UNIVERSITY OF CALIFORNIA SAN DIEGO

Chemical Tools for the Study of Lipids in Biology

A dissertation submitted in partial satisfaction of the requirements for the degree Doctor of Philosophy

in

Chemistry

by

Andrew K. Rudd

Committee in charge:

Professor Neal K. Devaraj, Chair
Professor Arnold L. Rheingold
Professor Sunil K. Sinha
Professor Navtej Toor
Professor Brian M. Zid

2019

The Dissertation of Andrew K. Rudd is approved, and it is acceptable in quality and form for publication on microfilm and electronically:

Chair

University of California San Diego

2019

Epigraph

It always seems impossible, until it is done.

Nelson Mandela

Table of Contents

List of Figures

List of Schemes

Acknowledgements

I would like to acknowledge the individuals who have played an instrumental role in my past and current success. First, I have to thank my parents, Neil and Anne Rudd, whose commitment, love, guidance, and support made me the person I am today. Thank you for fostering my curiosity and always supporting me in everything I do. You set an example of dedication and character which I strive to emulate. Thank you to my brother, Peter, for keeping me humble and for always looking up to me. Thank you to my girlfriend, Sarah Kranau, for her support and understanding throughout my Ph.D.

I would like to think my exceptional teachers whose commitment to my education was integral to my intellectual and personal growth. Mrs. Palese, thank you for your countless hours of work in and outside of the classroom. Your kindness and commitment stay with me to this day. Mrs. Hubbard, thank you for helping a shy child to come out of his shell.

I attribute much of my success to the sport of wrestling and the lessons it provided me. My participation in wrestling taught me perseverance, toughness, leadership, and character which is hard to find anywhere else. Thank you Coach Arlis and Coach Bayer for introducing me to the sport of wrestling and always pushing me to be the best that I could be. Through your coaching, I learned that I was capable of achieving things that I never thought possible. The lessons that I learned from you have shaped me into the person I am and continue to serve me every day.

I would like to thank my undergraduate research advisor Dr. Laura Listenberger for giving me the opportunity to engage in research in her lab. Her help and guidance gave me confidence in myself as a scientist. Without your help, I would not be where I am today. Thank you for encouraging and supporting my curiosity in the lab and for setting an example for exceptional

science. Your mentorship undeniably shaped my future in science and without your help, I may never have had the courage to pursue a Ph.D.

I must thank my current advisor, Dr. Neal Devaraj. Thank you for giving me the opportunity to join your lab. Your passion and attitude towards science inspire me every day. Thank you for always treating me as a colleague and encouraging me to aim high. Your guidance has been invaluable to my development as a scientist and an individual.

Finally, I must thank the members of the Devaraj Lab. You have all been irreplaceable mentors, collaborators, and friends. Thank you, Christian Cole, for sharing your incredible biological knowledge and experimental skill with me. Thank you, Michael Hardy, for immediately welcoming me into the Devaraj lab and lending invaluable advice during my Ph.D. Dr. Haoxing Wu, thank you for imparting some small amount of your incredible synthetic knowledge to me. I would like to thank Brandon Cisneros and Eric Zhou, the two incredible scientists who joined the Devaraj lab the same year as me. It has been a privilege to work alongside you both. I have to give a special thanks to Dr. Roberto J. Brea. You have been an outstanding mentor and friend. I have incredible admiration for you as a scientist and a person. I owe much of my success at UCSD to you. Thank you for instilling in me your meticulous attention to detail and care for the mentorship of others.

Notes About the Chapters

Chapter two, in full, is a reprint (with co-author permission) of the material as it appears in the publication; **A. K. Rudd**, J. V. Cuevas, N. K. Devaraj "SNAP-tag Reactive Lipid Anchors Enable Targeted and Spatiotemporally Controlled Localization of Proteins to Phospholipid Membranes," *J. Am. Chem. Soc.*, 2015, 137 (15) 4884–4887. I would like to thank Joan Cuevas for his assistance in performing vesicle microdomain experiments and Neal Devaraj for his scientific oversight and assistance in preparing the manuscript. The author of the dissertation is the primary author of this manuscript.

Chapter three, in full, is a reprint (with co-author permission) of the material as it appears in the publication; R. J. Brea, **A. K. Rudd,** N. K. Devaraj "Nonenzymatic biomimetic remodeling of phospholipids in synthetic liposomes," *Proc. Natl. Acad. Sci. U.S.A.,* 2016, 133 (31) 8589-8594. My contribution to this chapter was in the design and execution of all giant unilamellar vesicle (GUV) and microscopy experiments. I thank Roberto Brea and Neal Devaraj for their contributions to this chapter. Roberto Brea conceived and synthesized all compounds presented in this chapter and performed all experiments related to the characterization of these compounds and their reaction products as well as their unique chemical behavior. Neal Devaraj provided scientific oversight and assistance in the preparation of the manuscript.

Chapter four, in full, is a reprint (with co-author permission) of the material as it appears in the publication; **A. K. Rudd,** N. K. Devaraj "Traceless Synthesis of Ceramides in Living Cells Reveals Saturation Dependent Apoptotic Effects," *Proc. Natl. Acad. Sci. U.S.A.,* 2018, 115 (29) 7485-7490. I would like to thank Neal Devaraj for his invaluable advice and assistance in preparing the manuscript. The author of the dissertation is the primary author of this manuscript.

Chapter five, in full, is a reprint (with co-author permission) of the material as it appears in the publication; **A. K. Rudd**, R. J. Brea, N. K. Devaraj "Amphiphile-Mediated

Depalmitoyolation of Proteins in Living Cells," *J. Am. Chem. Soc.*, 2018, 140 (50) 17374-17378. I would like to sincerely thank Roberto Brea for his assistance with this work. Roberto Brea synthesized all compounds presented in this chapter and provided valuable scientific advice. I thank Neal Devaraj for his guidance and insight in designing experiments and preparing the manuscript. The author of the dissertation is the primary author of this manuscript.

Vita

Education

2013 Bachelor of Arts, Chemistry, St. Olaf College, Northfield, MN

2019 Doctor of Philosophy, Chemistry, University of California San Diego

Publications

A. K. Rudd, R. J. Brea, N. K. Devaraj "Amphiphile-Mediated Depalmitoyolation of Proteins in Living Cells," *J. Am. Chem. Soc.*, 2018, 140 (50) 17374-17378.

A. K. Rudd, N. K. Devaraj "Traceless Synthesis of Ceramides in Living Cells Reveals Saturation Dependent Apoptotic Effects," *Proc. Natl. Acad. Sci. U.S.A.,* 2018, 115 (29) 7485-7490.

R. J. Brea, **A. K. Rudd,** N. K. Devaraj "Nonenzymatic biomimetic remodeling of phospholipids in synthetic liposomes," *Proc. Natl. Acad. Sci. U.S.A.,* 2016, 133 (31) 8589-8594.

A. K. Rudd, J. V. Cuevas, N. K. Devaraj "SNAP-tag Reactive Lipid Anchors Enable Targeted and Spatiotemporally Controlled Localization of Proteins to Phospholipid Membranes," *J. Am. Chem. Soc.*, 2015, 137 (15) 4884–4887.

Fellowships and Awards

2017 Biochemistry of Growth and Regulation Trainee

2016 Inamori Fellowship Award

2016 Teddy Traylor Award

2016 Distinguished Graduate Student Award

2014 San Diego Fellowship

Presentations

2018 Oral – ACS New Orleans

2017 Oral – ACS Washington DC

2017 Poster – ACS San Francisco

2016 Oral - ACS San Diego

2015 Oral – Pacifichem

Abstract of the Dissertation

Chemical Tools for the Study of Lipids in Biology

By

Andrew K. Rudd

Doctor of Philosophy in Chemistry

University of California San Diego, 2019

Professor Neal K. Devaraj, Chair

This dissertation will first explore methods to selectively direct proteins to phospholipid membranes. The natural mechanisms that tether proteins to membranes are typically complex, requiring multiple steps and accessory components. It would be advantageous to develop simplified methods to direct proteins of interest to phospholipid membranes in a single step. We have developed a modular method for membrane localization of proteins by using chemically modified phospholipid anchors capable of covalent attachment to O6-methylguanine DNA methyltransferase (SNAP-tag) fusion proteins. We demonstrate that photocaged lipid precursors

enable light-triggered spatial and temporal control over protein localization. The anchoring system is compatible with cell-free expression, allowing for genetic targeting of proteins to lipid membranes of giant unilamellar vesicles. This technique can be used to control membrane curvature effects, similar to what has been previously observed with certain membrane-bound proteins. This work addresses a current need in synthetic biology for simplified and robust methods to control membrane localization of expressed proteins and shows promise as a general tool for protein targeting to lipid vesicles and cellular membranes.

In the second investigation, this dissertation will discuss a new method for the nonenzymatic remodeling of lipid membranes. Cell membranes have a vast repertoire of phospholipid species whose structures can be dynamically modified by enzymatic remodeling of acyl chains and polar head groups. Lipid remodeling plays important roles in membrane biology and dysregulation can lead to disease. Although there have been tremendous advances in creating artificial membranes to model the properties of native membranes, a major obstacle has been developing straightforward methods to mimic lipid membrane remodeling. Stable liposomes are typically kinetically trapped and are not prone to exchanging diacylphospholipids. An approach relies on transthioesterification/acyl shift reactions that occur spontaneously and reversibly between tertiary amides and thioesters. We demonstrate exchange and remodeling of both lipid acyl chains and head groups. Using our synthetic model system, we demonstrate the ability of spontaneous phospholipid remodeling to trigger changes in vesicle spatial organization, composition, and morphology as well as recruit proteins that can affect vesicle curvature. Membranes capable of chemically exchanging lipid fragments could be used to help further understand the specific roles of lipid structure remodeling in biological membranes.

In the third section of this dissertation, a novel approach for the in situ synthesis of natural lipids in living cells will be presented. Mammalian cells synthesize thousands of distinct lipids,

yet the function of many of these lipid species is unknown. Ceramides, a class of sphingolipid, are implicated in several cell-signaling pathways, but poor cell permeability and lack of selectivity in endogenous synthesis pathways have hampered direct study of their effects. Here we report a strategy that overcomes the inherent biological limitations of ceramide delivery by chemoselectively ligating lipid precursors in vivo to yield natural ceramides in a traceless manner. Using this method, we uncovered the apoptotic effects of several ceramide species and observed differences in their apoptotic activity based on acyl-chain saturation. Additionally, we demonstrate spatiotemporally controlled ceramide synthesis in live cells through photoinitiated lipid ligation. Our in situ lipid ligation approach addresses the long-standing problem of lipid-specific delivery and enables the direct study of unique ceramide species in live cells.

Finally, this dissertation will discuss the development of small molecules for the depalmitoylation of proteins in vivo. Post-translational S-palmitoylation plays a central role in protein localization, trafficking, stability, aggregation, and cell signaling. Dysregulation of palmitoylation pathways in cells can alter protein function and is the cause of several diseases. Considering the biological and clinical importance of S-palmitoylation, tools for direct, in vivo modulation of this lipid modification would be extremely valuable. Here, we describe a method for the cleavage of native S-palmitoyl groups from proteins in living cells. Using a cell permeable, cysteine-functionalized amphiphile, we demonstrate the direct depalmitoylation of cellular proteins. We show that amphiphile-mediated depalmitoylation (AMD) can effectively cleave S-palmitoyl groups from the native GTPase HRas and successfully depalmitoylate mislocalized proteins in an infantile neuronal ceroid lipofuscinosis (INCL) disease model. AMD enables direct and facile depalmitoylation of proteins in live cells and has potential therapeutic applications for diseases such as INCL, where native protein thioesterase activity is deficient.

CHAPTER 1

1 Introduction

1.1 The Birth of Lipid Chemistry

Michel Eugene Chevreul was born in Angers, France on August 31st, 1786. Chevreul was born into a family of apothecaries and surgeons, his father was a pioneer in obstetrics and received the honor of surgeon to Louis, Duke of Anjou (who would later be known as Louis the 18th of France). In 1799, Michel Eugene attended Ecole Centrale where he studied for four years. In 1803, when it came time to choose a career, he broke from his family's tradition of medical practice and instead chose to pursue chemistry. In 1804, he joined the laboratory of Vauquelin Fourcroy. Vauquelin, who was developing methods to separate natural materials into their fundamental constituents, introduced Chevreul to the study of biological compounds. During his time in Vauquelin's lab, Chevreul worked to isolate natural dyes from biological sources. In 1811, Vauquelin tasked him with examining a sample of soap. This simple assignment had tremendous consequences for the world of chemistry. Chevreul found that fats were composed of two key components, fatty acids and glycerol. Furthermore, he discovered that the fats he studied were composed of not one but many distinct species of fatty acids. In 1813, Michel Eugene received a position at Lycée Charlemagne as a professor of physics where he continued to explore the chemistry of fats. During this time, he discovered that lard contained two types of fats. One (stearine) was solid at room temperature while the other (elaine) remained liquid. Chevreul went on to identify specific fatty acids including stearic, capric, oleic and butyric acids as well as cholesterol as key constituents of animal fats.[1,2]

1.2 From Fat to Structure

The next big discovery in lipid chemistry was that of a new class of lipids, phospholipids, first described by Theodore Gobley in 1847. Through the careful extraction and analysis of egg yolk, Gobley identified an organic component containing phosphorus. This "phosphoric matter" could be degraded into fatty acids and glycerophosphoric acid, suggesting the existence of a new biological lipid composed of fatty acids, glycerol and phosphate. He named these compounds lecithins (these would later be known as phosphatidylcholines). The discovery of these polar lipids set the stage for a new revelation in the field of lipid chemistry. This breakthrough would come by way of an English scientist, Ernest Overton. As a student and lecturer at the University of Zürich, Overton published extensively on his observations on cell meiosis and the osmotic properties of cells. From 1895-1902 he pioneered the concept of a cellular membrane composed of lipids. He discovered that these lipid boundary layers were involved in the process of solute exchange between cells and their environment. He also found that the flow of sodium and potassium across the membranes of muscle and nerve cells was responsible for their activity.[3] This fundamental discovery shed new light on the importance of lipids in cellular structure and function. A further understanding was gained from studies by Evert Gorter and François Grendal in their landmark 1924 paper where they demonstrated that the cellular membrane is composed of a layer of lipids two molecules thick. This first model of a lipid bilayer set the framework for our modern day understanding of phospholipid membranes.[4]

1.3 A Medical Link

At the same time that lipids came into focus as essential structural components of the cell, their potential role in human health was thrust onto the main stage. In 1913, a Russian pathologist by the name of Nikolai N. Anitschkow was searching for the underlying cause of atherosclerosis. Atherosclerosis, the buildup of plaque in arteries, was well described in 1913 but was often

considered an unavoidable part of the aging process. One hypothesis suggested that the pathogenesis of this disease was due to excessive consumption of animal proteins. In an attempt to test this hypothesis, Anitschkow fed rabbits a diet of milk, eggs and meat. He found that, indeed, these rabbits developed the kind of plaque buildup associated with atherosclerosis. To elucidate the exact dietary culprit, Anitschkow systematically eliminated foods from the Rabbits' diets until the disease was no longer observed. He found that while whole eggs and egg yolk induced vascular buildup, egg whites did nothing. Anitschkow then extracted and purified cholesterol from egg yolks and found that this lipid alone could replicate the results, demonstrating that atherosclerosis was due not to a protein but a lipid, cholesterol.[5] For the first time, lipids had been linked to the progression of a disease.

While it was becoming clear that dietary lipids played a significant role in health, the underlying mechanisms were unknown. It had been well understood that fats and oils were a good source of nutritional energy, but it wasn't until 1929 that it was discovered that certain dietary fats were essential. In a seminal study by George and Mildred Burr, they found that feeding rats a fat-free diet led to a deficiency disease. By reintroducing specific fats, they discovered that a single fatty acid, linoleic acid, was a necessary part of the rat's diet. This work shifted the scientific thinking on fats, and it became apparent that not all required fats could be synthesized from carbohydrates and proteins.[6] The exact reason for this remained unknown until the late 1940's when Ralph Holman discovered that in rats, linoleic acid was metabolized to arachidonic acid, an essential cell signaling molecule. Holman went on to extensively study dietary fatty acids and classify their metabolic products. This work led to the discovery that the terminal end of fatty acids remains unaltered in biology. Because of this, he introduced the omega (ω) naming structure for fatty acids in which carbons are counted starting from the terminus of fatty acids.[7]

1.4 Lipids in the 21st Century

At the turn of the century, the advance of new analytic tools made it possible to peer deeper into biology than ever before. Mass spectroscopy techniques were now capable of exquisite sensitivity, allowing for the analysis of global lipid populations in complex biological samples. These advances led to the discovery of thousands of new lipid species and sparked the lipidomics revolution. It soon became possible to identify and quantify specific lipid species in cells and to begin to piece together the dynamic metabolism of these molecules.[8] This birthed efforts such as the Lipid Maps project which has drastically accelerated the discovery of unique lipid species and cataloged over 40,000 specific lipid species to date.[9] With this vast new knowledge of lipid diversity, came a new question, what are they all for?

Mammalian cells contain thousands of distinct lipid species, but the reason for such diversity is widely unknown. We can classify lipid structure but still know very little about lipid behavior and function. A big reason for this is the lack of available tools for asking such questions. Tools for studying lipid localization, interactions and biological function are severely lacking. One main area of inquiry is the interactions between lipids and proteins. One approach in this area has been to metabolically incorporate lipids bearing bioorthogonal tags and then pull down proteins which interact with these lipids. This approach has been used to study the lipid-protein interactions of fatty acids, isoprenoids and phospholipids in live cells.[10] Recently, powerful tools have been developed which allow for the study of the effects of specific lipids in live-cells. Carsten Schultz's group has developed photocaged sphingosine molecules which enable controlled release of sphingosine in living cells and led to the finding that sphingosine can control the release of calcium from lysosomes.[11] Work out of Dirk Trauner's group has demonstrated that synthetic photoswitchable diacylglycerols can be used to spatially control protein kinase C activity in cells.[12] Genetic manipulation of endogenous lipid synthesis pathways has also emerged as a powerful

method for the study to specific lipid species in vivo. Itay Budin and Jay Keasling demonstrated that by engineering the fatty acid biosynthesis pathway in E. coli they could modulate the lipid composition of the inner membrane and study the effect of membrane fluidity on respiratory metabolism.[13]

Another ongoing area of lipid research studies these molecules in the context of the origin of life. Groundbreaking work by Jack Szostak's group has demonstrated how simple lipids can assemble into membrane bilayers.[14] Their work has shown how these simple lipid bilayers can engage in the behaviors necessary for the growth and propagation of protocells. Further work by Neal Devaraj's group has taken a chemistry-based approach to answer some of these same questions. By developing methods for the de novo synthesis of lipids under biological conditions, the Devaraj group has shown that chemical reactions can be coupled to the synthesis, growth and division of protocell membranes.[15,16]

This dissertation will explore the development of new chemical tools for the study of lipids in both artificial and biological systems. Recent work will be presented which lends new biomimetic functionality to model membrane systems. The lessons learned from these minimal systems were then used to develop tools for the chemoselective reaction of lipid molecules inside of living cells. These new methods enable the study of previously intractable biological questions and represent a fundamentally new approach toward the study of lipids in biology.

CHAPTER 2

2 SNAP-tag-Reactive Lipid Anchors Enable Targeted and Spatiotemporally Controlled Localization of Proteins to Phospholipid Membranes

2.1 Introduction

Membrane-bound proteins are critical for regulating signaling, transport, binding interactions, and curvature.[17–19] Thus, controlled localization of proteins to discrete regions of the cellular membrane is essential for all organisms. Cells accomplish this task through several transport and lipidation pathways, often requiring enzymes specific to the target protein.[20,21] Current techniques for incorporating mem- brane proteins into phospholipid membranes involve the growth of isolated cellular membranes[22] or require the use of proteoliposomes and detergent,[23,24] making in situ protein localization difficult. Approaches to facilitate membrane localization of proteins of interest include the use of transmembrane domain and isoprenylation sequence fusions,[25–27] membrane- localizing ligands,[28] optogenetics,[29] or supramolecular interactions.[30]

These techniques, while useful, have several drawbacks, including a lack of covalent membrane attachment and the inability to control interactions in a spatiotemporal manner. A tool that overcomes these hurdles would allow for controlled studies on topics such as protein signaling and induced membrane curvature, where efficient and localized protein attachment is required to elicit specific responses.[17,18] Furthermore, such tools would be capable of guiding in situ synthesized proteins to membranes for synthetic biology applications. Here we present a simplified approach to membrane localization that results in the selective and covalent linkage of proteins to the lipid bilayer. This approach utilizes benzylguanine (BG)-modified lipid anchors and the well-

established mutant O^6-methylguanine- DNA methyltransferase, SNAP-tag,[31] to tether proteins to phospholipid membranes. Additionally, it allows for photo- activation of protein to defined vesicles or portions of a single vesicle membrane with spatial resolution on the order of micrometers. To our knowledge, this is the first demonstration of the use of the SNAP-tag reaction to anchor proteins to BG- functionalized phospholipid membranes.

SNAP-tag technology has seen increasing use in biomolecular imaging due to its several attractive features, which include the ability to access a broad range of bright and stable synthetic fluorophores, the availability of fluorogenic probes, and the relatively small size of the reactive protein (~20 kDa).[32–35] The remarkable versatility of SNAP-tag has enabled numerous applications beyond imaging, such as the detection of drug-protein interactions,[36] conjugation of biomolecules,[37,38] proximity ligation of oligonucleotides[39] and immobilization of protein on self-assembled monolayers.[40] However, despite these past results, SNAP-tags have not been explored for lipid membrane modification. We thus set out to investigate whether reactive lipid anchors on phospholipid membranes could capture SNAP-tag proteins.

2.2 SNAP-tag Lipid Anchors: Design and Optimization

To determine if SNAP-tags could be used for lipid membrane modification, we synthesized several SNAP-tag reactive BG lipid anchors. Interestingly, initial experiments without a linker and with a short 7-member poly(ethylene glycol) (PEG) linker between the BG and lipid headgroup failed to promote localization of SNAP-tag to model phospholipid membranes (compounds **7** and **9**, Figure 2.1). Reasoning that the phospholipid membrane-bound BG group may have hindered access to the active site of the SNAP-tag protein,[41] we chose to explore longer and more flexible linkers and found that 17- and 45-member PEG linkers (DOPE-PEG17-BG and DSPE-PEG45-BG) were able to maintain reactivity of membrane-bound BG with SNAP-tag proteins (Figure

2.1). To confirm the covalent reactivity of DSPE-PEG45-BG, the lipid was incubated with a purified SNAP-tag protein at 37 °C overnight. SDS-PAGE gel analysis of the completed reaction showed an expected increase in protein mass, indicating covalent linkage of SNAP-tag and the lipid anchor (Figure 2.2). The sensitivity of the membrane reaction to linker structure offers a possible explanation for why past attempts to extend SNAP-tags to phospholipid membrane modification have not met with success.[42] PEG linkers are an attractive solution to this problem because they increase the flexibility of the reactive substrate while still maintaining a short end-to-end distance. Modeling experiments suggest that 18-member poly(ethylene oxide) molecules, very similar in length and structure to the linker region of DOPE- PEG17-BG, have an average length of 25.3 Å.[43]

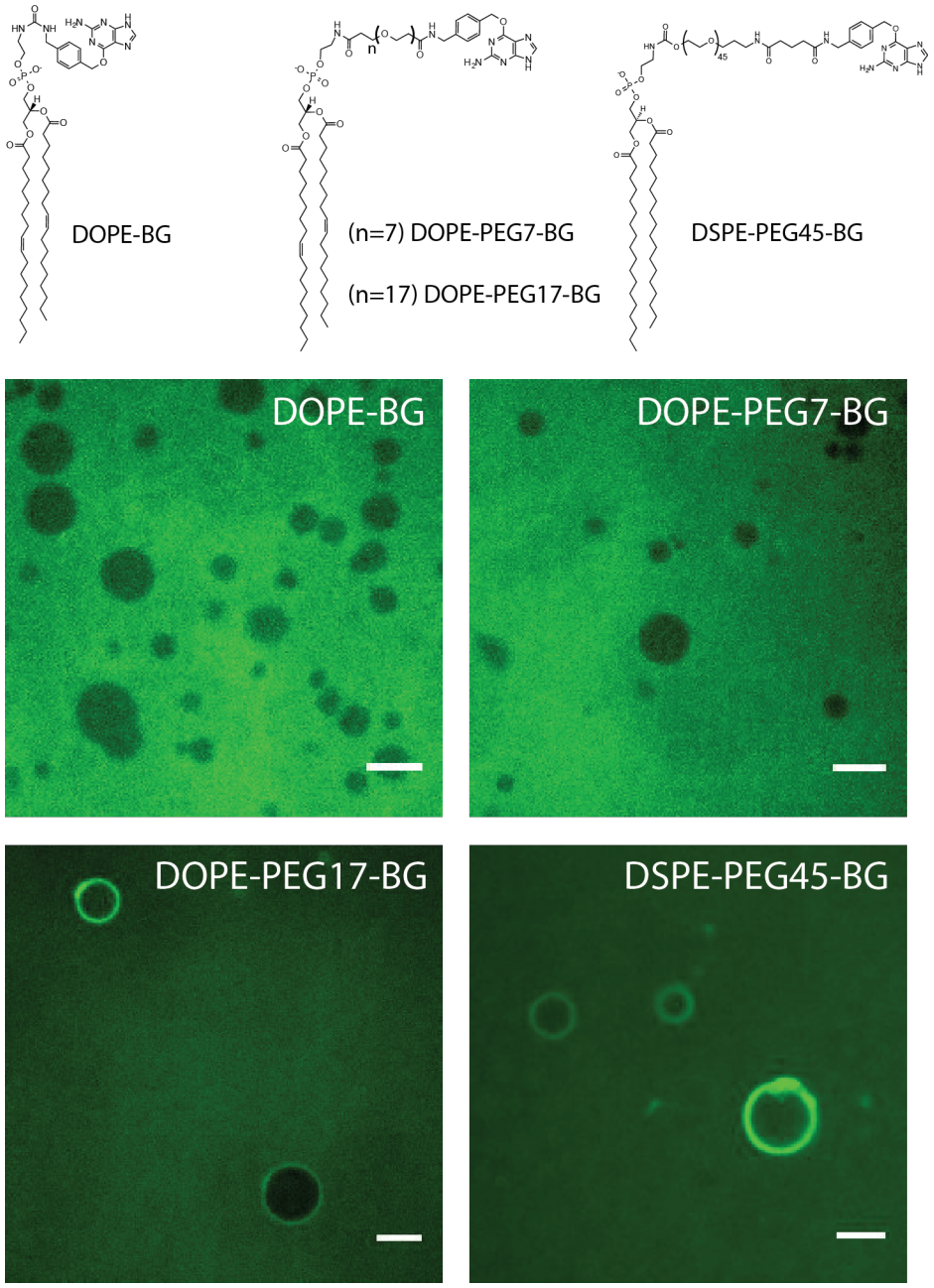

Figure 2.1 Full field images of vesicle populations containing 5 % lipid anchor after incubation with AF488 labeled SNAP-tag protein. No binding was observed in the vesicle population when using no linker (DOPE-BG) or a short linker (DOPE-PEG7-BG). Binding was observed, however, in all vesicles of populations possessing longer linkers (DOPE-PEG17-BG and DSPE-PEG45-BG) (Scale bar 10 μm). Structures of all four lipids are given above for reference.

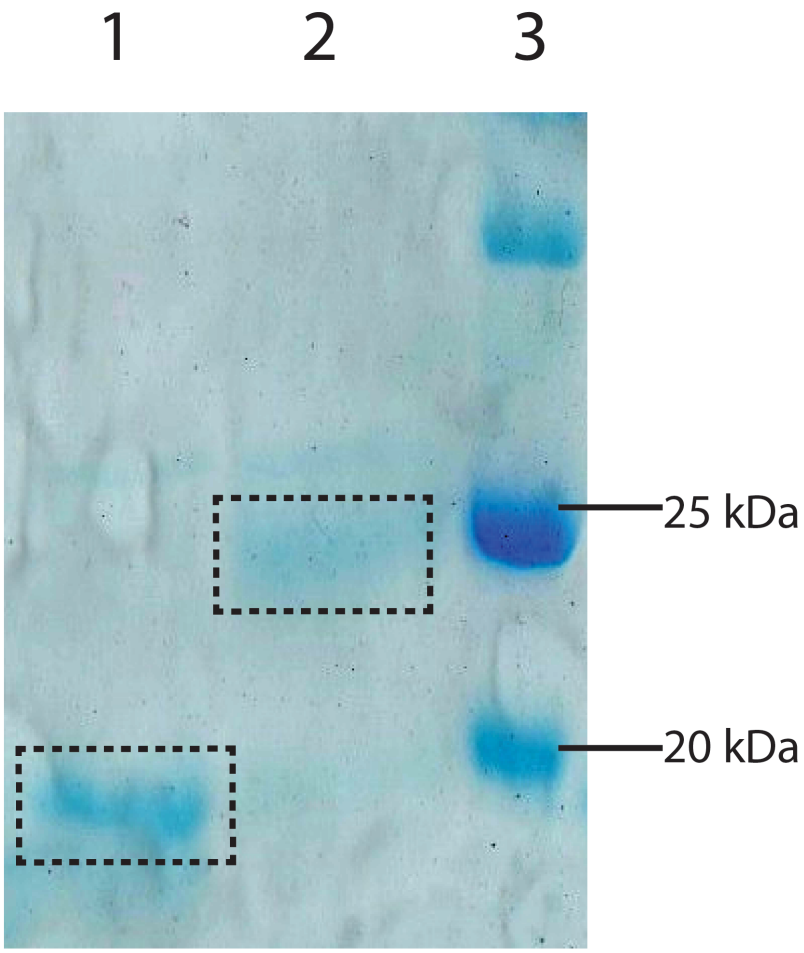

Figure 2.2 SDS-PAGE on a 15% polyacrylamide gel of purified SNAP-tag protein (Lane 1) and purified SNAP-tag protein reacted with compound **1** (Lane 2). MW marker (Lane 3). Major bands are highlighted in each lane. The roughly 5 kDa shift is different than the expected 3 kDa shift most likely due to the lower mobility of PEG in SDS-PAGE as compared to protein.[44]

2.3 Selective Protein Modification of Phospholipid Membranes

To investigate the utility of these anchors for phospholipid membrane modification (Figure 2.3B), dioleoylphosphatidylcholine (DOPC) giant unilamellar vesicles (GUVs) containing 5 mol % DSPE-PEG45-BG were formed by adapting a previously published inverse emulsion technique.[45] Formed vesicles were incubated with 3 μM Alexa Fluor 488 (AF488) dye-labeled SNAP-tag for 1 h at 37 °C. Fluorescent microscopy showed excellent membrane localization of SNAP-tag to DSPE-PEG45-BG containing membranes (Figure 2.3C). To confirm that the

localization we observed was due to reaction with the lipid anchor and not other nonspecific interactions, we incubated AF488-labeled bovine serum albumin with DSPE-PEG45-BG vesicles and observed no membrane localization. Additionally, AF488-SNAP-tag incubated with DOPC vesicles lacking the reactive lipid anchor showed no localization to the membrane, indicating that the fluorescent SNAP-tag protein does not bind due to inherent phospholipid membrane affinity (Figure 2.4).

Having determined that DSPE-PEG45-BG is capable of reacting with SNAP-tag protein, we next explored whether the lipids could be used to target specific microdomains formed on mixed phospholipid vesicles. Previous studies have shown that mixtures of saturated and unsaturated phospholipids, along with cholesterol, can produce vesicles with two distinct lipid phases.[46,47] Using a 1:1:1 mixture of DOPC:distearoylphosphatidylcholine (DSPC):cholesterol (Chol) with 5 mol % DSPE- PEG45-BG, we electroformed GUVs with two lipid phases. After introduction of AF488-labeled SNAP-tag, specific labeling of the less ordered lipid domains occurred, evidenced by colocalization with the fluorescent lipid Texas Red DHPE (Figure 2.5). These results suggest that BG-modified lipids could serve as a valuable tool for studying the effect of lipid domains on the function and structure of embedded proteins.

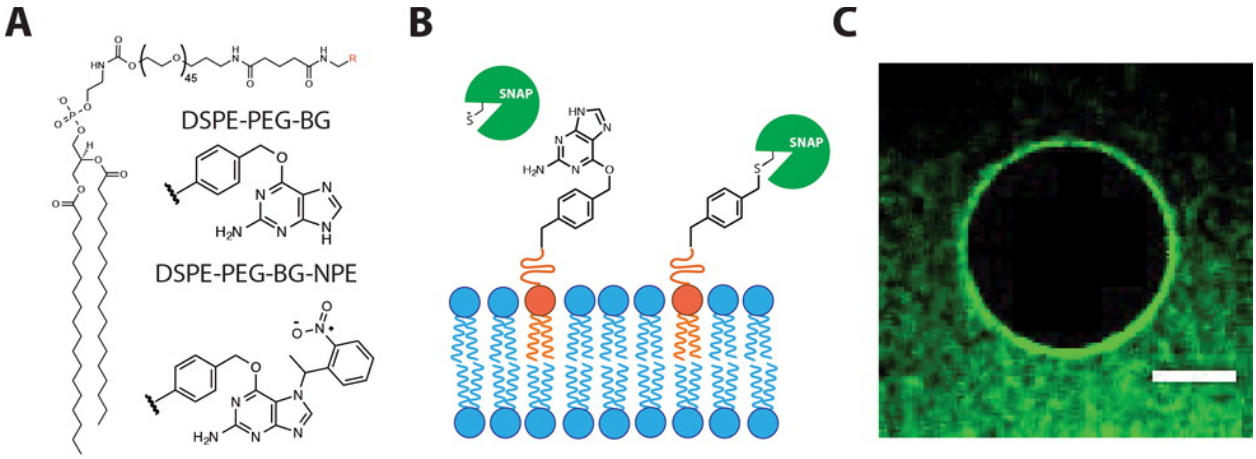

Figure 2.3 SNAP-tag lipid anchors. (A) DSPE-PEG lipid anchor with benzylguanine (BG) and photocaged benzylguanine (BG-NPE) head groups. (B) Proposed reaction of SNAP-tag protein with a membrane embedded DSPE-PEG lipid-anchored BG substrate. Transfer of the benzyl group to the active site of the SNAP-tag results in covalent attachment of the protein to the phospholipid membrane. (C) Visualizing membrane localization of a fluorescently tagged (AF-488) SNAP-tag protein on a giant unilamellar vesicle. The vesicle was formed with 5 mol % DSPE-PEG45-BG lipid anchors, which captures the SNAP-tag protein (scale bar 10 μm).

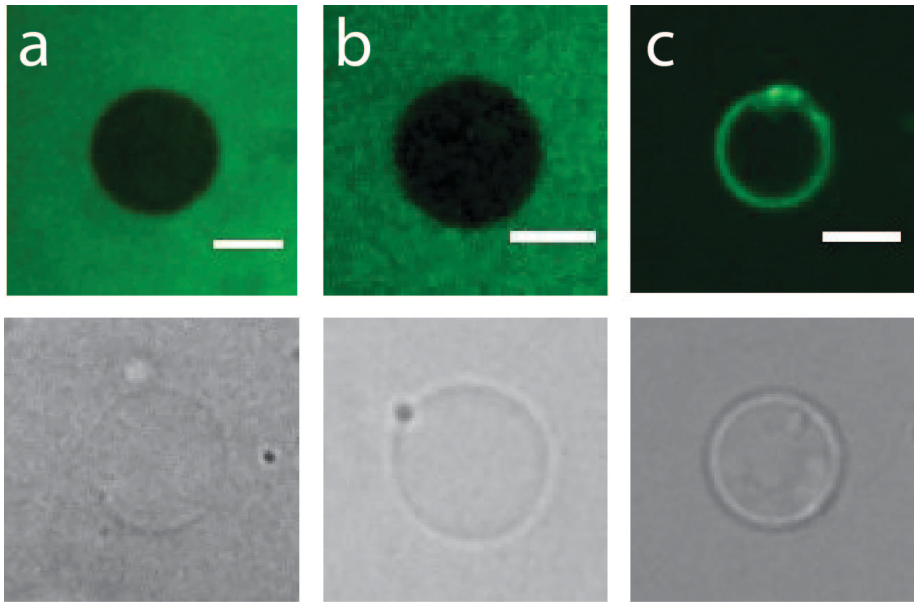

Figure 2.4 DSPE-PEG45-BG results in specific binding of SNAP-tag to vesicle membranes. Top Row: AlexaFluor 488, Bottom Row: DIC (a) Incubation of AlexaFluor 488 labeled SNAP-tag with DOPC GUVs, (b) Incubation of AlexaFluor 488 labeled BSA with 5 % DSPE-PEG45-BG GUVs, (c) Incubation of AlexaFluor 488 labeled SNAP-tag with 5 % DSPE-PEG45-BG GUVs (scale bar 10 μm).

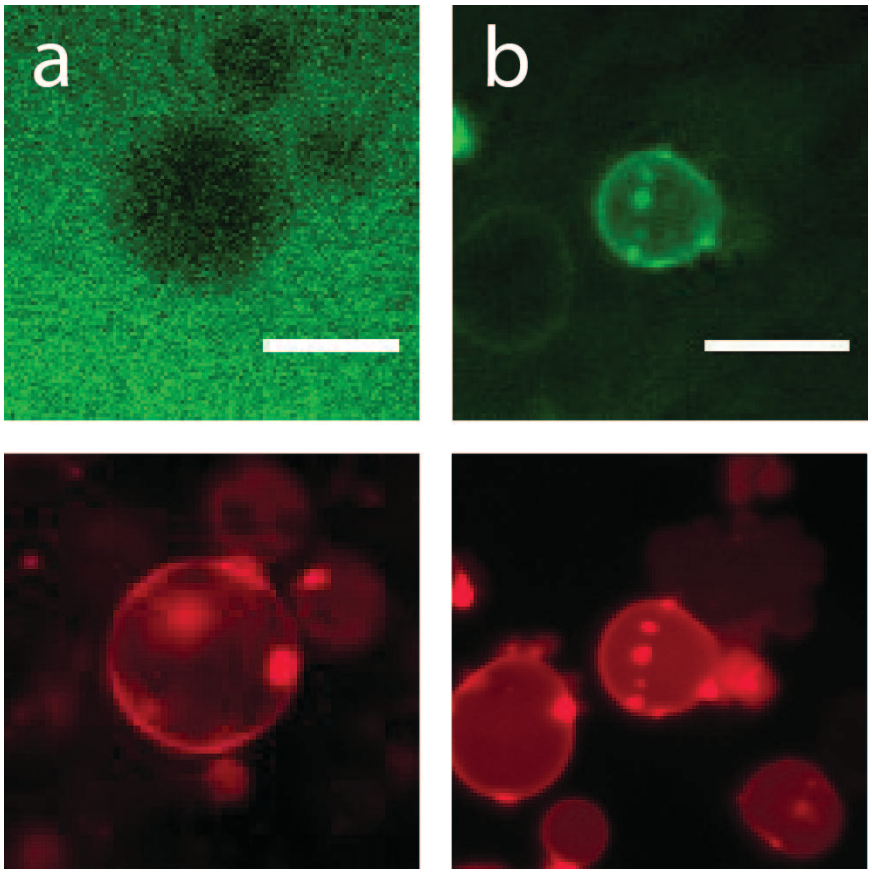

Figure 2.5 Localization of Alexa Fluor 488 labeled SNAP-tag to DSPE-PEG-BG containing membrane microdomains. Top Row: AlexaFluor 488, Bottom Row: Texas Red (a) 1:1:1 DOPC:DSPC:Chol GUVs (b) 1:1:1 DOPC:DSPC:Chol GUVs with 5 % DSPE-PEG45-BG (scale bar 20 μm).

2.4 Spatiotemporally Controlled Membrane Protein Modification

A major advantage of using SNAP-tag reactive lipids is the potential to spatiotemporally control membrane protein modification. Elegant work has established that photocaged alkylguanosines can be activated with light to trigger binding with SNAP-tagged proteins.[48] With this in mind, we explored the feasibility of light-activated protein immobilization using a photocaged lipid anchor (DSPE-PEG45-BG-NPE) (Figure 2.3A). Kinetic studies showed rapid uncaging of the lipid in vesicles ($t_{1/2}$ = 80 s) upon irradiation with 360 nm light. To test the reactivity of the DSPE-PEG45-BG-NPE vesicles to SNAP- tag, DOPC GUVs were synthesized containing 5 mol % DSPE- PEG45-BG-NPE. Obtained vesicles were irradiated with 360 nm light

for 10 min and then incubated with AF488-labeled SNAP- tag protein for 1 h (see 2.7 Experimental Methods for full details). The UV activated vesicles showed marked localization of protein to the membrane compared to nonactivated vesicles, which lacked any discernible binding even after 2 h of incubation with SNAP-tag proteins (Figure 2.6). An exciting feature of this technique is its compatibility with laser scanning confocal microscopy. By controlling the region of light exposure with a 405 nm diode laser, we were able to activate a selected vesicle of a population without triggering protein localization in neighboring vesicles. Activation was rapidly accomplished using 4.5 s of light exposure. After deprotection, SNAP-tag protein localization occurred within minutes (Figure 2.7B). We next synthesized DPPC GUVs containing 5 mol % DSPE-PEG45-BG-NPE using a solvent evaporation method.[49] By employing DPPC (T_m = 41 °C) as the main component of the phospholipid membrane, we were able to produce vesicles possessing a gel phase membrane at ambient temperature. Because the vesicle membranes are in the gel phase, lateral diffusion of constituent phospholipids is extremely slow, thus preventing lipid anchors from translating throughout the membrane.[50] This characteristic allowed us to photo-uncage lipid anchors on only a portion of the membrane. Vesicles were incubated with 230 μM SNAP-tag GFP and then irradiated for 2 s on one side of a vesicle membrane. After exposure, protein localization was observed within 90 s and after 10 min no further binding was evident. This unique capability may allow for the controlled decoration of membranes with several different fusion proteins at specific locations on a vesicle, an area that is of interest for drug delivery applications.[51,52]

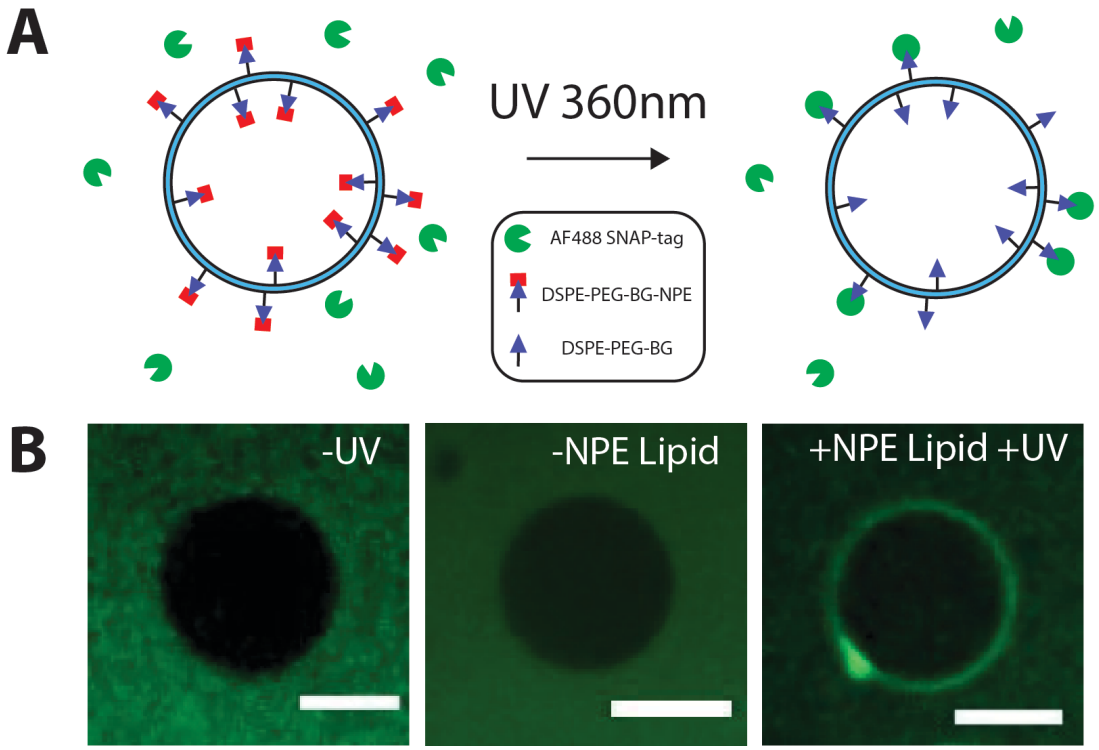

Figure 2.6 Light activated binding of SNAP-tag GFP to vesicles. (A) Exposure of DSPE-PEG45-BG-NPE containing vesicles to 360 nm UV light results in loss of the NPE caging group and activates binding of SNAP-tag to the membrane. (B) Left: 5% DSPE-PEG45-BG-NPE vesicles were incubated for 2 h with dye (AF488) labeled SNAP-tag with no UV exposure (scale bar 10 µm). Middle: DOPC vesicles exposed to 360 nm UV light for 10 min and incubated for 2 h with dye (AF488) labeled SNAP-tag (scale bar 15 µm). Right 5% DSPE-PEG45-BG-NPE vesicles exposed to 360 nm UV light for 10 min and incubated for 2 h with dye (AF488) labeled SNAP-tag (scale bar 10 µm).

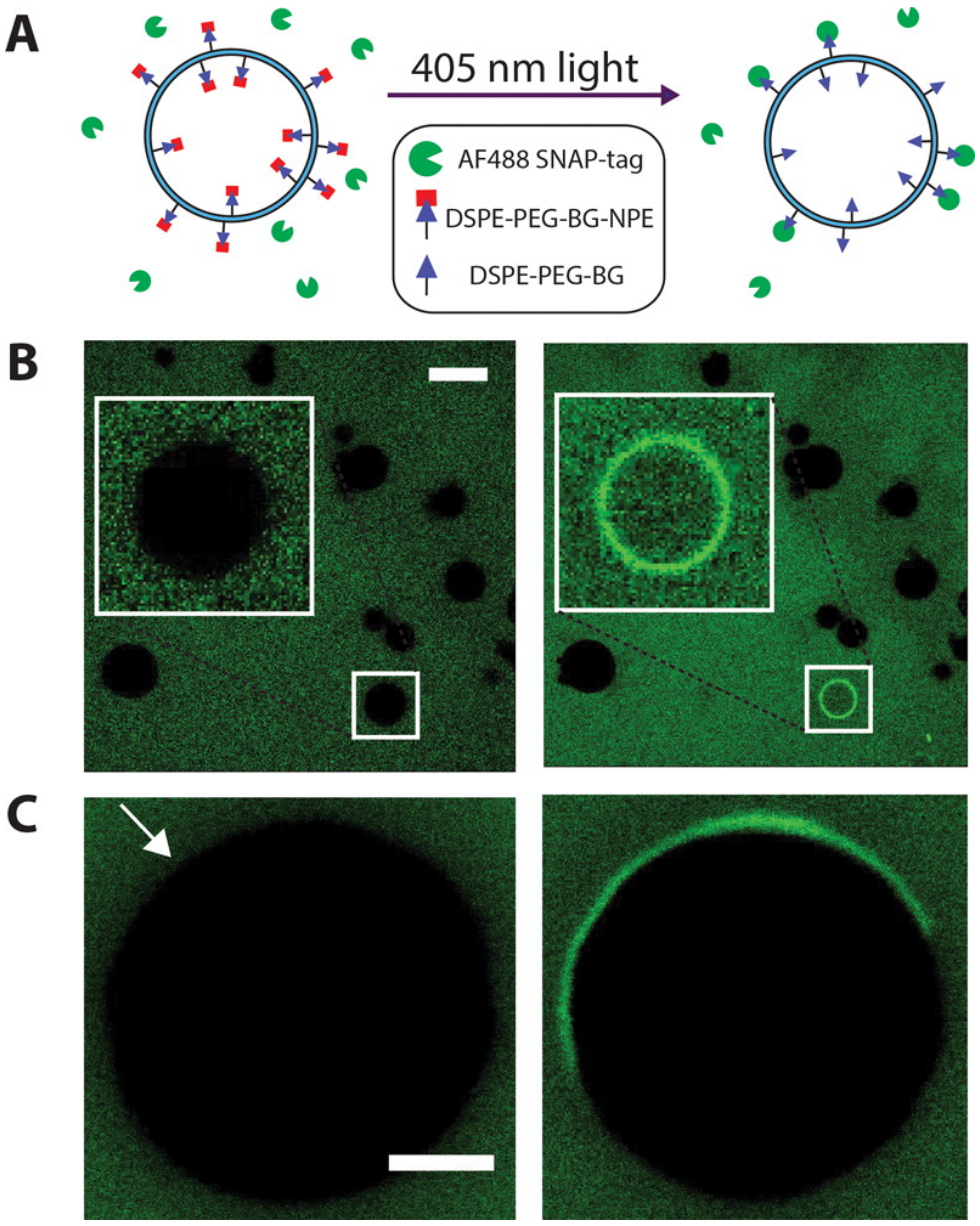

Figure 2.7 Spatiotemporally controlled binding of SNAP-tag proteins to vesicles. (A) Exposure of DSPE-PEG-BG-NPE containing vesicles to a 405 nm laser results in the loss of the NPE caging group and spatiotemporally activates binding of SNAP-tag proteins to the membrane. (B) Left: 20:1 DOPC:DSPE-PEG-BG-NPE vesicles incubated with dye (AF488)-labeled SNAP-tag before photoactivation (scale bar 30 μm).: A single vesicle of the population was irradiated with the 405 laser line for 4.5 s (white box). Right: After 10 min, protein has bound specifically to the uncaged vesicle. (C) Left: 20:1 DPPC:DSPE-PEG45-BG-NPE vesicles incubated with SNAP-tag GFP fusion before photoactivation (scale bar 2 μm). A portion of the vesicle was exposed to the 405 laser line (white arrow) for 2 s. Right: after 10 min protein binding is observed only on the selected portion of the gel phase membrane.

2.4 Genetically Targeted Protein Localization in a Minimal Cell System

Recently there has been increasing interest in the use of vesicle encapsulated cell free expression systems as cell mimics. Applications include fundamental studies on the essential elements for cellular function, minimal cells for synthetic biology, and drug delivery.[53,54] Seminal work in this area has demonstrated the efficient expression of protein in GUVs that encapsulate either E. coli lysate or the recombinant PURE system.[26,55] A challenge in this area has been to target in situ-synthesized proteins to the GUV membrane. Having this capability is essential for the reconstitution of natural membrane protein function and the design of new artificial systems in self-contained minimal cells. While there have been elegant demonstrations using spontaneous incorporation of certain integral membrane proteins,[28] and reconstitution of the Sec translocon to create lipid/protein membranes,[56] the use of SNAP-tag reactive lipids could offer a simple method to genetically target a much wider range of proteins to the surrounding lipid bilayer (Figure 2.8A). We therefore examined whether DSPE-PEG45-BG lipids could be utilized in con- junction with cell free expression systems to genetically trigger membrane localization of a SNAP-tag fusion protein. Plasmid encoding for a SNAP-tag GFP fusion protein and an S30 T7 protein expression system were encapsulated in GUVs containing 5 mol % DSPE-PEG45-BG using a modified inverse emulsion method. After protein expression at 37 °C for 1 h, vesicles containing lipid anchor showed excellent localization of expressed fusion protein to the vesicle membrane (Figure 2.8B). Control experiments with vesicles lacking reactive lipid or using a control GFP resulted in no localization of membrane protein. This result demonstrates the ability of the SNAP-tag reactive lipid system to effectively emulate cellular protein trafficking and allow for genetically targeted control over membrane localization.

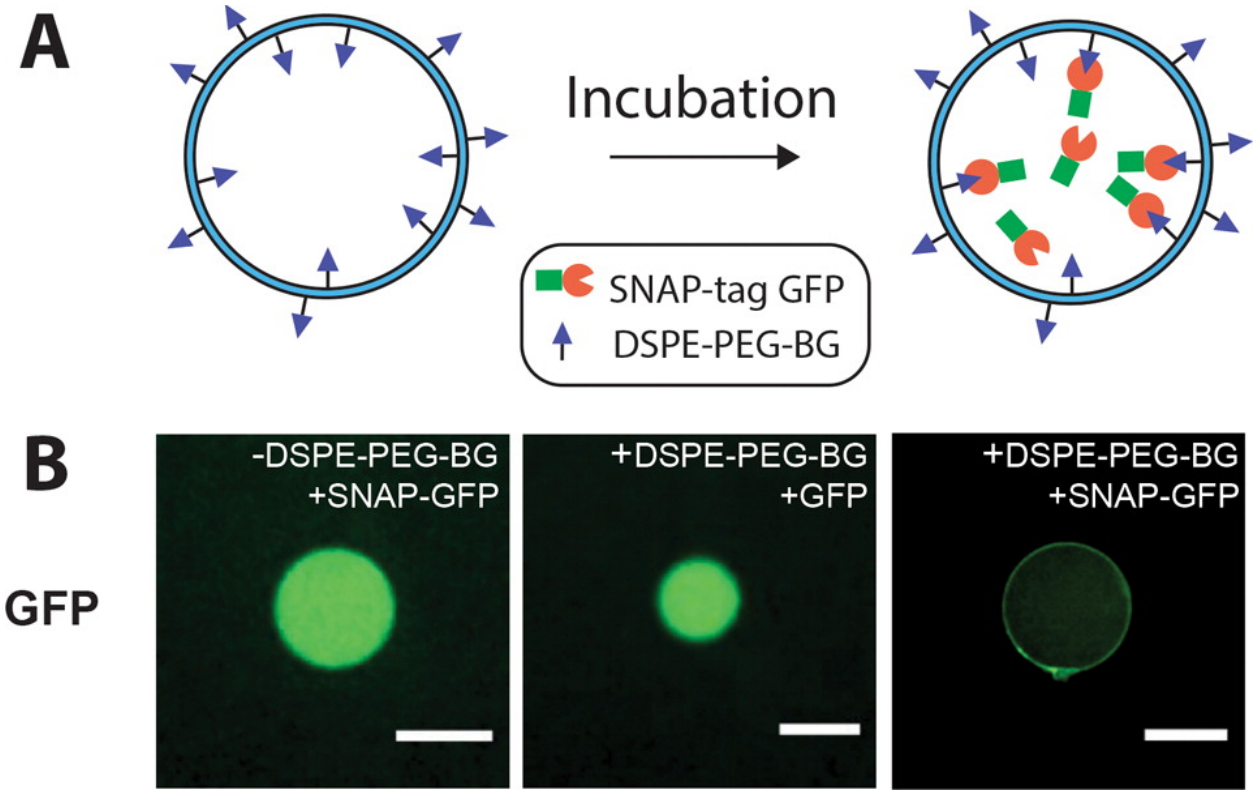

Figure 2.8 Binding of in situ synthesized SNAP-tag GFP to vesicle membranes. (A) Expression by E. coli lysate encapsulated in 5 mol % DSPE-PEG-BG vesicles leads to subsequent membrane localization of SNAP-tag GFP fusion protein. (B) GUVs expressing fluorescent protein (green channel, bottom row). Left: DOPC GUVs with no DSPE-PEG-BG expressing SNAP-tag GFP fusion (scale bar 15 μm). Middle: 5 mol % DSPE-PEG45-BG vesicles expressing GFP (scale bar 10 μm). Right: 5 mol % DSPE-PEG45-BG vesicles expressing SNAP-tag GFP fusion (scale bar 25 μm).

2.5 Lipid Anchored Proteins Induce Membrane Curvature

Having demonstrated the wide range of capabilities and control offered by SNAP-tag reactive lipid anchors, we wished to explore if this technique could be used to recreate membrane effects caused by natural phospholipid-bound proteins. Recently it has been shown that some natural membrane-bound proteins such as epsin1 are able to induce membrane curvature changes due to crowding effects alone and that even tethering GFP to the membrane at high concentration can result in membrane tubulation. We therefore reasoned that our membrane anchor could be used to induce membrane curvature via crowding by tethering protein near the membrane in high

concentration.[57] Electroformed vesicles possessing disordered microdomains were synthesized containing 5 mol % DSPE-PEG45-BG. Upon incubation with 185 μM SNAP-GFP, membrane tubulation and deformation was observed within 90 s (Figure 2.9), while controls lacking membrane anchor displayed no noticeable change in membrane morphology (Figure 2.10). Membrane curvature phenomenon could also be observed with lower concentrations of SNAP-GFP, down to 10 μM (Figure 2.11). These results demonstrate that the protein is anchored close enough to the membrane to allow for collective protein behavior to be transmitted to the lipid anchor and result in a dramatic change in membrane curvature.

While this technology offers several opportunities for modifying model phospholipid membranes, there is also tremendous interest in directing proteins to living cellular membranes for applications ranging from live cell imaging, drug delivery, and biochemical studies. Given that the SNAP-tag technology has seen extensive use for live-cell imaging applications, we reasoned that our lipid anchors would be suitable for directing proteins to the membranes of living cells. Cells treated with lipid anchor showed strong surface staining by fluorescently tagged protein, while control cells lacking the lipid anchor showed minor background (Figure 2.12). In this capacity, DSPE-PEG45-BG could be useful in cell signaling or adhesion studies by offering a simple method for membrane tethering of proteins or polypeptides.[58] Unfortunately, due to the charged and relatively large nature of the lipid linker and SNAP-tag protein, studies would be limited to the outer leaflet of the cellular membrane.

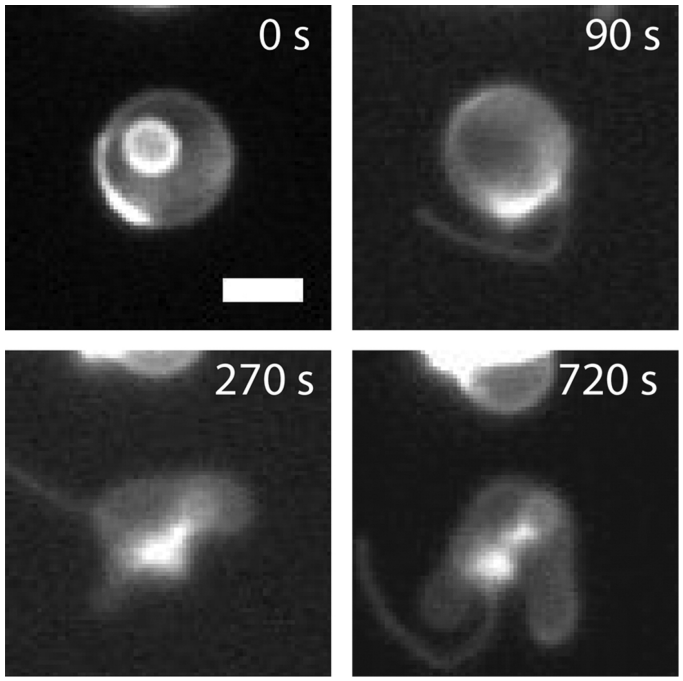

Figure 2.9 Introduction of an excess of SNAP-tag GFP fusion protein to microdomain containing GUVs results in significant membrane deformation.Images show a representative GUV, labeled with 0.1 mol % Texas Red DHPE, undergoing tubulation and blebbing events on the minute time scale. Time noted in seconds after introduction of protein (scale bar 5 μm).

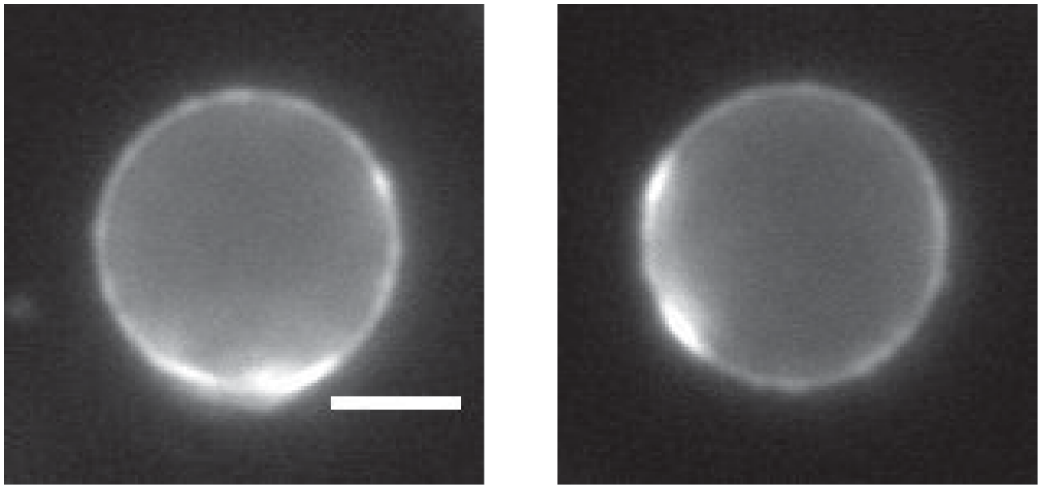

Figure 2.10 A representative 1:2:1.2 DOPC:DPPC:Chol GUV with no DSPE-PEG45-BG exposed to 190 μM SNAP-gfp fusion shows no change in membrane morphology. Left: GUV before SNAP-gfp addition, Right: GUV after 17 min incubation with 190 μM SNAP-gfp. Vesicles labeled with 0.1 mol % Texas Red DHPE (Scale bar 10 μm).

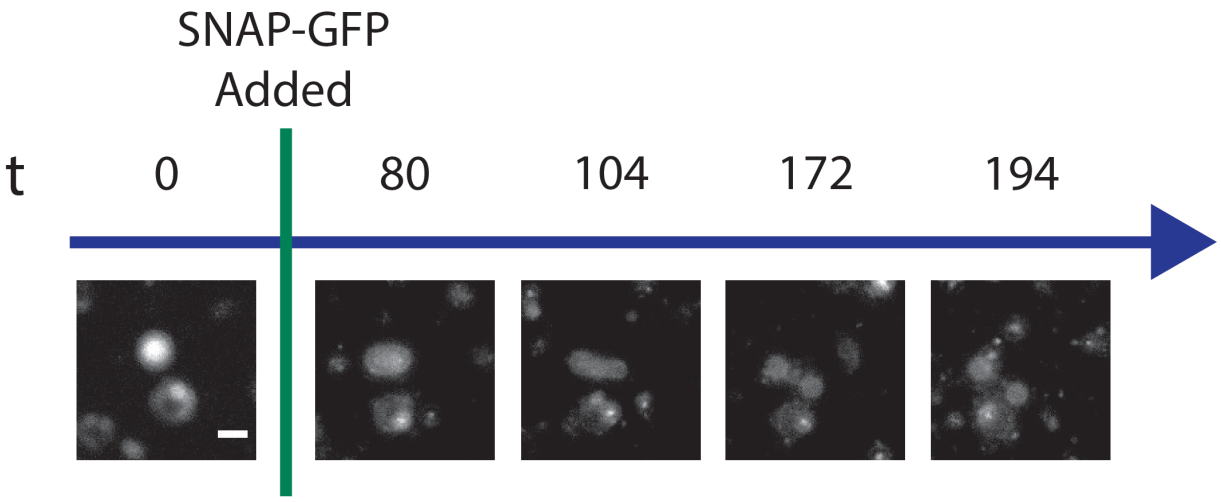

Figure 2.11 Introduction of SNAP-tag GFP fusion protein to 1:2:1.2 DOPC:DPPC:Chol GUVs results in significant membrane deformation even at low concentration. Images show a representative GUV, labeled with 0.1 mol % Texas Red DHPE, undergo tubulation events. Time noted in minutes after introduction of protein to a final concentration of 10 µM (scale bar 10 µm).

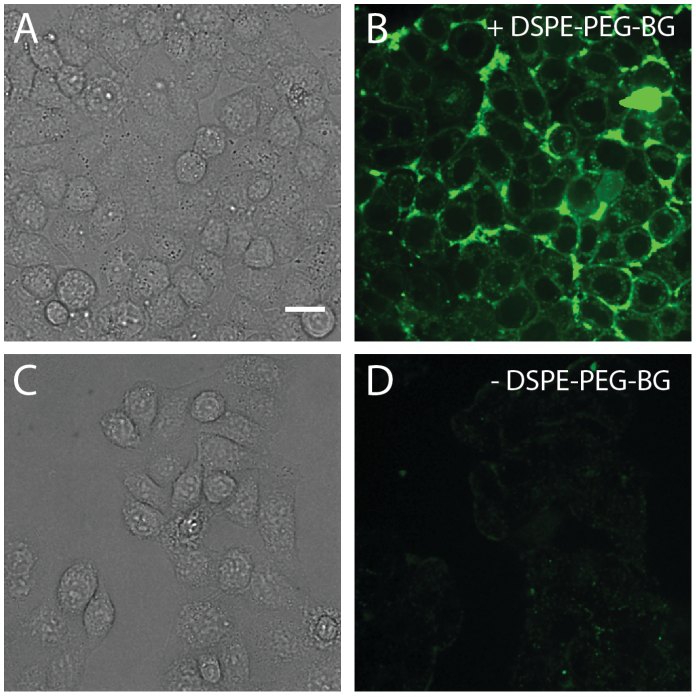

Figure 2.12 Incubation of HeLa cells with DSPE-PEG45-BG results in localization of AlexaFluor 488 labeled SNAP-tag to the cellular membrane. DIC (A) and fluorescent (B) images of cells incubated for 1 hr with DSPE-PEG45-BG. DIC (C) and fluorescent (D) images of cells not incubated with DSPE-PEG45-BG (scale bar 20 µm).

2.6 Conclusion

In summary, we have demonstrated a straightforward and robust method for targeting proteins to phospholipid membranes in a controlled and homogeneous fashion using SNAP- tags. With photocaged lipids, this technique enables light-driven spatiotemporal control over the formation of protein-modified membranes. Additionally, the use of native phospholipids as building blocks suggests that various natural lipids could be used to direct SNAP-tag reactive anchors to defined regions of cells or multiphasic artificial membranes. SNAP-tag reactive lipid anchors serve as a versatile tool for the controlled localization of proteins to phospholipid membranes and may have potential therapeutic, synthetic biology, and cellular biology applications, which we are currently exploring in our laboratory.

2.7 Experimental Methods

2.7.1 Materials

All chemicals and reagents were of reagent grade, obtained from Sigma Aldrich (St. Louis, MO), and used without further purification unless otherwise stated. 2-dioleoyl-sn- glycero-3-phosphocholine (DOPC) and 1,2-distearoyl-*sn*-glycero-3-phosphocholine (DSPC) were purchased from Avanti Polar Lipids, Inc. (Alabaster, AL). N-(Carbonyl- methoxypolyethyleneglycol 2000)-1,2-distearoyl-sn-glycero-3-phosphoethanolamine (NHS-PEG-DSPE) was purchased from NOF America Corp. (White Plains, NY) and mass verified by MS (ESI): m/2z $[M+2H]^+$ calc 1521.5; found 1521.3. Due to the disperse PEG lengths in the compound, several peaks appear 22 mass units apart. Representative peaks corresponding to expected masses are highlighted in mass spectra.

2.7.2 Plasmids

SNAP-tag GFP fusion plasmid was purchased from Addgene (Plasmid 46846: pIVEX-SNAP-GFP, deposited by Florian Hollfelder) and stored as an *E. coli* glycerol stock at -80º C. A miniprep was performed using AccuPrep Plasmid Mini Extraction Kit (Bioneer, Alameda, CA) and the recovered DNA stored in water at 4º C. SNAP-tag_EGFP_Hisx6 fusion plasmid was constructed using standard molecular biology techniques. sfEGFP plasmid was generously provided by Simpson Joseph (University of California San Diego) and used without further purification.

2.7.3 Protein Purification

BL21 competent *E. coli* cells (Agilent Technologies, Santa Clara, CA) were transformed with SNAP-tag_EGFP_Hisx6 plasmid per the manufacturers protocol. Cells were grown in a 1 L culture at 37º C with constant shaking and induced with 1 mM IPTG once the culture reached 0.6 O.D. After induction, the culture was grown for 4 additional hrs after which *E. coli* were pelleted and stored at 4 oC until purification. His-tag purification was performed by the manufacturer's specifications using Ni-NTA resin (Thermo, Rockford, IL). Purified protein was exchanged into 1xPBS with 1 mM DTT using a 10 kDa molecular weight cutoff microcentrifuge filter and stored at -80º C. Final protein concentration was determined via UV-vis analysis.

2.7.4 Cell Free Expression System

S30 T7 High-Yield Protein Expression System was purchased from Promega (Madison, WI) and reactions were performed per the manufacturer's instructions. Reactions contained 20 μL of S30 premix, 18 μL S30 T7 extract, 1 μg plasmid DNA, with the addition of sucrose to a final concentration of 200 mM and Cy5 azide to a final concentration of 1 mM.

2.7.5 Fluorescent Labeling of SNAP-tag protein

(15 μL, 0.75 nmol) SNAP-tag purified protein solution (New England Biolabs, Ipswich, MA) was washed with 100 mM $NaHCO_3$ pH 8.3 four times by spinning in a 10 kDa molecular weight cutoff microcentrifuge filter (EMD Millipore, Darmstadt, Germany). To the remaining $NaHCO_3$ protein solution was added (0.94 μL, 0.75 nmol) AlexaFluor 488 NHS ester (Life Technologies, Grand Island, NY). This solution was reacted at RT with shaking for 1 hr after which it was washed four times with 1x PBS containing 1 mM DTT using a 10 kDa molecular weight cutoff microcentrifuge filter. This procedure yielded 50 μL of protein solution. UV-Vis analysis of the protein sample showed the concentration of SNAP-tag to be 2 μM and confirmed that AlexaFluor 488 had been attached in a 1:1 molar ratio with SNAP-tag.

2.7.6 General Procedure for External Binding of SNAP-tag Protein to Vesicles

DOPC or 20:1 DOPC:Lipid Anchor **1, 6, 7, 9 or 11** lipid mixtures were prepared from chloroform stocks. Lipid solutions were dried into a film under nitrogen and then a volume of heavy mineral oil (Fisher Scientific, Waltham, MA) was added to yield a 5 mg/mL solution of lipid in oil. This solution was capped under nitrogen and sonicated in a bath sonicator for 1 hr at RT. 10 μL of 200 mM sucrose, 1x PBS pH 7.5 was added to the oil and the mixture was agitated violently to emulsify. The resultant oil-in-water emulsion was layered on top of a solution of 200 mM glucose, 1x PBS pH 7.5 and centrifuged for 10 min (RT, 10,000 rcf). The oil layer was removed by aspiration, leaving the vesicle containing aqueous layer. 39 μL vesicle solution, 1 μL 50 mM DTT and 10 μL of 2 μM AlexaFluor 488 labeled SNAP-tag protein solution were combined and incubated at 37º C for 1 hr. If applicable, the mixture was transferred to a quartz cuvette and exposed to 360 nm UV light in a photochemical reactor for 10 min (Southern New England

Ultraviolet Company, Brandford, CT). The mixture was removed from the cuvette and incubated for an additional 1 hr at 37º C before imaging.

2.7.7 Spatially Controlled Binding of SNAP-tag Protein to Vesicles

For the localization of protein to one vesicle 20:1 DOPC:Lipid Anchor **6** lipid mixture was prepared from chloroform stocks. The lipid solution was dried into a film under nitrogen and then a volume of heavy mineral oil (Fisher Scientific, Waltham, MA) was added to yield a 1 mg/mL solution of lipid in oil. This solution was capped under nitrogen and sonicated in a bath sonicator for 1 hr at RT. 10 μL of 200 mM sucrose, 1x PBS pH 7.5 was added to the oil and the mixture was agitated violently to emulsify. The resultant oil-in-water emulsion was layered on top of a solution of 200 mM glucose, 1x PBS pH 7.5 and centrifuged for 10 min (RT, 10,000 rcf). The oil layer was removed by aspiration, leaving the vesicle containing aqueous layer. 39 μL vesicle solution, 1 μL 50 mM DTT and 10 μL of 2 μM AlexaFluor 488 labeled SNAP-tag protein solution were combined and a small volume prepared on a glass slide for laser scanning microscopy.

Images were acquired on a LSM 780 built around an Axio Observer Z1 motorized inverted microscope (Carl Zeiss Microscopy GmbH, Germany) with a 40x, 1.20 NA water immersion objective using ZEN imaging software (Carl Zeiss Microscopy GmbH, Germany). Fluorophores were excited with a 458 nm, 25 mW Argon Laser, green. NPE groups were removed from selected vesicles in the image frame by scanning a circular region around the vesicle 10 times in 10 z-planes (1.93 μm apart) with a pixel dwell time of 12.6 μs using a 405 nm, 30 mW Diode at 100% power (total exposure time 4.5 sec).

For the localization of protein to one portion of a vesicle a 20:1 mixture of DPPC:Lipid Anchor **6** was prepared from chloroform stocks. The total lipid concentration was brought to 2 mM in a volume of 100 µL chloroform and 10 µL methanol. The solution was placed in a 1 dram glass vial and topped with 700 µL 1xPBS. Organic solvent was removed via rotary evaporation at 50 oC to yield a slightly turbid solution of vesicles in buffer. 5 µL of vesicle solution, 1 µL 50 mM DTT and 4 µL 570 µM SNAP- tag_EGFP_Hisx6 fusion protein in 1xPBS were mixed and a small volume prepared on a glass slide for laser scanning microscopy.

Images were acquired on a LSM 780 built around an Axio Observer Z1 motorized inverted microscope (Carl Zeiss Microscopy GmbH, Germany) with a 63x, 1.40 NA oil immersion objective using ZEN imaging software (Carl Zeiss Microscopy GmbH, Germany). Fluorophores were excited with a 458 nm, 25 mW Argon Laser, green. NPE groups were removed from selected vesicles in the image frame by scanning a circular region on one side of the vesicle 10 times with a pixel dwell time of 3.0 µs (total exposure time 2 sec) using a 405 nm, 30 mW Diode at 100% power.

2.7.8 General Procedure for Encapsulation of Cell Free Expression System

DOPC or 20:1 DOPC:Lipid Anchor **1** lipid mixtures were prepared from chloroform stocks. Lipid solutions were dried into a film under nitrogen and then a volume of heavy mineral oil (Fisher Scientific, Waltham, MA) was added to yield a 5 mg/mL solution of lipid in oil. This solution was capped under nitrogen and sonicated in a bath sonicator for 1 hr at RT. 10 µL of cell free expression reaction was added to the oil and the mixture was agitated violently to emulsify. The resultant oil-in-water emulsion was layered on top of a solution of 200 mM Glucose, 300 mM HEPES pH 7.5

and centrifuged for 10 min (RT, 10,000 rcf). The oil layer was removed by aspiration and the vesicle containing aqueous layer was imaged.

2.7.9 Procedure for electroformation of GUV's

For microdomain binding experiments a 5 mM lipid mixture of 1:1:1 DOPC:DSPC:Chol with 0.1% Texas Red DHPE (Life technologies, Eugene, OR) with or without 5% DSPE-PEG45-BG **1** was prepared in chloroform. 20 µl of lipid solution was placed on the conductive side of an ITO coated slide and dried *in vacuo* for 30 min. An O-ring sealed with vacuum grease was placed around the dry lipid film and 250 µL of 150 mM Sucrose was added to the center of the O-ring. The ITO slide was placed in the vesicle prep pro and the conductive side of a second ITO slide was placed above facing the solution such that the conductive sides of the ITO slides touched the conductive pads. The vesicles were electroformed with the following parameters; Frequency 5 Hz, Amplitude 3 V, Temp. 36 oC, Rise 3 min, Main 120 min, Fall 5 min. Indium-tin oxide (ITO) slides, O-ring and *vesicle prep pro*® all supplied by (Nanion Technologies, North Brunswick, NJ). For membrane deformation experiments a 5 mM lipid mixture of 1:2:1.2 DOPC:DPPC:Chol with 0.1 % Texas Red DHPE with or without 5% DSPE-PEG45-BG **1** was prepared in chloroform and vesicles formed as above.

2.7.10 Fluorescent labeling of Bovine Serum Albumin (BSA)

A 45 µM stock solution of Bovine Serum Albumin (EMD chemicals, Inc., San Diego, CA) was prepared in 10 mL of $NaHCO_3$ pH 8.3. 0.6 µL of AlexaFluor488-NHS (0.8 mM) was added and the solution incubated at RT with shaking for 1 hr. Solution was washed four times with 1x PBS containing 1 mM DTT using a 10 kDa molecular weight cutoff microcentrifuge filter. Labeled protein was used immediately.

2.7.11 Microdomain SNAP-tag Binding

After electroformation, 39 μL of vesicle solution was added to a 0.6 mL eppendorf tube along with 1 μL of freshly prepared 50 mM DTT and 10 μL of 2 μM AlexaFluor 488 labeled SNAP-tag solution and reaction performed for 1 hr at 37 oC. As DSPE-PEG45- BG **1** is structurally similar to phospholipid dyes used in past studies,[46] it would be expected to partition into less ordered membrane microdomains. Indeed, our results indicate that exposure of mixed phospholipid vesicles to fluorescent SNAP-tag protein results in specific labeling of the less ordered lipid domains, by colocalization with the fluorescent lipid Texas Red DHPE. Notably, the labeled vesicle microdomains retained the ability to rapidly diffuse within the membrane. Experiments performed in the absence of DSPE-PEG-BG **1** resulted in no SNAP-tag binding to vesicles.

2.7.12 Membrane Curvature Experiments

After electroformation, 1 μL of vesicle solution was diluted in 48 μL 1xPBS and 1 μL 50 mM DTT. 10 μL of the diluted solution was transferred to a 384 glass bottom well plate. While imaging, 5 μL of 570 μM (Figure 4) or 5 μL of 30 μM (Figure S7) SNAP- tag_EGFP_Hisx6 was added and images taken every 10 sec (Figure 4) or 2 min (Figure S9) for the duration of the experiment.

2.7.13 Live-Cell SNAP-tag Binding

HeLa cells were grown overnight on a LabTek chamber slide (Thermo, Rockford, IL) maintained in McCoy's 5A, 1X (Iwakata & Grace Mod.) with L-glutamine (10% fetal bovine serum and 1% penicillin/streptomycin). Cells were washed with McCoy's 5A without serum and antibiotics and then incubated in that same media containing 50 mM DSPE-PEG-BG **1** for 1 hr at 37 oC. Cells were washed again with McCoy's 5A without serum and antibiotics and incubated in that same media containing 70 nM AlexaFluor 488 labeled SNAP-tag for 20 min at 37 oC. Cells were washed with additional McCoy's 5A without serum and antibiotics before imaging.

2.7.14 Epifluorescence Microscopy

All Images, unless otherwise indicated, were acquired on a Yokagawa spinning disk system (Yokagawa, Japan) built around an Axio Observer Z1 motorized inverted microscope (Carl Zeiss Microscopy GmbH, Germany) with a 40x, 1.40 NA oil immersion objective to an Evolve 512x512 EMCCD camera (Photometrics, Canada) using ZEN imaging software (Carl Zeiss Microscopy GmbH, Germany). Fluorophores were excited with a 405 nm, 50 mW DPSS laser, blue; 635 nm, 30 mw DPSS laser, far red; and 488 nm, 100 mW OPSL laser, green.

Images of microdomains and membrane deformation were acquired on an Axio Observer D1 inverted microscope (Carl Zeiss Microscopy GmbH, Germany) with a 40x, 0.6 NA air immersion objective to and ORCA-ER camera (Hamamatsu, Japan) using Micro-manager 7.4.12 software.[59] Fluorophores were excited with a HXP 120 metal halide arc lamp (Carl Zeiss Microscopy GmbH, Germany).

2.7.15 Verification of SNAP-tag reaction with DSPE-PEG-BG 1

Purified SNAP-tag protein (20 μg, 1.02 nmol) (New England Biolabs, Ipswich, MA) was dissolved in 200 μL buffer (50 mM Tris-HCl, 100 mM NaCl, 1 mM DTT, pH 7.5), with or without **1** (0.33 mg, 102 nmol). The reaction shaken at 37 oC overnight after which the reaction solution was concentrated to 50 μL by centrifugation in a 10 kDa molecular weight cutoff microcentrifuge filter (Millipore, Billerica, MA). Samples were loaded with laemmli buffer (Bio Rad, Hercules, CA) onto a 15% SDS-PAGE gel. The gel was stained with coomassie brilliant blue (Bio Rad, Hercules, CA) and imaged (Figure S2).

2.7.16 Photouncaging of Compound 6

1-(2-nitrophenyl)ethyl derivatives that carry a leaving group at the benzylic position release the protected group when irradiated. This reaction proceeds via aci- nitro intermediates that are observable by flash photolysis at λmax≈400 nm.[60] This behavior has been demonstrated via exposure to a 100W Hg lamp with an emission maximum of 365 nm[48] and by irradiation with a 405 nm laser source.[61,62] In order to verify the efficacy of benzylguanine uncaging, we performed MS analysis of compound **6** before and after 10 min exposure to 360 nm light in a photochemical reactor using 8 360 nm bulbs (Southern New England Ultraviolet Company, Brandford, CT). **6** was dissolved in MeOH at 2.5 mg/mL and analyzed via MS. MS (ESI) calc 1673.1; found 1673.5. The solution was then exposed to UV light in a quartz cuvette and analyzed again by MS. MS (ESI) m/2z $[M+2H]^+$ calc 1598.6; found 1598.4. Due to the disperse PEG lengths in the compound, several peaks appear 22 mass units apart. Representative peaks corresponding to expected masses are highlighted (S40-41).

Additionally, we determined the kinetics of compound **6** uncaging in vesicles. LUVs containing 20% **6** were synthesized using a well-established extrusion method. DOPC (1.53 μmol) and **6** (3.8 μmol) were added to a glass vial as chloroform solutions. A lipid film was formed by rotating the vial under a stream of N_2 and dried for an additional 10 min under N_2. 1 mL of PBS (pH 7.4) was added to the vial and it was mixed end-over-end for 1 hr at RT. The solution was then vortexed and submitted to 10 freeze/thaw cycles using a dry ice/ethanol bath and a warm water bath (vortexing between each cycle). The vesicle solution was then extruded 10 times through a 200 nm polycarbonate membrane (GE Healthcare, Pittsburgh, PA) using an Avanti Mini Extruder (Avanti Polar Lipids, Alabaster, AL). The vesicle solution was then added to a quartz cuvette, sealed with a stopper and parafilm and exposed to 360 nm light using a photochemical reactor. 20

μL of solution was removed at set time points and aliquots submitted to analysis by reverse-phase HPLC. The formation of the 1-nitro-2- ethylbenzene product was monitored by absorbance at 280 nm and relative concentration determined by integration of the elution peak. Absorbance values were plotted relative to time using GraphPad Prism software and the corresponding data fit calculated ($k = 0.00868\ M^{-1}s^{-1}$, $t_{1/2} = 79.9$ s).

2.7.17 Synthesis of DSPE-PEG45-BG (1)

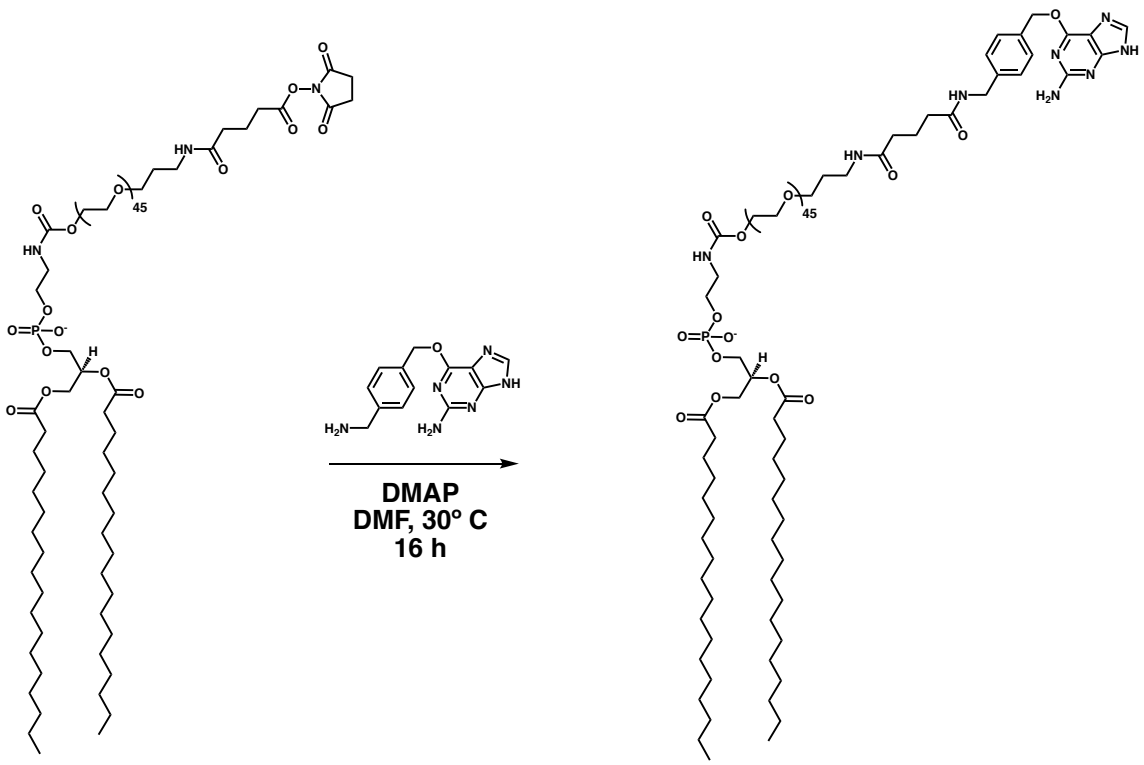

Scheme 2.1 Synthesis of DSPE-PEG45-BG (**1**)

6-((4-(aminomethyl)benzyl)oxy)-7*H*-purin-2-amine (1.6 mg, 6.1 µmol) and DMAP (1.0 mg, 8.1 µmol) were dissolved in 250 µL anhydrous DMF. DSPE-PEG-NHS (10 mg, 3.3 µmol) was dissolved in 250 µL dry DMF. The solutions were combined and triethylamine (0.69 µL, 5.0 µmol) was added. The reaction was heated to 30 ºC and stirred for 16 hrs. After cooling, the solvent was evaporated the resulting orange solid dissolved in 100 µL of MeOH. The solution was purified by preparatory reverse-phase HPLC, eluted with H_2O/MeOH containing 0.1% formic acid to yield compound **1** as a colorless solid (6.2 mg, 58%). ^{1}H NMR (500 MHz, $CDCl_3$): δ7.92 (bs, 1H), 7.50 (bs, 1H), 7.30 (d, 2H), 7.24 (d, 2H), 7.03 (bs, 1H), 6.30 (bs, 1H), 5.45 (bs, 2H), 5.20 (bs, 1H), 4.41-4.30 (m), 4.20-3.96 (m), 3.38 (m, 2H), 3.28 (m, 2H), 2.28 (m, 6H), 2.20 (m, 2H), 1.91 (m, 2H), 1.73 (m, 2H), 1.56 (m, 4H), 1.22 (m, 56H), 0.85 (t, 6H). ^{13}C NMR (125 MHz, $CDCl_3$): δ173.7,

173.6, 173.4, 173.3, 160.6, 156.7, 155.2, 139.8, 133.3, 128.9, 128.0, 70.7, 65.8, 64.5, 63.9, 62.4, 51.1, 43.2, 41.9, 37.9, 35.5, 34.4, 34.3, 32.1, 29.9, 29.8, 29.6, 29.3, 29.0, 25.1, 22.9, 22.3, 14.4. MS (ESI) m/2z $[M-2H]^-$ calc 1597.06; found 1597.65. HPLC (ELSD) Eclipse Plus C8 4.6 x 50mm 3.5 µm / H_2O:MeOH / 0-15min 5%-95% MeOH, 15-22min 95% MeOH.

2.7.18 Synthesis of 1-(1-bromoethyl)-2-nitrobenzene (2)

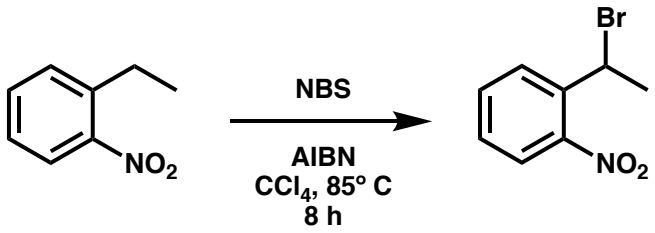

Scheme 2.2 Synthesis of 1-(1-bromoethyl)-2-nitrobenzene (**2**)

Adapting a previous protocol,[63] 1-ethyl-2-nitrobenzene (1.0 g, 8.3 mmol) and N-bromosuccinimide (1.3 g, 7.3 mmol) were dissolved in 3.5 mL CCl_4. AIBN (11.3 mg, 68.8 µmol) was added to the solution and it was stirred under N_2 at 85 ºC for 8 hrs. After cooling, insoluble products were filtered and the filtrate concentrated *in vacuo.* The concentrated filtrate was diluted in 20 mL of ethyl acetate and washed with water and brine. Solvent was removed under reduced pressure and purified by flash column chromatography. Yield: 601.8 mg (3.0 mmol, 36%) as a brown liquid. ^{1}H NMR (500 MHz, $CDCl_3$): δ 7.88 (dd, J= 8.0,1.3, 1H), 7.83 (dd, J= 8.3, 1.3, 1H), 7.64 (t, J= 7.6, 1H), 7.43(t, J=7.7, 1H), 5.80 (q, J= 6.9, 1H), 2.08 (d, J= 6.9, 1H). ^{13}C NMR (125MHz, $CDCl_3$): δ 147.4, 137.8, 133.6, 130.0, 129.1, 124.5, 42.0, 27.3. HPLC (A280) Eclipse Plus C8 4.6 x 50mm 3.5 µm / H_2O:MeOH / 0-15min 5%-95% MeOH, 15-18min 95% MeOH.

2.7.19 Synthesis of BG-Boc (3)

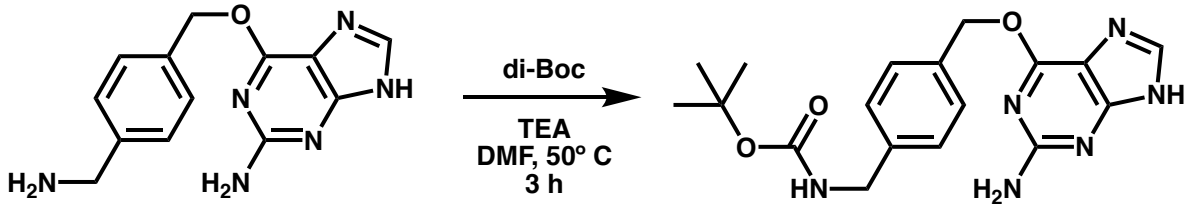

Scheme 2.3 Synthesis of BG-Boc (**3**)

6-((4-(aminomethyl)benzyl)oxy)-7*H*-purin-2-amine (53.9 mg, 199 µmol) was suspended in 10 mL anhydrous DMF with the addition of TEA (77 µL, 555 µmol) and stirred at 50 ºC for 5 min before adding di-*tert*-butyl dicarbonate (49.4 mg, 226 µmol). The reaction was stirred at 50 ºC for 3 hr and then solvent was removed *in vacuo* and residue dissolved in a minimal amount of DCM. The solution was added to an excess of water and 1 M HCL added dropwise until a precipitate formed. Precipitate was recovered via vacuum filtration. Yield: 45.8 mg (123 µmol, 62%) as a colorless solid. MS (ESI) m/z: $[M+H^+]$ calc 371.2; found 370.9. ^{1}H NMR (500 MHz, $(CD_3)_2SO$): δ12.41(s, 1H), 7.80 (s, 1H), 7.43 (d, J=7.9, 2H), 7.24 (d, J=7.9, 2H), 6.29(s, 2H), 5.45 (s, 2H), 4.13 (d, J=6.0, 2H), 1.39 (s, 9H). ^{13}C NMR (125 MHz, $(CD_3)_2SO$): δ 159.9, 158.6, 155.8, 155.2, 140.0, 137.8, 135.1, 128.5, 126.9, 113.5, 77.8, 67.5, 43.2, 28.3, 26.9. HPLC (ELSD) Eclipse Plus C8 4.6 x 50mm 3.5 µm / H_2O:MeOH / 0-15min 5%-95% MeOH, 15-18min 95% MeOH

2.7.20 Synthesis of ^{N7}NPE-BG-Boc (4) and ^{N9}NPE-BG-Boc (5)

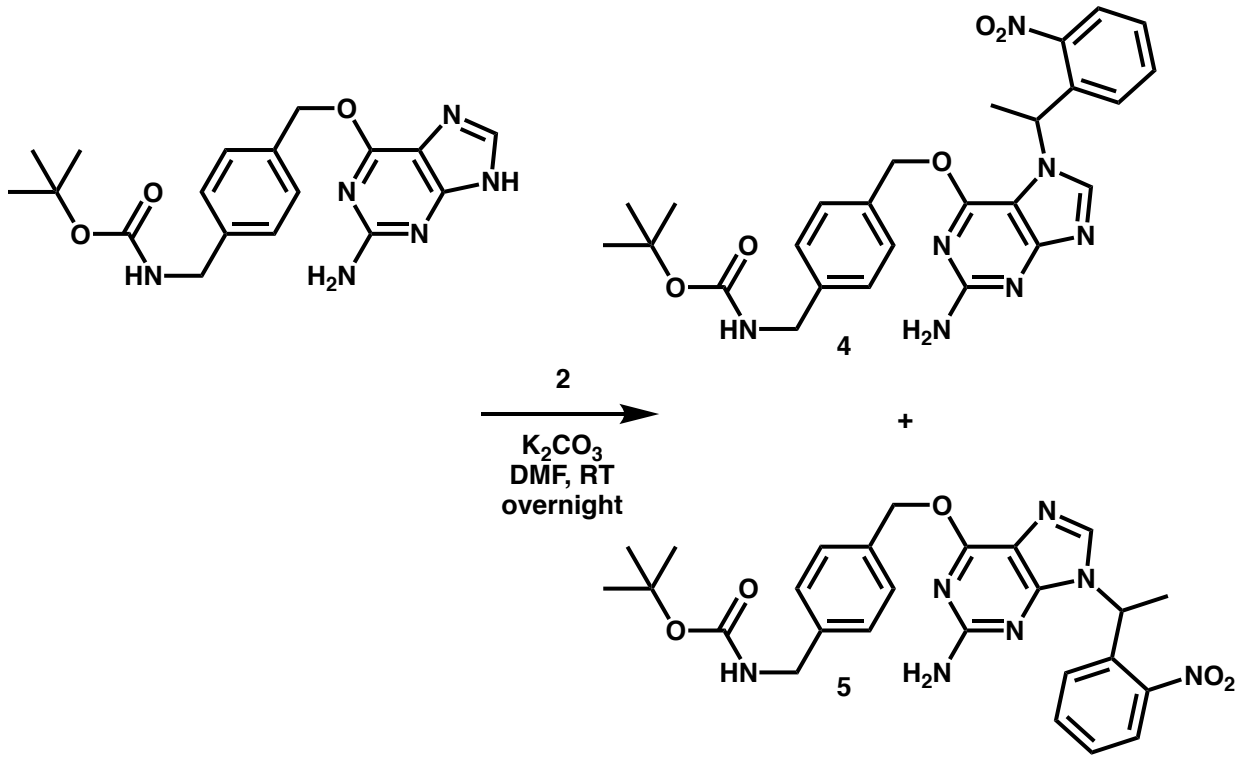

Scheme 2.4 Synthesis of ^{N7}NPE-BG-Boc (**4**) and ^{N9}NPE-BG-Boc (**5**)

Adapting a previous protocol,[63] (**3**) (45.8 mg, 124 µmol) and K_2CO_3 (52.3 mg, 378 µmol) were dissolved in 200 µL anhydrous DMF. 1-(bromoethyl)-2-nitrobenzene (**2**) (73.0 mg, 379 µmol) was dissolved in 100 µL anhydrous DMF before adding to the reaction and stirring under N_2 overnight. Insoluble material was filtered out and solvent was removed *in vacuo.* The resulting residue was dissolved in 3 mL DCM and extracted 3x with 3 mL water. The DCM fraction was concentrated *in vacuo* and separated via flash chromatography with 20:1 DCM:MeOH as the mobile phase. Eluted fractions of the same isomer were combined and solvent removed *in vacuo.* ^{N7}NPE-BG-Boc (4) Yield: 9.1 mg (17.4 µmols, 14.1 %) as a colorless solid, ^{N9}NPE-BG-Boc (5) Yield: 6.7 mg (12.9 µmols, 10.4%) as a colorless solid.

*^{N7}NPE-BG-Boc (**4**)*

MS (ESI) m/z: [M+H$^+$] calc 520.2; found 520.2. ^{1}H NMR (500 MHz, CD_3OD): δ 8.46 (s, 1H), 7.92 (d, J= 8.1, 1H), 7.55 (t, J= 7.5, 1H), 7.45 (t, J=8,1H), 7.15 (d, J=8.1, 2H), 7.09 (d, J=7.9, 2H), 6.98 (d, J=7.6, 1H), 6.38 (q, J= 7.0, 1H) 5.33 (d, J= 12.1, 1H), 5.26 (dd, J=12.1, 22.0 1H), 4.20 (s, 2H), 2.04 (d, J= 7.0, 3H), 1.46 and 1.24(rotameric, 9H). ^{13}C NMR (500 MHz, CD_3OD): δ 164.6, 161.7, 158.6, 149.3, 144.4, 141.1, 138.9, 138.6,136.2, 135.4, 130.6, 130.5, 130.2, 130.0, 128.2, 128.1, 126.3, 125.5, 107.7, 80.4, 68.5, 55.1, 42.7, 28.9 and 27.1(rotameric $C(CH_3)_3$), 21.2. HPLC (ELSD) Eclipse Plus C8 4.6 x 50mm 3.5 µm / H_2O:MeOH / 0-15min 5%-95% MeOH, 15-18min 95% MeOH.

*^{N9}NPE-BG-Boc (**5**)*

MS (ESI) m/z [M+H$^+$] calc 520.2; found 520.2. ^{1}H NMR (500 MHz, CD_3OD): δ 8.14 (s, 1H), 8.02 (d, J= 8.2, 1H), 7.63 (t, J= 7.9, 1H), 7.51 (t, J= 8.0, 1H), 7.46 (d, J= 7.6, 2H), 7.37 (d, J= 7.9, 1H), 7.28 (d, J= 7.8, 2H), 6.29 (q, J= 7.1, 1H), 5.49(s, 2H), 4.22 (s, 2H), 2.04 (d, J= 7.1, 3H), 1.43 (s, 9H). ^{13}C NMR (125 MHz, CD_3OD): δ 160.5, 160.2, 153.6, 148.3, 139.5, 137.8, 135.2, 133.6, 128.2, 127.5, 126.8, 124.6, 113.9, 78.8, 67.3, 49.8, 43.3, 27.3, 19.2. HPLC (ELSD) Eclipse Plus C8 4.6 x 50mm 3.5 µm / H_2O:MeOH / 0-15min 5%-95% MeOH, 15-18min 95% MeOH.

2.7.21 Synthesis of DSPE-PEG45-BG-NPE (6)

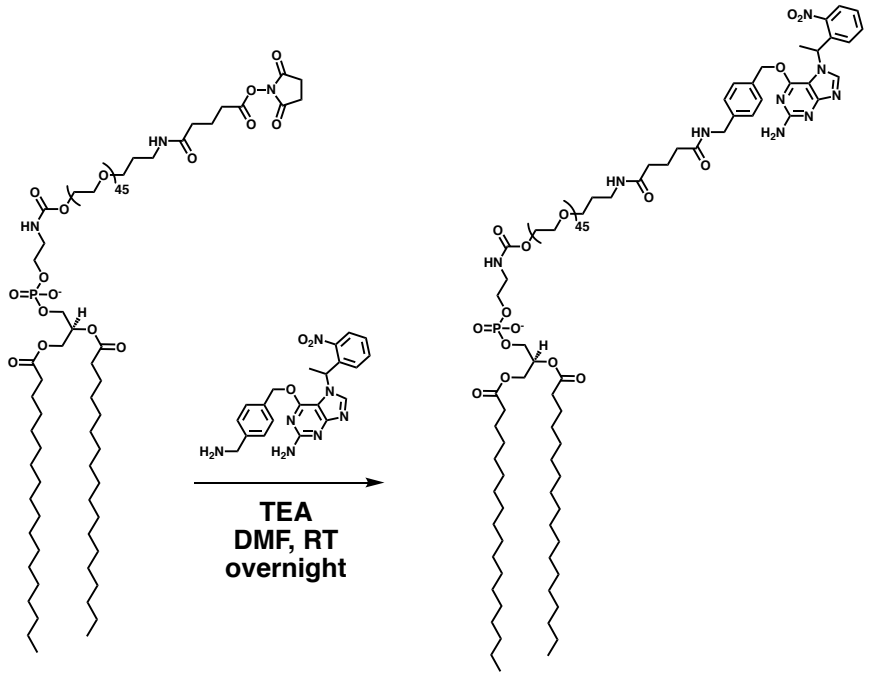

Scheme 2.5 Synthesis of DSPE-PEG45-BG-NPE (**6**)

(**4**) (1.5 mg, 2.9 µmol) was dissolved in 1mL of trifluoroacetic acid and stirred for 30 min. Compound **4** was utilized in binding experiments because of previous work showing its superior inertness to SNAP-tag.[63] Reaction completion was verified by MS and a quantitative yield assumed. Solvent and reaction byproducts were removed *in vacuo* to yield a colorless solid. This solid was dissolved in 100 µL anhydrous DMF before adding triethylamine (1.4µL, 100 µmol). This solution was stirred for 5 min and then NHS-PEG-DSPE (5.0 mg, 17 µmol) dissolved in 200 µL anhydrous DMF was added and the reaction stirred overnight at RT. After reaction, solvent was removed *in vacuo* and the residue dissolved in 100 µL MeOH and purified by preparatory reverse-phase HPLC, eluted with H_2O/MeOH containing 0.1% formic acid to yield compound **6** as a colorless solid. Yield: 4.5 mg (1.3 µmol, 81 %). ^{1}H NMR (500 MHz, CD_3OD): δ8.26 (bs, 1H), 7.96 (s, 1H), 7.58 (bs, 1H), 7.50 (bs, 1H), 7.07 (m, 2H), 6.86 (s, 1H), 6.74 (s, 1H), 6.43 (s, 1H),

5.84 (m, 2H), 5.34 (dd, J = 11.2, 24.5, 2H), 4.51-3.43 (m), 3.42 (m, 2H), 3.37 (m, 2H), 2.50-1.68 (m), 1.57 (m, 4H), 1.23 (m, 56H), 0.86 (t, 6H). ^{13}C NMR (125 MHz, CD_3OD): δ173.3, 172.9, 145.7, 133.3, 70.6, 69.5, 66.5, 64.0, 61.9, 38.6, 35.2, 34.2, 34.0, 33.0, 31.9, 29.7, 29.4, 29.3, 29.2, 29.1, 28.6, 24.9, 22.7, 14.1. MS (ESI) m/2z $[M+2H]^+$ calc 1673.1; found 1673.5. HPLC (ELSD) Eclipse Plus C8 4.6 x 50mm 3.5 µm / H_2O:MeOH / 0-15min 5%-95% MeOH, 15-18min 95% MeOH.

2.7.22 Synthesis of DOPE-BG (7)

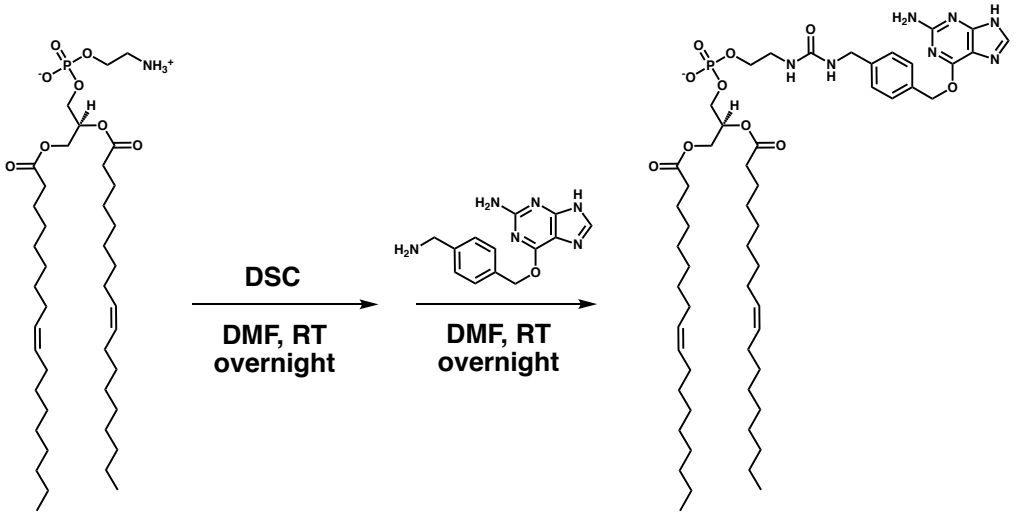

Scheme 2.6 Synthesis of DOPE-BG (**7**)

DOPE (18.1 mg, 24.3 µmol) and *N,N′*-disuccinimidyl carbonate (6.9 mg, 26.8 µmol) were dissolved in 1 mL anhydrous DMF. TEA (7 µL, 50.2 µmol) was added to the solution before stirring under N_2 at RT overnight. Reaction completion was verified by TLC and then 6-((4-(aminomethyl)benzyl)oxy)-7*H*-purin-2-amine (12.5 mg, 46.3 µmol) was added to the reaction before stirring under N_2 at RT overnight. Solvent was removed *in vacuo* and the resulting solid dissolved in 500 µL of MeOH. The solution was purified by preparatory reverse-phase HPLC, eluted with H_2O/MeOH containing 0.1% formic acid to yield compound 7 as a colorless solid. Yield: 7 mg (6.7 µmol, 28%). 1H NMR (500 MHz, CDCl3): δ 8.06 (s, 1H), 7.35 (m, 4H), 7.04 (bs, 1H), 6.35 (bs, 2H), 5.35 (s, 4H), 5.26 (m, 1 H), 4.40 (m, 2H), 4.19 (m, 2H), 4.08 (m, 4H), 3.62 (s, 1H), 3.54 (bs, 1H), 2.30 (m, 4H), 1.98 (m, 8H), 1.57 (m, 4H), 1.35-1.15 (m, 40H), 0.85 (t, J= 7.2, 6H). 13C NMR (125 MHz, CDCl3): δ173.5, 173.2, 163.5, 160.4, 158.5, 158.0, 154.4, 152.6, 152.0, 142.3, 137.5, 130.9, 130.5, 130.0, 129.7, 127.8, 105.9, 70.0, 64.0, 62.4, 31.9, 29.7, 29.3, 29.1, 27.2, 24.9, 22.7, 14.2. MS (ESI) m/z [M-H]- calc 1038.64; found 1038.92. HPLC (ELSD)

Eclipse Plus C8 4.6 x 50mm 3.5 µm / H2O:MeOH / 0-15min 5%-95% MeOH, 15-22min 95% MeOH.

2.7.23 Synthesis of DOPE-PEG7-PFP (8)

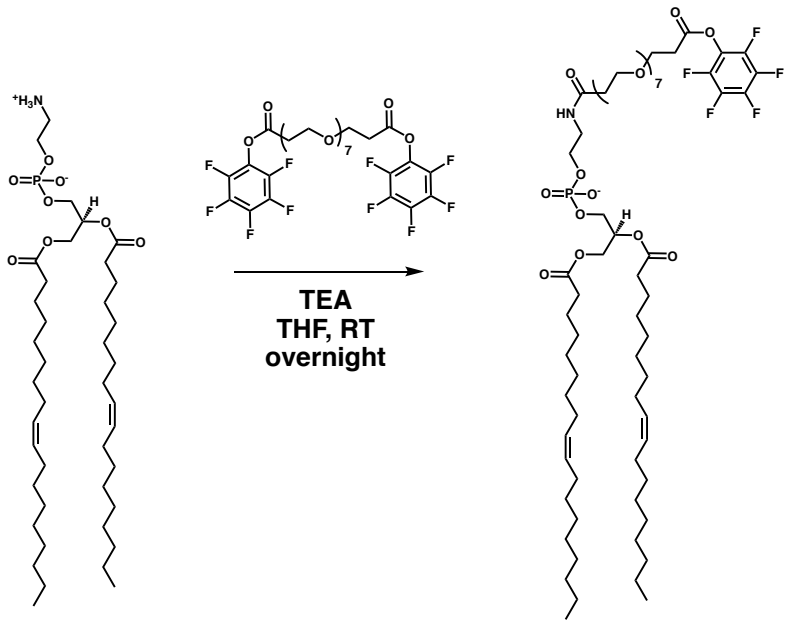

Scheme 2.7 Synthesis of DOPE-PEG7-PFP (**8**)

DOPE (4.3 mg, 5.8 µmol) and PEG7 Bis-PFP Ester (Conju-Probe, San Diego, CA) (20.0 mg, 26.4 µmol) were dissolved in 0.5 mL anhydrous THF. TEA (2.3 µL, 16.1 µmol) was added and the solution stirred at RT overnight. Solvent was removed *in vacuo* and the residue dissolved in a minimal volume of DCM. The DCM solution was loaded onto a prep-TLC plate (.25mm x 20cm x 20cm, EMD Millipore, Darmstadt, Germany) and developed with 10:1 DCM:MeOH. The product band was collected and washed with 10:1 DCM:MeOH and solvent removed *in vacuo.* Yield: 3.5 mg (2.7 µmol, 50%) as a colorless solid. ^{1}H NMR (500 MHz, $CDCl_3$): δ5.31 (m, 4H), 5.18 (bs, 1H), 4.35 (m, 1H), 4.12 (m, 1H), 3.93 (m, 4H), 3.85 (t, J = 6.2, 2H), 3.79-3.53 (m, 26H), 3.42 (bs, 2H), 2.92 (m, 2H), 2.49 (m, 2H), 2.24 (q, J = 7.2, 4H), 1.98 (m, 8H), 1.55 (m, 4H), 1.24

(m, 40H), 0.85 (t, 6H). ^{13}C NMR (125 MHz, $CDCl_3$): δ173.6, 173.2, 167.7, 142.2, 140.7, 140.3, 139.0, 138.7, 137.0, 130.2, 129.9, 70.8, 70.5, 70.2, 67.8, 66.2, 64.5, 63.8, 62.9, 34.6, 34.5, 34.3, 32.1, 31.2, 29.7, 29.5, 29.4, 27.4, 25.1, 22.9, 14.3. MS (ESI) m/z $[M+Na]^+$ calc 1340.72; found 1340.61

2.7.24 Synthesis of DOPE-PEG7-BG (9)

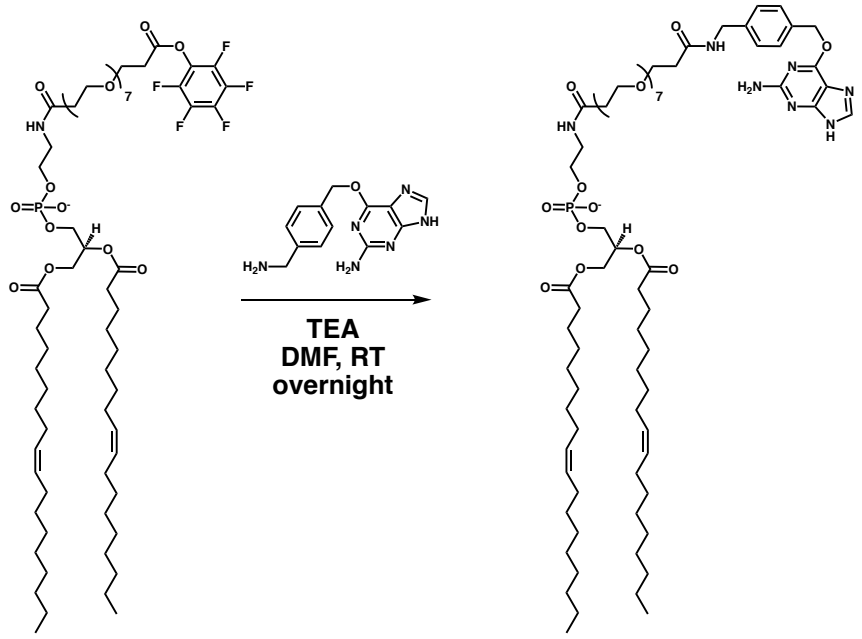

Scheme 2.8 Synthesis of DOPE-PEG7-BG (**9**)

Compound **8** (3.5 mg, 2.7 µmol) and 6-((4-(aminomethyl)benzyl)oxy)-7*H*-purin-2-amine (2.5 mg, 9.3 µmol) were dissolved in 0.5 mL anhydrous DMF. TEA (1.1µL, 8.0 µmol) was added and the solution stirred at RT overnight. Solvent was removed *in vacuo* and the residue dissolved in MeOH. The solution was purified by preparatory reverse-phase HPLC, eluted with H_2O/MeOH containing 0.1% formic acid to yield compound **9** as a colorless solid. Yield: 0.9 mg (0.7 µmol, 24%).^{1}H NMR (500 MHz, $CDCl_3$): δ8.00 (bs, 1H), 7.84 (bs, 1H), 7.36 (d, J = 7.7, 2H), 7.29 (d, J = 7.7, 2H), 5.52 (bs, 2H), 5.32 (m, 4H), 5.25 (s, 1H), 4.47 (d, J = 5.7, 2H), 4.38 (m, 1H), 4.20 (m,

1H), 4.09-3.93 (m, 6H), 3.79-3.27 (m, 30H), 2.61-2.43 (m, 4H), 2.27 (m, 4H), 1.98 (m, 8H), 1.57 (m, 4H), 1.37-1.19 (m, 40H), 0.86 (t, 6H). ^{13}C NMR (125 MHz, $CDCl_3$): δ173.6, 173.3, 172.1, 171.5, 139.8, 133.9, 130.2, 129.9, 129.1, 127.9, 70.4, 67.7, 67.5, 64.9, 64.1, 62.7, 43.1, 41.0, 37.1, 34.8, 34.3, 31.1, 30.0, 29.8, 29.6, 29.4, 26.3, 27.4, 25.1, 22.9, 14.4. MS (ESI) m/z $[M+H]^+$ calc 1404.9; found 1404.2. HPLC (ELSD) Eclipse Plus C8 4.6 x 50mm 3.5 µm / H_2O:MeOH / 0-15min 5%-95% MeOH, 15-22min 95% MeOH.

2.7.25 Synthesis of DOPE-PEG17-NHS (10)

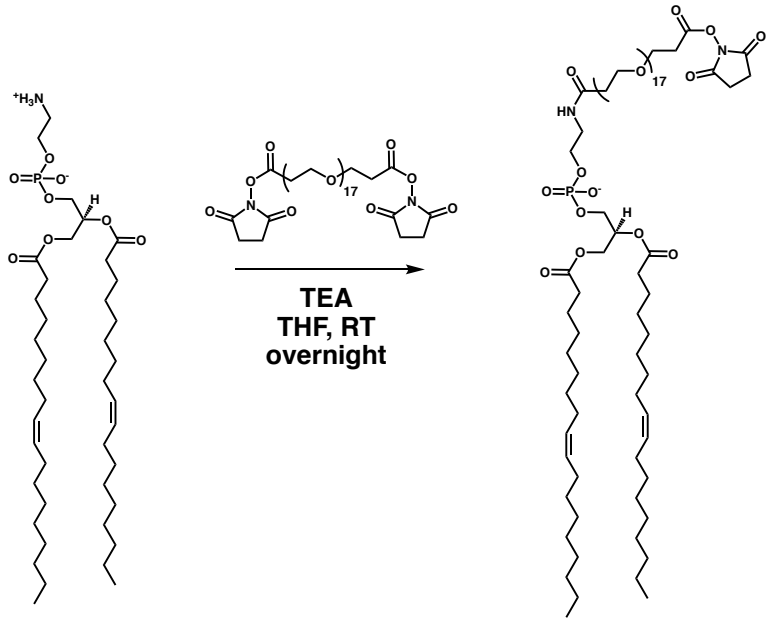

Scheme 2.9 Synthesis of DOPE-PEG17-NHS (**10**)

DOPE (4.5 mg, 6.1 µmol) and PEG17 Bis-NHS Ester (Broadpharm, San Diego, CA) (28.0 mg, 26.4 µmol) were dissolved in 0.5 mL anhydrous THF. TEA (2.5 µL, 18.8 µmol) was added and the reaction stirred under nitrogen overnight at RT. Solvent was removed *in vacuo* and the residue dissolved in a minimal volume of DCM. The DCM solution was loaded onto a prep-TLC plate (.25mm x 20cm x 20cm, EMD Millipore, Darmstadt, Germany) and developed with 10:1

DCM:MeOH. The product band was collected and washed with 10:1 DCM:MeOH and solvent removed *in vacuo.* Yield: 3.5 mg (1.9 µmol, 36%) as a colorless solid. ^{1}H NMR (500 MHz, $CDCl_3$): δ5.32 (m, 4H), 5.16 (bs, 1H), 4.32 (m, 1H), 4.12 (m, 1H), 3.93 (m, 4H), 3.83 (t, 2H), 3.80-3.56 (m, 66H), 3.41 (m, 2H), 2.68 (bs, 4H), 2.61-2.48 (m, 4H), 2.27 (m, 4H), 1.99 (m, 8H), 1.56 (m, 4H), 1.44-1.04 (m, 40H), 0.86 (t, 6H). ^{13}C NMR (125 MHz, $CDCl_3$): δ173.5, 173.1, 168.9, 166.7, 130.0, 129.7, 70.5, 67.3, 65.7, 62.7, 36.2, 34.2, 34.1, 32.2, 31.9, 29.8, 29.7, 29.5, 29.3, 29.2, 29.1, 27.2, 24.9. 22.7, 14.1. MS (ESI) m/z $[M-H]^-$ calc 1688.02; found 1687.98.

2.7.26 Synthesis of DOPE-PEG17-BG (11)

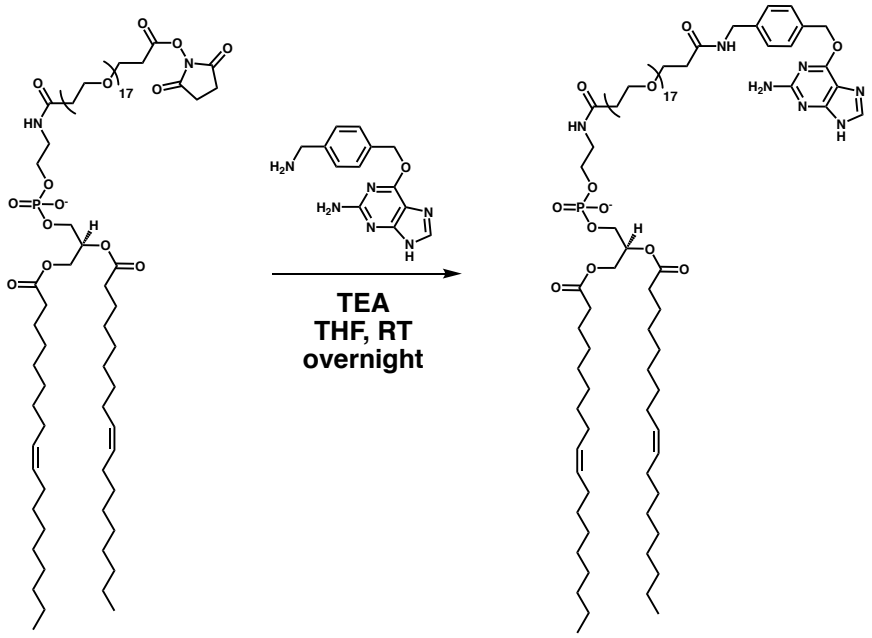

Scheme 2.10 Synthesis of DOPE-PEG17-BG (**11**)

Compound **10** (3.5 mg, 2.1 µmol) and 6-((4-(aminomethyl)benzyl)oxy)-7*H*-purin-2-amine (1.7 mg, 6.2 µmol) were added to 0.5 mL anhydrous DMF. TEA (1µL, 7.1 µmol) was added and the reaction stirred under nitrogen overnight at RT. Solvent was removed *in vacuo* and the residue dissolved in MeOH. The solution was purified by preparatory reverse-phase HPLC, eluted with

H_2O/MeOH containing 0.1% formic acid to yield compound **11** as a colorless solid. Yield: 1.2 mg (0.7 µmol, 32%). ^{1}H NMR (500 MHz, $CDCl_3$): δ7.69 (bs, 1H), 7.42 (d, J = 7.6, 2H), 7.31 (d, J = 7.6, 2H), 5.58, (bs, 2H), 5.32 (m ,4H), 5.22 (bs, 1H), 4.46 (m, 2H), 4.36 (m, 1H), 4.20-4.05(m, 4H), 4.00 (m, 1H), 3.84-3.36 (m, 70H), 2.52 (m, 4H), 2.26 (m, 4H), 2.18-1.47 (m), 1.47-1.05 (m, 40H), 0.86 (t, 6H). ^{13}C NMR (125 MHz, $CDCl_3$): δ130.2, 130.0, 129.2, 128.1, 70.7, 67.5, 51.1, 43.1, 34.4, 34.3, 32.1, 30.0, 29.8, 29.6, 27.5, 25.1, 22.9, 14.4. MS (ESI) m/z $[M-H]^-$ calc 1843.11; found 1843.13. HPLC (ELSD) Eclipse Plus C8 4.6 x 50mm 3.5 µm / H_2O:MeOH / 0-15min 5%-95%.

Notes about the chapter:

Chapter two, in full, is a reprint (with co-author permission) of the material as it appears in the publication; **A. K. Rudd**, J. V. Cuevas, N. K. Devaraj "SNAP-tag Reactive Lipid Anchors Enable Targeted and Spatiotemporally Controlled Localization of Proteins to Phospholipid Membranes," *J. Am. Chem. Soc.*, 2015, 137(15) 4884–4887. I would like to thank Joan Cuevas for his assistance in performing vesicle microdomain experiments and Neal Devaraj for his scientific oversight and assistance in preparing the manuscript. The author of the dissertation is the primary author of this manuscript.

CHAPTER 3

3 Nonenzymatic Biomimetic Remodeling of Phospholipids in Synthetic Liposomes

3.1 Introduction

Living organisms carry out the de novo synthesis of phospholipid membranes, in part, by using membrane-bound acyltransferases and reactive thioester precursors (Figure 3.1A).[64] Subsequently, de novo synthesized phospholipid membranes can be remodeled by acyltransferases and transacylases in the presence of different lysolipid, phospholipid, and fatty acid precursors (Figure 3.1A).[65] Such natural mechanisms allow cells to fine-tune properties of biological membranes by changing the composition and organization of their constituent lipids and proteins.[66] Membrane remodeling is an essential component of numerous cellular functions including the formation of organelles,[67] division,[68] trafficking,[69] and signaling.[70] Many experimental and theoretical studies have examined membrane remodeling due to enzymatically driven changes in lipid composition.[71] For instance, the disruption of the transacylase activity of the enzyme tafazzin leads to alterations in the mitochondrial lipid cardiolipin and the disease known as Barth's syndrome.[72,73]

Model membranes composed of well-defined synthetic lipids are useful tools for studying questions related to membrane biology.[74] The importance of lipid remodeling in biology underscores the need for straightforward methods to remodel lipid composition in artificial model membranes. Unfortunately, nonenzymatic methods to exchange lysolipid fragments in synthetic vesicles have previously not been feasible. This is likely due to the high kinetic stability of phospholipid membranes, which do not readily exchange diacylphospholipid species between membranes.[75] Because the composition of phospholipids controls the physical properties of the

resulting membranes, synthetic phospholipid remodeling could be used to gain control over the function and form of artificial membranes, for instance by enabling dynamic changes in vesicle morphology. Here, we demonstrate efficient de novo generation and remodeling of phospholipid vesicles at neutral pH through application of the native chemical ligation (NCL)[76–81] and reversible native chemical ligation (RNCL)[82] (Figures 3.1B-C and 3.2-3.5). Our strategy uses reversible covalent coupling reactions and reactive single-chain lipid precursors, which are known to rapidly exchange between membranes.[83] We demonstrate that our protein-free synthetic membranes can be used to test the effects of lipid fragment exchange on membrane properties such as curvature, microdomain formation, and protein recruitment. Advanced model membranes could be harnessed to further understand the effects of chemical lipid remodeling on membrane biology and enable dynamic control over properties of preformed vesicles such as size, shape, and charge.

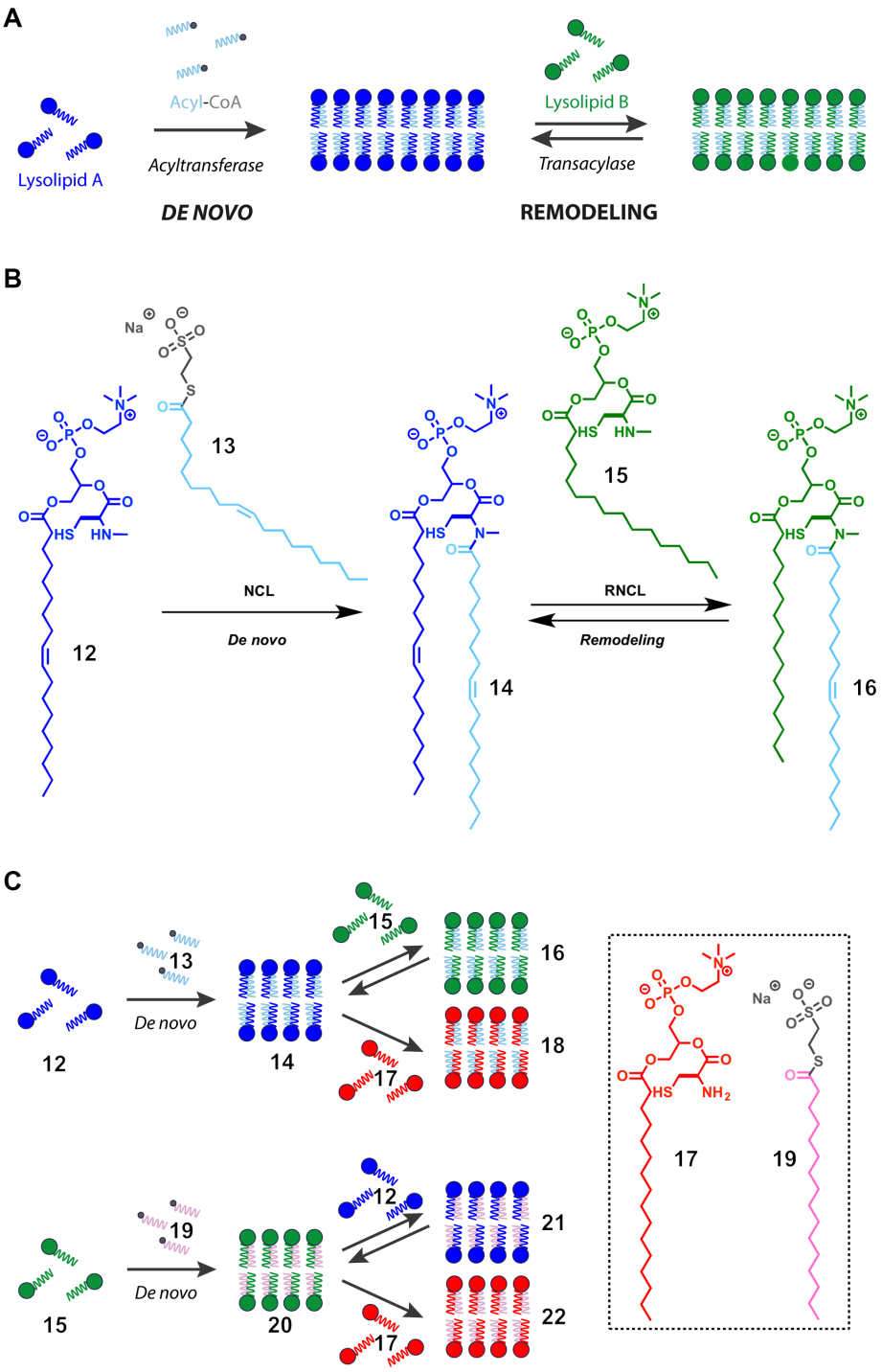

Figure 3.1 De novo formation and remodeling of phospholipid membrane architecture. A, Enzymatic acyl chain incorporation into membranes during the de novo and remodeling phospholipid synthesis pathways [CoA: coenzyme A]. B, De novo synthesis of phospholipids by NCL reaction of an N-methylated cysteine-functionalized lysolipid (12) and MESNA oleoyl thioester (13), followed by subsequent remodeling of the corresponding phospholipids by RNCL in the presence of another N-methylated cysteine-functionalized lysolipid (15). C, Schematic representation of phospholipid libraries obtained by NCL-based de novo formation and RNCL-based remodeling approaches.

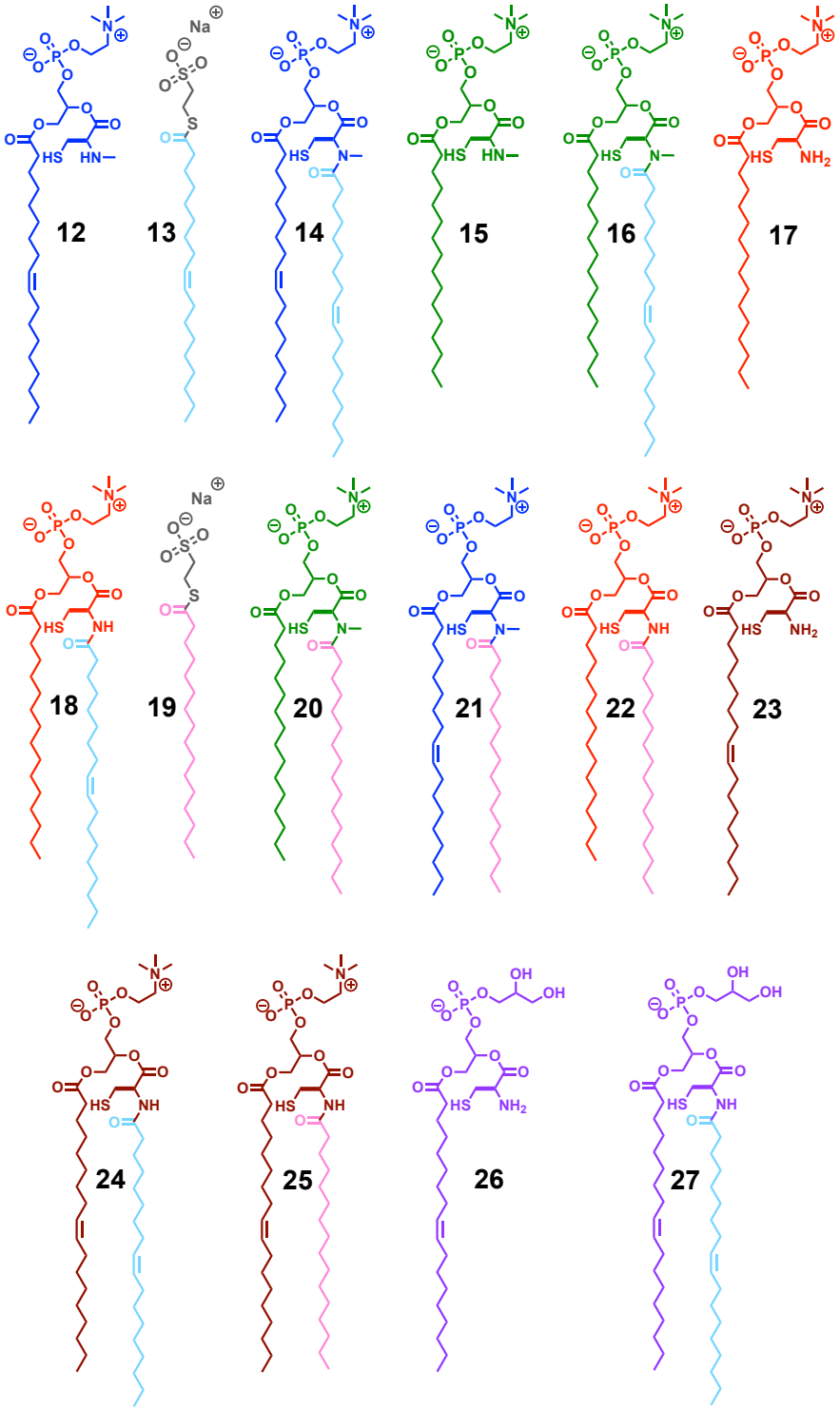

Figure 3.2 Chemical structures of all the lipids used in this study.

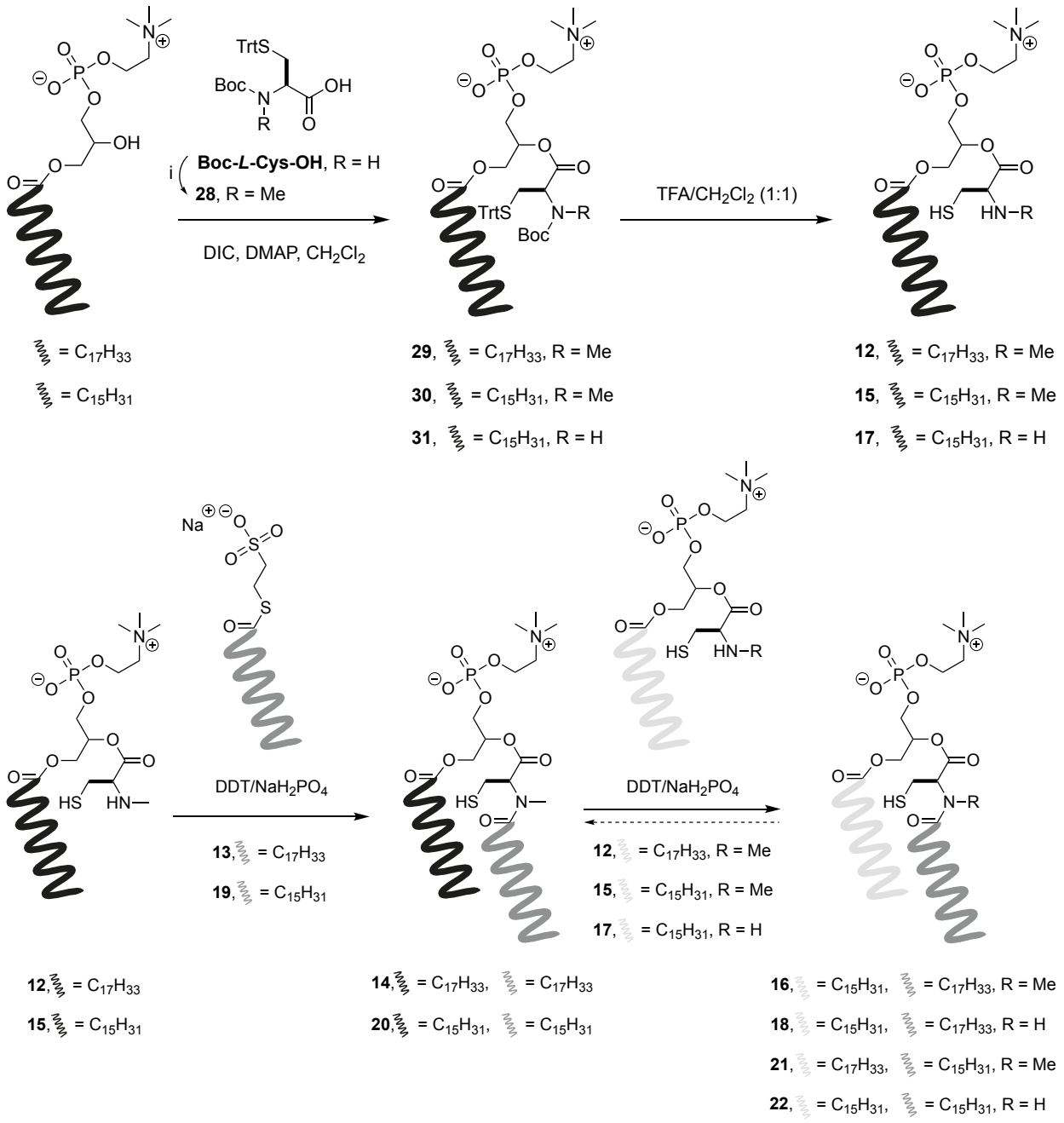

Figure 3.3 De novo formation and remodeling of phospholipid membranes. Top, Synthesis of N-methylated and un-N-methylated cysteine-functionalized lysolipids. Bottom, De novo synthesis of phospholipids by NCL reaction of an N-methylated cysteine-functionalized lysolipid (12 or 15) and MESNA acyl thioester (oleoyl 2 or palmitoyl 8), followed by subsequent remodeling of the corresponding phospholipids (14 or 20) by RNCL in the presence of another cysteine-functionalized lysolipid (N-methylated 15 or 12; un-N-methylated 17).

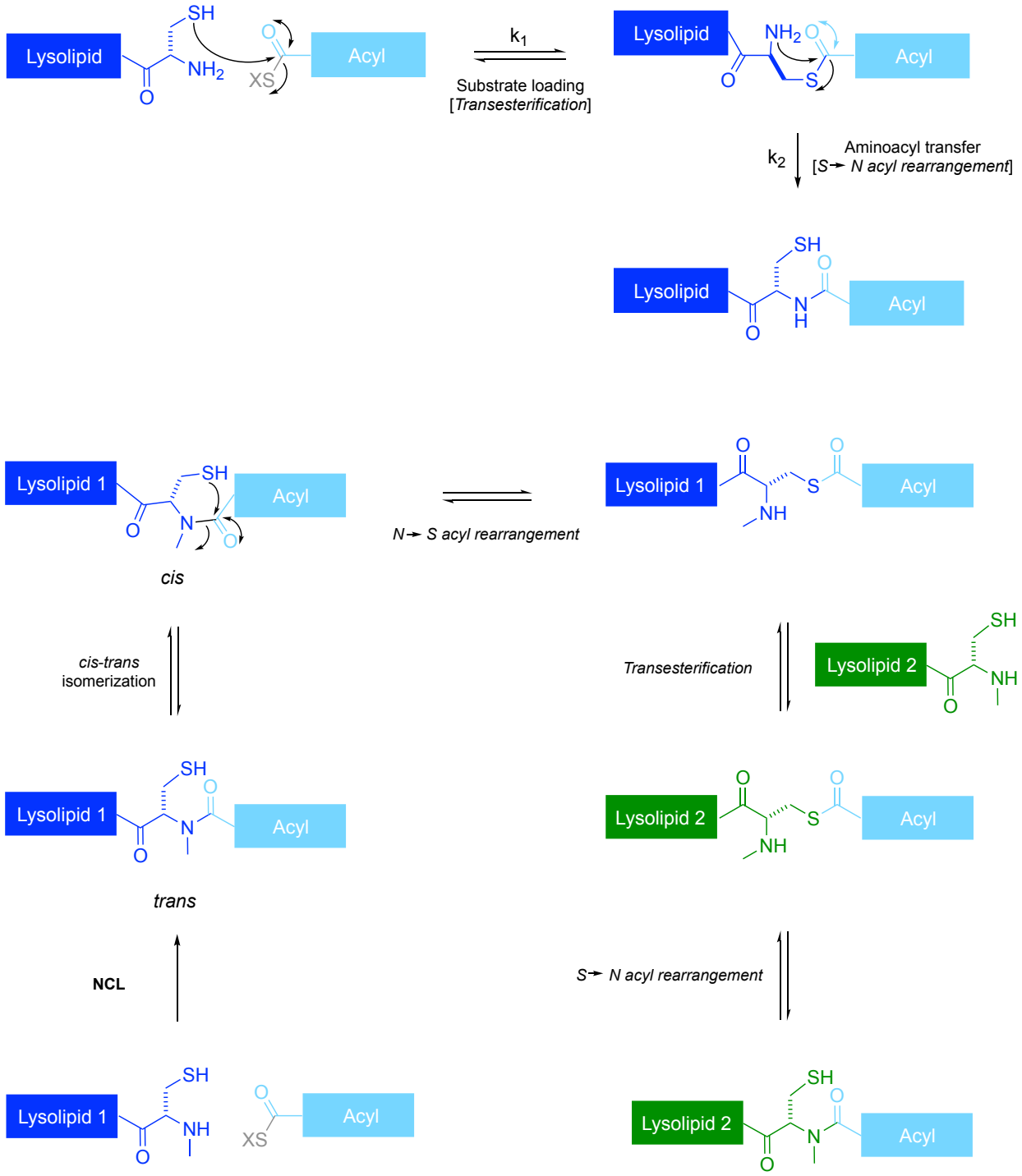

Figure 3.4 Reaction mechanisms of NCL and RNCL. Top, Mechanism of NCL. The mechanism involves a two-step process consisting of a thiol-exchange step between a C-terminal acyl thioester and the sulfhydryl moiety of an N-terminal cysteine residue in a lysolipid, which prompts an intramolecular nucleophilic attack by the α-amino group of the cysteine (S-to-N acyl rearrangement) to form the final amide bond. Bottom, Mechanism of RNCL. The mechanism involves a sequence of cis-trans isomerization, N-to-S acyl rearrangement, transthioesterification, and S-to-N acyl shift.

Compound	Head[a]	Lipid chain	N-R'	Transition temperature	Cmc's	Micelle size
Lysolipid **1**	PC	R = Oleoyl	N-Me		<100 μM	4.54 nm
Thioester **2**		R = Oleoyl			<10 μM	3.79 nm
Phospholipid **3**	PC	R_1 = Oleoyl R_2 = Oleoyl	N-Me	<263 K		
Lysolipid **4**	PC	R = Palmitoyl	N-Me		<100 μM	6.74 nm
Phospholipid **5**	PC	R_1 = Palmitoyl R_2 = Oleoyl	N-Me	270 K		
Lysolipid **6**	PC	R = Palmitoyl	N-H		<100 μM	5.32 nm
Phospholipid **7**	PC	R_1 = Palmitoyl R_2 = Oleoyl	N-H	270 K		
Thioester **8**		R = Palmitoyl			<10 μM	3.53 nm
Phospholipid **9**	PC	R_1 = Palmitoyl R_2 = Palmitoyl	N-Me			
Phospholipid **10**	PC	R_1 = Oleoyl R_2 = Palmitoyl	N-Me			
Phospholipid **11**	PC	R_1 = Palmitoyl R_2 = Palmitoyl	N-H			
Lysolipid **12**	PC	R = Oleoyl	N-H			
Phospholipid **13**	PC	R_1 = Oleoyl R_2 = Oleoyl	N-H	<263 K		
Phospholipid **14**	PC	R_1 = Oleoyl R_2 = Palmitoyl	N-H			
Lysolipid **15**	PG	R = Oleoyl	N-H			
Phospholipid **16**	PG	R_1 = Oleoyl R_2 = Oleoyl	N-H			

[a] PC: phosphocholine, PG: phosphoglycerol

Figure 3.5 Characteristics of all the lipids used in this study.

3.2 NCL-based Phospholipid Synthesis

We initially synthesized two substrates to mimic the native precursors of the common phospholipid 1-oleoyl-2-oleoyl-sn-glycero-3-phosphocholine (DOPC): an N-methylated cysteine-functionalized analog of the lysolipid 1-oleoyl-sn-glycero-3-phosphocholine (**12**) and a sodium 2-mercaptoethanesulfonate (MESNA) oleoyl thioester **13** in lieu of oleoyl-CoA (Figures 3.1B-C, 3.2, 3.3 and 3.5). Precursors **12** and **13** are water-soluble amphiphiles, forming micelles of ~4.5 and 3.8 nm in diameter, respectively, with critical micelle concentrations below 100 μM (for **12**) and 10 μM (for **13**) (Figures 3.6 and 3.7). The high water solubility of both precursors facilitated initial de novo phospholipid synthesis by NCL using mild conditions and millimolar concentrations of lipid precursors. Under typical NCL conditions (NaH2PO4 buffer, pH 7.1, containing DTT as reducing agent), unprotected segment **12** and **13** coupled over 30 min to afford amidophospholipid **14**, a novel phospholipid that resembles DOPC, with the exception of an N-methylated cysteine-amido linker (Figures 3.1B-C, 3.2, 3.3 and 3.5). Phospholipid formation was analyzed using combined liquid chromatography, MS, and evaporative light scattering detection (ELSD) measurements (Figure 3.8).

As expected, neither the N-methylated cysteine-modified lysolipid **12** nor the MESNA thioester **13** formed membranes in aqueous solution. However, the amidophospholipid product **14** readily formed membrane vesicles in situ (Figure 3.9). Lipid vesicular structures were initially identified by fluorescence microscopy using the membrane staining dye Texas Red DHPE (Figure 3.10). Confirmation that the resulting structures were membrane compartments was also achieved by transmission electron microscopy (TEM) (Figures 3.11A and 3.12). In this case, aliquots of the in situ phospholipid samples were collected over 400 mesh Cu/Rh grids, which were then negatively stained with uranyl acetate. Under these conditions, electron microscopy revealed the presence of several populations of spherical vesicles that were between 50–950 nm wide. The

efficient in situ encapsulation ability of the vesicles was determined by inclusion of a polar fluorophore, 8-hydroxypyrene-1,3,6-trisulfonic acid (HPTS), in the hydration media, followed by vesicle characterization using fluorescence microscopy (Figure 3.11B and 3.13). Finally, we determined the gel-to-liquid-phase transition temperature of the resulting membranes by performing steady-state anisotropy measurements as a function of temperature with the membrane fluidity probe 1,6-diphenyl-1,3,5-hexatriene (DPH). The measurements indicate that the amidophospholipid membranes composed from **14** have fluidity and chain melting temperatures comparable to those of native DOPC membranes (Tc = 256 K) (Figures 3.11C, 3.14 and 3.15).

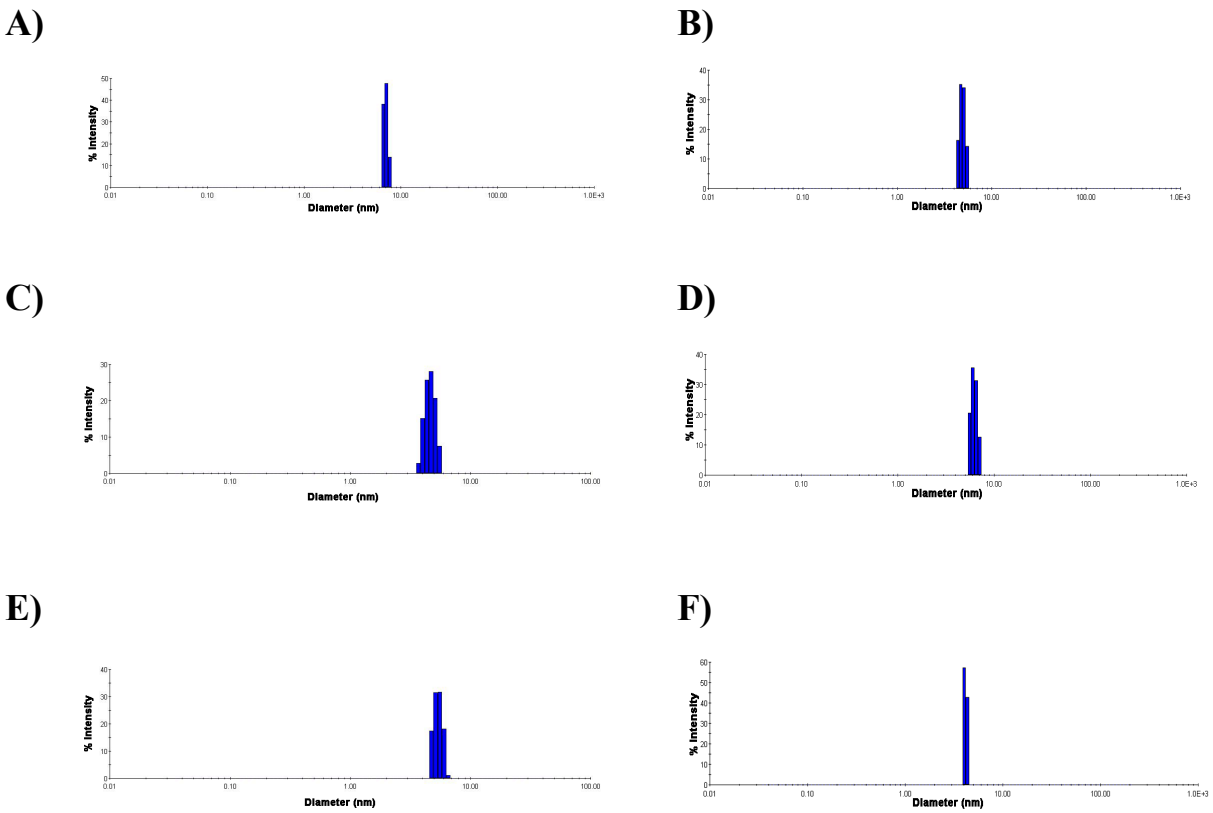

Figure 3.6 Dynamic Light Scattering experiments. Dynamic Light Scattering corresponding to 1.0 mM aqueous solution of 1-palmitoyl-2-hydroxy-sn-glycero-3-phosphocholine Lyso C16 PC-OH (A), 1-oleoyl-2-(L-MeN-Cys)-sn-glycero-3-phosphocholine 12 (B), MESNA thiooleate 13 (C), 1-palmitoyl-2-(L-MeN-Cys)-sn-glycero-3-phosphocholine 15 (D), 1-palmitoyl-2-(L-Cys)-sn-glycero-3-phosphocholine 17 (E), and MESNA thiopalmitate 19 (F). Lysolipids show critical micelle concentrations (cmc's) below 100 μM, whereas MESNA thiooesters present cmc's below 10 μM.

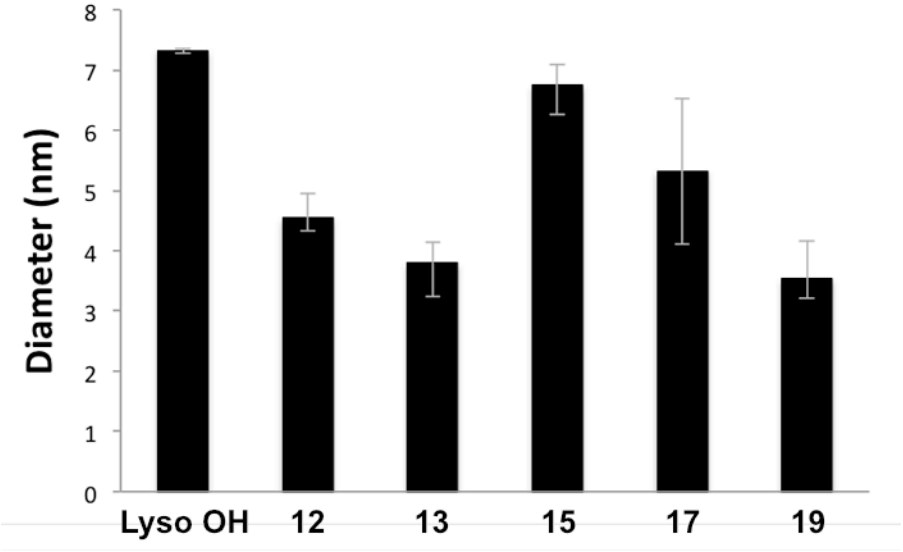

Figure 3.7 Micelle size measurements. Micelle sizes estimated from DLS studies corresponding to 1.0 mM aqueous solution of 1-palmitoyl-2-hydroxy-sn-glycero-3-phosphocholine (Lyso C16 PC-OH) (7.32 nm in diameter), 1-oleoyl-2-(MeN- L-Cys)-sn-glycero-3-phosphocholine 12 (4.54 in diameter), MESNA thiooleate 13 (3.79 nm in diameter), 1-palmitoyl-2-(L-MeN-Cys)-sn-glycero-3-phosphocholine 15 (6.74 nm), 1-palmitoyl-2-(L-Cys)-sn-glycero-3-phosphocholine 17 (5.32 nm), and MESNA thiopalmitate 19 (3.53 nm in diameter).

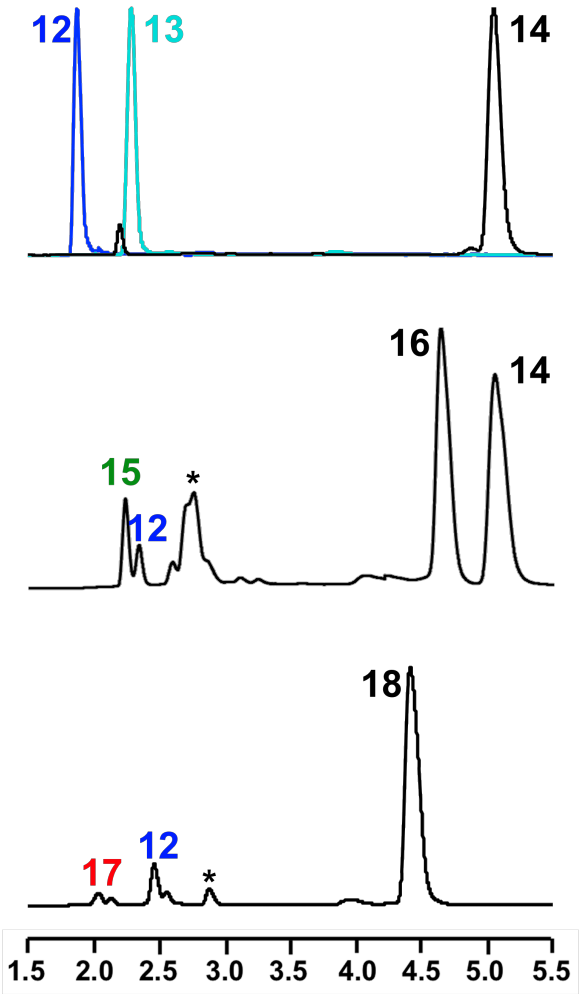

Figure 3.8 HPLC/ELSD spectra monitoring the *de novo* phospholipid membrane formation and subsequent remodeling driven by non-enzymatic reactions. A, ELSD spectra showing the progress of the *in situ* phospholipid formation of **14** by NCL reaction. Addition of MESNA thioester **13** to the cysteine-based lysolipid **12** in 25 mM DTT in 200 mM NaH_2PO_4 pH 7.1 buffer immediately led to amidophospholipid formation, and this process progressed to near completion over a period of 30 min using millimolar concentrations of reactants. B, ELSD spectra corresponding to the RNCL exchange reaction between the phospholipid **14** and the N-methylated cysteine-functionalized lysolipid **15**, leading to an equimolar mixture of **14** and **16**. C, ELSD spectra corresponding to the RNCL exchange reaction between the phospholipid **14** and cysteine-functionalized lysolipid **17**, leading to the selective formation of **18**. Retention times (R_t's) for lysolipids (**12**, **15** and **17**), MESNA oleoyl thioester (**13**) and phospholipids (**14, 16** and **18**) were verified by mass spectrometry. Extra peaks (*) correspond with oleoyl-DTT intermediate and/or side products resulting from lysolipid hydrolysis.

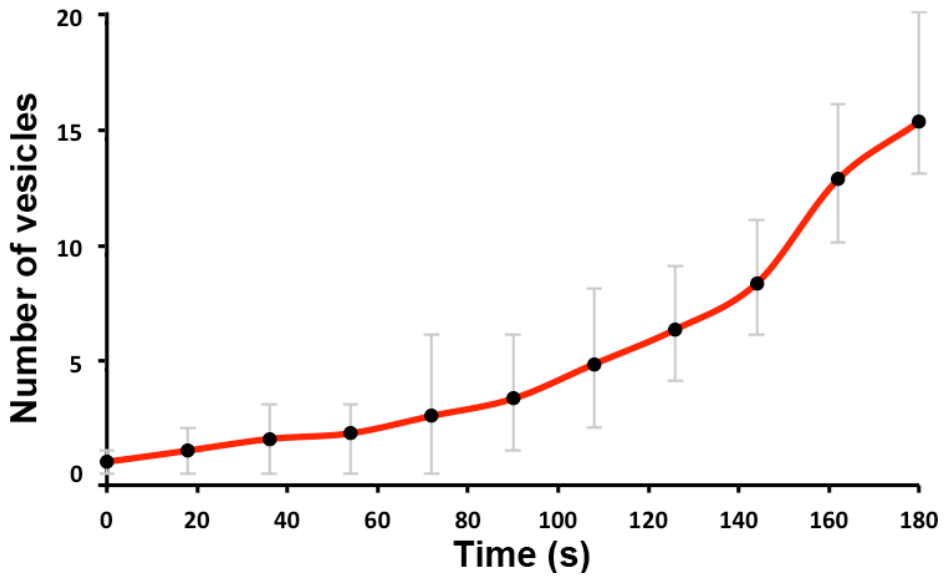

Figure 3.9 Kinetics of in situ vesicle formation. An aqueous solution of MESNA thiooleate **13** (4 mM) was added to another aqueous solution of N-methylated cysteine-based lysolipid **12** (4 mM) and DTT (20 mM in 200 mM NaH2PO4 buffer pH 7.1). The population of phospholipid **14** vesicles larger than 1 μm in diameter was counted every 18 s over a period of 3 min in four different 26×26 μm regions.

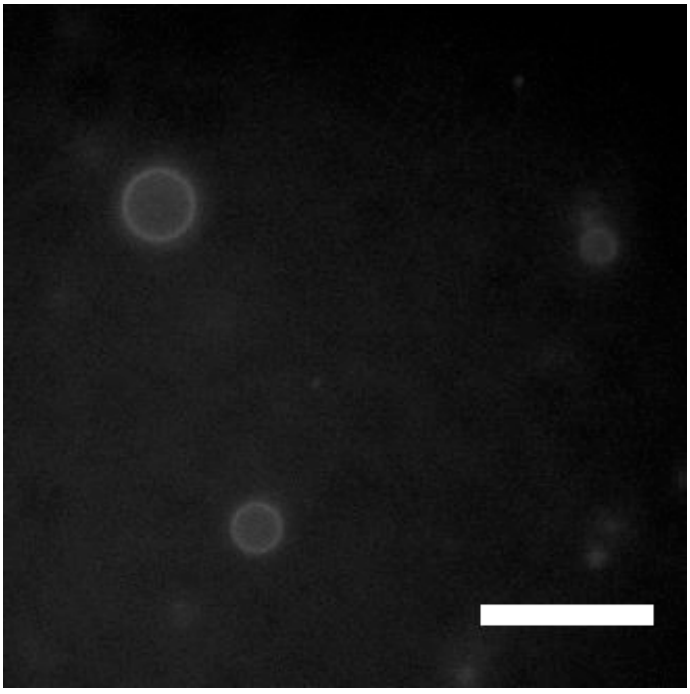

Figure 3.10 Fluorescence microscopy image of membrane-containing vesicles formed by hydration of a thin film of phospholipid **14**. Membranes were stained with 100 μM of Texas Red® DPHE. Scale bar denotes 10 μm.

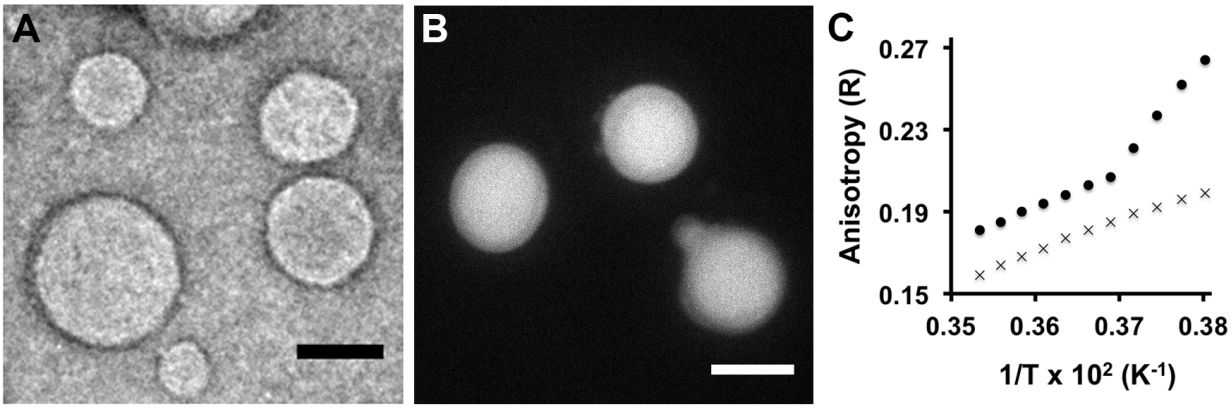

Figure 3.11 Characterization of the amidophospholipid vesicular architecture. A, TEM image of negatively stained vesicular structures formed by spontaneous de novo NCL-based synthesis of phospholipid **14**. Scale bar denotes 100 nm. B, Fluorescence microscopy image demonstrating the in situ encapsulation of HPTS within membrane vesicles during de novo synthesis of phospholipid **14**. Scale bar denotes 10 μm. C, Anisotropy of 1,6-diphenyl-1,3,5-hexatriene (DPH) as a function of temperature within membranes formed from phospholipid **14** (X) and **16** (•). A sudden change in the slope of the anisotropy indicates a transition from a gel to liquid-crystalline phase. The melting temperature of the lipid chains in membranes formed from **16** was detected at 270 K, comparable to the transition temperature of analogous POPC membranes. In contrast, within the temperatures tested (263-283 K), a phase transition was not detected in membranes formed from **14**, as predicted by comparing to analogous DOPC membranes (Tc = 256 K). The unitless anisotropy ratio (R) is a measure of the acyl packing of the bilayer, with higher values indicating a more ordered membrane.

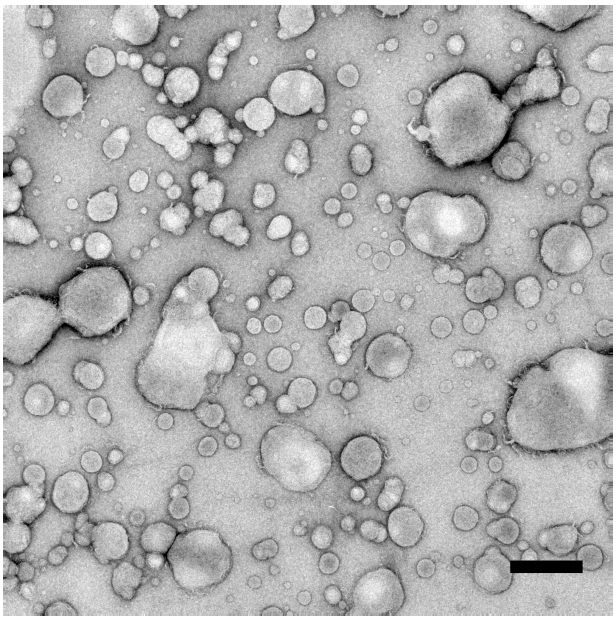

Figure 3.12 TEM images of in situ formed phospholipid **14** sample, showing the presence of vesicles. Scale bar denotes 500 nm.

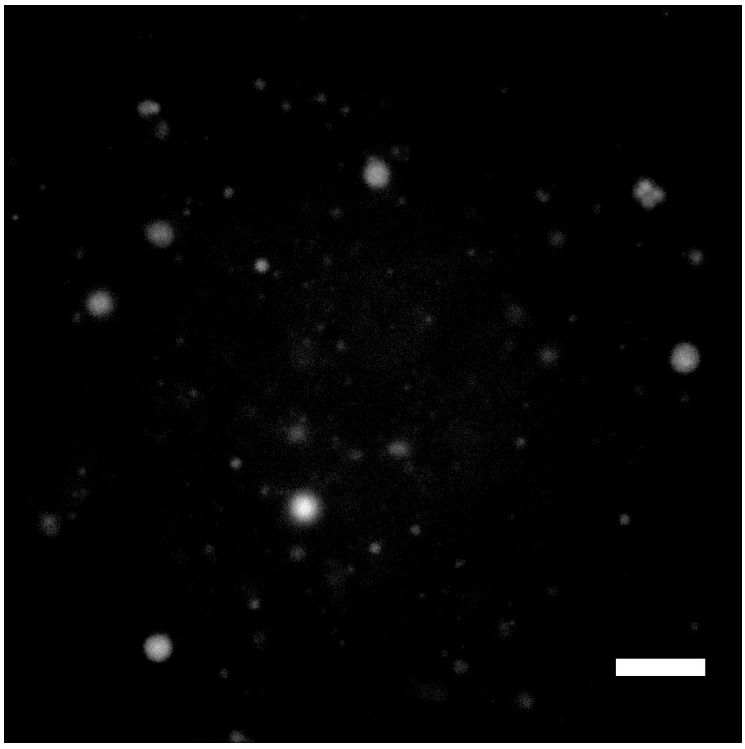

Figure 3.13 Fluorescence microscopy images corresponding to the *in situ* encapsulation of polar fluorescent dye 8-hydroxypyrene-1,3,6-trisulfonic acid (HPTS) in phospholipid **14** membrane vesicles. Scale bar denotes 25 μm.

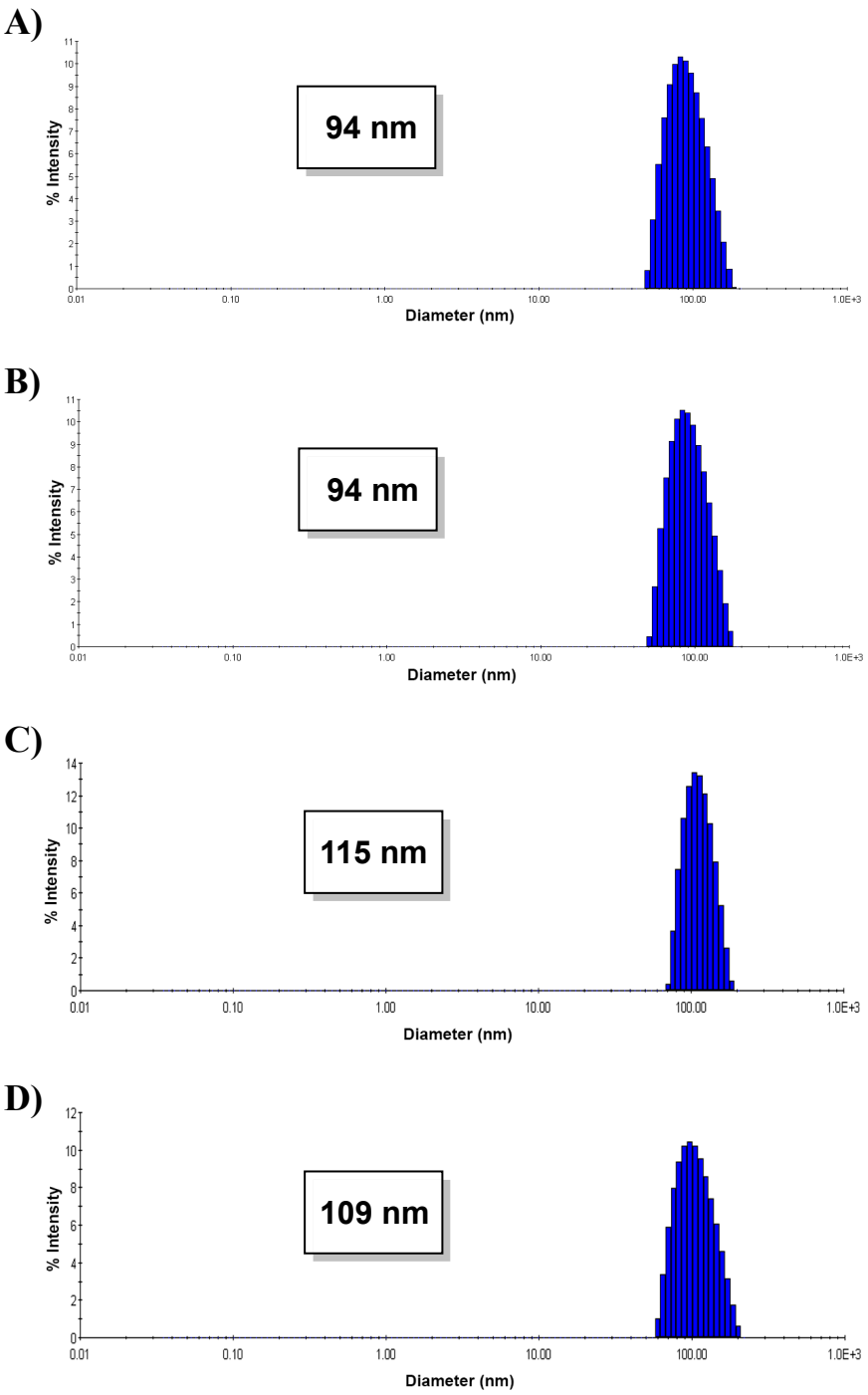

Figure 3.14 Dynamic Light Scattering corresponding to the 100 nm extruded DOPC (A), POPC (B), phospholipid 3 (C) and phospholipid 5 (D) membrane vesicles.

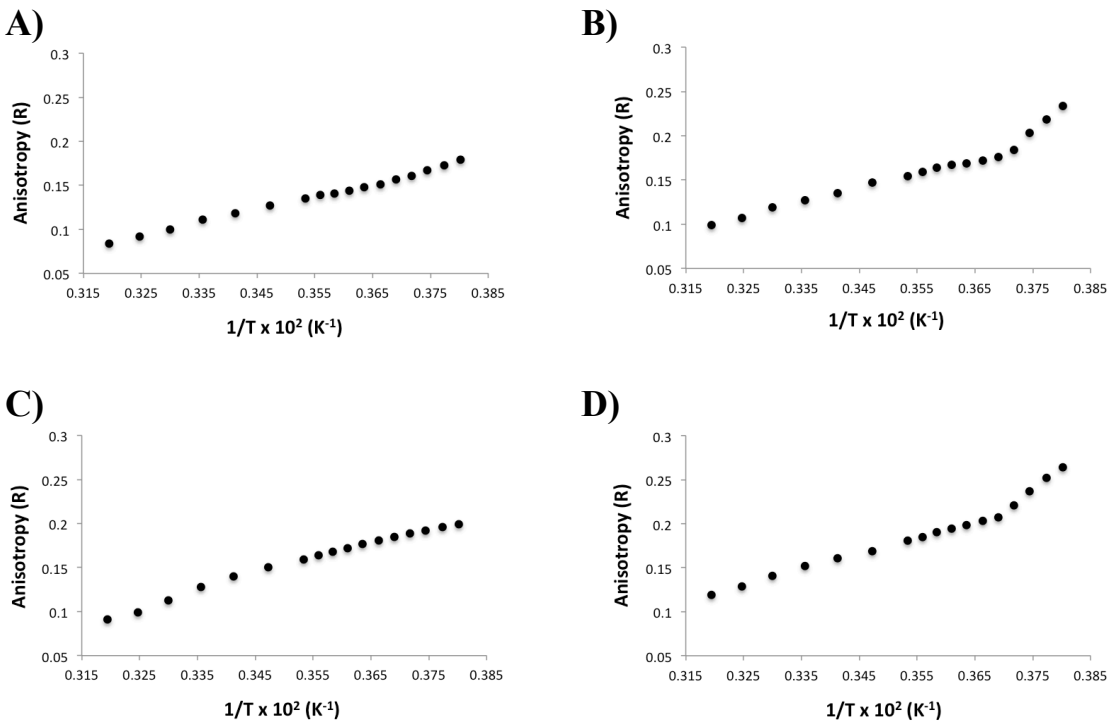

Figure 3.15 Chain melting temperatures of different phospholipids. 1,6-diphenyl-1,3,5-hexatriene (DPH) anisotropy was used as a function of temperature to measure phase transitions of the lipid chains. A sudden change in the slope of the anisotropy indicates a transition from a gel to liquid-crystalline phase. A, DPH anisotropy graph corresponding to the sample of DOPC vesicles. Within the temperatures tested (263-313 K), a phase transition was not detected in membranes from DOPC phospholipid, consistent with previous measurements. B, DPH anisotropy graph corresponding to the sample of POPC vesicles. The melting temperature of the lipid chains in POPC membranes was detected at 270 K, consistent with previous measurements. C, DPH anisotropy graph corresponding to the sample of phospholipid **14** vesicles. Within the temperatures tested (263-313 K), a phase transition was not detected in membranes formed from **14**, as predicted by comparing to analogous DOPC membranes. D, DPH anisotropy graph corresponding to the sample of phospholipid **16** vesicles. The melting temperature of the lipid chains in **16** membranes was detected at 270 K, comparable to the transition temperature of analogous POPC membranes.

3.3 In Situ Phospholipid Remodeling

Using RNCL, we explored the remodeling of amidophospholipid membranes. Initially, we tested the ability of phospholipids to react by RNCL using giant unilamellar vesicles (GUVs) formed by electroformation using interdigitated ITO electrodes.[84] This technique allowed for the formation of GUVs (1–100 μm) from amidophospholipid **14** with excellent yield. Confirmation of the lipid vesicular structure was achieved by fluorescence microscopy using the membrane staining dye Bodipy FL DHPE (Figure 3.16). GUVs from phospholipid **14** were then used to study

the dynamics of the RNCL by following the reaction with N-methylated lysolipids at pH 7.1 in a phosphate buffer containing DTT (Figure 3.17). When we combined an aqueous solution of GUVs composed of lipid **14** with 1.0 equivalent of the N-methylated cysteine-functionalized palmitoyl lysolipid **15**, we observed the appearance in the ELSD spectrum of a new peak corresponding to amidophospholipid **16** (Figures 3.2, 3.5 and 3.17). This confirmed the dynamic covalent character of the RNCL and the ability to remodel **14** to form new phospholipids. Despite their different lipid tail saturation, oleoyl- and palmitoyl-derivatized phospholipids (**14** and **16**, respectively) were present in almost equal concentrations (1:1 ratio), which implies that both species have similar stabilities in the equilibria. Modifications of phospholipid tail saturation can change the physical state of the membrane. Consequently, lipid exchange-based remodeling affords a straightforward approach to modulate the order and fluidity of synthetic phospholipid membranes. As expected, the chain melting temperature for membranes composed of phospholipid **16** was estimated to be 270 K, which is comparable to native 1-palmitoyl-2-oleoyl-sn-glycero-3-phosphocholine (POPC) membranes (Figures 3.11 and 3.15). Also, the anisotropy ratio (R) for dyes embedded in membranes formed from phospholipid **16** is higher compared with phospholipid **14**, suggesting that **16** forms more ordered membranes.

We tested whether the equilibria during remodeling could be shifted by using cysteine lysolipids, which irreversibly form stable amide bonds with thioesters. Remodeling of phospholipid membranes spontaneously took place upon the addition of 1.0 equivalent of cysteine-functionalized palmitoyl lysolipid **17** to a solution of GUVs formed from phospholipid **14**, resulting in the appearance of a new peak that corresponded to phospholipid **18** (Figures 3.2, 3.5 and 3.17). The new phospholipid was the dominant species in the equilibrium, ~30-fold more abundant than the initial N-methylated phospholipid **14**, which at 298 K corresponds to an energy difference of 2.0 kcal·mol−1. It seems likely that the equilibrium is driven by the higher stability

of amidophospholipid **18**, which, in the absence of an N-methylated residue avoids the formation of a significant amount of the cis isomer, a necessary intermediate for the reversible nonenzymatic process (Figure 3.4).

To combine the nonenzymatic de novo and remodeling phospholipid membrane synthesis pathways, we proceeded to study the lipid tail exchange in spontaneously formed vesicles. We initially formed phospholipid **14** by de novo synthesis (Figures 3.9 and 3.18A). Sequential addition of 1.0 equivalent of N-methylated cysteine-functionalized palmitoyl lysolipid **15** to the de novo vesicle population of **14** resulted in lipid remodeling, loss of **12**, and the formation of phospholipid **16**, indicating that RNCL took place (Figures 3.8, 3.18B and 3.19). As expected from our previous GUV experiments, the oleoyl- and palmitoyl-derivatized phospholipids (**14** and **16**, respectively) were present in equimolar concentrations (1:1 ratio), demonstrating that both species have analogous stabilities and are in equilibrium. Addition of more than 1.0 equivalent of lysolipid **15** leads to a corresponding shift in the final **14**:**16** lipid ratio, caused by the increase of phospholipid **16** (Figure 3.20). This finding suggests that the final phospholipid membrane composition can be controlled through the stoichiometry of the starting reactive lipids. Alternatively, the de novo-formed vesicles of **14** could be irreversibly remodeled by addition of the cysteine-functionalized palmitoyl lysolipid **17**, selectively forming vesicles composed of phospholipid **18** (Figures 3.8 and 3.18C).

During remodeling, the phospholipid chains can be modulated by changing the reactive precursors (Figures 3.1C and 3.3). For instance, addition of saturated MESNA thioester **19** to the N-methylated cysteine-based lysolipid **15** led to de novo synthesis of fully saturated amidophospholipid **20** (Figures 3.2, 3.3 and 3.5). Phospholipid **20** could be remodeled by subsequent addition of N-methylated cysteine-based lysolipid **12** or cysteine lysolipid **17**, affording amidophospholipid **21** or **22**, respectively (Figures 3.2, 3.3 and 3.5).

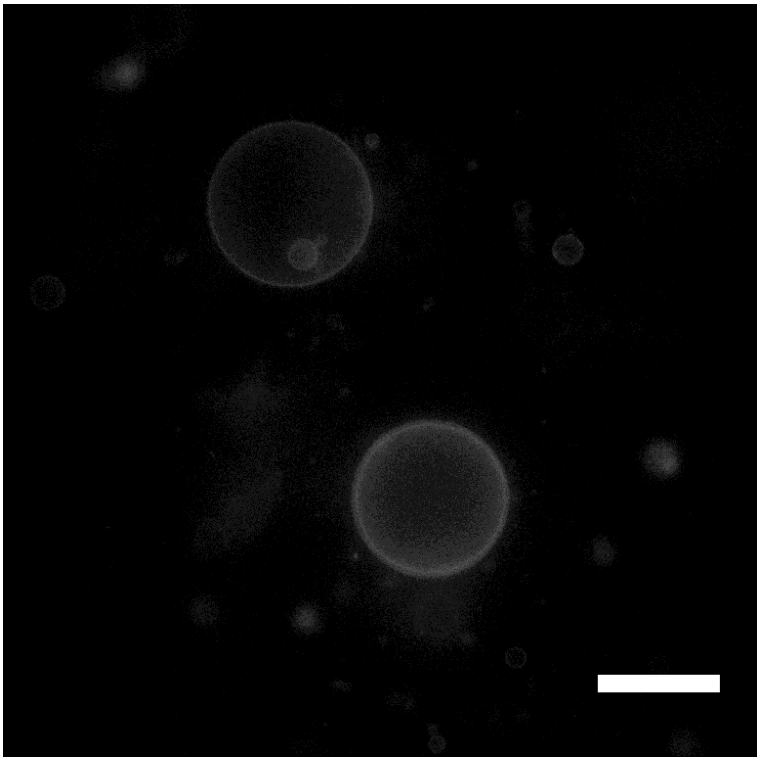

Figure 3.16 Characterization of the giant unilamellar vesicular structure. Fluorescence microscopy image of membrane-containing giant unilamellar vesicles (GUVs) formed by electroformation of phospholipid **14**. Membranes were stained using 0.1 mol% of Bodipy® FL DHPE. Scale bar denotes 25 μm.

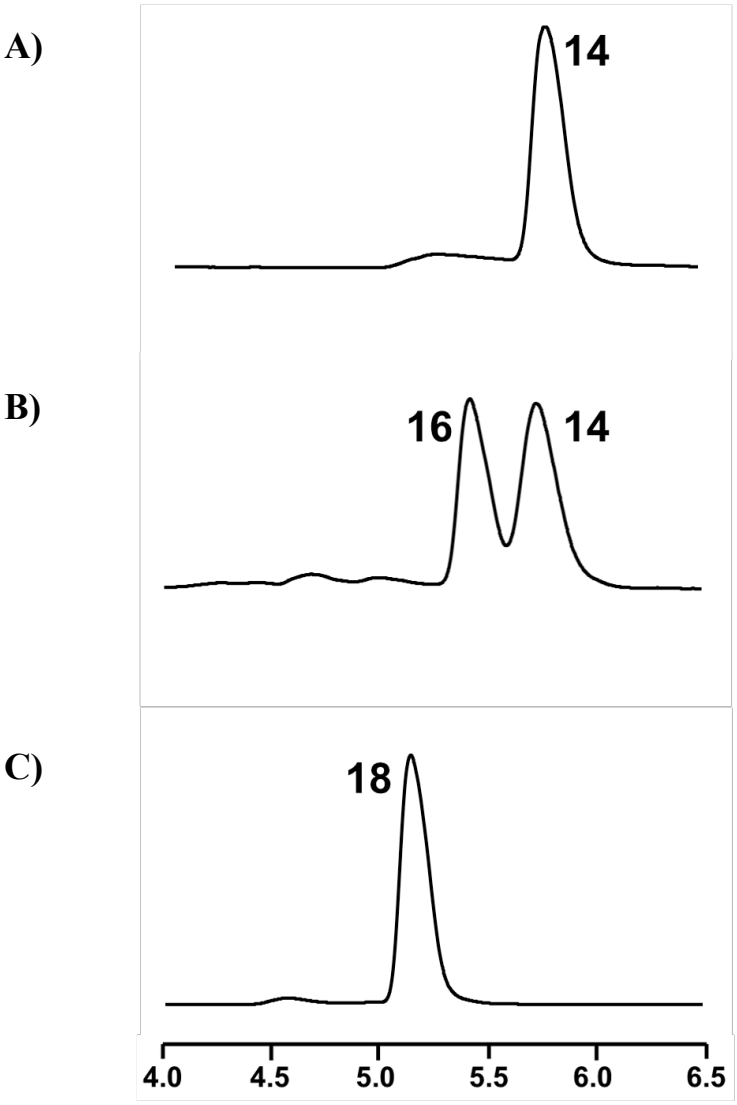

Figure 3.17 HPLC/ELSD spectra monitoring the remodeling of phospholipid membrane GUVs driven by RNCL. A, ELSD spectra showing the GUVs from phospholipid **14**. B, ELSD spectra corresponding to the RNCL exchange reaction between the GUVs from phospholipid **14** and the N-methylated cysteine-functionalized lysolipid **15**, leading to an equimolar mixture of **14** and **16**. C, ELSD spectra corresponding to the RNCL exchange reaction between the GUVs from phospholipid **14** and cysteine-functionalized lysolipid **17**, leading to the selective formation of **18**. Retention times (R_t's) for phospholipids (**14, 16** and **18**) were verified by mass spectrometry.

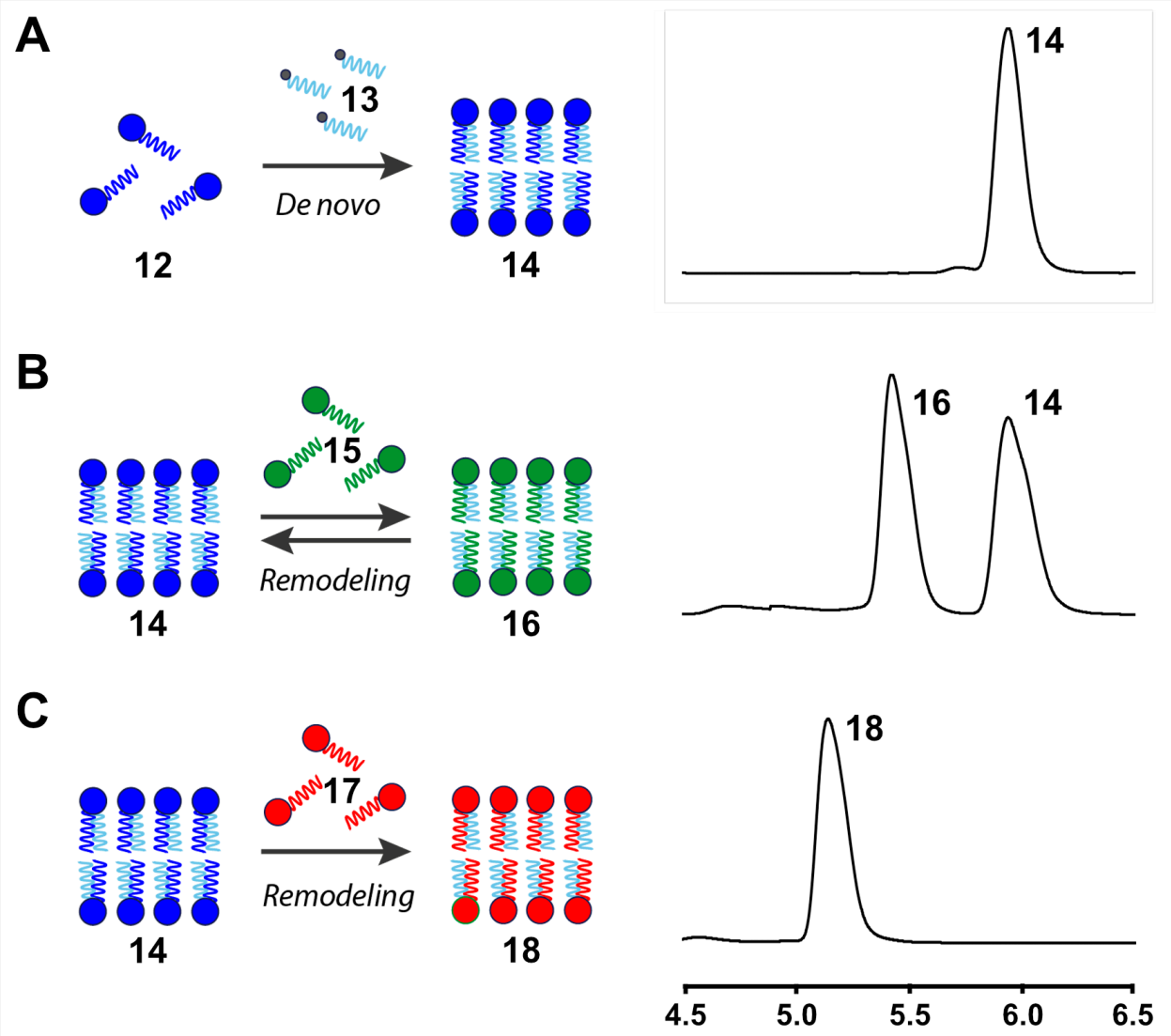

Figure 3.18 Sequential *de novo* phospholipid membrane formation and remodeling driven by non-enzymatic reactions. A, ELSD spectra corresponding to the *in situ* phospholipid formation of **14**. B, ELSD spectra corresponding to the RNCL exchange reaction between *in situ* formed phospholipid **14** and the N-methylated cysteine-functionalized lysolipid **15**, leading to an equimolar mixture of **14** and **16**. C, ELSD spectra corresponding to the RNCL exchange reaction between *in situ* formed phospholipid **14** and cysteine-functionalized lysolipid **17**, leading to the selective formation of **18**.

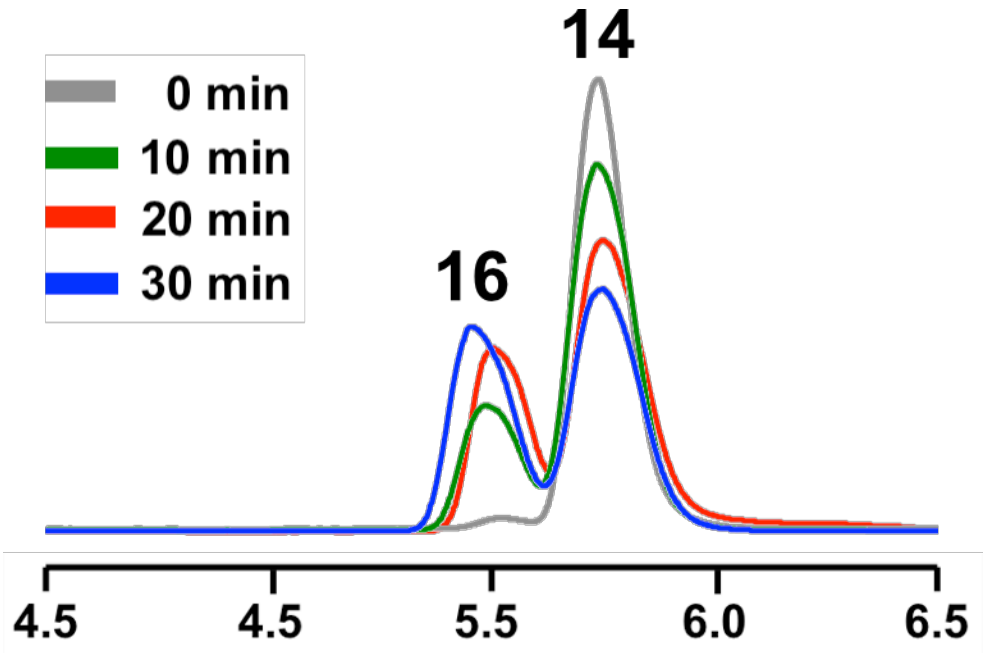

Figure 3.19 HPLC/ELSD traces monitoring the progress of the remodeling. ELSD spectra corresponding to the RNCL exchange reaction between phospholipid **14** and the N-methylated cysteine-functionalized lysolipid **15**, leading to an equimolar mixture of **14** and **16**. The retention times for all the species were verified by mass spectrometry and the use of known standards.

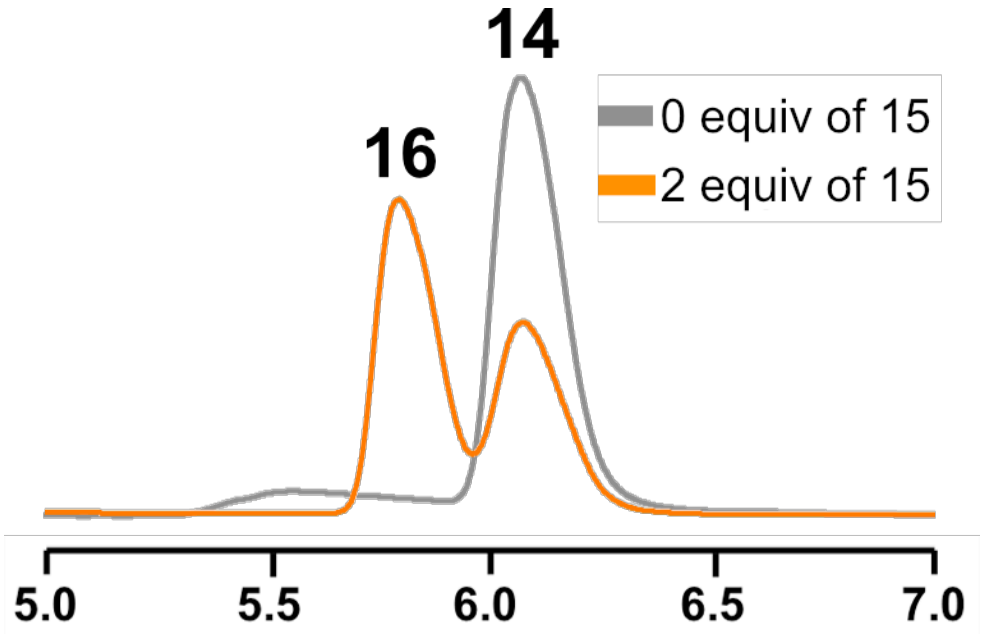

Figure 3.20 ELSD spectra corresponding to the RNCL exchange reaction between phospholipid **14** and 2.0 equivalents of the N-methylated cysteine-functionalized lysolipid **15**, leading to an approximately 1:2 mixture of **14** and **16**. The retention times for all the species were verified by mass spectrometry and the use of known standards.

3.4 Biomimetic Membrane Remodeling

Living cells chemically remodel phospholipids to alter larger-scale physical properties of their membranes.[65,66] An important example is the formation of phase-separated compositional lipid microdomains known as "lipid rafts".[85] Lipid rafts have been implicated in a number of important cellular processes including signal transduction,[86] membrane trafficking,[87] and protein sorting,[88] where changes in lipid organization can have a profound impact on the function of membrane proteins. Additionally, lipid raft domains facilitate budding,[86] disease states,[89] viral assembly,[90] and infection.[91] Phase transitions in lipid mixtures with the same hydrophilic head are driven by differences in the order state of lipid tails.[46,92] Significantly, the degree of unsaturation in phospholipid tails can change the liquid–gel transition temperature and, therefore, the order state of the chain. With this in mind, we determined whether lipid remodeling of N-methylated amidophospholipids could trigger significant changes in vesicle composition and spatial organization. We used electroformation in the presence of 0.1 mol % of Texas Red DHPE dye to create labeled GUVs containing a mixture of phospholipids **14** and **21** with cholesterol in a molar ratio of 1:1:0.8. Upon addition of 1.0 equivalent of lysolipid **17**, formation of a new class of GUVs composed of phospholipids **18**, **22**, and cholesterol was detected. Consequently, a dramatic shift from one miscible phase to two immiscible phases was observed, as indicated by the partitioning of Texas Red DHPE dye into discrete circular regions of the membrane (Figure 3.21). These events occurred within 2–3 min and were apparent in nearly all vesicles observed. Alternatively, microdomain formation was not detected over the same observed period when GUVs composed of **14**, **21**, and cholesterol were treated with the unreactive lysolipid 1-palmitoyl-2-hydroxy-sn-glycero-3-phosphocholine. Furthermore, remodeling of the same GUVs by addition of the reactive oleoyl lysolipid **23** (Figures 3.2 and 3.5) to generate the phospholipids **24** and **25** (Figures 3.2 and 3.5) showed no microdomain formation, suggesting that the presence of fully saturated lipid

species is necessary to promote such events. We postulate that lipid microdomains emerge as the composition of the phospholipid membrane shifts to mixtures similar to those known to create two immiscible domains. In situ remodeling of phospholipids by lipid tail exchange leads to subsequent micrometer-scale changes in membrane composition and morphology.

In addition to controlling membrane fluidity, cells are able to modulate their plasmalemma charge through the metabolism of phospholipids bearing different head groups.[64,93] The ability to precisely control membrane charge is crucial for a number of cell functions including signaling,[94] lipid trafficking,[95] and phagocytosis.[93] For instance, during phagocytosis the negative charge of the inner membrane is critical for recruitment and anchoring of proteins required for phagosome formation.[93] The subsequent loss of membrane charge, induced by metabolism of negatively charged phospholipids, enables dissociation of membrane-bound proteins during phagosome maturation and sealing.[93] By using a lysolipid possessing a negatively charged head group, we hypothesized that we could modulate the membrane association of amphiphysin,[96,97] a similar membrane-associated protein. Amphiphysin is a protein involved in endocytosis that is known to bind to negatively charged phospholipid membranes and induce positive curvature in the surface.[96] To determine whether remodeling our model membranes could drive similar effects, we first synthesized GUVs composed of neutral N-methylated phosphatidylcholine phospholipid **14** and then added 1.0 equivalent of negatively charged phosphatidylglycerol lysolipid **26** (Figures 3.2, 3.5 and 3.22), observing the formation of a new class of GUVs composed of phosphatidylglycerol phospholipid **27** (Figures 3.2, 3.5, 3.22, and 3.23). After reaction completion, amphiphysin (Figure 3.24) was subsequently added to the mixture, and dramatic curvature events were observed in the negatively charged GUVs of **27** within 1 min of protein addition (Figure 3.25). This behavior was not observed in phospholipid **14** GUVs before the addition of **26** or as a result of the remodeling itself, indicating that the change in membrane charge is responsible for the observed protein

binding behavior. Analogous remodeling experiments in the presence of the protein epsin 1[98] (Figure 3.24) showed identical membrane curvature events (Figure 3.26). Alternatively, morphological transformations were not detected over the same observed period when controls were carried out. In addition, treatment of phospholipid **14** GUVs with the neutral oleoyl phosphatidylcholine lysolipid **23** resulted in phospholipid **24** membranes that were not deformed in the presence of amphiphysin or epsin 1, suggesting that the membrane remodeling alone is not responsible for protein activity.

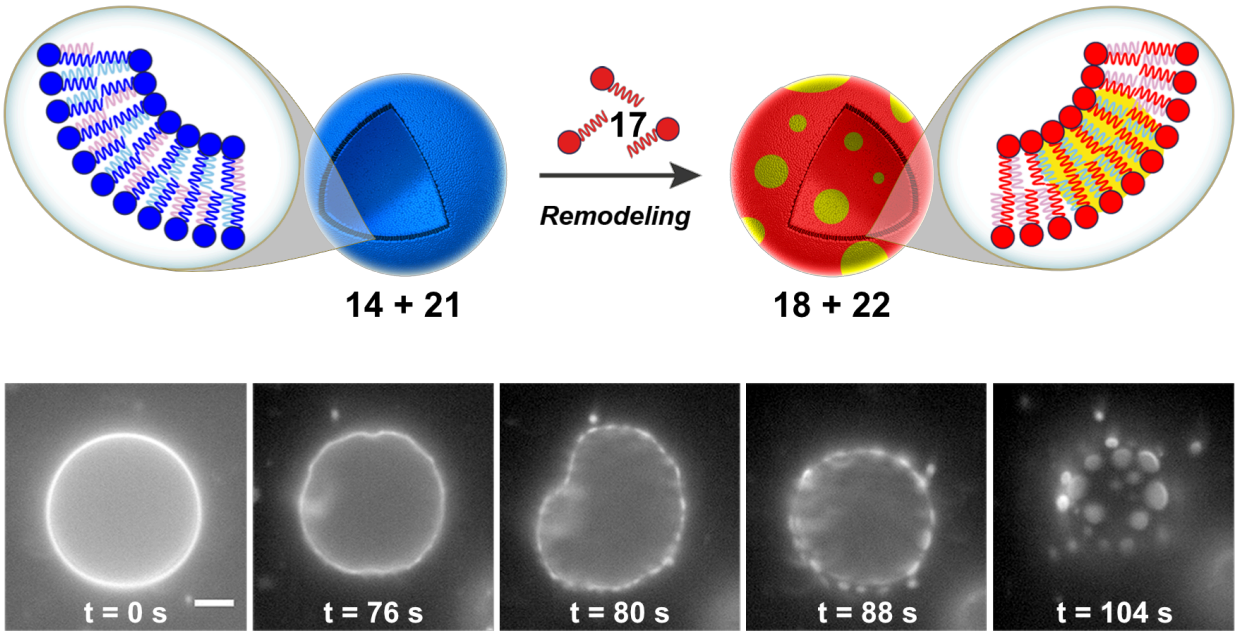

Figure 3.21 Lipid microdomain formation induced by RNCL-based remodeling. Top, Schematic representation of microdomain generation directed by membrane remodeling of phospholipid vesicles. GUVs composed of **14**, **21**, and cholesterol (molar ratio of 1:1:0.8) containing 0.1 mol % of Texas Red® DHPE dye are remodeled by RNCL exchange reactions with cysteine-functionalized lysolipid **17**, leading to the formation of a new class of GUVs composed of **18**, **22** and cholesterol. Consequently, a dramatic shift from one miscible phase to two immiscible phases takes place. Bottom, Fluorescence microscopy images tracking membrane remodeling and subsequent microdomain formation driven by the RNCL exchange reactions. An aqueous buffer solution of **14**:**21**:cholesterol GUVs (400 μM) and cysteine-functionalized lysolipid **17** (400 μM) in the presence of DTT (2 mM) was imaged at different times after initial mixing (from 0 to 104 s). Initially, lipid microdomains were not present. However, shortly after the species had been mixed, lipid remodeling took place and microdomain formation was observed, as indicated by the partitioning of Texas Red® DHPE dye into discrete circular regions of the membrane. Scale bar denotes 10 μm.

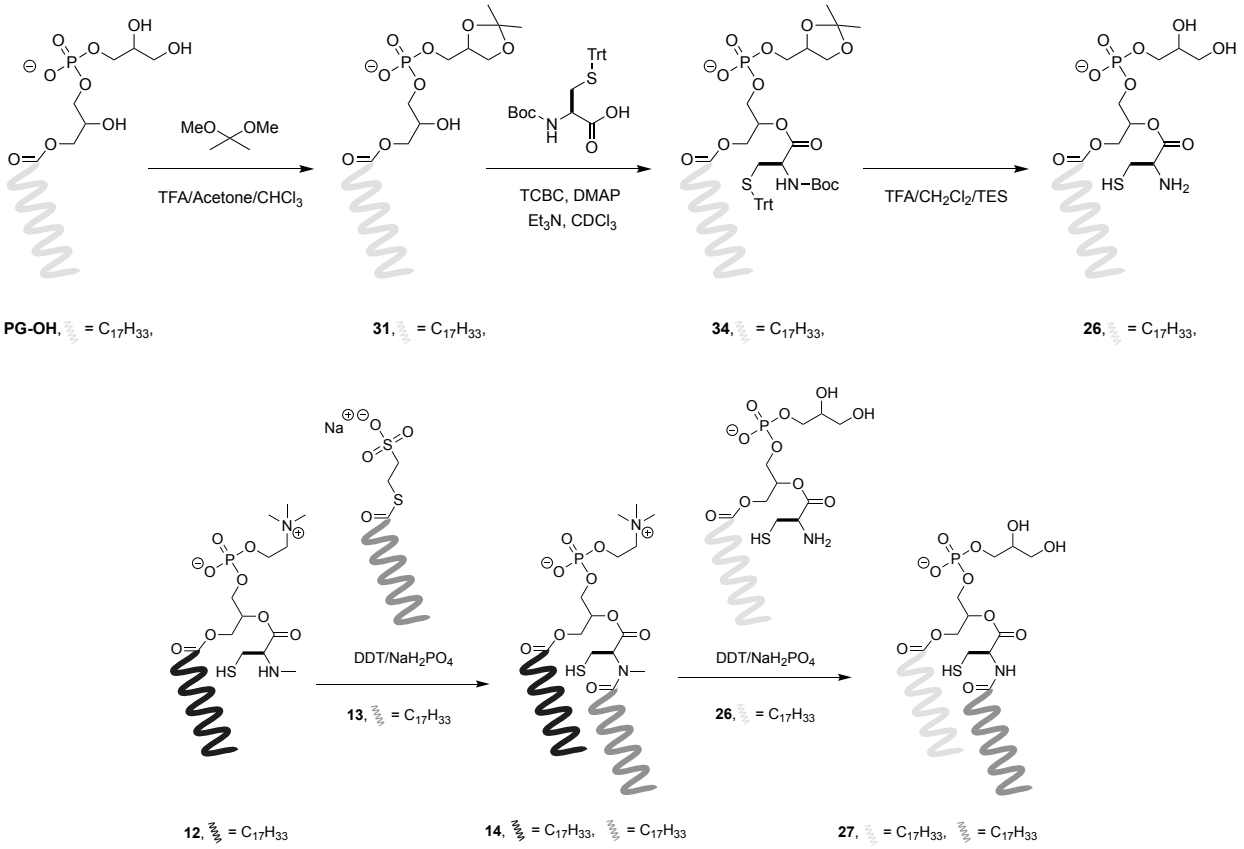

Figure 3.22 De novo formation and head group remodeling of phospholipid membranes. Top, Synthesis of negatively charged cysteine-functionalized phosphatidylglycerol lysolipid **26**. Bottom, De novo synthesis of phospholipids by NCL reaction of the N-methylated cysteine-functionalized phosphatidylcholine lysolipid **12** and MESNA oleoyl thioester **13**, followed by subsequent head group remodeling of the corresponding neutral phospholipid **14** by RNCL in the presence of the cysteine-functionalized phosphatidylglycerol lysolipid **26**.

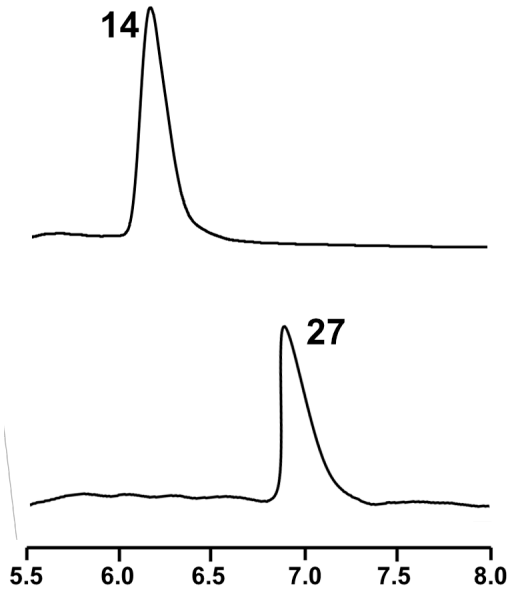

Figure 3.23 HPLC/ELSD spectra monitoring the head group remodeling of phospholipid membrane GUVs driven by RNCL. A, ELSD spectra showing the GUVs from phospholipid **14**. B, ELSD spectra corresponding to the RNCL exchange reaction between the GUVs from phospholipid **14** and the cysteine-functionalized lysolipid **26**, leading to the selective formation of **27**. Retention times (Rt's) for phospholipids (**14** and **27**) were verified by mass spectrometry.

A)

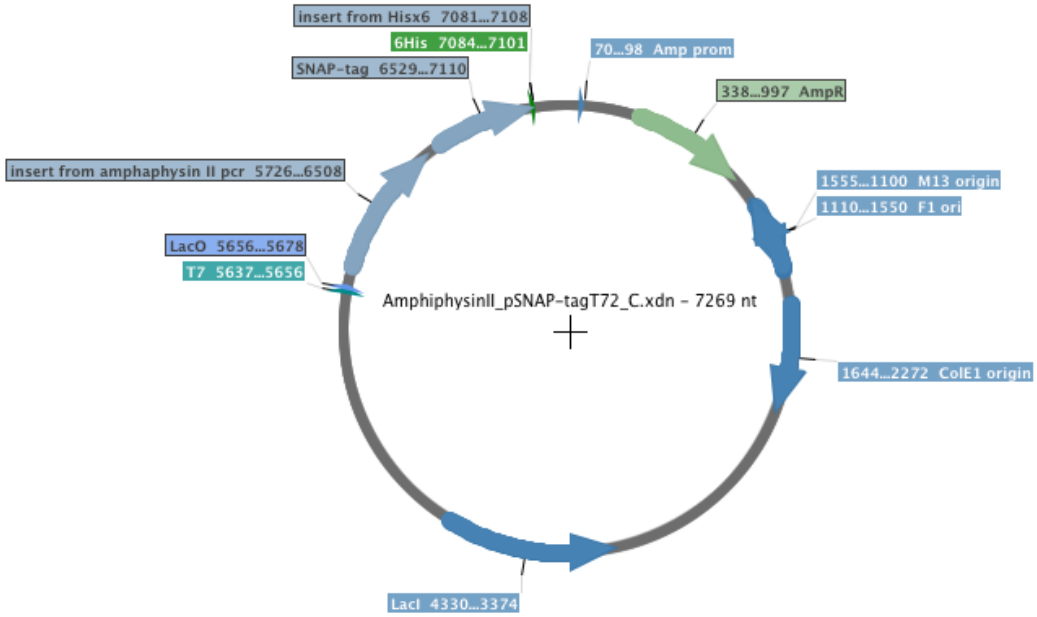

B)

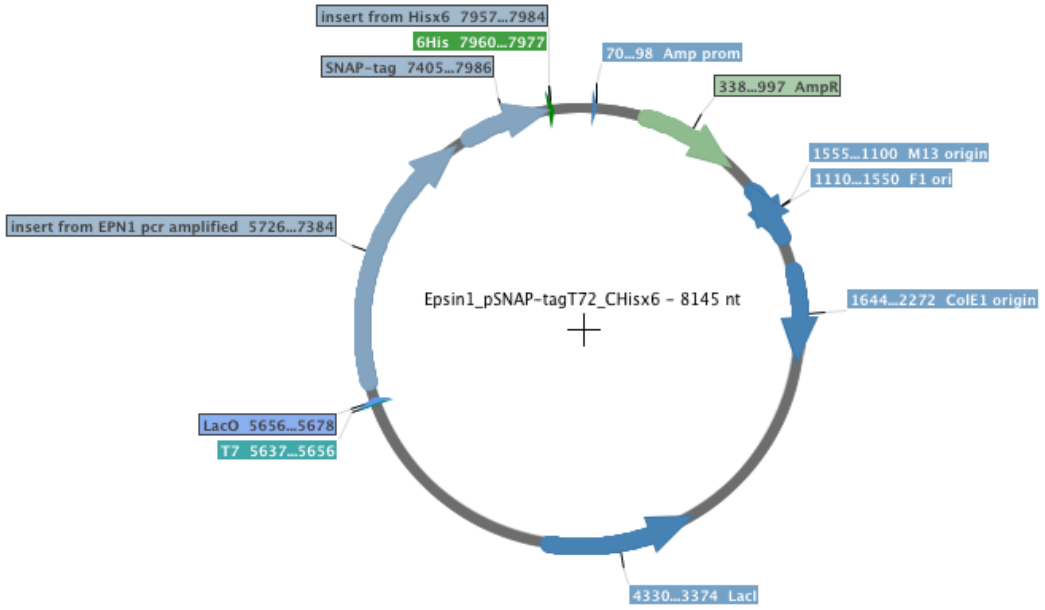

Figure 3.24 Plasmid maps corresponding to amphiphysinII_pSNAP-tagT72_C.xdn - 7269 nt (A) and epsin1_pSNAP-tagT72_CHisx6 - 8145 nt (B).

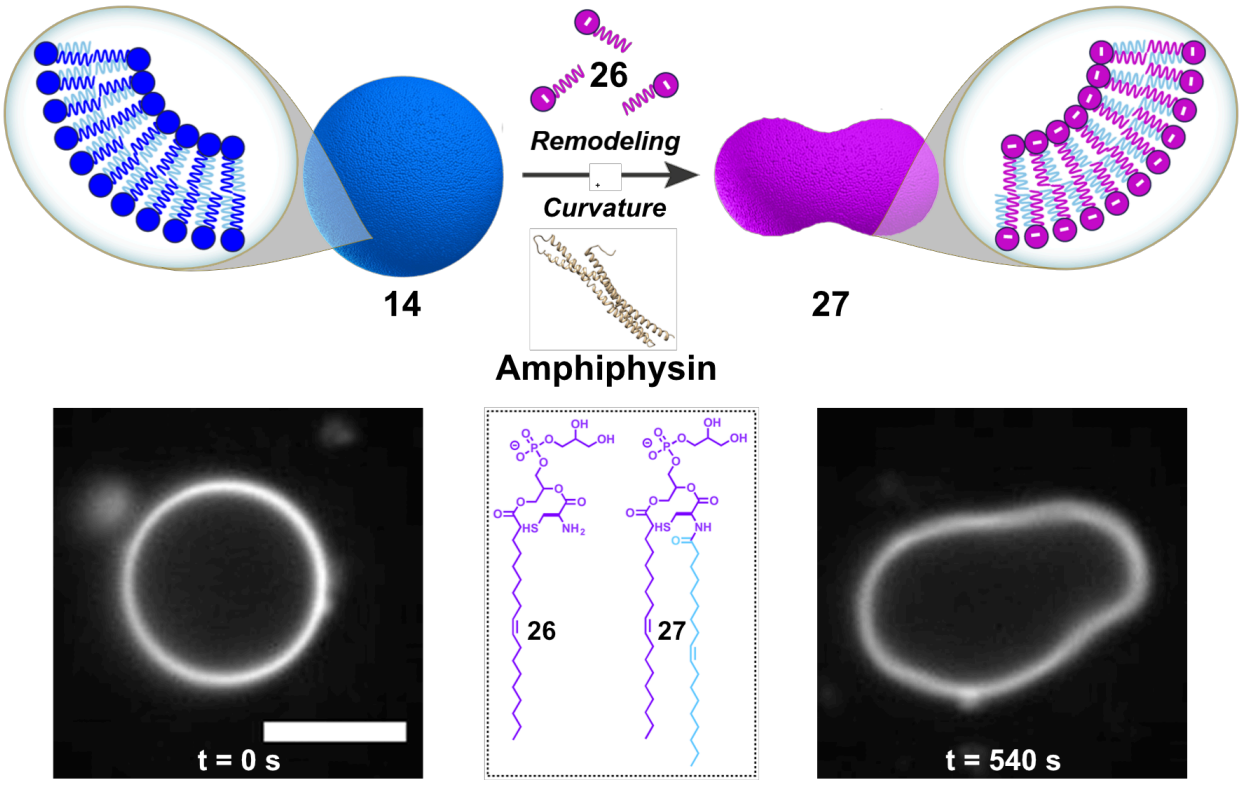

Figure 3.25 Membrane curvature induced by RNCL-based remodeling. GUVs composed of neutral phospholipid **14** containing 0.1 mol % of Bodipy® FL DHPE dye are remodeled by RNCL exchange reactions with negatively charged lysolipid **26**, leading to the formation of a new class of GUVs composed of **27**. After addition of amphiphysin to the mixture, dramatic membrane curvature events in the negatively charged GUVs **27** were observed as a result of the protein binding. Scale bar denotes 5 μm.

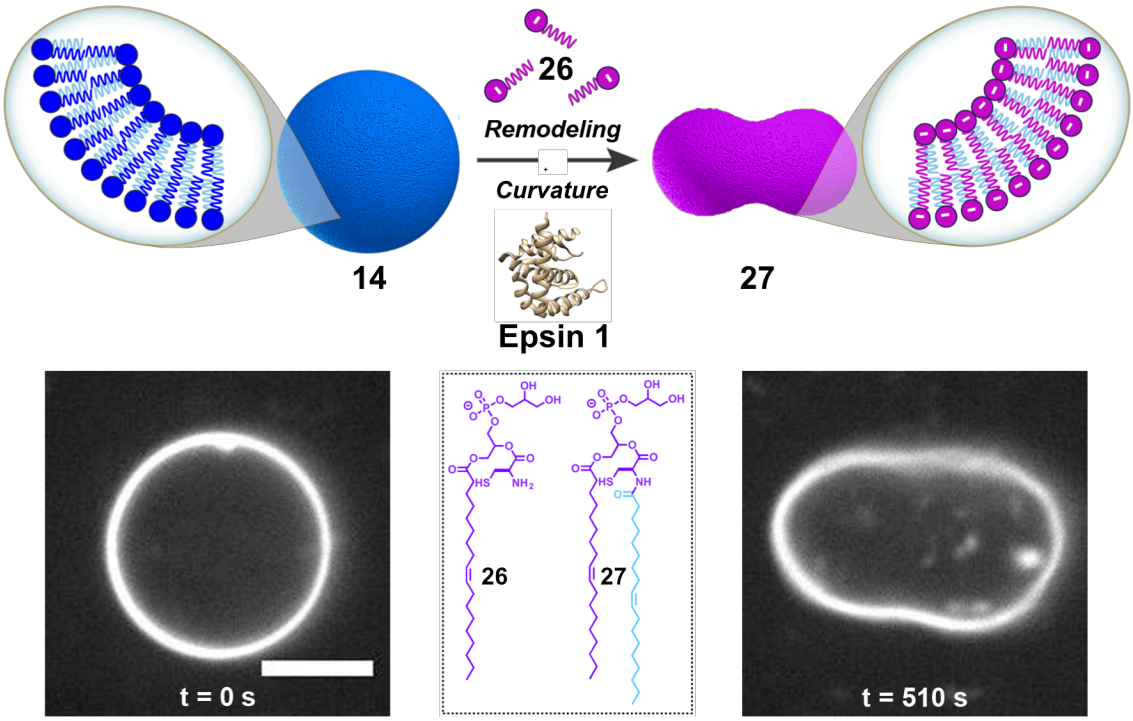

Figure 3.26 Membrane curvature induced by RNCL-based remodeling. GUVs composed of neutral phospholipid **14** containing 0.1 mol % of Bodipy® FL DHPE dye are remodeled by RNCL exchange reactions with negatively charged lysolipid **26**, leading to the formation of a new class of GUVs composed of **27**. After addition of epsin 1 to the mixture, dramatic membrane curvature events in the negatively charged GUVs **27** were observed as a result of the protein binding. Scale bar denotes 10 μm.

3.5 Conclusion

In conclusion, we have developed for the first time, to our knowledge, simplified model membranes that mimic how native phospholipid membranes are synthesized and remodeled. The NCL reaction can be efficiently used for the preparation of amidophospholipids that self-assemble in situ to form membrane vesicles. We demonstrate subsequent membrane remodeling directed by the RNCL reaction for the construction of dynamic membranes that can spontaneously change their composition and morphology. Our approach overcomes kinetic barriers to lipid remodeling that are faced with standard liposome preparations. As such, future opportunities could involve exploiting our system to further study the specific effects of lipid remodeling on membrane curvature and organization. Furthermore, our methodology might be harnessed to lower the barrier

to changing the size and shape of preformed vesicles in the presence of appropriate stabilizing scaffolds, such as membrane coat proteins,[99] provided that N-terminal cysteine residues are absent. The described NCL-based de novo lipid formation and RNCL-based lipid remodeling combined approach should be applicable for studying and exploiting the effects of membrane exchange in minimal model membranes.

3.7 Experimental Methods

3.7.1 General Considerations

Commercially available 1-palmitoyl-2-hydroxy-sn-glycero-3-phosphocholine (Lyso C16 PC-OH), 1-oleoyl-2-hydroxy-sn-glycero-3-phosphocholine (Lyso C18 PC-OH), 1-oleoyl-2-hydroxy-sn-glycero-3-phospho-(1'-rac-glycerol) (sodium salt) (Lyso C18 PG-OH) and 1-palmitoyl-2-oleoyl-sn-glycero-3-phosphocholine (POPC) were used as obtained from Avanti® Polar Lipids. N-Boc-L-Cys(Trt)-OH, iodomethane (IMe), sodium hydride (NaH), tetrahydrofuran (THF), N,N'-diisopropylcarbodiimide (DIC), 4-dimethylaminopyridine (DMAP), trifluoroacetic acid (TFA), triethylsilane (TES), 2,2-dimethoxypropane (DMP), 2,4,6-trichlorobenzoyl chloride (TCBC), oleic acid, N-(3-dimethylaminopropyl)-N'-ethylcarbodiimide hydrochloride (EDC.HCl), sodium 2-mercaptoethanesulfonate (MESNA), sodium phosphate monobasic monohydrate (NaH2PO4.H2O), dithiothreitol (DTT), 8-hydroxypyrene-1,3,6-trisulfonic acid (HPTS), 1,6-diphenyl-1,3,5-hexatriene (DPH) and cholesterol were obtained from Sigma-Aldrich. Texas Red® 1,2-dihexadecanoyl-sn-glycero-3-phosphoethanolamine, triethylammonium salt (Texas Red® DHPE) and Bodipy® 1,2-dihexadecanoyl-sn-glycero-3-phosphoethanolamine, triethylammonium salt (Bodipy® FL DHPE) were obtained from Life Technologies. Deuterated chloroform (CDCl3), methanol (CD3OD) and dimethyl sulfoxide (d6-DMSO) were obtained from Cambridge Isotope

Laboratories. All reagents obtained from commercial suppliers were used without further purification unless otherwise noted. Analytical thin-layer chromatography was performed on E. Merck silica gel 60 F254 plates. Compounds, which were not UV active, were visualized by dipping the plates in a ninhydrin or potassium permanganate solution and heating. Silica gel flash chromatography was performed using E. Merck silica gel (type 60SDS, 230-400 mesh). Solvent mixtures for chromatography are reported as v/v ratios. HPLC analysis was carried out on an Eclipse Plus C8 analytical column with Phase A/Phase B gradients [Phase A: H2O with 0.1% formic acid; Phase B: MeOH with 0.1% formic acid]. HPLC purification was carried out on Zorbax SB-C18 semipreparative column with Phase A/Phase B gradients [Phase A: H2O with 0.1% formic acid; Phase B: MeOH with 0.1% formic acid]. Proton nuclear magnetic resonance (1H NMR) spectra were recorded on a Varian VX-500 MHz or Jeol Delta ECA-500 MHz spectrometers, and were referenced relative to residual proton resonances in CDCl3 (at 7.24 ppm), CD3OD (at 4.87 or 3.31 ppm) or d6-DMSO (at 2.50 ppm). Chemical shifts were reported in parts per million (ppm) relative to tetramethylsilane (0.00). 1H NMR splitting patterns are assigned as singlet (s), doublet (d), triplet (t), quartet (q) or pentuplet (p). All first-order splitting patterns were designated on the basis of the appearance of the multiplet. Splitting patterns that could not be readily interpreted are designated as multiplet (m) or broad (br). Carbon nuclear magnetic resonance (13C NMR) spectra were recorded on a Varian VX-500 MHz or Jeol Delta ECA-500 MHz spectrometers, and were referenced relative to residual proton resonances in CDCl3 (at 77.23 ppm), CD3OD (at 49.15 ppm) or d6-DMSO (at 39.51 ppm). Electrospray Ionization-Time of Flight (ESI-TOF) spectra were obtained on an Agilent 6230 Accurate-Mass TOFMS mass spectrometer. Anisotropy measurements were obtained on a SPEX FluoroMax-3 spectrofluorometer. Transmission electron microscopy images were recorded on a FEI TecnaiTM Sphera 200 kV microscope equipped with a LaB6 electron gun, using the standard cryotransfer holders developed by Gatan, Inc. Giant

unilamellar vesicle (GUV) electroformation was carried out on a Vesicle Prep Pro® device developed by Nanion Technologies.

3.7.2 Micelle Sizes: Critical Micelle Concentrations (cmc's)

100.0 µL of aqueous solutions (10 mM, 1 mM, 100 µM, 10 µM and 1 µM) of the control (lysolipid1-palmitoyl-2-hydroxy-sn-glycero-3-phosphocholine, Lyso C16 PC-OH) and the precursors (**12**, **13**, **15**, **17** or **19**) were analyzed by Dynamic Light Scattering (DLS) in order to determine the micelle sizes and the critical micelle concentrations (cmc's).

3.7.3 De Novo Phospholipid Synthesis

General procedure. N-methylated cysteine-modified lysolipid **12** (3.20 mg, 5.01 µmol) and MESNA thiooleate **13** (2.14 mg, 5.01 µmol) were dissolved in 1.00 mL of 25 mM DTT in 200 mM NaH2PO4 pH 7.1 buffer and stirred under N2 for 30 min at rt, affording the phospholipid **14**. Phospholipids **16**, **18**, **20**, **21** and **22** were also prepared in the same way, using the corresponding lysolipids **12**, **15** or **17**, and MESNA thioesters **13** or **19**.

3.7.4 De Novo Phospholipid Synthesis: In Situ Vesicle Formation

5.0 µL of a 25 mM DTT solution in 200 mM NaH2PO4 pH 7.1 buffer were added to 2.5 µL of a 10 mM solution of N-methylated cysteine-based lysolipid **12** in 200 mM NaH2PO4 pH 7.1 buffer. Afterward, 2.5 µL of a 10 mM solution of MESNA thiooleate **13** in NaH2PO4 pH 7.1 buffer were added, and the mixture was briefly agitated. The resulting solution was added to a glass microscope slide and covered with a glass coverslip supported with vacuum grease. The sample was then monitored by phase contrast microscopy in order to analyze the in situ phospholipid **14** vesicle formation.

3.7.5 Remodeling: Lipid Chain RNCL Exchange

General procedure. 100.0 μL of a previously de novo formed phospholipid **14** solution were added to cysteine-modified lysolipid (N-methylated **15** or un-N-methylated **17**; 0.50 μmol), and stirred under N_2 for 30 min at rt, affording the corresponding remodeled phospholipids (equimolar mixture of N-methylated phospholipids **14** and **16** or un-N-methylated phospholipid **18**). Phospholipids **21** and **22** were also prepared in the same way, using the corresponding de novo formed phospholipid **20**, and lysolipids **12** or **17**.

3.7.6 Remodeling: Head Group RNCL Exchange

General procedure. 100.0 μL of a previously de novo formed N-methylated phosphatidylcholine phospholipid **14** solution were added to cysteine-modified phosphatidylglycerol lysolipid **26** (0.50 μmol), and stirred under N_2 for 30 min at rt, affording the corresponding remodeled phosphatidylglycerol phospholipid **27**.

3.7.7 LC/MS Analysis

De novo formation (NCL reaction) and remodeling (RNCL reaction) of phospholipid membranes were performed in the appropriate buffer (200 mM NaH2PO4 pH 7.1 buffer containing 25 mM DTT) as described above. Aliquots of 1.5 μL of sample were taken at various time points, diluted with 50.0 μL of MeOH and analyzed using an Eclipse Plus C8 analytical column (5% Phase A in Phase B, 5.5 min) with an Evaporative Light Scattering Detector (ELSD) at a flow of 1.0 mL/min. For all LC/MS runs, solvent Phase A consisted of H2O with 0.1% formic acid and solvent Phase B of MeOH with 0.1% formic acid.

3.7.8 Fluorescence Microscopy of Phospholipid Membrane Vesicles: Texas Red® DHPE

In situ vesicle formation. 5.0 μL of a 25 mM DTT solution in 200 mM NaH2PO4 pH 7.1 buffer were added to 2.5 μL of a 10 mM solution of N-methylated cysteine-based lysolipid **12** in 200 mM NaH2PO4 pH 7.1 buffer. Afterward, 2.5 μL of a 10 mM solution of MESNA thiooleate **13** in NaH2PO4 pH 7.1 buffer were added, and the mixture was briefly agitated. Then, 5.0 μL of the resulting solution were mixed with 0.1 μL of a 100 μM Texas Red® DPHE dye solution in EtOH, and the resulting solution was added to a glass microscope slide and covered with a glass coverslip supported with vacuum grease. The corresponding sample was then monitored by fluorescence and phase contrast microscopy in order to analyze the in situ vesicle formation and determine the corresponding vesicular structure.

Hydration Method

10.0 μL of a 20 mM solution of phospholipid **14** in CHCl3 were added to a 1 mL vial, placed under N_2 and dried for 15 min to prepare a lipid film. Then, 200.0 μL of H_2O were added and the solution was tumbled at 25 ºC for 1 h. Afterward, to 10.0 μL of this 1 mM aqueous solution of phospholipid **14** were added 0.1 μL of a 100 μM Texas Red® DPHE dye solution in EtOH, and the mixture was briefly agitated. The corresponding sample was finally monitored by fluorescence and phase contrast microscopy in order to determine the vesicle structure.

Sonication Method

10.0 μL of a 20 mM solution of phospholipid **14** in CHCl3 were added to a 1 mL vial, placed under N_2 and dried for 15 min to prepare a lipid film. Then, 200.0 μL of H_2O were added, and the resulting mixture was sonicated with heat (≈55ºC) for 1 h. Afterward, to 10.0 μL of this 1 mM aqueous solution of phospholipid **14** were added 0.1 μL of a 100 μM Texas Red® DPHE dye

solution in EtOH, and the mixture was briefly agitated. The corresponding sample was finally monitored by fluorescence and phase contrast microscopy in order to determine the vesicle structure.

3.7.9 Transmission Electron Microscopy (TEM) Studies

General. A deposition System Balzers Med010 was used to evaporate a homogeneous layer of carbon. The samples were collected over 400 mesh Cu grids. The grids were then negatively stained with a solution of 1% (w/w) uranyl acetate. Micrographs were recorded on a FEI TecnaiTM Sphera microscope operating at 200 kV and equipped with a LaB6 electron gun, using the standard cryotransfer holders developed by Gatan, Inc. For image processing, micrographs were digitized in a Zeiss SCAI scanner with different sampling windows.

TEM measurements. Copper grids (formvar/carbon-coated, 400 mesh copper) were prepared by glow discharging the surface at 20 mA for 1.5 min. Once the surface for vesicle adhesion is ready, 3.5 μL of a 5 mM solution of phospholipid **14** in H_2O (previously sonicated at ≈55 ºC for 1 h) was deposited on the grid surface. This solution was allowed to sit for 10 seconds before being washed away with 10 drops of glass distilled H_2O and subsequent staining with 3 drops of 1% w/w uranyl acetate. The stain was allowed to sit for 10 seconds before wicking away with filter paper. All grid treatments and simple depositions were on the dark/shiny/glossy formvar-coated face of the grid (this side face up during glow discharge). Samples were then imaged via TEM, revealing the presence of several populations of spherical compartments (50-950 nm in diameter), consistent with the vesicle architecture.

In situ TEM measurements. Copper grids (formvar/carbon-coated, 400 mesh copper) were prepared by glow discharging the surface at 20 mA for 1.5 min. Once the surface for vesicle adhesion is ready, 3.5 μL of a previously in situ formed phospholipid **14** sample in 200 mM NaH2PO4 pH 7.1 buffer was deposited on the grid surface. This solution was allowed to sit for 10 seconds before being washed away with 10 drops of glass distilled H_2O and subsequent staining with 3 drops of 1% w/w uranyl acetate. The stain was allowed to sit for 10 seconds before wicking away with filter paper. All grid treatments and simple depositions were on the dark/shiny/glossy formvar-coated face of the grid (this side face up during glow discharge). Samples were then imaged via TEM, revealing the presence of several populations of spherical compartments (50-950 nm in diameter), consistent with the vesicle architecture.

3.7.10 Encapsulation Experiments

Encapsulation of HPTS (Standard method)

60.0 μL of a 20 mM solution of phospholipid **14** in $CHCl_3$ were added to a 1 mL vial, placed under N_2 and dried for 15 min to prepare a lipid film. Then, 240.0 μL of a 100 μM HPTS solution in H_2O were added and the mixture was tumbled at 25 ºC for 1 h. Afterwards, the solution was transferred to a 100K spin filter and centrifuged for 10 min at 9000-10000 rcf in order to remove the non-encapsulated HPTS. Then, the sample was washed and centrifuged with H_2O (5 × 250 μL). The lipid-containing solution was finally examined by fluorescence microscopy, observing vesicles containing the desired HPTS.

Encapsulation of HPTS (Inverse emulsion method)

60.0 µL of a 20 mM solution of phospholipid **14** in CHCl3 were added to a 1 mL vial, placed under N_2 and dried for 15 min to prepare a lipid film. Then, 200.0 µL of mineral oil (Fisher Chemical, O122-1) were added and placed under N_2 to displace the air above the mineral oil. The resulting mixture was sonicated with heat (≈55ºC) for 1 h. Afterward, 100.0 µL of the amidophospholipid oil was added to a 1 mL eppendorf. Then, 10.0 µL of the upper buffer [50 µM HPTS + 200 mM sucrose in 100 mM HEPES buffer pH 7.5 solution] was added, and the resulting mixture was flicked and vortexed until it was a cloudy emulsion. The corresponding emulsion was added to a 1 mL eppendorf containing 100.0 µL of the lower buffer [200 mM glucose in 100 mM HEPES buffer pH 7.5 solution], so it floated on top. Then, we waited for 10 min. After this time, the sample was centrifuged for 10 min at 9000-10000 rcf. The sample was separated from the oil (either aspirating off the oil or using a syringe/needle to collect the sample from the bottom). The corresponding sample contained vesicles encapsulating HPTS that were observed using fluorescence microscopy.

In situ encapsulation of HPTS

1-oleoyl-2-(MeN-L-Cys)-sn-glycero-3-phospho-choline (**12**, 0.50 mg, 0.78 µmol) was dissolved in 78.0 µL of a 100 µM solution of HPTS in 200 mM NaH2PO4 pH 7.1 buffer. Then, 78.0 µL of a 50 mM DTT solution in 200 mM NaH2PO4 pH 7.1 buffer was added. Finally, MESNA-thiooleate **13** (0.34 mg, 0.78 µmol) was added and the resulting mixture was stirred under N_2 at rt. After 30 min, the reaction was transferred to a 100K spin filter and centrifuged for 10 min at 9000-10000 rcf in order to remove the non-encapsulated HPTS. Then, the sample was washed and centrifuged with a 200 mM solution of NaH_2PO_4 pH 7.1 buffer (5 × 250 µL). The lipid-containing solution was finally examined by fluorescence microscopy, observing vesicles containing the desired HPTS.

3.7.11 Anisotropy Studies

Vesicle preparation and extrusion

10.0 µL of a 100 mM solution of phospholipid (DOPC, POPC, **14**, **16** or **18**) in $CHCl_3$ were added to a 1 mL vial, placed under N_2 and dried for 15 min to prepare a lipid film. The dried film was hydrated in 500.0 µL of H_2O [Final concentration of phospholipid: 2 mM]. The lipid solution was briefly vortexed and then sonicated with heat (≈55ºC) for 45 min. Once the sample was fully hydrated, the vesicles were extruded through 100 nm membrane. Extruded vesicles were finally analyzed by Dynamic Light Scattering (DLS).

Anisotropy measurements

5.0 µL of a 500 µM solution of DPH in EtOH were added to 495.0 µL of 100 nm phospholipid (DOPC, POPC, **14**, **16** or **18**) extruded vesicles [Final concentration of DPH: 5 µM, 1% v/v]. The solution was tumbled at 25 ºC overnight. Steady-state anisotropy was measured at different temperatures (from -10 to 40 ºC) on a Perkin spectrophotometer with a manual polarizer accessory and peltier temperature controller.

3.7.12 Fluorescence Microscopy of Giant Unilamellar Vesicles (GUVs): Bodipy® FL DHPE

GUVs preparation: electroformation method. 20.0 µL of a 5 mM solution of phospholipid **14** containing 0.1 mol% Bodipy® FL DHPE in $CHCl_3$ were placed on the conductive side of an indium tin oxide (ITO) slide. The slide was then dried in vacuo for 1 h, after which a rubber O-ring was placed around the dried lipid film and filled with 260.0 µL of 150 mM sucrose solution. A second ITO slide was placed onto of the first and everything assembled within a Vesicle Prep Pro® device. The giant unilamellar vesicles were electroformed with the following parameters:

Frequency 5 Hz, Amplitude 3 V, Temperature 55 ºC, Rise time 10 min, Main time 120 min, Fall time 10 min. The corresponding sample was finally monitored by fluorescence and phase contrast microscopy in order to determine the giant unilamellar vesicle structure.

3.7.13 GUVs Remodeling: RNCL Exchange

GUVs preparation: electroformation method. 20.0 µL of a 5 mM solution of phospholipid **14** in $CHCl_3$ were placed on the conductive side of an indium tin oxide (ITO) slide. The slide was then dried in vacuo for 1 h, after which a rubber O-ring was placed around the dried lipid film and filled with 260.0 µL of 150 mM sucrose solution. A second ITO slide was placed on top of the first and everything assembled within a Vesicle Prep Pro® device. The giant unilamellar vesicles were electroformed with the following parameters: Frequency 5 Hz, Amplitude 3 V, Temperature 55 ºC, Rise time 10 min, Main time 120 min, Fall time 10 min.

RNCL exchange. 100.0 µL of previously electroformed 3 GUVs solution (Final concentration of phospholipid **14**: 400 µM) and 2.0 µL of 100 mM DTT in 150 mM NaH_2PO_4 pH 7.1 buffer were added to cysteine-modified lysolipid (N-methylated **15** or un-N-methylated **17**; 0.04 µmol), and stirred under N_2 for 30 min at rt, affording the corresponding remodeled GUVs (GUVs from equimolar mixture of N-methylated phospholipids **14** and **16** or GUVs from un-N-methylated phospholipid **18**).

LC/MS analysis. Remodeling (RNCL reaction) of phospholipid GUV membranes were performed in the appropriate buffer as described above. Aliquots of 50.0 µL were analyzed using an Eclipse Plus C8 analytical column (5% Phase A in Phase B, 5.5 min) with an Evaporative Light Scattering

Detector (ELSD) at a flow of 1.0 mL/min. For all LC/MS runs, solvent Phase A consisted of H_2O with 0.1% formic acid and solvent Phase B of MeOH with 0.1% formic acid.

3.7.14 GUVs Remodeling: In Situ Formation of Lipid Microdomains

GUVs preparation: electroformation method. 20.0 μL of a solution of **14**:**21**:cholesterol [Final concentration of phospholipid mixture: 5 mM] in a 1:1:0.8 molar ratio containing 0.1 mol% Texas Red® DHPE in $CHCl_3$ were placed on the conductive side of an indium tin oxide (ITO) slide. The slide was then dried in vacuo for 1 h, after which a rubber O-ring was placed around the dried lipid film and filled with 260.0 μL of 150 mM sucrose solution. A second ITO slide was placed onto of the first and everything assembled within a Vesicle Prep Pro® device. The giant unilamellar vesicles were electroformed with the following parameters: Frequency 5 Hz, Amplitude 3 V, Temperature 55 ºC, Rise time 10 min, Main time 120 min, Fall time 10 min.

In situ formation of microdomains. 9.0 μL of previously electroformed **14**:**21**:cholesterol GUVs (Final concentration of phospholipid mixture: 400 μM), 1.0 uL of 50 mM DTT in 150 mM NaH_2PO_4 pH 7.1 buffer and 9.0 μL of a 400 μM solution of lysolipid **17** in 150 mM NaH2PO4 pH 7.1 buffer were subsequently mixed. Then, 3.0 μL of the resulting solution were added to a glass microscope slide and covered with a glass coverslip supported with vacuum grease. Fluorescence microscope images of microdomain formation were acquired at different times after initial mixing on an Axio Observer Z1 inverted microscope (Carl Zeiss Microscopy GmbH, Germany) with a 60x, 1.4 NA oil immersion objective to an ORCA-Flash 4.0 camera using the manufacturers software (Hamamatsu, Japan). Texas Red® DHPE fluorophore was excited with an HXP 120 metal halide arc lamp (Carl Zeiss Microscopy GmbH, Germany).

3.7.15 GUVs Remodeling: Membrane Curvature

Plasmid construction. Amphiphysin and epsin 1 were cloned from plasmids obtained from Addgene (Plasmid #22213) and DNAsu (Plasmid ID: HsCD00403825) respectively, and inserted into SNAP-tag_EGFP_Hisx6 plasmid as N-terminal fusions. BL21 competent E. coli cells (Agilent Technologies, Santa Clara, CA) were transformed with each plasmid per the manufacturers protocol. Cells were grown in a 1 L culture at 37 ºC with constant shaking and induced with 1 mM IPTG once the culture reached 0.6 O.D. After induction, the culture was grown for 4 additional h after which E. coli were pelleted and stored at 4 ºC until purification. His-tag purification was performed by the manufacturer's specifications using Ni-NTA resin (Thermo, Rockford, IL). Purified protein was exchanged into 1×PBS using a 10 kDa molecular weight cutoff microcentrifuge filter and stored at -80 ºC. Final protein concentration was determined via UV-Vis analysis.

GUVs preparation: electroformation method. 20.0 µL of a solution of phospholipid **14** [Final concentration of phospholipid **14**: 5 mM] containing 0.1 mol% Bodipy® FL DHPE in $CHCl_3$ were placed on the conductive side of an indium tin oxide (ITO) slide. The slide was then dried in vacuo for 1 h, after which a rubber O-ring was placed around the dried lipid film and filled with 265.0 µL of 150 mM sucrose solution. A second ITO slide was placed onto of the first and everything assembled within a Vesicle Prep Pro® device. The giant unilamellar vesicles were electroformed with the following parameters: Frequency 5 Hz, Amplitude 3 V, Temperature 55 ºC, Rise time 10 min, Main time 120 min, Fall time 10 min.

Membrane curvature experiments: remodeling with subsequent addition of protein. 9.0 µL of previously electroformed **14** GUVs (Final concentration of phospholipid **14**: 380 µM), 1.0 uL of

50 mM DTT in 150 mM NaH_2PO_4 pH 7.1 buffer and 9.0 µL of a 380 µM solution of lysolipid **26** in 150 mM NaH_2PO_4 pH 7.1 buffer were subsequently mixed. After incubation during 2 h, 9.0 µL of the resulting solution were added to 1.0 µL of protein (Amphiphysin: 728 µM solution, final concentration: 72.8 µM; Epsin 1: 27.7 µM solution, final concentration: 2.8 µM). Fluorescence microscope images of membrane curvature events were acquired at different times after initial mixing on an Axio Observer Z1 inverted microscope (Carl Zeiss Microscopy GmbH, Germany) with a 60x, 1.4 NA oil immersion objective to an ORCA-Flash 4.0 camera using the manufacturers software (Hamamatsu, Japan). Bodipy® FL DHPE fluorophore was excited with an HXP 120 metal halide arc lamp (Carl Zeiss Microscopy GmbH, Germany).

Membrane curvature experiments: without remodeling but with subsequent addition of protein. (Control). 9.0 µL of previously electroformed 3 GUVs (Final concentration of phospholipid **14**: 380 µM), 1.0 uL of 50 mM DTT in 150 mM NaH2PO4 pH 7.1 buffer and 9.0 µL of 150 mM NaH_2PO_4 pH 7.1 buffer were subsequently mixed. After incubation during 2 h, 9.0 µL of the resulting solution were added to 1.0 µL of protein (Amphiphysin: 728 µM solution, final concentration: 72.8 µM; Epsin 1: 27.7 µM solution, final concentration: 2.8 µM) or H_2O (Control). Fluorescence microscope images of membrane curvature events were acquired at different times after initial mixing on an Axio Observer Z1 inverted microscope (Carl Zeiss Microscopy GmbH, Germany) with a 60x, 1.4 NA oil immersion objective to an ORCA-Flash 4.0 camera using the manufacturers software (Hamamatsu, Japan). Bodipy® FL DHPE fluorophore was excited with a HXP 120 metal halide arc lamp (Carl Zeiss Microscopy GmbH, Germany). No observable membrane curvature events were detected.

Membrane curvature experiments: remodeling without subsequent addition of protein (Control). 9.0 µL of previously electroformed 3 GUVs (Final concentration of phospholipid **14**: 380 µM), 1.0 uL of 50 mM DTT in 150 mM NaH_2PO_4 pH 7.1 buffer and 9.0 µL of a 380 µM solution of lysolipid **26** in 150 mM NaH_2PO_4 pH 7.1 buffer were subsequently mixed. After incubation during 2 h, 9.0 µL of the resulting solution were added to 1.0 µL of H_2O. Fluorescence microscope images were acquired at different times after initial mixing on an Axio Observer Z1 inverted microscope (Carl Zeiss Microscopy GmbH, Germany) with a 60x, 1.4 NA oil immersion objective to an ORCA-Flash 4.0 camera using the manufacturers software (Hamamatsu, Japan). Bodipy® FL DHPE fluorophore was excited with an HXP 120 metal halide arc lamp (Carl Zeiss Microscopy GmbH, Germany). No observable membrane curvature events were detected.

3.7.16 Synthesis of N-(*tert*-butoxycarbonyl)-N-methyl-*S*-trityl-L-cysteine [N-Boc-^{Me}N-*L*-Cys(Trt)-OH] (28)

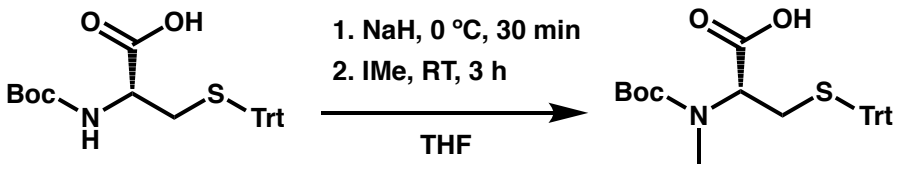

Scheme 3.1 Synthesis of N-(*tert*-butoxycarbonyl)-N-methyl-*S*-trityl-L-cysteine [N-Boc-^{Me}N-*L*-Cys(Trt)-OH] (**28**)

A solution of N-Boc-*L*-Cys(Trt)-OH (1.00 g, 2.16 mmol) in dry THF (16 mL) was treated with NaH (60% in mineral oil, 0.26 g, 6.48 mmol) and stirred at 0 ºC for 30 min. Then, iodomethane (404.0 µL, 6.48 mmol) was added and the resulting mixture was stirred at rt for 3 h. After quenching with water, the THF was removed and the resulting aqueous solution was washed with Et_2O (3 × 10 mL), acidified to pH 3 by addition of HCl (10%), and finally extracted with CH_2Cl_2 (3 × 20 mL). The combined organic layers were dried over Na_2SO_4 and concentrated under reduced

pressure, giving a pale-yellow foam. The corresponding crude was purified by flash chromatography (0-5% MeOH in CH_2Cl_2), affording 0.91 g of **28** as a white foam [89%, R_f = 0.28 (5% MeOH in CH_2Cl_2)]. ^{1}H NMR ($CDCl_3$, 500.13 MHz): 7.41 (d, J = 7.9 Hz, 6H, 6 × CH_{Ar}), 7.30-7.24 (m, 6H, 6 × CH_{Ar}), 7.22-7.16 (m, 3H, 3 × CH_{Ar}), 3.85 (m, 0.5H, 0.5 × CH), 3.59 (m, 0.5H, 0.5 × CH), 2.83-2.75 (m, 1H, 0.5 × CH_2), 2.70-2.55 (m, 4H, 0.5 × CH_2 + 1 × N-CH_3), 1.42 (s, 4.5H, 1.5 × CH_3), 1.35 (s, 4.5H, 1.5 × CH_3). ^{13}C NMR ($CDCl_3$, 125.77 MHz): 176.2 and 175.3, 153.3 and 154.9, 144.6, 129.8, 128.2, 127.0, 81.3 and 81.0, 67.2 and 67.1, 60.6 and 59.7, 34.4 and 33.8, 31.7 and 31.0, 28.5 and 28.4. MS (ESI-TOF) [m/z (%)]: 500 ([M +Na]$^+$, 100). HRMS (ESI-TOF) calculated for $C_{28}H_{31}NO_4SNa$ ([M +Na]$^+$) 500.1866, found 500.1868.

3.7.17 Synthesis of 1-oleoyl-2-[N-Boc-^{Me}N-*L*-Cys(Trt)]-*sn*-glycero-3-phosphocholine (29)

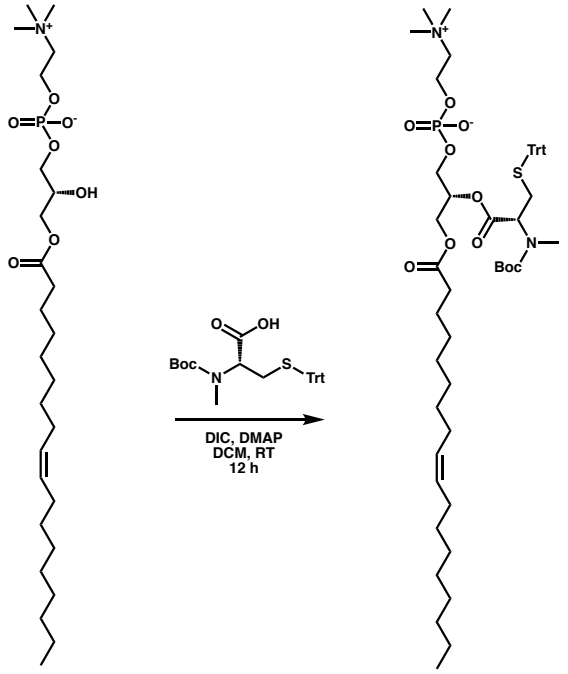

Scheme 3.2 Synthesis of 1-oleoyl-2-[N-Boc-^{Me}N-*L*-Cys(Trt)]-*sn*-glycero-3-phosphocholine (**29**)

A solution of N-Boc-^{Me}N-*L*-Cys(Trt)-OH (**28**, 91.5 mg, 191.7 µmol) in CH_2Cl_2 (7.5 mL) was stirred at rt for 10 min, and then DIC (45.0 µL, 287.5 µmol) and DMAP (11.7 mg, 95.8 µmol) were successively added. After 10 min stirring at rt, 1-oleoyl-2-hydroxy-*sn*-glycero-3-phosphocholine (**Lyso C_{18} PC-OH**, 25.0 mg, 47.9 µmol) was added. After 12 h stirring at rt, the solvent was removed under reduced pressure, and the crude was purified by HPLC, affording 43.1 mg of **29** as a colorless foam [92%, R_t = 9.2 min (Zorbax SB-C18 semipreparative column, 100% *Phase B*, 15.5 min)]. ^{1}H NMR ($CDCl_3$, 500.13 MHz): 7.41-7.33 (d, *J* = 7.9 Hz, 6H, 6 × CH_{Ar}), 7.30-7.23 (m, 6H, 6 × CH_{Ar}), 7.22-7.16 (m, 3H, 3 × CH_{Ar}), 5.39-5.25 (m, 2H, 2 × CH), 5.14-4.97 (m, 1H, 1 × CH), 4.38-4.16 (m, 3H, 1.5 × CH_2), 4.05-3.80 (m, 4H, 1 × CH + 1.5 × CH_2), 3.75-3.61 (m, 2H, 1 × CH_2), 3.24 (s, 9H, 3 × CH_3), 2.77-2.68 (m, 1H, 0.5 × CH_2), 2.62 (s, 3H, 1 × N-CH_3), 2.46-2.56 (m, 1H, 0.5 × CH_2), 2.23-2.07 (m, 2H, 1 × CH_2), 2.04-1.92 (m, 4H, 2 × CH_2), 1.56-1.43

(m, 2H, 1 × CH_2), 1.39 (s, 4.5H, 1.5 × CH_3), 1.36 (s, 4.5H, 1.5 × CH_3), 1.34-1.16 (m, 20H, 10 × CH_2), 0.85 (t, J = 7.1 Hz, 3H, 1 × CH_3). ^{13}C NMR ($CDCl_3$, 125.77 MHz): 173.3, 169.7, 163.9, 155.7, 144.4, 130.0, 129.7, 129.5, 128.0, 126.8, 80.8 and 80.3, 71.8, 67.0, 66.4, 63.1, 62.4, 59.1, 54.5, 33.9, 32.9, 31.9, 31.5, 31.2, 29.8, 29.8, 29.5, 29.3, 29.3, 29.2, 29.2, 29.1, 28.4, 27.2, 27.2, 24.8, 22.7, 14.2. MS (ESI-TOF) [m/z (%)]: 981 ([MH]$^+$, 100). HRMS (ESI-TOF) calculated for $C_{54}H_{82}N_2O_{10}PS$ ([MH]$^+$) 981.5422, found 981.5420.

3.7.18 Synthesis of 1-oleoyl-2-(^{Me}N-*L*-Cys)-*sn*-glycero-3-phosphocholine (12)

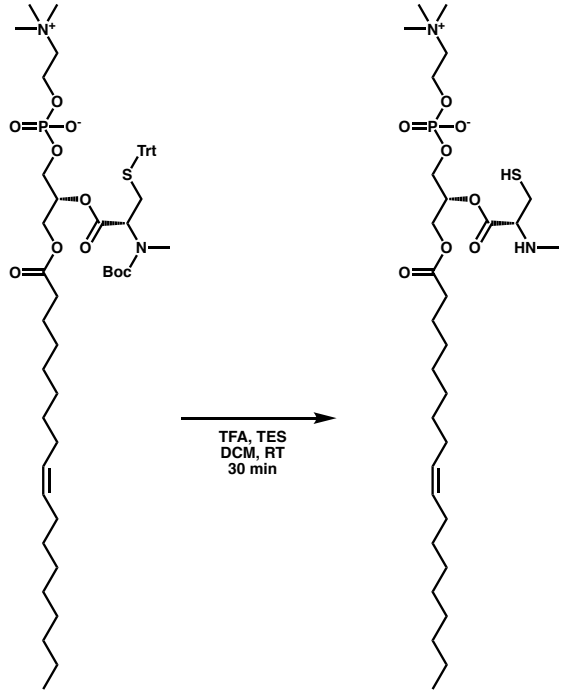

Scheme 3.3 Synthesis of 1-oleoyl-2-(^{Me}N-*L*-Cys)-*sn*-glycero-3-phosphocholine (**12**)

A solution of 1-oleoyl-2-[N-Boc-^{Me}N-*L*-Cys(Trt)]-*sn*-glycero-3-phosphocholine (**29**, 20.0 mg, 20.4 µmol) in 4 mL of TFA/CH_2Cl_2/TES (1.9:1.9:0.2) was stirred at rt for 30 min. After removal of the solvent, the residue was dried under high vacuum for 3 h. Then, the corresponding residue was diluted in MeOH (1 mL), filtered using a 0.2 µm syringe-driven filter, and the crude solution

was purified by HPLC, affording 11.7 mg of the lysolipid **12** as a colorless oil [78%, Rt = 8.7 min (Zorbax SB-C18 semipreparative column, 50% *Phase A* in *Phase B*, 5 min, and then 5% *Phase A* in *Phase B*, 10 min)]. ^{1}H NMR (CD_3OD, 500.13 MHz): 5.47-5.24 (m, 3H, 3 × CH), 4.50-4.37 (m, 1H, 0.5 × CH_2), 4.33-4.20 (m, 3H, 1.5 × CH_2), 4.16-4.00 (m, 2H, 1 × CH_2), 3.98-3.80 (m, 1H, 1 × CH), 3.72-3.59 (m, 2H, 1 × CH_2), 3.45-3.18 (m, 2H, 1 × CH_2), 3.23 (s, 9H, 3 × CH_3), 2.55 (s, 3H, 1 × N-CH_3), 2.35 (t, J = 7.6 Hz, 2H, 1 × CH_2), 2.12-1.92 (m, 4H, 2 × CH_2), 1.73-1.52 (m, 2H, 1 × CH_2), 1.42-1.20 (m, 20H, 12 × CH_2), 0.91 (t, J = 7.0 Hz, 3H, 1 × CH_3). ^{13}C NMR (CD_3OD, 125.77 MHz): 175.0, 171.6, 130.9, 73.9, 67.6, 65.0, 63.5, 62.9, 60.7, 54.8, 35.0, 34.1, 33.2, 31.0, 31.0, 30.8, 30.8, 30.6, 30.6, 30.5, 30.5, 30.4, 28.3, 28.3, 26.1, 23.9, 14.7. MS (ESI-TOF) [m/z (%)]: 639 ($[MH]^+$, 100). HRMS (ESI-TOF) calculated for $C_{30}H_{40}N_2O_8PS$ ($[MH]^+$) 639.3803, found 639.3804.

3.7.19 Synthesis of 1-palmitoyl-2-[N-Boc-^{Me}N-*L*-Cys(Trt)]-*sn*-glycero-3-phosphocholine (30)

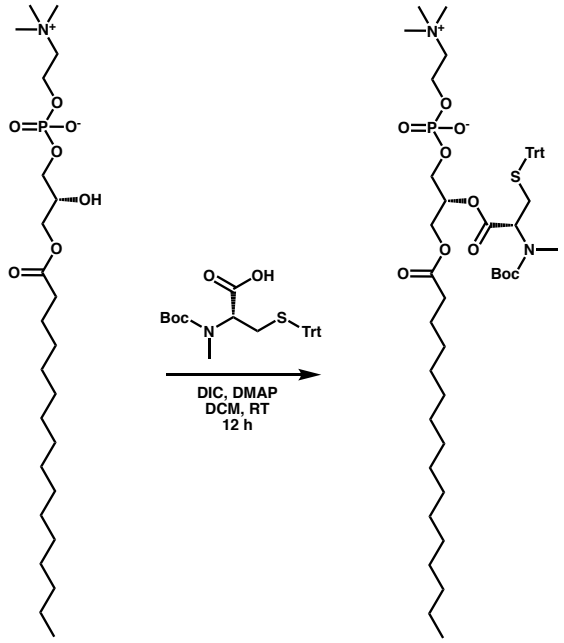

Scheme 3.4 Synthesis of 1-palmitoyl-2-[N-Boc-^{Me}N-*L*-Cys(Trt)]-*sn*-glycero-3-phosphocholine (**30**)

A solution of N-Boc-^{Me}N-*L*-Cys(Trt)-OH (**28**, 77.1 mg, 161.6 µmol) in CH_2Cl_2 (6 mL) was stirred at rt for 10 min, and then DIC (37.0 µL, 242.4 µmol) and DMAP (9.9 mg, 80.8 µmol) were successively added. After 10 min stirring at rt, 1-palmitoyl-2-hydroxy-*sn*-glycero-3-phosphocholine (**Lyso C_{16} PC-OH**, 20.0 mg, 40.4 µmol) was added. After 12 h stirring at rt, the solvent was removed under reduced pressure, and the crude was purified by HPLC, affording 29.7 mg of **30** as a colorless foam [77%, R_t = 8.8 min (Zorbax SB-C18 semipreparative column, 100% *Phase B*, 15.5 min)]. ^{1}H NMR ($CDCl_3$, 500.13 MHz, □): 7.38 (d, *J* = 7.8 Hz, 6H, 6 × CH_{Ar}), 7.29-7.23 (m, 6H, 6 × CH_{Ar}), 7.22-7.16 (m, 3H, 3 × CH_{Ar}), 5.18-5.01 (m, 1H, 1 × CH), 4.36-4.17 (m, 3H, 1.5 × CH_2), 4.08-3.99 (m, 1H, 1 × CH), 3.99-3.81 (m, 3H, 1.5 × CH_2), 3.74-3.60 (m, 2H, 1 × CH_2), 3.22 (s, 9H, 3 × CH_3), 2.77-2.69 (m, 1H, 0.5 × CH_2), 2.62 (s, 3H, 1 × N-CH_3), 2.56-2.48 (m, 1H, 0.5 × CH_2), 2.29-2.08 (m, 2H, 1 × CH_2), 1.57-1.43 (m, 2H, 1 × CH_2), 1.39 (s, 4.5H, 1.5 × CH_3), 1.36 (s, 4.5H, 1.5 × CH_3), 1.30-1.17 (m, 24H, 12 × CH_2), 0.85 (t, *J* = 7.0 Hz, 3H, 1 × CH_3). ^{13}C NMR ($CDCl_3$, 125.77 MHz, □): 173.5, 169.9, 164.0, 155.9, 144.6, 129.7, 128.2, 127.0, 81.1 and 80.6, 71.8, 67.2, 66.6, 63.4, 62.4, 59.4, 54.7, 34.1, 33.2, 32.1, 31.7, 31.3, 29.9, 29.9, 29.9, 29.7, 29.6, 29.5, 29.4, 28.6, 28.5, 25.0, 22.9, 14.4. MS (ESI-TOF) [m/z (%)]: 977 ([M +Na]$^+$, 21), 955 ([MH]$^+$, 100). HRMS (ESI-TOF) calculated for $C_{52}H_{80}N_2O_{10}PS$ ([MH]$^+$) 955.5266, found 955.5255.

3.7.20 Synthesis of 1-palmitoyl-2-(^{Me}N-*L*-Cys)-*sn*-glycero-3-phosphocholine (15)

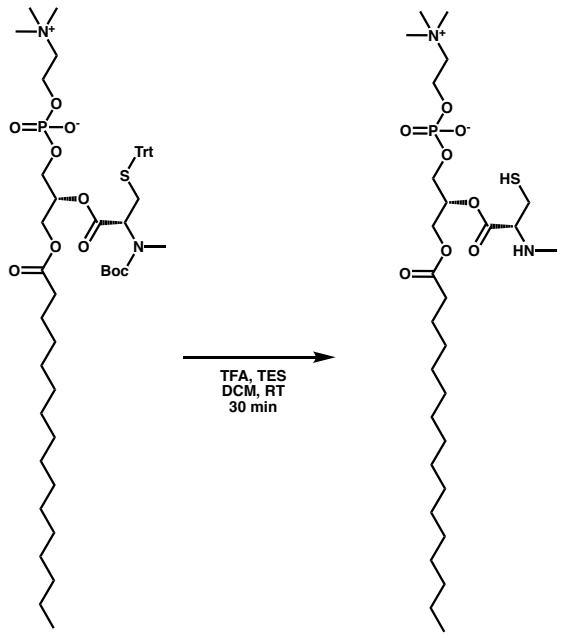

Scheme 3.5 Synthesis of 1-palmitoyl-2-(^{Me}N-*L*-Cys)-*sn*-glycero-3-phosphocholine (**15**)

A solution of 1-palmitoyl-2-[N-Boc-^{Me}N-*L*-Cys(Trt)]-*sn*-glycero-3-phosphocholine (**30**, 20.0 mg, 20.9 µmol) in 4 mL of TFA/CH_2Cl_2/TES (1.9:1.9:0.2) was stirred at rt for 30 min. After removal of the solvent, the residue was dried under high vacuum for 3 h. Then, the corresponding residue was diluted in MeOH (1 mL), filtered using a 0.2 µm syringe-driven filter, and the crude solution was purified by HPLC, affording 13.7 mg of the lysolipid **15** as a colorless oil [92%, Rt = 8.5 min (Zorbax SB-C18 semipreparative column, 50% *Phase A* in *Phase B*, 5 min, and then 5% *Phase A* in *Phase B*, 10 min)]. ^{1}H NMR (CD_3OD, 500.13 MHz): 5.37 (m, 1H, 1 × CH), 4.51-4.42 (m, 1H, 0.5 × CH_2), 4.32-4.22 (m, 3H, 1.5 × CH_2), 4.18-4.01 (m, 3H, 1 × CH + 1 × CH_2), 3.69-3.61 (m, 2H, 1 × CH_2), 3.24 (s, 9H, 3 × CH_3), 3.18-3.02 (m, 2H, 1 × CH_2), 2.68 (s, 3H, 1 × N-CH_3), 2.35 (t, J = 7.5 Hz, 2H, 1 × CH_2), 1.68-1.54 (m, 2H, 1 × CH_2), 1.39-1.21 (m, 24H, 12 × CH_2), 0.90 (t, J = 6.9 Hz, 3H, 1 × CH_3). ^{13}C NMR (CD_3OD, 125.77 MHz): 175.0, 166.7, 74.7, 67.5, 65.1, 63.9, 63.4, 60.7, 54.8, 35.0, 33.3, 31.0, 31.0, 30.9, 30.9, 30.8, 30.8, 30.7, 30.7, 30.6, 30.5, 30.4, 26.1,

26.1, 23.9, 14.6. MS (ESI-TOF) [m/z (%)]: 613 ([MH]$^+$, 100). HRMS (ESI-TOF) calculated for $C_{28}H_{58}N_2O_8PS$ ([MH]$^+$) 613.3646, found 613.3647.

3.7.21 Synthesis of 1-palmitoyl-2-[N-Boc-*L*-Cys(Trt)]-*sn*-glycero-3-phosphocholine (31)

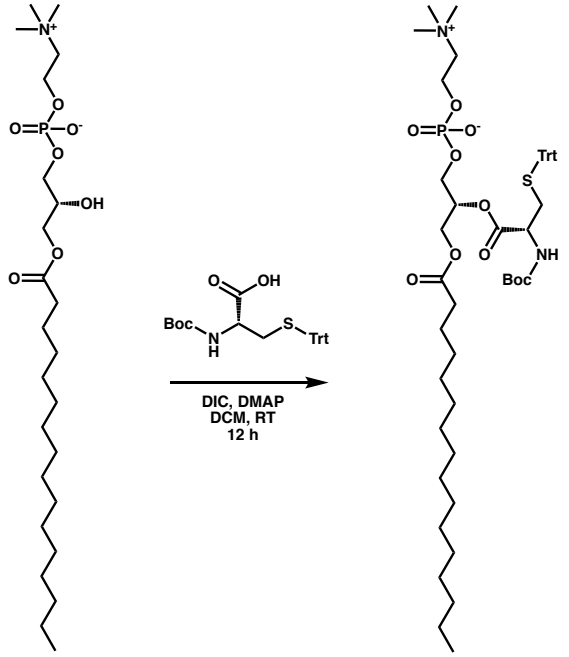

Scheme 3.6 Synthesis of 1-palmitoyl-2-[N-Boc-*L*-Cys(Trt)]-*sn*-glycero-3-phosphocholine (**31**)

A solution of N-Boc-*L*-Cys(Trt)-OH (93.7 mg, 201.6 µmol) in CH_2Cl_2 (7.5 mL) was stirred at rt for 10 min, and then DIC (47.0 µL, 302.4 µmol) and DMAP (12.3 mg, 100.8 µmol) were successively added. After 10 min stirring at rt, 1-palmitoyl-2-hydroxy-*sn*-glycero-3-phosphocholine (**Lyso C_{16} PC-OH**, 25.0 mg, 50.4 µmol) was added. After 12 h stirring at rt, the solvent was removed under reduced pressure, and the crude was purified by HPLC, affording 29.6 mg of **31** as a colorless foam [88%, R_t = 12.5 min (Zorbax SB-C18 semipreparative column, 5% *Phase A* in *Phase B*, 15.5 min)]. ^{1}H NMR ($CDCl_3$, 500.13 MHz): 7.38-7.31 (d, J = 8.0 Hz, 6H, 6 × CH_{Ar}), 7.30-7.23 (m, 6H, 6 × CH_{Ar}), 7.22-7.16 (m, 3H, 3 × CH_{Ar}), 5.25-5.13 (m, 1H, 1 × CH),

5.10 (d, J = 7.8 Hz, 0.3H, 1 × NH), 5.01 (d, J = 7.8 Hz, 0.7H, 1 × NH), 4.38-4.21 (m, 3H, 1.5 × CH_2), 4.20-4.11 (m, 1H, 1 × CH), 4.10-3.87 (m, 3H, 1.5 × CH_2), 3.86-3.66 (m, 2H, 1 × CH_2), 3.25 (s, 9H, 3 × CH_3), 2.73-2.45 (m, 2H, 1 × CH_2), 2.33-2.06 (m, 2H, 1 × CH_2), 1.62-1.43 (m, 2H, 1 × CH_2), 1.38 (s, 9H, 3 × CH_3), 1.31-1.16 (m, 24H, 12 × CH_2), 0.85 (t, J = 7.0 Hz, 3H, 1 × CH_3). ^{13}C NMR ($CDCl_3$, 125.77 MHz): 173.6, 170.4, 163.9, 155.3, 144.5, 129.7, 128.3, 121.2, 80.2, 72.2, 67.3, 66.4, 64.1, 62.6, 59.9, 54.7, 52.8, 34.2, 34.1, 32.1, 29.9, 29.9, 29.9, 29.7, 29.6, 29.5, 29.4, 29.3, 28.6, 24.9, 22.9, 14.3. MS (ESI-TOF) [m/z (%)]: 941 ($[MH]^+$, 100). HRMS (ESI-TOF) calculated for $C_{51}H_{78}N_2O_{10}PS$ ($[MH]^+$) 941.5109, found 941.5111.

3.7.22 Synthesis of 1-palmitoyl-2-(*L*-Cys)-*sn*-glycero-3-phosphocholine (17)

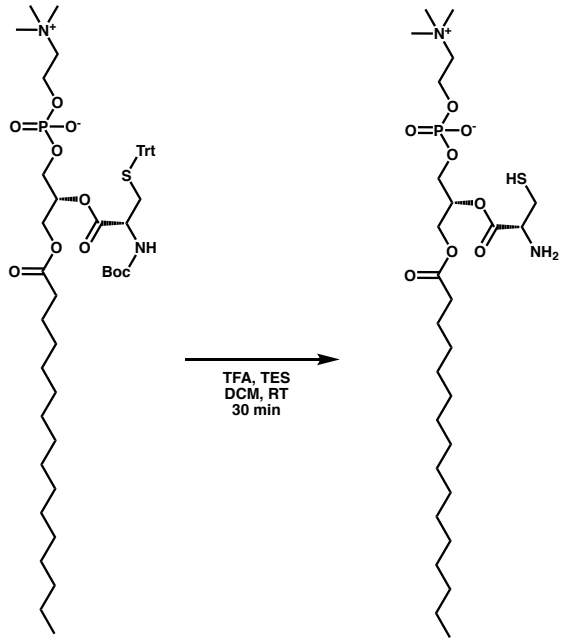

Scheme 3.7 Synthesis of 1-palmitoyl-2-(*L*-Cys)-*sn*-glycero-3-phosphocholine (**17**)

A solution of 1-pal-mitoyl-2-[N-Boc-*L*-Cys(Trt)]-*sn*-glycero-3-phosphocholine (**20**, 30.0 mg, 31.9 μmol) in 6 mL of TFA/CH_2Cl_2/TES (2.85:2.85:0.3) was stirred at rt for 30 min. After removal of the solvent, the residue was dried under high vacuum for 3 h. Then, the corresponding residue was

diluted in MeOH (1 mL), filtered using a 0.2 □m syringe-driven filter, and the crude solution was purified by HPLC, affording 14.2 mg of the lysolipid **17** as a colorless foam [64%, Rt = 9.0 min (Zorbax SB-C18 semipreparative column, 50% *Phase A* in *Phase B*, 5 min, and then 5% *Phase A* in *Phase B*, 10 min)]. ^{1}H NMR (CD_3OD, 500.13 MHz): 5.37 (m, 1H, 1 × CH), 4.43-4.36 (m, 1H, 0.5 × CH_2), 4.35-4.28 (m, 1H, 1 × CH), 4.27-4.14 (m, 3H, 1.5× CH_2), 4.13-3.98 (m, 2H, 1 × CH_2), 3.63-3.56 (m, 2H, 1 × CH_2), 3.17 (s, 9H, 3 × CH_3), 3.16-2.99 (m, 2H, 1 × CH_2), 2.33-2.25 (m, 2H, 1 × CH_2), 1.60-1.49 (m, 2H, 1 × CH_2), 1.31-1.19 (m, 24H, 12 × CH_2), 0.84 (t, J = 6.9 Hz, 3H, 1 × CH_3). ^{13}C NMR (CD_3OD, 125.77 MHz): 175.0, 168.5, 75.0, 67.5, 65.1, 63.3, 60.7, 55.9, 54.8, 34.9, 33.2, 31.0, 31.0, 30.9, 30.9, 30.9, 30.8, 30.7, 30.6, 30.4, 26.1, 25.5, 25.3, 23.9, 14.6. MS (ESI-TOF) [m/z (%)]: 599 ($[MH]^+$, 100). HRMS (ESI-TOF) calculated for $C_{27}H_{56}N_2O_8PS$ ($[MH]^+$) 599.3490, found 599.3484.

3.7.23 Synthesis of 1-oleoyl-2-[N-Boc-*L*-Cys(Trt)]-*sn*-glycero-3-phosphocholine (32)

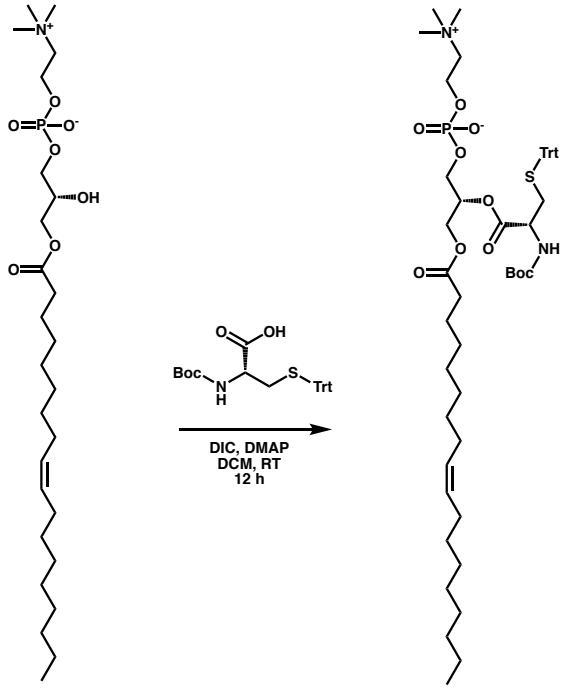

Scheme 3.8 Synthesis of 1-oleoyl-2-[N-Boc-*L*-Cys(Trt)]-*sn*-glycero-3-phosphocholine (**32**)

A solution of N-Boc-*L*-Cys(Trt)-OH (88.9 mg, 191.7 µmol) in CH_2Cl_2 (7.5 mL) was stirred at rt for 10 min, and then DIC (45.0 µL, 287.5 µmol) and DMAP (11.7 mg, 95.8 µmol) were successively added. After 10 min stirring at rt, 1-oleoyl-2-hydroxy-*sn*-glycero-3-phosphocholine (**Lyso C_{18} PC-OH**, 25.0 mg, 47.9 µmol) was added. After 12 h stirring at rt, the solvent was removed under reduced pressure, and the crude was purified by HPLC, affording 34.6 mg of **32** as a colorless foam [75%, R_t = 7.8 min (Zorbax SB-C18 semipreparative column, 100% *Phase B*, 15.5 min)]. ^{1}H NMR ($CDCl_3$, 500.13 MHz): 7.38 (d, *J* = 7.5 Hz, 6H, 6 × CH_{Ar}), 7.33-7.26 (m, 6H, 6 × CH_{Ar}), 7.25-7.19 (m, 3H, 3 × CH_{Ar}), 5.40-5.29 (m, 2H, 2 × CH), 5.27-5.13 (m, 1H, 1 × CH), 5.07 (d, *J* = 9.0 Hz, 1H, 1 × NH), 4.41-3.88 (m, 7H, 3 × CH_2 + 1 × CH), 3.77-3.57 (m, 2H, 1 × CH_2), 3.25 (s, 9H, 3 × CH_3), 2.74-2.48 (m, 2H, 1 × CH_2), 2.31-2.09 (m, 2H, 1 × CH_2), 2.07-1.93 (m, 4H, 2 × CH_2), 1.61-1.43 (m, 2H, 1 × CH_2), 1.42 (s, 9H, 3 × CH_3), 1.31-1.17 (m, 20H, 10 ×

CH_2), 0.88 (t, J = 7.0 Hz, 3H, 1 × CH_3). ^{13}C NMR ($CDCl_3$, 125.77 MHz): 173.5, 170.4, 163.9, 155.3, 144.4, 130.1, 129.9, 129.7, 129.6, 128.2, 128.2, 127.1, 80.1, 72.3, 67.2, 66.5, 63.8, 62.7, 59.4, 54.6, 52.7, 34.1, 34.1, 34.0, 32.0, 29.9, 29.9, 29.7, 29.5, 29.5, 29.4, 29.4, 29.3, 29.2, 29.2, 28.5, 28.5, 27.4, 27.3, 24.9, 24.8, 22.8, 14.3. MS (ESI-TOF) [m/z (%)]: 967 ($[MH]^+$, 100), 989 ($[M +Na]^+$, 20). HRMS (ESI-TOF) calculated for $C_{53}H_{80}N_2O_{10}PS$ ($[MH]^+$) 967.5266, found 967.5269.

3.7.24 Synthesis of 1-oleoyl-2-(*L*-Cys)-*sn*-glycero-3-phosphocholine (23)

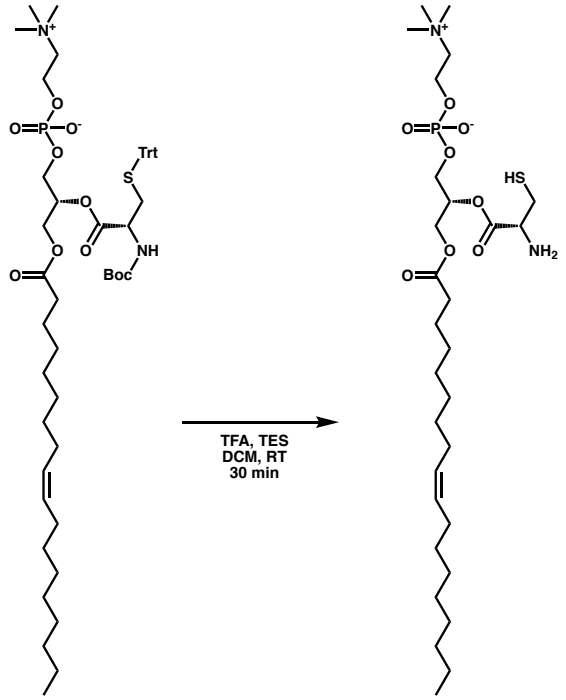

Scheme 3.9 Synthesis of 1-oleoyl-2-(*L*-Cys)-*sn*-glycero-3-phosphocholine (**23**)

A solution of 1-oleoyl-2-[N-Boc-*L*-Cys(Trt)]-*sn*-glycero-3-phosphocholine (**32**, 20.0 mg, 20.7 μmol) in 4 mL of TFA/CH_2Cl_2/TES (1.9:1.9:0.2) was stirred at rt for 30 min. After removal of the solvent, the residue was dried under high vacuum for 3 h. Then, the corresponding residue was diluted in MeOH (1 mL), filtered using a 0.2 μm syringe-driven filter, and the crude solution was

purified by HPLC, affording 11.2 mg of the lysolipid **23** as a colorless foam [75%, Rt = 8.1 min (Zorbax SB-C18 semipreparative column, 50% *Phase A* in *Phase B*, 5 min, and then 5% *Phase A* in *Phase B*, 10 min)]. MS (ESI-TOF) [m/z (%)]: 625 ([MH]$^+$, 100). HRMS (ESI-TOF) calculated for $C_{29}H_{58}N_2O_8PS$ ([MH]$^+$) 625.3651, found 625.3647.

3.7.25 Synthesis of Acetonide-protected 1-oleoyl-2-hydroxy-*sn*-glycero-3-phosphoglycerol (33)

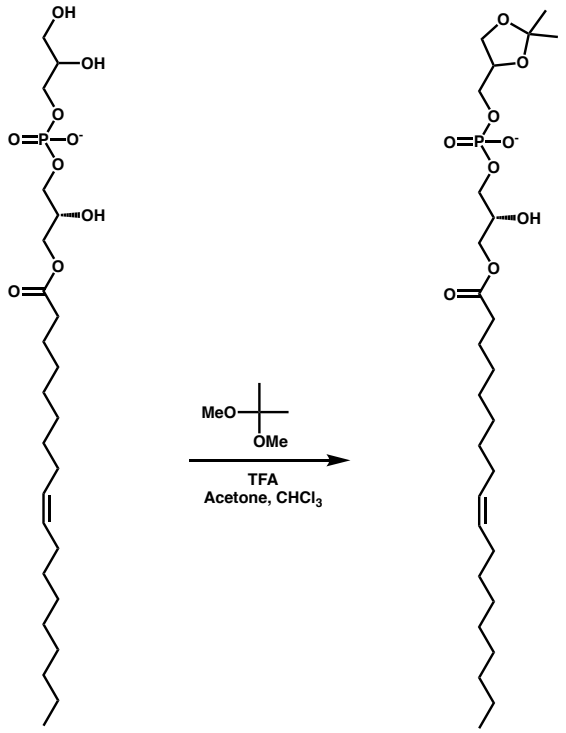

Scheme 3.10 Synthesis of Acetonide-protected 1-oleoyl-2-hydroxy-*sn*-glycero-3-phosphoglycerol (**33**)

A suspension of 1-oleoyl-2-hydroxy-*sn*-glycero-3-phospho-(1'-rac-glycerol) (sodium salt) (**Lyso C_{18} PG-OH**, 75.0 mg, 141.0 μmol) in acetone (1 mL) was subsequently treated with 2,2-dimethoxypropane (DMP, 65 mL) and a catalytic amount of TFA (40 μL). After 5 min stirring at rt, $CHCl_3$ (65 mL) was added until the lysolipid was fully dissolved. The reaction mixture was

stirred for 60 h at rt. After evaporation of solvent under reduced pressure, the residue was dried *in vacuo* for 30 min to remove the TFA. The product was then re-dissolved in dry $CHCl_3$ (10 mL) (do not use wet $CHCl_3$ as this will react with the acetonide moiety), and the solvent was removed by rotary evaporation. This was repeated a total of three times to remove trace TFA in the oily residue. The corresponding residue was dried *in vacuo* for 5 h to give a pale yellow oil, which was used without further purification. ^{1}H NMR ($CDCl_3$, 500.13 MHz): 8.28 (br s, 1H, 1 × OH), 5.45-5.20 (m, 2H, 2 × CH), 4.33-4.21 (m, 1H, 1 × CH), 4.19-4.10 (m, 1H, 0.5 × CH_2), 4.09-3.96 (m, 4H, 2 × CH_2), 3.95-3.83 (m, 3H, 1.5 × CH_2), 3.77-3.66 (m, 1H, 1 × CH), 2.29 (t, J = 7.5 Hz, 2H, 1 × CH_2), 2.08-1.90 (m, 4H, 2 × CH_2), 1.67-1.49 (m, 2H, 1 × CH_2), 1.38 (s, 3H, 1 × CH_3), 1.32 (s, 3H, 1 × CH_3), 1.30-1.17 (m, 20H, 10 × CH_2), 0.85 (t, J = 6.9 Hz, 3H, 1 × CH_3). ^{13}C NMR ($CDCl_3$, 125.77 MHz): 174.3, 130.2, 129.9, 110.1, 74.5, 69.0, 67.8, 67.2, 66.1, 64.4, 34.2, 32.1, 30.0, 29.9, 29.7, 29.5, 29.5, 29.5, 29.4, 29.4, 27.4, 27.4, 26.8, 25.3, 25.0, 22.9, 14.3. MS (ESI-TOF) [m/z (%)]: 549 ([M]$^-$, 100). HRMS (ESI-TOF) calculated for $C_{27}H_{50}O_9P$ ([M]$^-$) 549.3198, found 549.3193.

3.7.26 Synthesis of Acetonide-protected 1-oleoyl-2-[N-Boc-*L*-Cys(Trt)]-*sn*-glycero-3-phosphoglycerol (34)

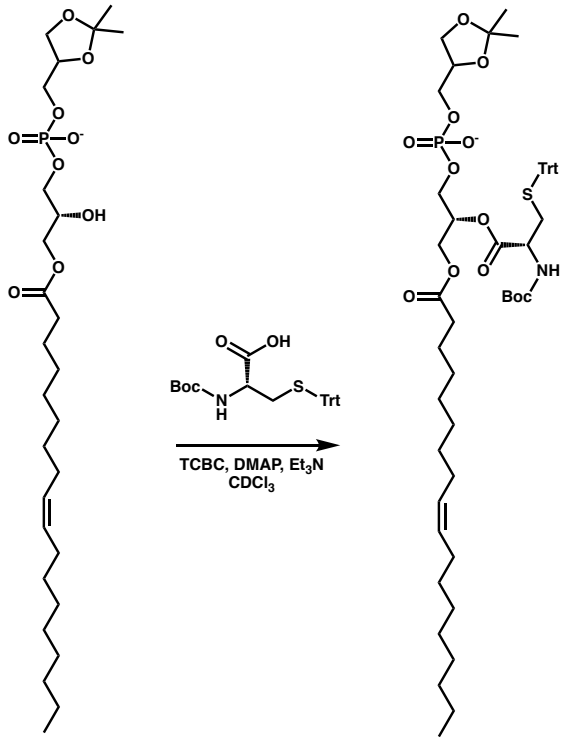

Scheme 3.11 Synthesis of Acetonide-protected 1-oleoyl-2-[N-Boc-*L*-Cys(Trt)]-*sn*-glycero-3-phosphoglycerol (**34**)

A solution of acetonide-protected 1-oleoyl-2-hydroxy-*sn*-glycero-3-phosphoglycerol (**33**, 40.0 mg, 69.9 µmol), N-Boc-*L*-Cys(Trt)-OH (81.0 mg, 174.7 µmol), DMAP (51.2 mg, 419.4 µmol) and Et_3N (34 µL) in $CDCl_3$ (2.5 mL) was stirred for 10 min at rt. Then, 2,4,6-trichlorobenzoyl chloride (TCBC, 71 µL) was added and the reaction was stirred for 12 h at rt. Afterwards, H_2O (75 µL) was added to the reaction mixture to quench the acid chloride, and the solvent was removed by rotary evaporation to give a yellow oil. The crude was dissolved in 500 µL of $CHCl_3$ and purified by flash column chromatography (0-20% MeOH in $CHCl_3$), affording 55.8 mg of **34** as a pale yellow oil [78%, R_f = 0.57 (20% MeOH in $CHCl_3$)]. ^{1}H NMR ($CDCl_3$, 500.13 MHz): 7.45-7.31 (m, 6H, 6 × CH_{Ar}), 7.30-7.22 (m, 6H, 6 × CH_{Ar}), 7.21-7.13 (m, 3H, 3 × CH_{Ar}), 5.45-5.4 (m, 2H, 2 × CH),

5.26-5.07 (m, 1H, 1 × NH), 5.09-4.90 (m, 1H, 1 × CH), 4.64-3.38 (m, 10H, 4 × CH_2 + 2 × CH), 3.38-3.07 (m, 1H, 0.5 × CH_2), 2.75-2.44 (m, 1H, 0.5 × CH_2), 2.36-2.07 (m, 2H, 1 × CH_2), 2.08-1.84 (m, 4H, 2 × CH_2), 1.64-1.44 (m, 2H, 1 × CH_2), 1.43-1.17 (m, 35H, 10 × CH_2 + 5 × CH_3), 0.86 (t, J = 6.4 Hz, 3H, 1 × CH_3). ^{13}C NMR ($CDCl_3$, 125.77 MHz): 173.2, 169.7, 158.1, 144.9, 130.2, 130.2, 129.9, 129.8, 128.2, 127.0, 82.2, 74.8, 72.0, 71.4, 68.0, 67.1, 66.4, 54.8, 34.1, 32.1, 30.0, 30.0, 29.9, 29.8, 29.6, 29.5, 29.5, 29.4, 29.4, 28.6, 27.5, 27.4, 27.0, 25.6, 24.9, 22.9, 14.3. MS (ESI-TOF) [m/z (%)]: 994 ([M]$^-$, 100). HRMS (ESI-TOF) calculated for $C_{54}H_{77}NO_{12}PS$ ([M]$^-$) 994.4910, found 994.4907.

3.7.27 Synthesis of 1-oleoyl-2-(*L*-Cys)-*sn*-glycero-3-phosphoglycerol (26)

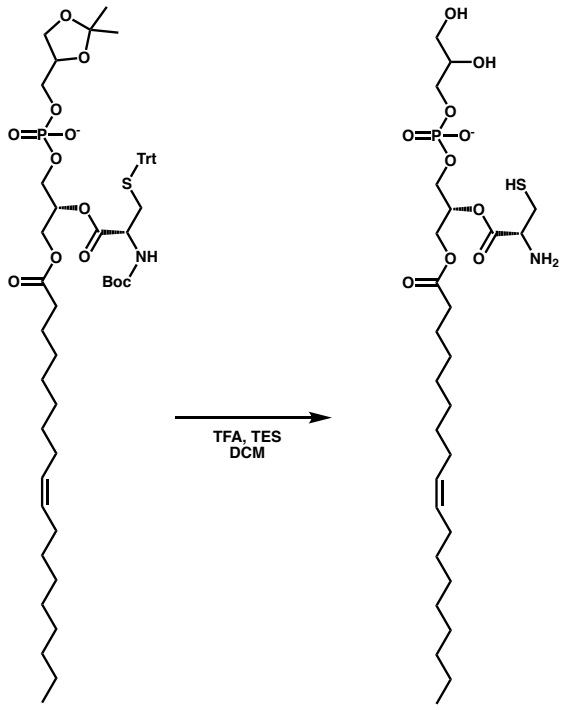

Scheme 3.12 Synthesis of 1-oleoyl-2-(*L*-Cys)-*sn*-glycero-3-phosphoglycerol (**26**)

A solution of acetonide-protected 1-oleoyl-2-[N-Boc-*L*-Cys(Trt)]-*sn*-glycero-3-phosphoglycerol (**34**, 10.0 mg, 9.80 µmol) in 2 mL of TFA/CH_2Cl_2/TES (0.95:0.95:0.1) was stirred at rt for 30 min.

After removal of the solvent, the residue was dried under high vacuum for 3 h. Then, the corresponding residue was diluted in MeOH (500 µL), filtered using a 0.2 µm syringe-driven filter, and the crude solution was purified by HPLC, affording 4.7 mg of the lysolipid **26** as a colorless oil [65%, Rt = 9.9 min (Zorbax SB-C18 semipreparative column, 50% *Phase A* in *Phase B*, 5 min, and then 5% *Phase A* in *Phase B*, 10 min)]. ^{1}H NMR (MeOD, 500.13 MHz): 5.43-5.25 (m, 3H, 3 × CH), 4.49-4.38 (m, 1H, 1 × CH), 4.39-4.21 (m, 2H, 1 × CH_2), 4.19-4.01 (m, 2H, 1 × CH_2), 3.98-3.81 (m, 2H, 1 × CH_2), 3.80-3.73 (m, 1H, 1 × CH), 3.67-3.52 (m, 2H, 1 × CH_2), 3.29-2.99 (m, 2H, 1 × CH_2), 2.35 (t, J = 7.6 Hz, 2H, 1 × CH_2), 2.10-1.94 (m, 4H, 2 × CH_2), 1.72-1.52 (m, 2H, 1 × CH_2), 1.45-1.16 (m, 20H, 10 × CH_2), 0.90 (t, J = 6.8 Hz, 3H, 1 × CH_3). ^{13}C NMR (MeOD, 125.77 MHz): 175.0, 169.9, 131.1, 130.9, 74.9, 72.7, 72.7, 68.0, 65.0, 64.0, 63.3, 35.0, 33.8, 33.2, 33.2, 31.0, 30.9, 30.8, 30.6, 30.5, 30.5, 30.4, 28.3, 28.3, 26.1, 23.9, 14.6. MS (ESI-TOF) [m/z (%)]: 612 ($[M]^-$, 100). HRMS (ESI-TOF) calculated for $C_{27}H_{51}NO_{10}PS$ ($[M]^-$) 612.2977, found 612.2974.

3.7.28 Synthesis of MESNA thiooleate (13)

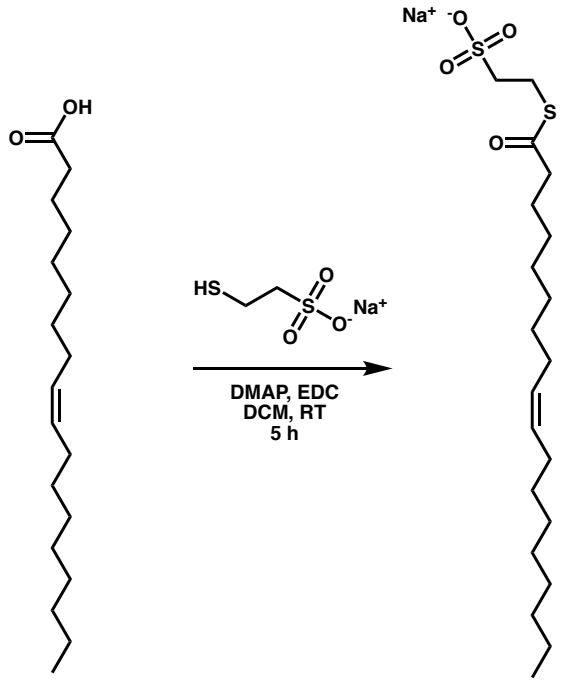

Scheme 3.13 Synthesis of MESNA thiooleate (**13**)

A solution of oleic acid (189.2 mg, 670.0 µmol) in CH_2Cl_2 (5 mL) was stirred at 0 ºC for 10 min, and then DMAP (7.4 mg, 60.9 µmol) and EDC.HCl (128.4 mg, 670.0 µmol) were successively added. After 10 min stirring at 0 ºC, sodium 2-mercaptoethanesulfonate (MESNA, 100.0 mg, 609.1 µmol) was added. After 5 h stirring at rt, the mixture was extracted with H_2O (2 × 3 mL) and the combined aqueous phases were washed with EtOAc (3 mL). After evaporation of H_2O under reduced pressure, the residue was washed with CH_3CN (5 mL), and then filtered to yield 194.7 mg of **13** as a white solid [75%]. ^{1}H NMR (d_6-DMSO, 500.13 MHz): 5.36-5.27 (m, 2H, 2 × CH), 3.05-2.99 (m, 2H, 1 × CH_2), 2.60-2.51 (m, 4H, 2 × CH_2), 2.02-1.92 (m, 4H, 2 × CH_2), 1.58-1.49 (m, 2H, 1 × CH_2), 1.34-1.18 (m, 20H, 10 × CH_2), 0.85 (t, J = 6.9 Hz, 3H, 1 × CH_3). ^{13}C NMR (d_6-DMSO, 125.77 MHz): 198.7, 129.8, 129.7, 51.0, 43.4, 31.4, 29.2, 29.1, 28.9, 28.8, 28.7, 28.6,

28.5, 28.3, 26.7, 26.6, 25.1, 24.4, 22.2, 14.1. MS (ESI-TOF) [m/z (%)]: 429 ([MH]$^+$, 100). HRMS (ESI-TOF) calculated for $C_{20}H_{38}NaO_4S_2$ ([MH]$^+$) 429.2104, found 429.2105.

3.7.29 Synthesis of MESNA thiopalmitate (19)

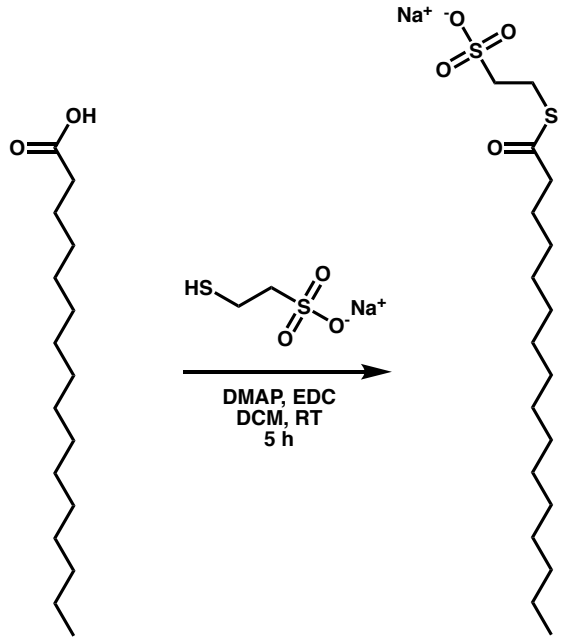

Scheme 3.14 Synthesis of MESNA thiopalmitate (**19**)

A solution of palmitic acid (171.8 mg, 670.0 µmol) in CH_2Cl_2 (5 mL) was stirred at 0 ºC for 10 min, and then DMAP (7.4 mg, 60.9 µmol) and EDC.HCl (128.4 mg, 670.0 µmol) were successively added. After 10 min stirring at 0 ºC, sodium 2-mercaptoethanesulfonate (MESNA, 100.0 mg, 609.1 µmol) was added. After 5 h stirring at rt, the mixture was extracted with H_2O (2 × 3 mL) and the combined aqueous phases were washed with EtOAc (3 mL). After evaporation of H_2O under reduced pressure, the residue was washed with CH_3CN (5 mL), and then filtered to yield 189.3 mg of **19** as a white solid [77%]. ^{1}H NMR (d_6-DMSO, 500.13 MHz): 3.08-2.96 (m, 2H, 1 × CH_2), 2.62-2.50 (m, 4H, 2 × CH_2), 1.62-1.45 (m, 2H, 1 × CH_2), 1.34-1.14 (m, 24H, 12 ×

CH_2), 0.85 (t, J = 7.0 Hz, 3H, 1 × CH_3). ^{13}C NMR (d_6-DMSO, 125.77 MHz): 198.7, 50.9, 43.3, 31.3, 29.1, 29.1, 29.1, 29.0, 29.0, 29.0, 28.9, 28.8, 28.7, 28.2, 25.1, 24.3, 22.1, 14.0. MS (ESI-TOF) [m/z (%)]: 379 ([M -Na]$^-$, 100). HRMS (ESI-TOF) calculated for $C_{18}H_{35}O_4S_2$ ([M -Na]$^-$) 379.1971, found 379.1973.

3.7.30 Synthesis of 1-oleoyl-2-[^{Me}N-*L*-Cys-(oleoyl)]-*sn*-glycero-3-phosphocholine (14)

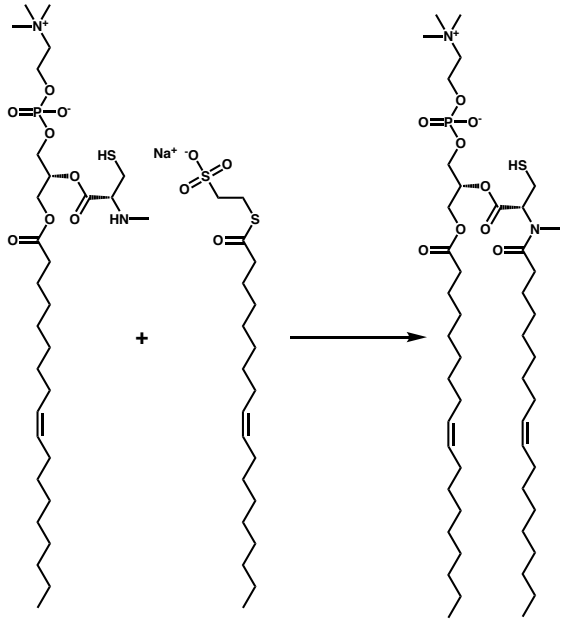

Scheme 3.15 Synthesis of 1-oleoyl-2-[^{Me}N-*L*-Cys-(oleoyl)]-*sn*-glycero-3-phosphocholine (**14**)

1-oleoyl-2-(^{Me}N-*L*-Cys)-*sn*-glycero-3-phosphocholine (**12**, 7.50 mg, 11.75 μmol) and MESNA-thiooleate (**13**, 5.03 mg, 11.75 μmol) were dissolved in 1.18 mL of 50 mM DTT in 200 mM NaH_2PO_4 pH 7.1 buffer and stirred under N_2 at rt. After 30 min, the corresponding mixture was filtered using a 0.2 μm syringe-driven filter, and the crude solution was purified by HPLC, affording 7.5 mg of the amidophospholipid **14** as a colorless oil [71%, R_t = 15.6 min (Zorbax SB-C18 semipreparative column, 100 % *Phase B*, 20.5 min)]. ^1H NMR ($CDCl_3$, 500.13 MHz): 5.38-5.27 (m, 4H, 4 × CH), 5.25-5.13 (m, 1H, 1 × CH), 5.14-4.95 (m, 1H, 1 × CH), 4.45-4.22 (m, 3H,

1.5 × CH_2), 4.17-3.91 (m, 3H, 1.5 × CH_2), 3.86-3.65 (m, 2H, 1 × CH_2), 3.31 (s, 9H, 3 × CH_3), 3.20-3.06 (m, 1H, 0.5 × CH_2), 2.98 (s, 3H, 1 × N-CH_3), 2.86-2.68 (m, 1H, 0.5 × CH_2), 2.35 (t, J = 7.5 Hz, 2H, 1 × CH_2), 2.26 (t, J = 7.5 Hz, 2H, 1 × CH_2), 2.10-1.85 (m, 8H, 4 × CH_2), 1.69-1.45 (m, 4H, 2 × CH_2), 1.39-1.12 (m, 41H, 20 × CH_2 + 1 × SH), 0.86 (t, J = 7.0 Hz, 6H, 2 × CH_3). ^{13}C NMR ($CDCl_3$, 125.77 MHz): 174.8, 173.7, 169.4, 130.7 and 130.4, 130.2 and 129.9, 72.7, 66.7, 63.9, 62.6, 59.9, 59.5, 54.8 and 54.7, 34.3, 33.8, 33.0, 32.9, 32.8, 32.1, 30.0, 30.0, 29.9, 29.9, 29.8, 29.7, 29.7, 29.6, 29.6, 29.6, 29.5, 29.5, 29.4, 29.4, 29.4, 29.3, 27.5, 27.4, 25.9, 25.3, 25.2, 25.1, 23.7, 22.9, 14.7. MS (ESI-TOF) [m/z (%)]: 925 ([M +Na]$^+$, 100), 903 ([MH]$^+$, 80). HRMS (ESI-TOF) calculated for $C_{48}H_{91}N_2O_9PSNa$ ([M +Na]$^+$) 925.6075, found 925.6073.

3.7.31 Synthesis of 1-palmitoyl-2-[^{Me}N-*L*-Cys-(oleoyl)]-*sn*-glycero-3-phosphocholine (16)

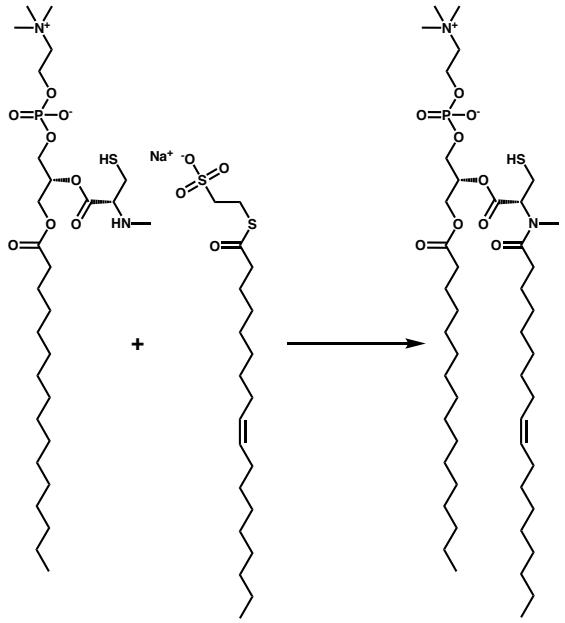

Scheme 3.16 Synthesis of 1-palmitoyl-2-[^{Me}N-*L*-Cys-(oleoyl)]-*sn*-glycero-3-phosphocholine (**16**)

1-palmitoyl-2-(^{Me}N-*L*-Cys)-*sn*-glycero-3-phosphocholine (**15**, 7.50 mg, 12.25 µmol) and MESNA-thiooleate (**13**, 5.24 mg, 12.25 µmol) were dissolved in 1.23 mL of 50 mM DTT in 200

mM NaH_2PO_4 pH 7.1 buffer and stirred under N_2 at rt. After 30 min, the corresponding mixture was filtered using a 0.2 μm syringe-driven filter, and the crude solution was purified by HPLC, affording 8.2 mg of the amidophospholipid **16** as a colorless oil [76%, R_t = 14.9 min (Zorbax SB-C18 semipreparative column, 100 % *Phase B*, 20.5 min)]. ^{1}H NMR ($CDCl_3$, 500.13 MHz): 5.38-5.28 (m, 2H, 2 × CH), 5.27-5.17 (m, 1H, 1 × CH), 5.09-5.02 (m, 1H, 1 × CH), 4.47-4.22 (m, 3H, 1.5 × CH_2), 4.18-3.92 (m, 3H, 1.5 × CH_2), 3.85-3.68 (m, 2H, 1 × CH_2), 3.30 (s, 9H, 3 × CH_3), 3.21-3.08 (m, 1H, 0.5 × CH_2), 2.98 (s, 3H, 1 × N-CH_3), 2.83-2.73 (m, 1H, 0.5 × CH_2), 2.35 (t, J = 8.3 Hz, 2H, 1 × CH_2), 2.26 (t, J = 8.3 Hz, 2H, 1 × CH_2), 2.06-1.85 (m, 4H, 2 × CH_2), 1.68-1.44 (m, 4H, 2 × CH_2), 1.38-1.17 (m, 45H, 22 × CH_2 + 1 × SH), 0.85 (t, J = 6.6 Hz, 6H, 2 × CH_3). ^{13}C NMR ($CDCl_3$, 125.77 MHz): 174.8, 173.7, 169.4, 130.7 and 130.4, 130.2 and 129.9, 72.6, 66.7, 63.9, 62.4, 59.9, 59.6, 54.8, 34.3, 33.8, 33.0, 32.9, 32.9, 32.1, 32.1, 30.0, 30.0, 29.9, 29.9, 29.9, 29.8, 29.8, 29.7, 29.6, 29.6, 29.6, 29.6, 29.5, 29.5, 29.5, 29.4, 29.4, 27.5, 27.4, 25.3, 25.0, 23.7, 22.9, 14.4. MS (ESI-TOF) [m/z (%)]: 899 ([M +Na]$^+$, 100), 877 ([MH]$^+$, 75). HRMS (ESI-TOF) calculated for $C_{46}H_{89}N_2O_9PSNa$ ([M +Na]$^+$) 899.5919, found 899.5917.

3.7.32 Synthesis of 1-palmitoyl-2-[*L*-Cys-(oleoyl)]-*sn*-glycero-3-phosphocholine (18)

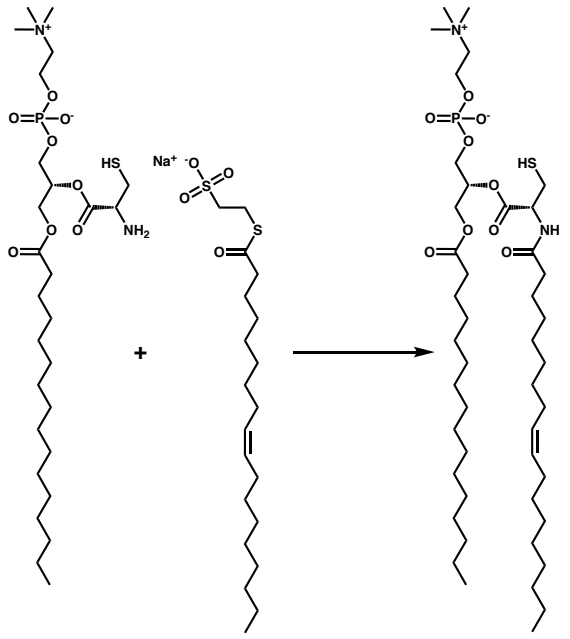

Scheme 3.17 Synthesis of 1-palmitoyl-2-[*L*-Cys-(oleoyl)]-*sn*-glycero-3-phosphocholine (**18**)

1-palmitoyl-2-(*L*-Cys)-*sn*-glycero-3-phosphocholine (**17**, 5.00 mg, 7.18 μmol) and MESNA-thiooleate (**13**, 3.07 mg, 7.18 μmol) were dissolved in 1.44 mL of 25 mM DTT in 200 mM NaH_2PO_4 pH 7.1 buffer and stirred under N_2 at rt. After 30 min, the corresponding mixture was filtered using a 0.2 μm syringe-driven filter, and the crude solution was purified by HPLC, affording 4.2 mg of the amidophospholipid **7** as a white solid [68%, R_t = 12.7 min (Zorbax SB-C18 semipreparative column, 100% *Phase B*, 15.5 min)]. ^{1}H NMR ($CDCl_3$, 500.13 MHz): 6.87 (d, 1H, 1 × NH, *J* = 7.5 Hz), 5.37-5.29 (m, 2H, 2 × CH), 5.28-5.18 (m, 1H, 1 × CH), 4.88-4.77 (m, 1H, 1 × CH), 4.46-4.24 (m, 3H, 1.5 × CH_2), 4.23-3.99 (m, 3H, 1.5 × CH_2), 3.98-3.80 (m, 2H, 1 × CH_2), 3.36 (s, 9H, 3 × CH_3), 3.08-2.81 (m, 2H, 1 × CH_2), 2.34-2.17 (m, 4H, 2 × CH_2), 2.04-1.87 (m, 4H, 2 × CH_2), 1.67-1.48 (m, 4H, 2 × CH_2), 1.35-1.16 (m, 45H, 22 × CH_2 + 1 × SH), 0.85 (t, *J* = 6.8 Hz, 6H, 2 × CH_3). ^{13}C NMR ($CDCl_3$, 125.77 MHz): 173.7, 169.9, 163.5, 130.7 and 130.4, 130.2 and 129.9, 72.3, 66.3, 64.6, 62.4, 60.2, 54.7, 53.7, 36.5, 34.2, 32.9, 32.1, 30.0, 29.9, 29.9,

29.9, 29.8, 29.7, 29.6, 29.6, 29.6, 29.5, 29.4, 29.4, 29.3, 27.4, 26.9, 25.9, 25.0, 22.9, 14.4. MS (ESI-TOF) [m/z (%)]: 885 ([M +Na]$^+$, 60), 863 ([MH]$^+$, 100). HRMS (ESI-TOF) calculated for $C_{45}H_{88}N_2O_9PS$ ([MH]$^+$) 863.5943, found 863.5948.

3.7.33 Synthesis of 1-palmitoyl-2-[^{Me}N-*L*-Cys-(palmitoyl)]-*sn*-glycero-3-phosphocholine (20)

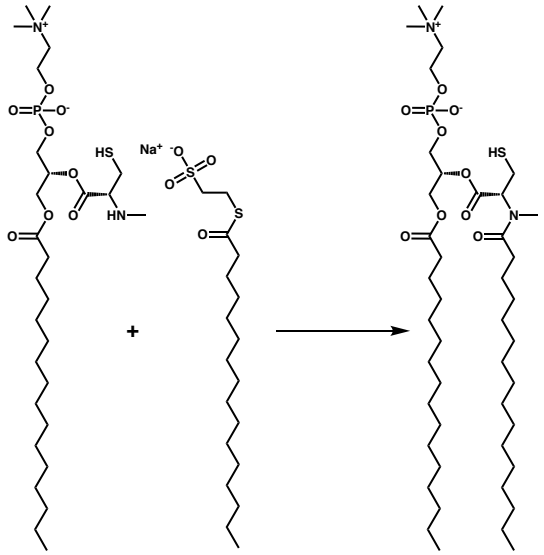

Scheme 3.18 Synthesis of 1-palmitoyl-2-[^{Me}N-*L*-Cys-(palmitoyl)]-*sn*-glycero-3-phosphocholine (**20**)

1-palmitoyl-2-(^{Me}N-*L*-Cys)-*sn*-glycero-3-phosphocholine (**15**, 5.00 mg, 8.17 µmol) and MESNA-thiopalmitate (**19**, 3.28 mg, 8.17 µmol) were dissolved in 1.63 mL of 25 mM DTT in 200 mM NaH_2PO_4 pH 7.1 buffer and stirred under N_2 at rt. After 30 min, the corresponding mixture was filtered using a 0.2 µm syringe-driven filter, and the crude solution was purified by HPLC, affording 4.0 mg of the amidophospholipid **20** as a colorless oil [57%, R_t = 15.8 min (Zorbax SB-C18 semipreparative column, 100 % *Phase B*, 20.5 min)]. ^{1}H NMR ($CDCl_3$, 500.13 MHz): 5.32-5.14 (m, 1H, 1 × CH), 5.11-5.00 (m, 1H, 1 × CH), 4.50-4.23 (m, 3H, 1.5 × CH_2), 4.21-3.96 (m, 3H, 1.5 × CH_2), 3.94-3.78 (m, 2H, 1 × CH_2), 3.36 (s, 9H, 3 × CH_3), 3.22-3.07 (m, 1H, 0.5 × CH_2), 2.98 (s, 3H, 1 × N-CH_3), 2.86-2.72 (m, 1H, 0.5 × CH_2), 2.35 (t, *J* = 7.2 Hz, 2H, 1 × CH_2), 2.27 (t,

J = 7.2 Hz, 2H, 1 × CH_2), 1.69-1.45 (m, 4H, 2 × CH_2), 1.34-1.17 (m, 49H, 24 × CH_2 + 1 × SH), 0.85 (t, J = 7.2 Hz, 6H, 2 × CH_3). ^{13}C NMR ($CDCl_3$, 125.77 MHz): 174.9, 173.8, 165.6, 72.3, 66.5, 66.3, 64.2, 62.3, 59.8, 54.8 and 54.7, 34.2, 33.8, 33.0, 32.1, 29.9, 29.9, 29.9, 29.9, 29.9, 29.8, 29.7, 29.7, 29.6, 29.6, 29.6, 29.4, 29.4, 25.3, 25.2, 25.1, 25.0, 23.7 22.9, 14.4. MS (ESI-TOF) [m/z (%)]: 873 ([M +Na]$^+$, 100), 851 ([MH]$^+$, 67). HRMS (ESI-TOF) calculated for $C_{44}H_{88}N_2O_9PS$ ([MH]$^+$) 851.5943, found 851.5939.

3.7.34 Synthesis of 1-oleoyl-2-[^{Me}N-*L*-Cys-(palmitoyl)]-*sn*-glycero-3-phosphocholine (21)

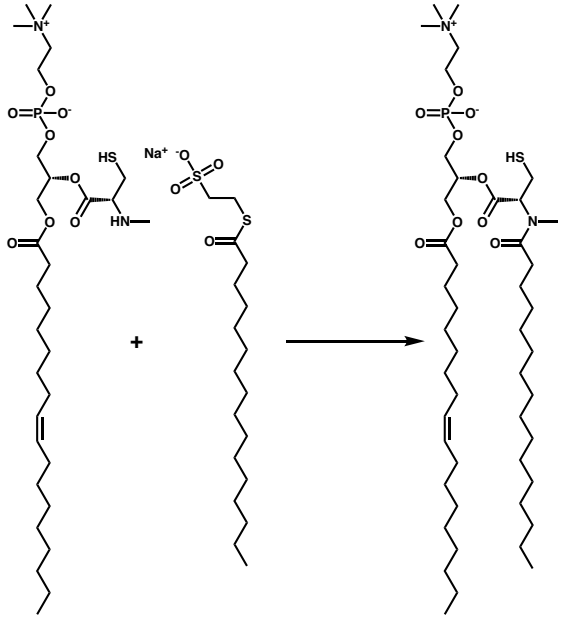

Scheme 3.19 Synthesis of 1-oleoyl-2-[^{Me}N-*L*-Cys-(palmitoyl)]-*sn*-glycero-3-phosphocholine (**21**)

1-oleoyl-2-(^{Me}N-*L*-Cys)-*sn*-glycero-3-phosphocholine (**12**, 2.00 mg, 3.14 µmol) and MESNA-thiopalmitate (**19**, 1.26 mg, 3.14 µmol) were dissolved in 625 µL of 25 mM DTT in 200 mM NaH_2PO_4 pH 7.1 buffer and stirred under N_2 at rt. After 30 min, the corresponding mixture was filtered using a 0.2 µm syringe-driven filter, and the crude solution was purified by HPLC, affording 1.5 mg of the amidophospholipid **21** as a colorless oil [68%, R_t = 16.9 min (Zorbax SB-

C18 semipreparative column, 100 % *Phase B*, 20.5 min)]. ^{1}H NMR ($CDCl_3$, 500.13 MHz): 5.43-5.28 (m, 2H, 2 × CH), 5.27-5.14 (m, 1H, 1 × CH), 5.13-5.00 (m, 1H, 1 × CH), 4.50-4.24 (m, 3H, 1.5 × CH_2), 4.20-3.97 (m, 3H, 1.5 × CH_2), 3.89-3.71 (m, 2H, 1 × CH_2), 3.33 (s, 9H, 3 × CH_3), 3.21-3.09 (m, 1H, 0.5 × CH_2), 2.98 (s, 3H, 1 × N-CH_3), 2.86-2.70 (m, 1H, 0.5 × CH_2), 2.38-2.22 (m, 4H, 2 × CH_2), 2.03-1.89 (m, 4H, 2 × CH_2), 1.67-1.43 (m, 4H, 2 × CH_2), 1.38-1.13 (m, 45H, 22 × CH_2 + 1 × SH), 0.85 (t, J = 7.1 Hz, 6H, 2 × CH_3). ^{13}C NMR ($CDCl_3$, 125.77 MHz): 174.7, 173.7, 169.4, 130.7 and 130.4, 130.2 and 129.9, 72.5, 66.7, 66.3, 64.1, 62.4, 59.9, 54.9 and 54.7, 34.3, 34.2, 33.8, 32.9, 32.8, 32.2, 32.1, 30.0, 30.0, 29.9, 29.9, 29.9, 29.9, 29.8, 29.7, 29.6, 29.6, 29.5, 29.4, 29.4, 29.4, 29.4, 29.3, 27.5, 27.4, 25.3, 25.2, 25.1, 23.7, 22.9, 14.4. MS (ESI-TOF) [m/z (%)]:899 ([M +Na]$^+$, 100), 877 ([MH]$^+$, 81). HRMS (ESI-TOF) calculated for $C_{46}H_{90}N_2O_9PS$ ([MH]$^+$) 877.6098, found 877.6099.

3.7.35 Synthesis of 1-palmitoyl-2-[*L*-Cys-(palmitoyl)]-*sn*-glycero-3-phosphocholine (22)

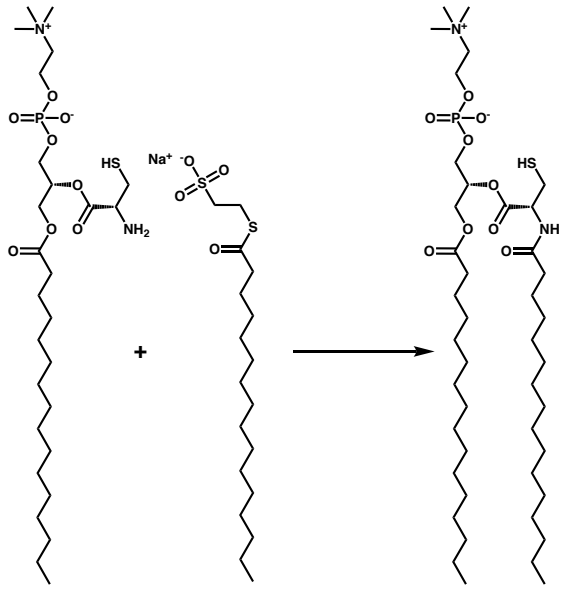

Scheme 3.20 Synthesis of 1-palmitoyl-2-[*L*-Cys-(palmitoyl)]-*sn*-glycero-3-phosphocholine (**22**)

1-palmitoyl-2-(*L*-Cys)-*sn*-glycero-3-phosphocholine (**17**, 3.00 mg, 5.01 μmol) and MESNA-thiopalmitate (**19**, 2.02 mg, 5.01 μmol) were dissolved in 1.00 mL of 25 mM DTT in 200 mM NaH_2PO_4 pH 7.1 buffer and stirred under N_2 at rt. After 30 min, the corresponding mixture was filtered using a 0.2 μm syringe-driven filter, and the crude solution was purified by HPLC, affording 2.4 mg of the amidophospholipid **22** as a colorless oil [57%, R_t = 14.9 min (Zorbax SB-C18 semipreparative column, 100 % *Phase B*, 20.5 min)]. MS (ESI-TOF) [m/z (%)]: 859 ([M +Na]$^+$, 46), 837 ([MH]$^+$, 100). HRMS (ESI-TOF) calculated for $C_{43}H_{86}N_2O_9PS$ ([MH]$^+$) 837.5792, found 837.5795.

3.7.36 Synthesis of 1-oleoyl-2-[*L*-Cys-(oleoyl)]-*sn*-glycero-3-phosphocholine (24)

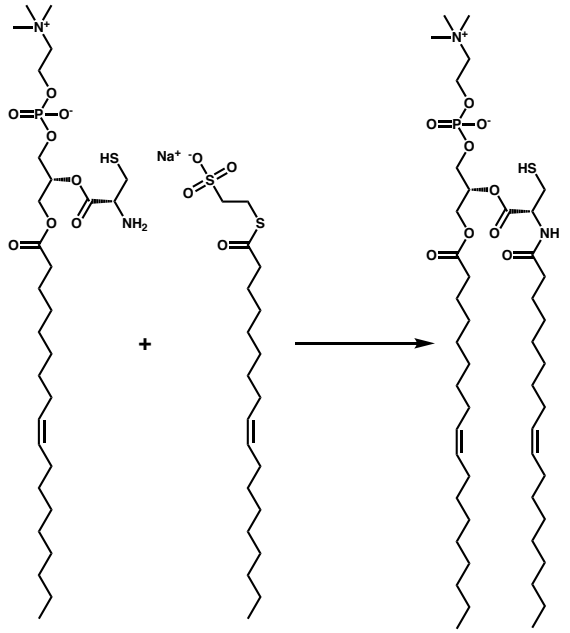

Scheme 3.21 Synthesis of 1-oleoyl-2-[*L*-Cys-(oleoyl)]-*sn*-glycero-3-phosphocholine (**24**)

1-oleoyl-2-(*L*-Cys)-*sn*-glycero-3-phosphocholine (**12**, 9.00 mg, 14.41 μmol) and MESNA-thiooleate (**13**, 6.20 mg, 14.41 μmol) were dissolved in 1.44 mL of 50 mM DTT in 200 mM $NaH_2PO_4.H_2O$ pH 7.1 buffer and stirred under N_2 at rt. After 30 min, the corresponding

mixture was filtered using a 0.2 μm syringe-driven filter, and the crude solution was purified by HPLC, affording 8.7 mg of the amidophospholipid **24** as a white foam [68%, R_t = 14.4 min (Zorbax SB-C18 semipreparative column, 100% *Phase B*, 20.5 min)]. ^{1}H NMR ($CDCl_3$, 500.13 MHz): 7.02 (d, 1H, 1 × NH, J = 7.9 Hz), 5.42-5.30 (m, 4H, 4 × CH), 5.29-5.22 (m, 1H, 1 × CH), 4.98-4.76 (m, 1H, 1 × CH), 4.44-3.92 (m, 6H, 3 × CH_2), 3.89-3.68 (m, 2H, 1 × CH_2), 3.33 (s, 9H, 3 × CH_3), 3.23-2.80 (m, 2H, 1 × CH_2), 2.38-2.17 (m, 4H, 2 × CH_2), 2.10-1.84 (m, 8H, 4 × CH_2), 1.71-1.45 (m, 4H, 2 × CH_2), 1.44-1.13 (m, 41H, 20 × CH_2 + 1 × SH), 0.85 (t, J = 6.8 Hz, 6H, 2 × CH_3). ^{13}C NMR ($CDCl_3$, 125.77 MHz): 173.7, 173.6, 170.0, 130.6, 130.3, 130.2, 129.8, 72.8, 66.6, 63.9, 62.6, 59.4, 54.8, 53.6, 36.5, 34.2, 34.1, 32.8, 32.7, 32.1, 30.0, 29.9, 29.8, 29.7, 29.7, 29.6, 29.5, 29.5, 29.4, 29.4, 29.4, 29.4, 29.3, 29.3, 27.4, 27.4, 27.3, 27.3, 26.9, 25.8, 25.8, 25.0, 22.9, 14.3. MS (ESI-TOF) [m/z (%)]: 889 ($[MH]^+$, 100), 911 ($[M+Na]^+$, 25). HRMS (ESI-TOF) calculated for $C_{47}H_{90}N_2O_9PS$ ($[MH]^+$) 889.6105, found 889.6102.

3.7.37 Synthesis of 1-oleoyl-2-[*L*-Cys-(palmitoyl)]-*sn*-glycero-3-phosphocholine (25)

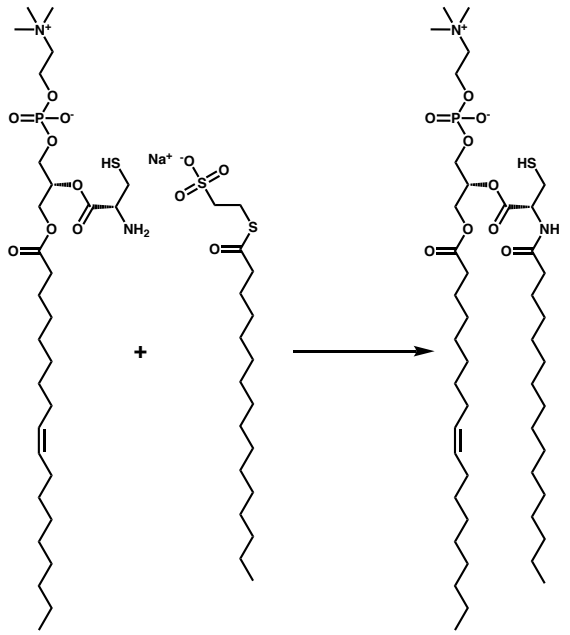

Scheme 3.22 Synthesis of 1-oleoyl-2-[*L*-Cys-(palmitoyl)]-*sn*-glycero-3-phosphocholine (**25**)

1-oleoyl-2-(*L*-Cys)-*sn*-glycero-3-phosphocholine (**23**, 5.00 mg, 8.01 μmol) and MESNA-thiopalmitate (**19**, 3.22 mg, 8.01 μmol) were dissolved in 0.80 mL of 50 mM DTT in 200 mM $NaH_2PO_4.H_2O$ pH 7.1 buffer and stirred under N_2 at rt. After 30 min, the corresponding mixture was filtered using a 0.2 μm syringe-driven filter, and the crude solution was purified by HPLC, affording 3.9 mg of the amidophospholipid **25** as a white foam [56%, R_t = 13.8 min (Zorbax SB-C18 semipreparative column, 100% *Phase B*, 20.5 min)]. MS (ESI-TOF) [m/z (%)]: 863 ($[M]^-$, 100). HRMS (ESI-TOF) calculated for $C_{45}H_{88}N_2O_9PS$ ($[MH]^+$) 863.5948, found 863.5947.

3.7.38 Synthesis of 1-oleoyl-2-[*L*-Cys-(oleoyl)]-*sn*-glycero-3-phosphoglycerol (27)

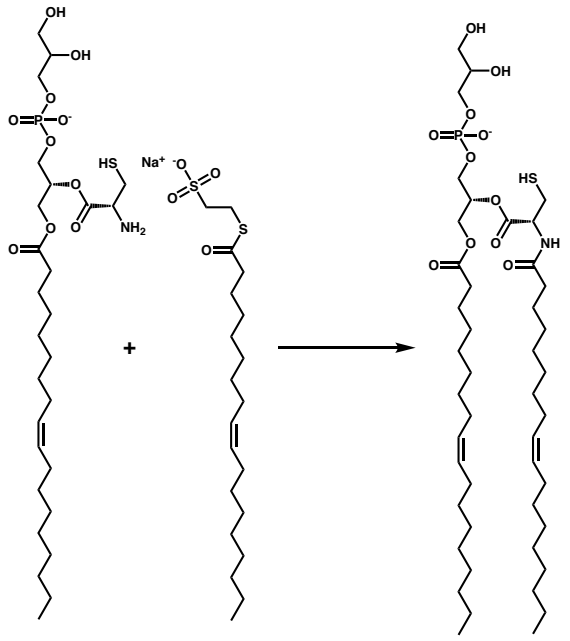

Scheme 3.23 Synthesis of 1-oleoyl-2-[*L*-Cys-(oleoyl)]-*sn*-glycero-3-phosphoglycerol (**27**)

1-oleoyl-2-(*L*-Cys)-*sn*-glycero-3-phosphoglycerol (**26**, 3.00 mg, 4.90 μmol) and MESNA-thiooleate (**13**, 2.10 mg, 4.90 μmol) were dissolved in 1.00 mL of 25 mM DTT in 200 mM NaH_2PO_4 pH 7.1 buffer and stirred under N_2 at rt. After 30 min, the corresponding mixture was filtered using a 0.2 μm syringe-driven filter, and the crude solution was purified by HPLC, affording 2.7 mg of the amidophospholipid **27** as a colorless oil [63%, R_t = 17.2 min (Zorbax SB-C18 semipreparative column, 100 % *Phase B*, 20.5 min)]. MS (ESI-TOF) [m/z (%)]: 877 ($[M]^-$, 100). HRMS (ESI-TOF) calculated for $C_{45}H_{83}NO_{11}PS$ ($[M]^-$) 876.5430, found 876.5435.

Notes about the chapter:

Chapter three, in full, is a reprint (with co-author permission) of the material as it appears in the publication; R. J. Brea, **A. K. Rudd,** N. K. Devaraj "Nonenzymatic biomimetic remodeling of phospholipids in synthetic liposomes," *Proc. Natl. Acad. Sci. U.S.A.,* 2016, 133(31) 8589-8594.

My contribution to this chapter was in the design and execution of all giant unilamellar vesicle and microscopy experiments. I thank Roberto Brea and Neal Devaraj for their contributions to this chapter. Roberto Brea conceived and synthesized all compounds presented in this chapter and performed all experiment related to the characterization of these compounds and their reaction products as well as their unique chemical behavior. Neal Devaraj provided scientific oversight and assistance in the preparation of the manuscript.

CHAPTER 4

4 Traceless Synthesis of Ceramides in Living Cells Reveals Saturation Dependent Apoptotic Effects

4.1 Introduction

Ceramides are produced within the cell through both *de novo* synthesis and salvage pathways and carry out diverse cellular functions.[100] Natural ceramide levels play an integral role in insulin resistance,[101] endosomal sorting pathways,[102] gene regulation,[103] and programmed cell death.[104] They are also implicated in tumor suppression and methods for their cellular delivery could be attractive as cancer therapeutics.[105] Despite considerable interest in the biological function of ceramides, direct study of their effects *in vivo* is limited by their impermeability to the cell membrane. As a result, current methods often rely on the use of unnatural short-chain ceramides. These analogs exhibit increased cell permeability but behave differently than natural ceramides in both physical membrane properties[106] and biological activity.[107] Testing how N-fatty acyl structure affects ceramide function is also not possible using short-chain analogs. Additionally, manipulation of native ceramide metabolism genetically or with inhibitors is limited by the broad substrate selectivity of endogenous ceramide synthases.[108] Recently, caged ceramides have been developed for the delivery of ceramide to macrophages but their biological activity, and efficacy in other cell lines, has not been reported.[109]

We developed a strategy to overcome these problems by synthesizing native ceramides *in situ* using two cell-permeable and chemoselective ligation partners. Previously, a salicylaldehyde ester-induced reaction has been reported for peptide ligation which relies on a C-terminal salicylaldehyde and N-terminal serine to selectively generate a peptide linkage.[110] This method, however, requires organic solvent, high reactant concentrations, and removal of the

salicylaldehyde group under acidic conditions. As an alternative, we sought to develop fatty acid salicylaldehyde esters that react selectively under physiological conditions with the sphingolipid backbone sphingosine to yield natural ceramides. Based on previous observations in our lab, we hypothesized that the organization of these reaction partners within membranes would accelerate the modest reaction rate of the salicylaldehyde-mediated ligation.[80,111] Furthermore, functionalizing the phenyl ring of the salicylaldehyde group with electron donating groups could increase the aqueous stability of the fatty acid ester and eliminate the need for organic solvent.

4.2 Chemoselective Synthesis of Ceramide in Model Membranes and Living Cells

To determine the feasibility of this approach, we synthesized a small collection of palmitic acid salicylaldehyde esters with different ring substituents, **35**-**37,** and performed ligation experiments in the presence of phospholipid vesicles as a model membrane. Upon incubation of 500 μM of palmitic acid salicylaldehyde ester with 250 μM sphingosine at 37 ºC in PBS (pH 7.4), C16:0 ceramide was formed within hours (Figure 4.1). The salicylaldehyde group is released spontaneously during the reaction, resulting in the traceless formation of ceramide, without the introduction of any extraneous chemical moieties (Figure 4.2A). From these initial experiments, we found that compound **3** offered superior hydrolytic stability, showing very little degradation (<2%) over 16 h (Figure 4.2B). Therefore, we chose to employ **37** as a sphingosine ligation partner in a method we term traceless ceramide ligation (TCL).

To investigate the chemoselectivity of this ligation we performed TCL in the presence of two potentially competing biomolecules, serine (Figure 4.2C) or lyso-sphingomyelin (Figure 4.2D). Serine possesses the same 2-aminoethanol moiety as sphingosine but is water soluble. Lysosphingomyelin is localized in the membrane but has only a free amine and not the terminal 2-aminoethanol functionality found in sphingosine. Under these conditions, TCL proceeded with

no observable decrease in yield or reaction rate, suggesting that both the terminal 2-aminoethanol functionality and localization in the phospholipid membrane are necessary for ligation. To determine if TCL could occur in live cells, we used a ^{13}C isotopic derivative of **37**, **37i**. HeLa cells were incubated in the presence of sphingosine, **37i,** or sphingosine and **37i** combined**,** for 16 h and then lysed. Cell fractionation was used to obtain crude mitochondrial fractions and enrich for the ceramide product formed in internal membranes (Figure 4.4).[112] Mass spectrometry analysis detected TCL-synthesized ceramide in the crude mitochondrial fraction only when both ligation partners were added to cells but not when they were added separately. Notably, we could not detect any TCL-synthesized ceramide when cells were treated with **37i** alone. This suggests that endogenous levels of sphingosine are insufficient for TCL. Additionally, the reaction was performed in the presence of an inhibitor of all six ceramide synthases, fumonisin B1 (FB1), which we determined was non-reactive towards **37** (Figure 4.5). Under these conditions, the isotopic ceramide product was still observed, confirming that it is not a metabolic product of **37i** (Figure 4.2E).[113] By performing a whole-cell lipid extraction,[114] we determined the total level of ^{13}C labeled ceramide produced in HeLa cells by TCL to be 136 ± 23 pmol/1x10^6 cells, indicating that physiological levels of ceramide can readily be synthesized *in situ* (Figure 4.6).[115]

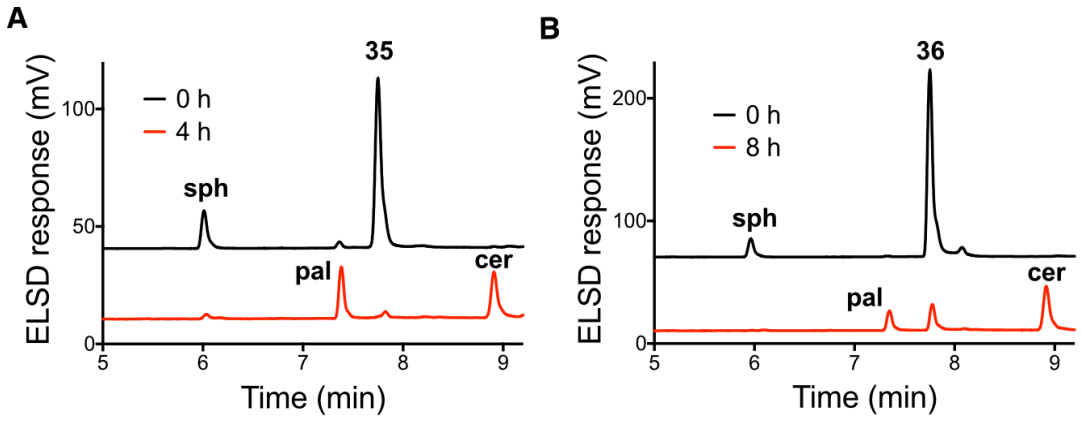

Figure 4.1 Fatty acid salicylaldehyde esters and sphingosine (sph) react in model membranes to form ceramide (cer). 250 μM sph and 500 μM **35** (A) or **36** (B) react to form ceramide (cer) at 37 ºC, pH 7.4 over a period of 4 or 8 h respectively. Palmitic acid (pal) is observed as a side product in the reaction due to background hydrolysis of the salicylaldehyde ester.

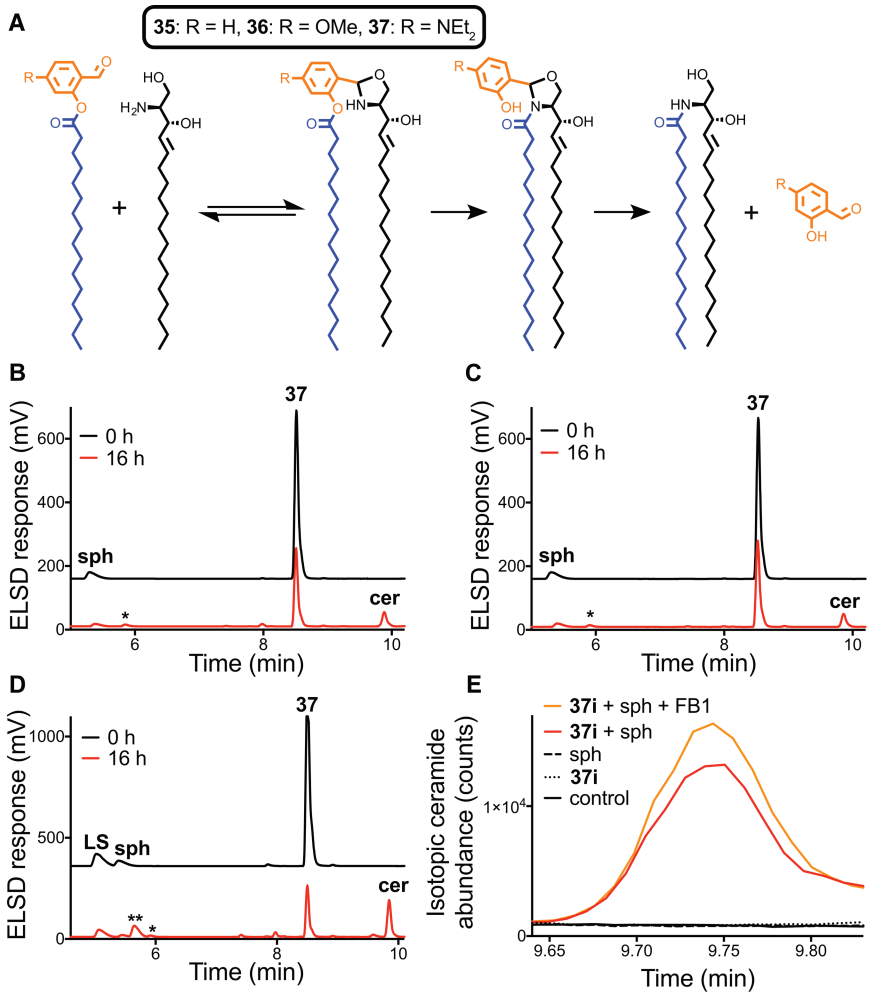

Figure 4.2 Fatty acid salicylaldehyde esters and sphingosine react chemoselectively in model membranes and live cells. A, Proposed reaction mechanism for traceless ceramide ligation. B, Sphingosine (sph) and **37** in model membranes react to form ceramide (cer) at 37 ºC, pH 7.4 over a period of 16 h. C and D, The reaction between sph and **37** forms cer chemoselectively in the presence of serine (C) and lyso-sphingomyelin (D). The production of a small quantity of reversibly formed byproduct **b1** {*} (B-D) and **b2** {**} (D) is also detected (Figure 4.3). E, Isotopic palmitic acid salicylaldehyde ester **37i** reacts with sph within live HeLa cells to form cer detectable in the crude mitochondrial cell fraction.

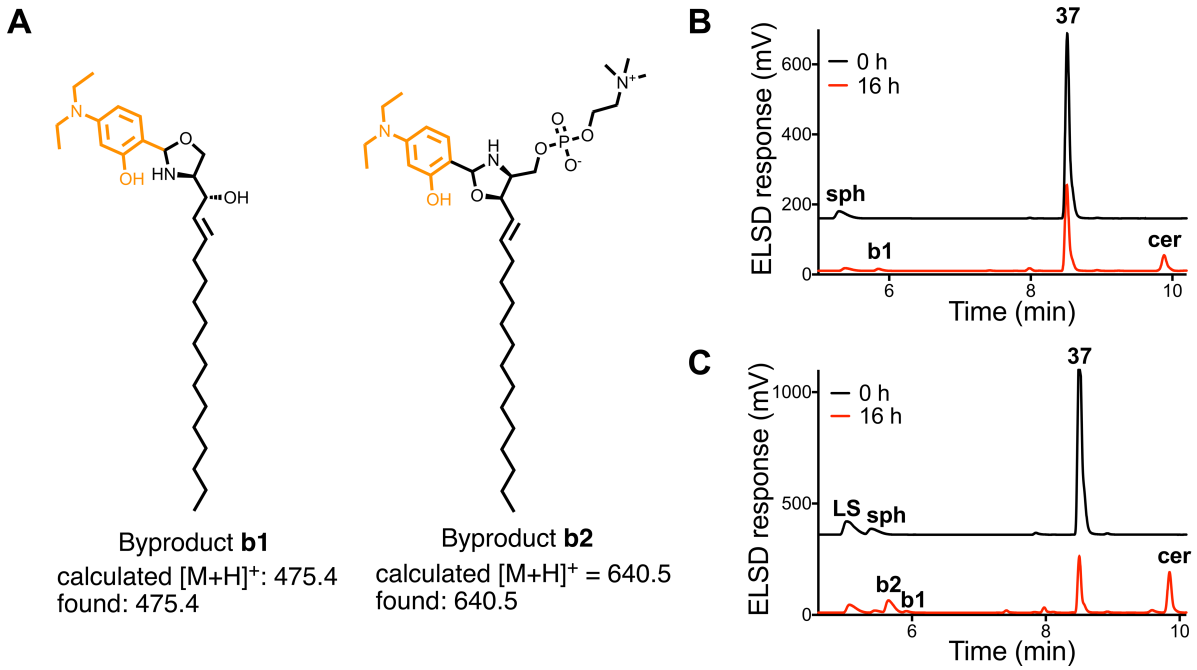

Figure 4.3 Reversible side products observed during TCL. A, Proposed structures of byproducts observed due to a reaction between the released salicylaldehyde auxiliary and sph (byproduct **b1**) and lysosphingomyelin (byproduct **b2**), analogous to intermediates proposed by Li.[110] B, **b1** is observed in the reaction between sph and **37**. C, **b1** and **b2** are observed in the reaction between sph and **37** in the presence of 1 eq. lysosphingomyelin (LS).

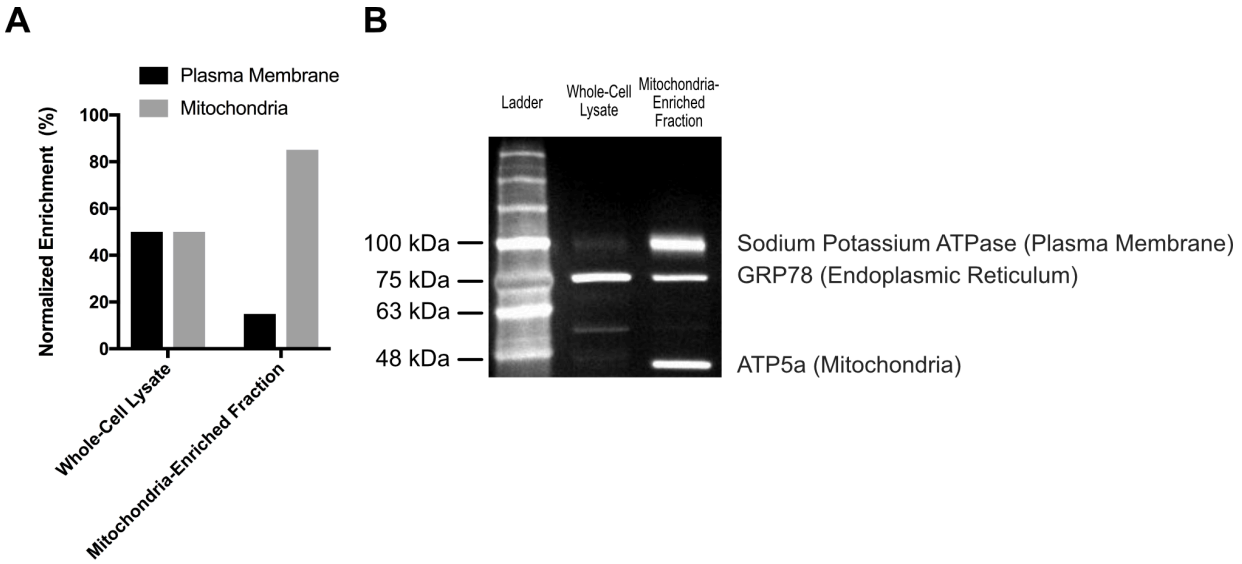

Figure 4.4 Validation of cell fractionation. A, Normalized enrichment of plasma membrane and mitochondria in whole-cell lysate and the mitochondria-enriched fraction (crude mitochondrial fraction). B, Western blot detection of markers specific to the plasma membrane, endoplasmic reticulum and mitochondria in the whole-cell lysate and mitochondria-enriched fraction.

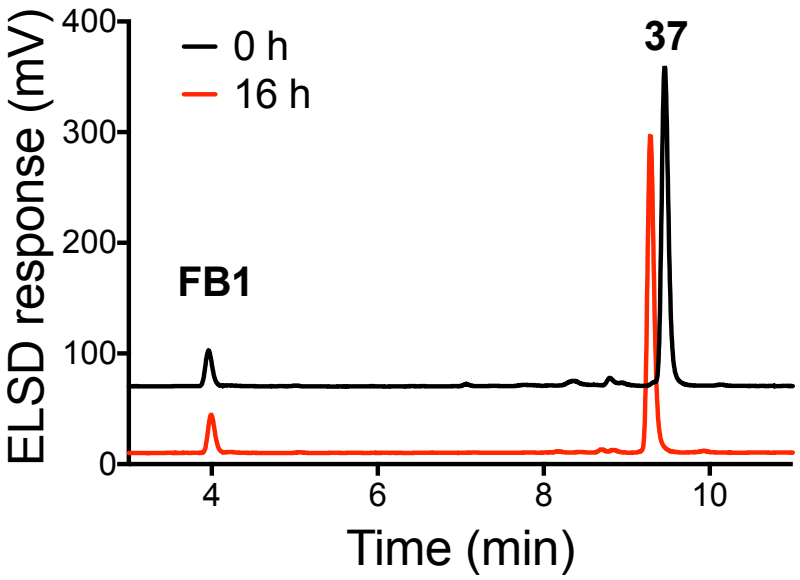

Figure 4.5 Fatty acid salicylaldehyde **37** and fumonisin B1 (**FB1**) do not react in model membranes. 250 μM FB1 and 500 μM 37 were incubated in phospholipid vesicles at 37 ºC, pH 7.4 over a period of 12 h. No degradation of FB1 or 37 was observed.

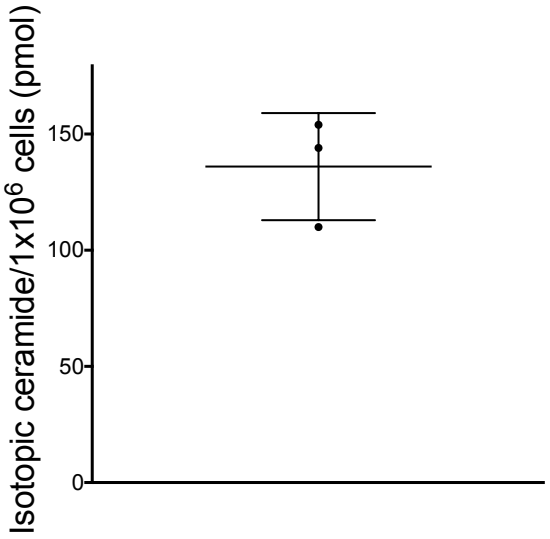

Figure 4.6 Quantification of TCL *in vivo*. Isotopic ceramide was detected in whole-cell lipid extracts of HeLa cells after performing TCL. Samples were analyzed by LCMS and the isotopic ceramide peak integrated to determine moles of ceramide based on a standard curve. This procedure was performed in triplicate and samples were normalized to the number of cells pre-lysis. Error bar represents standard deviation.

4.3 Synthesis of C16:0 Ceramide by TCL Triggers Apoptosis in Live Cells

Having confirmed the reaction proceeds in living cells, we investigated whether ceramide-induced apoptosis could be effected by TCL.[104,105] Certain ceramide species, most notably C16:0 ceramide, are known to increase in concentration during apoptosis.[116,117] Evidence suggesting that increases in levels of certain ceramides can directly trigger apoptosis is based on studies utilizing unnatural short-chain ceramides. These non-native ceramides exhibit substantial differences in structure, solubility, lipid ordering effects, and intracellular diffusion, raising concerns about the validity of these conclusions.[118,119] To test whether we could use TCL to study the apoptotic effects of natural C16:0 ceramide in cells, we incubated cultured HeLa cells in the presence of 100 μM **37** and varying concentrations of sphingosine. Cell viability was not impacted by **37** alone, but incubation with **37** and sphingosine together resulted in significantly lower cell viability compared to the same concentration of sphingosine alone (Figure 4.7A). Exogenous addition of 100 μM C16:0 ceramide had no effect on cell viability, highlighting the substantial increase in ceramide delivery through *in situ* TCL, and providing further evidence that TCL occurs intracellularly. Additionally, to confirm that the decrease in viability is due to TCL and not the metabolism of sphingosine to ceramide, we performed the same cell viability assay in the presence of FB1 and observed the same decrease in cell viability when cells were treated with **37** and sphingosine together compared to sphingosine alone (Figure 4.8). Visual quantification of cell death (Figure 4.7B) and fluorescent detection of caspase 3/7 activity (Figure 4.7C and Figure 4.9) confirmed that C16:0 ceramide delivered via TCL results in the activation of apoptotic caspases. To determine if TCL is compatible with cell lines other than HeLa cells, we performed the same viability experiments using NIH3T3 cells (Figure 4.10). Again, we observed significantly lower cell viability in cells treated with **37** and sphingosine as compared to **37** or sphingosine alone.

C16:0 ceramide is hypothesized to exert its proapoptotic function through the recruitment of the protein Bax to the mitochondria, which in turn triggers mitochondrial membrane permeabilization and eventual cell death[120–122]. This model, however, is based on a correlation between increased levels of cellular ceramide and Bax association with the mitochondria[121], or studies using unnatural short-chain ceramides[123]. Therefore, it remains unclear if C16:0 ceramide is an effector of Bax translocation *in vivo*. To determine whether an intracellular increase in C16:0 ceramide alone is sufficient to trigger Bax recruitment to mitochondria, we transiently expressed a Bax-GFP fusion protein in HeLa cells and observed the localization of Bax-GFP with respect to the mitochondrial staining dye Mitotracker. TCL-driven synthesis of C16:0 ceramide within cells resulted in Bax-GFP transitioning to a punctate distribution which partially colocalized to the mitochondria, consistent with previous reports of Bax localization during apoptosis[124,125] (Figure 4.7D and Figure 4.11). These results demonstrate that increases in intracellular C16:0 ceramide can directly trigger Bax translocation and suggest that this lipid plays a central role in Bax-induced apoptosis.

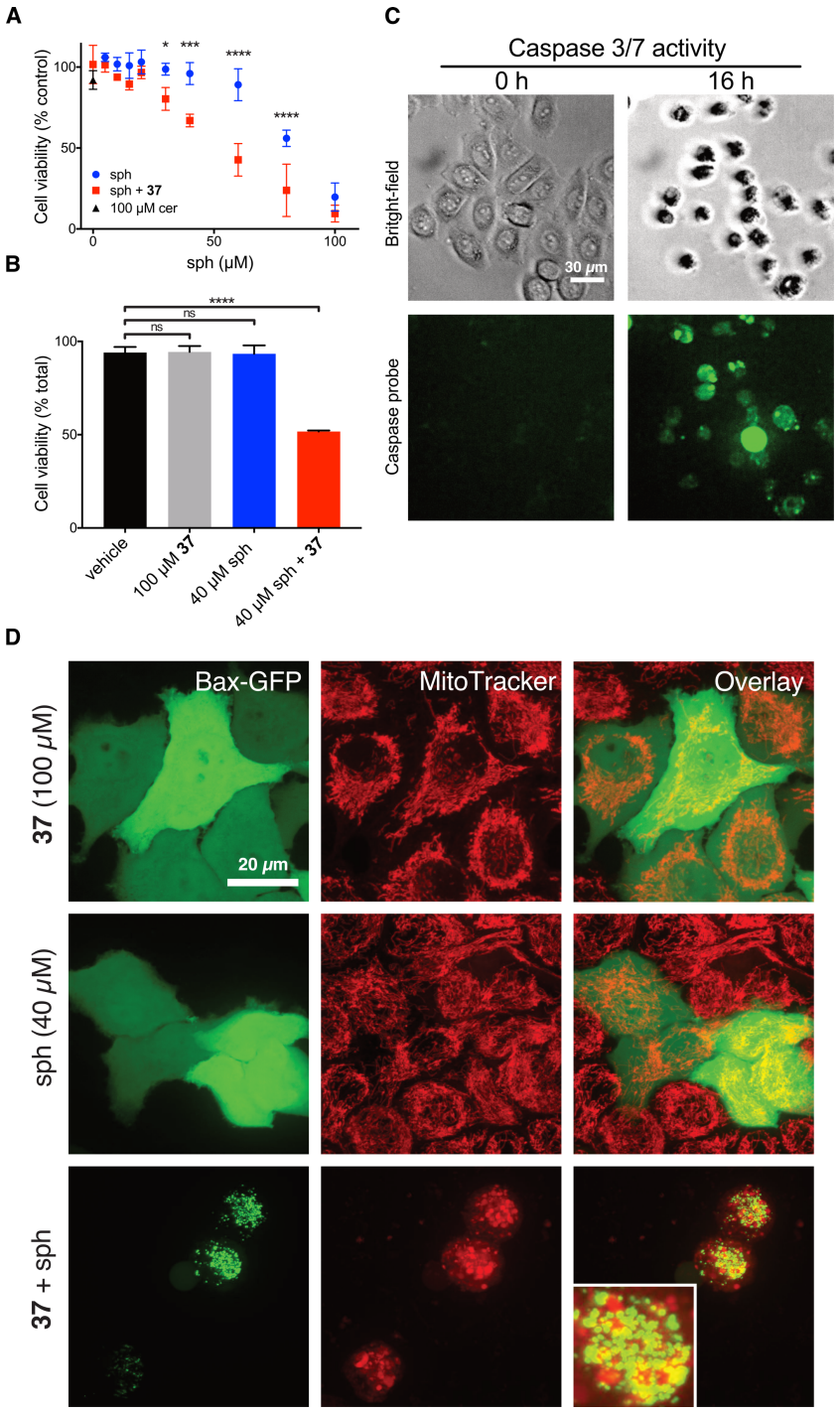

Figure 4.7 TCL in live cells triggers apoptosis. A and B, Treatment of cultured HeLa cells with 100 μM **37** and sph results in significantly more cell death than sph alone as monitored by a WST-1 proliferation assay (A) and total live cell count (B). Viability assays were performed in three biological replicates and shown as means ± SD. Statistically significant differences between points at a given sph concentration (A) or condition (B) are indicated *$p < 0.05$, **$p < 0.01$, ***$p < 0.001$, ****$p < 0.0001$. C, Treatment of HeLa cells with 100 μM **37** and 40 μM sph results in the activation of caspases necessary for apoptosis. D, Production of C16:0 ceramide during traceless ceramide ligation triggers translocation of Bax-GFP from the cytosol to mitochondria during apoptosis (images in (D) are maximum intensity Z-projections).

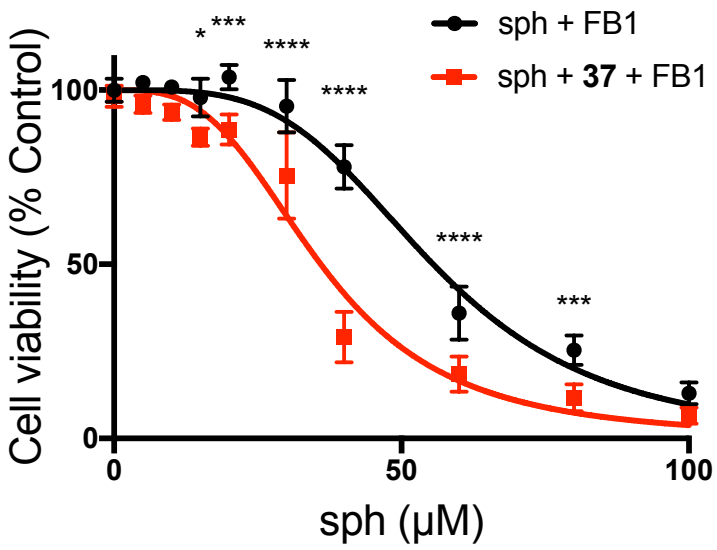

Figure 4.8 TCL induced cell death is not affected by the presence of a ceramide synthase inhibitor.Treatment of cultured HeLa cells with 100 μM **37** and sph results in significantly more cell death than sph alone in the presence of 25 μM fumonisin B1 (FB1) as monitored by a WST-1 proliferation assay. Viability assays were performed in three biological replicates and shown as means ± SD. Statistically significant differences between points at a given sph concentration are indicated *p < 0.05, ***p < 0.001, ****p < 0.0001.

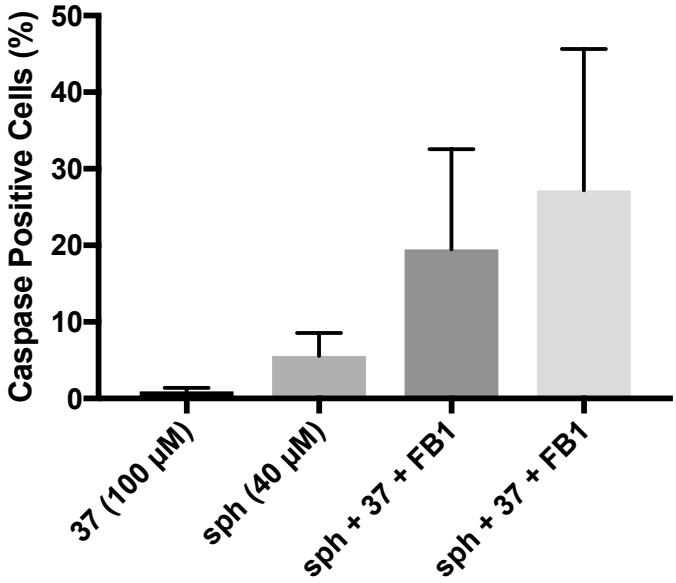

Figure 4.9 TCL triggers apoptosis in HeLa cells. Cells treated with sphingosine (sph) and 37, or sph, 37 and 25 μM fumonisin B1 (FB1) show higher levels of apoptosis compared to those treated with 37 or sph alone. Detection of Caspase 3/7 was performed using Cell Event Caspase-3/7 Green Detection Reagent (ThermoFisher). Four images at four different locations of the cell culture were taken for each condition using microscopy Method A. Percent caspase positive cells were counted and values shown as means ± SD.

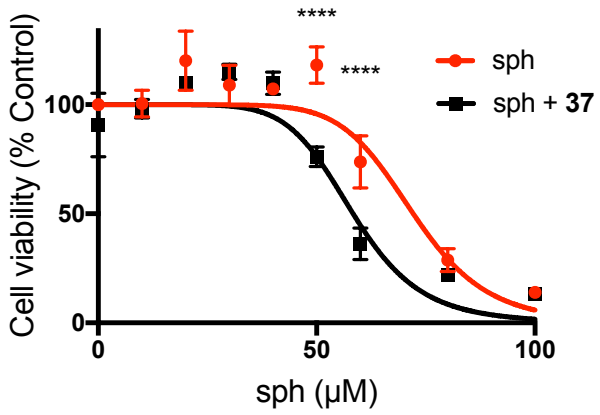

Figure 4.10 TCL triggers cell death in NIH3T3 cells. Treatment of cultured NIH3T3 cells with 100 μM **37** and sph results in significantly more cell death than sph alone as monitored by a WST-1 proliferation assay. Viability assays were performed in three biological replicates and shown as means ± SD. Statistically significant differences between points at a given sph concentration are indicated ****p < 0.0001.

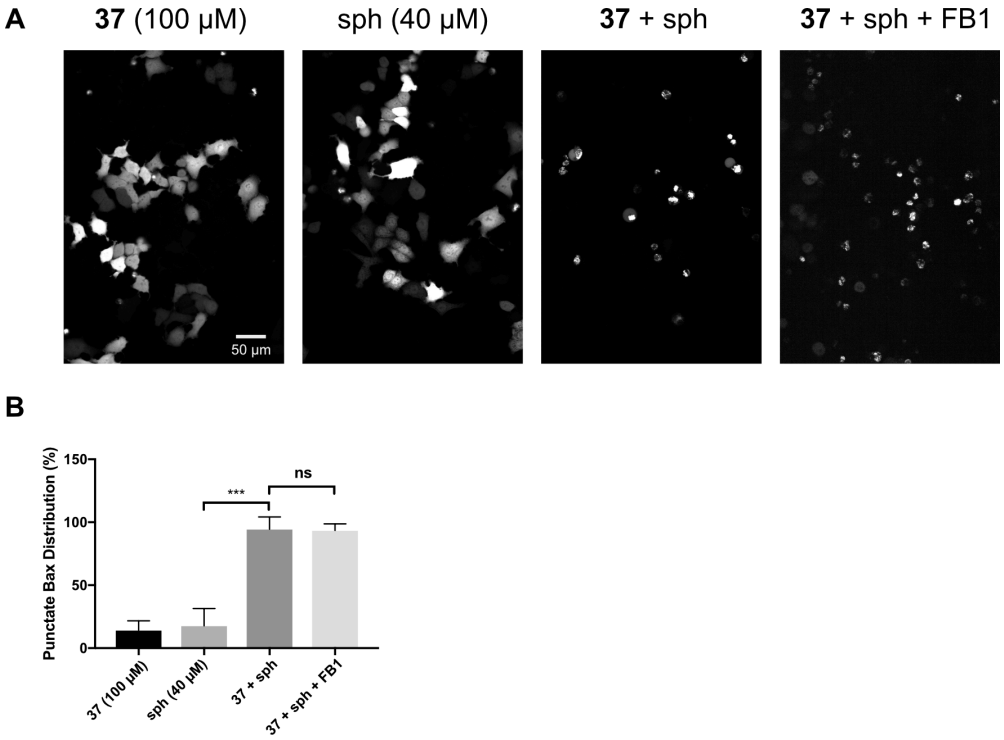

Figure 4.11 C16:0 ceramide triggers translocation of Bax-GFP from the cytosol to mitochondria during apoptosis. A, HeLa cells expressing Bax-GFP treated with sphingosine (sph) and **37**, or sph, **37** and 25 μM fumonisin B1 (FB1) show significantly more punctate Bax distribution compared to those treated with **37** or sph alone. B, Five images at five different locations of the cell culture were taken for each condition using microscopy Method A. Percent cells with a punctate Bax distribution were counted and values shown as means ± SD. ***p < 0.001.

4.4 TCL Can Synthesize Distinct Ceramide Species With Different Effects on Cell Viability

Cells produce numerous ceramide species with various N-fatty acyl groups.[126] Ceramides may exert differing biological effects depending on their acyl chain functionality.[100] Analyzing the roles of specific ceramide species are often confounded by the presence of six individual endogenous ceramide synthases (CerS1-6), which produce multiple ceramide products varying in both chain length and degree of unsaturation.[108] Additionally, many ceramide species are produced by more than one ceramide synthase, further hindering their study through traditional biochemical methods.[108,126] TCL offers the capability to deliver individual and specific ceramides to cells, something not possible through manipulation of cellular metabolism. As a proof of concept, we synthesized salicylaldehyde esters with differing fatty acid substituents **38**, **39** and **40**, and confirmed that they react with sphingosine to yield a range of ceramide products (Figure 4.12). We then generated the different ceramides in living HeLa cells and studied the effect of ceramide structure on cell viability. Delivery of fully saturated C16:0 or C18:0 ceramide using TCL resulted in a significant reduction in cell viability as compared to the sphingosine control (Figure 4.13A-B). In contrast, we observed no reduction in cell viability when monounsaturated C18:1 or C24:1 ceramide was delivered (Figure 4.13C-D). Differences in chain length did not affect the intracellular delivery of the precursors, as there was no significant difference in cellular levels of C16:0 and C18:1 ceramide formed after addition of sphingosine and isotopic salicylaldehyde esters **37i** and **38i** (Figure 4.14). We hypothesized that the observed difference in apoptotic activity of different ceramide species may be due to their ability to promote translocation of Bax to the mitochondria. To test this, we used TCL to synthesize C16:0 and C24:1 ceramide in HeLa cells expressing Bax-GFP. We found that Bax localized to the mitochondria significantly more when cells were treated with C16:0 ceramide (95 ± 2 % of cells) than when they were exposed to C24:1 ceramide (10 ± 6 % of cells) (Figure 4.13E-F and Figure 4.15). Our results suggest that ceramide

saturation plays a determinant role in the apoptotic activity of the molecule and support the hypothesis that ceramide-enriched membrane domains, formed preferentially by saturated ceramides, are required for the recruitment of Bax to the mitochondria and the activation of apoptosis pathways.[100,121,127]

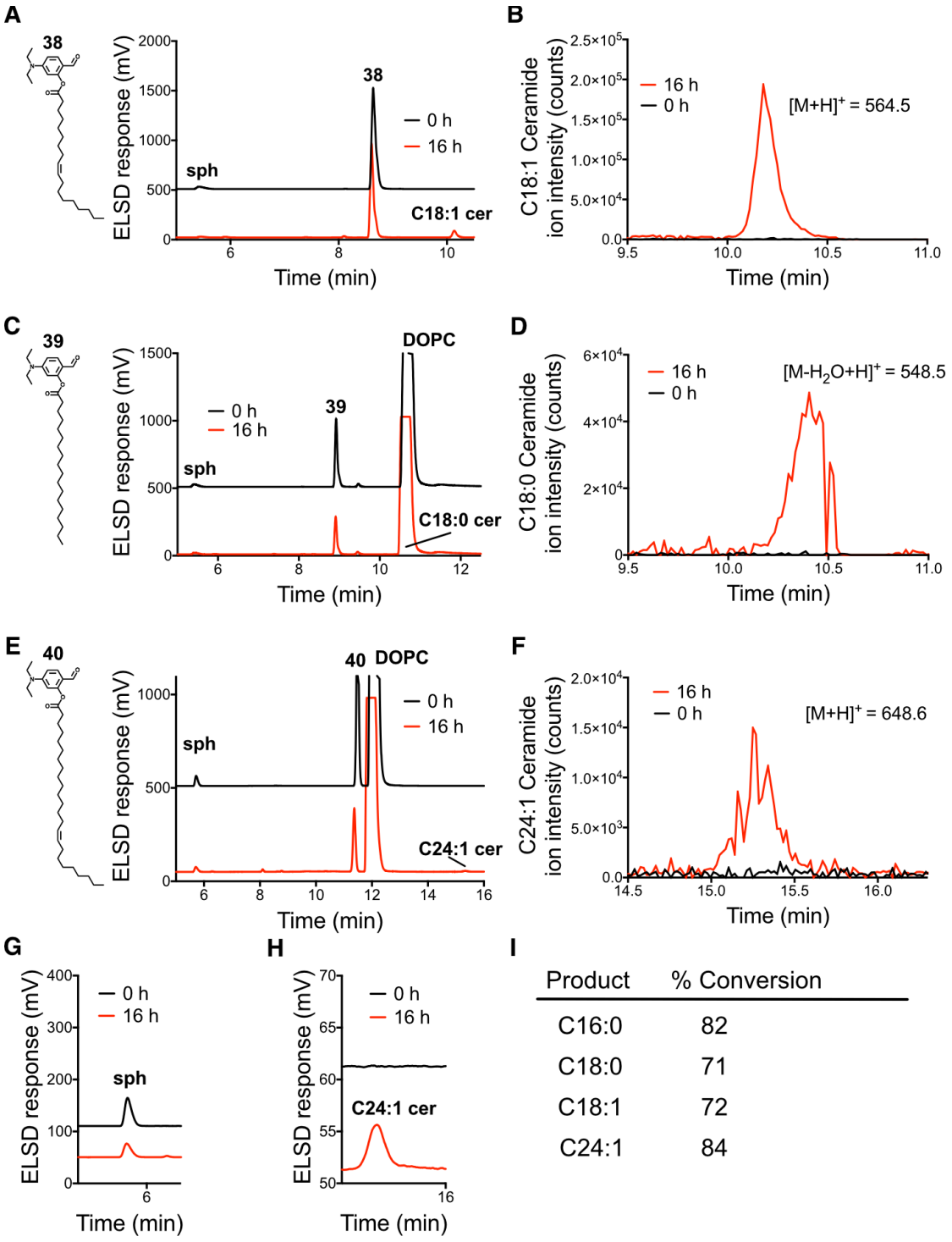

Figure 4.12 Fatty acid salicylaldehyde esters of different fatty acids react efficiently with sphingosine (sph) in model membranes to form the corresponding natural long chain ceramides (cer). HPLC traces of ELSD response (A, C, E), and MS detection of ceramide products (B, D, F) during TCL between sph and, **38** (A and B), **39** (C and D) and **40** (E and F). G and H, magnification of sph and cer peaks from HPLC trace in (E). I**,** Percent conversion of TCL reactions calculated by consumption of fatty acid salicylaldehyde ester precursors as monitored by HPLC peak absorbance at 280 nm.

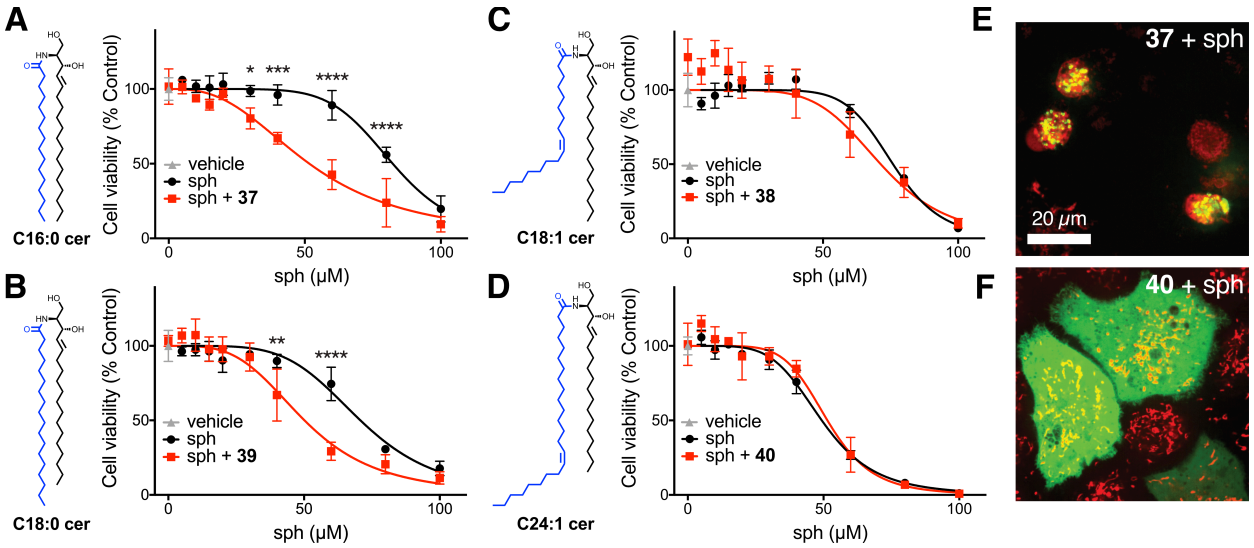

Figure 4.13 TCL delivery of specific ceramide species reveals an N-acyl chain saturation dependent effect on cell viability and Bax localization. A-D, Viability of cultured HeLa cells after 16 h incubation with TCL precursors as monitored by a WST-1 viability assay. Treatment of cells with 100 μM **37** (A) or 100 μM **39** (B) and sph results in significantly more cell death than sph alone. Cells treated with 100 μM **38** (C) or 100 μM **40** (D) and sph, or sph alone show no significant difference in cell viability. Viability assays were performed in three biological replicates and shown as means ± SD. Statistically significant differences between points at a given sph concentration are indicated *$p < 0.05$, **$p < 0.01$, ***$p < 0.001$, ****$p < 0.0001$. Lines represent a normalized dose-response curve with variable slope. E and F, Composite images of Bax-GFP (green) and MitoTracker (red) after treatment with 100 μM **37** or **40** and 40 μM sph for 16 h. Generation of C16:0 ceramide within HeLa cells promotes translocation of Bax-GFP to the mitochondria (E), while synthesis of C24:1 ceramide has no effect on Bax-GFP localization (F) (images are maximum intensity Z-projections).

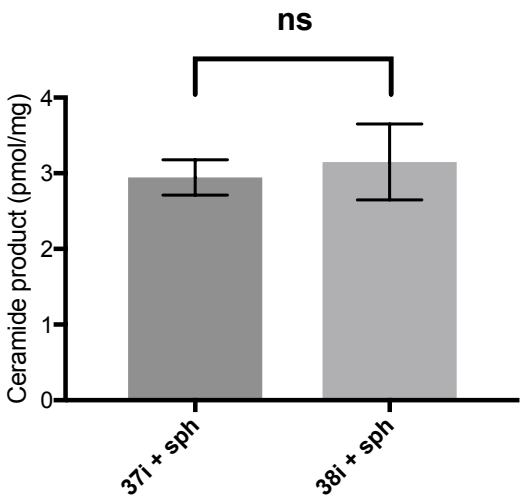

Figure 4.14 Quantification of TCL in crude mitochondrial cell fractions. Isotopic ceramide products of sphingosine and **37i** (n = 2) or sphingosine and **38i** (n = 3) were detected in crude mitochondrial fractions of HeLa cells after performing TCL. Samples were analyzed by LCMS and the isotopic ceramide peak integrated to determine moles of ceramide based on a standard curve. Ceramide formation is reported as pmol ceramide product per mg of total lipid extracted. Error bars represent standard deviation.

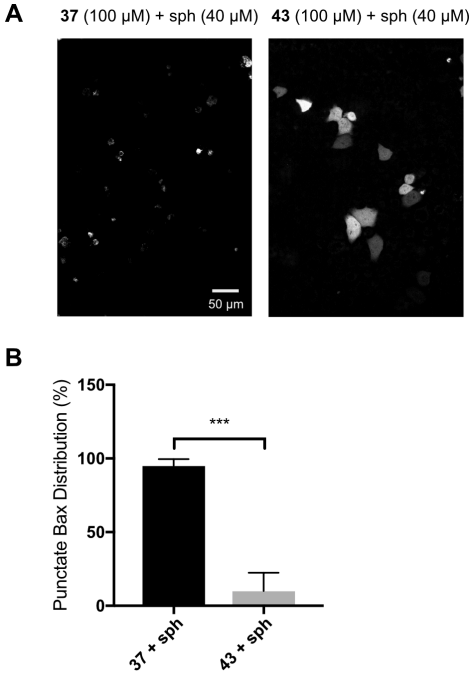

Figure 4.15 Saturation-specific effects of ceramide on Bax-GFP behavior. A, HeLa cells expressing Bax-GFP treated with sphingosine (sph) and **37** show significantly more punctate Bax distribution compared to those treated with sph and **40**. B, Five images at five different locations of the cell culture were taken for each condition using microscopy Method A. Percent cells with a punctate Bax distribution were counted and values shown as means ± SD. ***$p < 0.001$.

4.5 Photoinitiated TCL in Live Cells

Ceramide formation is stringently controlled in both time and space [64]. We sought to achieve a similar level of control using our ligation strategy. Previously, light reactive photocages have been developed for the protection and photoinitiated deprotection of biological lipids including sphingosine and ceramide [11,128,129]. While photocaged ceramide is an exceptional tool for the study of ceramide in model membranes [129], it has seen limited application in biological systems [109]. Modifying a previous synthetic scheme, we successfully synthesized a coumarin photocaged analog of sphingosine, **43**. We found that this compound was stable in HeLa cell lysate (Figure 4.16) and, upon UV exposure, was uncaged to yield sphingosine with a half-life of 10.6 s (Figure 4.17). We used the efficient uncaging and stability of this compound to spatiotemporally control ceramide synthesis in a live cell system. To determine the effect of **43** uncaging in cells, we cultured HeLa cells expressing Bax-GFP as a marker of apoptosis and then exposed them to a range of concentrations of the compound **43** (0-300 μM) and irradiated multiple regions of the cell culture with 405 nm laser and imaged over 10 h (Figure 4.18). We chose to use 50 μM **43** for TCL experiments because it did not result in significant cell death after irradiation but, based on cell viability experiments (Figure 4.7A), should provide a level of sphingosine sufficient for TCL. 100 μM **37** and 50 μM **43**. Using laser scanning microscopy, we uncaged **43** in a single cell using the 405 nm laser line and then imaged over a period of 12 hrs. We found that after 10 h, only the cell in which **43** was uncaged underwent apoptosis, evidenced by the shrinkage of the membrane and punctate Bax-GFP localization (Figure 4.19). Controls in which cells were incubated with **37** or **43** separately, and single cells irradiated under the same conditions, showed no apoptosis over the same period (Figure 4.20). To determine if this same behavior occurred when **43** was uncaged in multiple cells, we treated HeLa cells under the same conditions as before but irradiated multiple cells in several regions of the chamber slide. As expected, we found that irradiation of cells treated

with **37** and **43** resulted in significantly more cell death than irradiation of cells treated with **43** alone (Figure 4.21). Furthermore, we found that when cells were treated with precursors which form the unsaturated C24:1 ceramide (100 μM **40** and 50 μM **43**) and then irradiated under the same conditions, there was no significant difference in cell death as compared to cells treated with **43** alone (Figure 4.21). Spatiotemporally controlled TCL allows for the delivery of ceramides in a cell-selective manner. This could allow for modulation of specific ceramide levels in defined cells or regions of an organism, and help to uncover the roles of ceramide in development [130], neurodegeneration [131], and cancer [105].

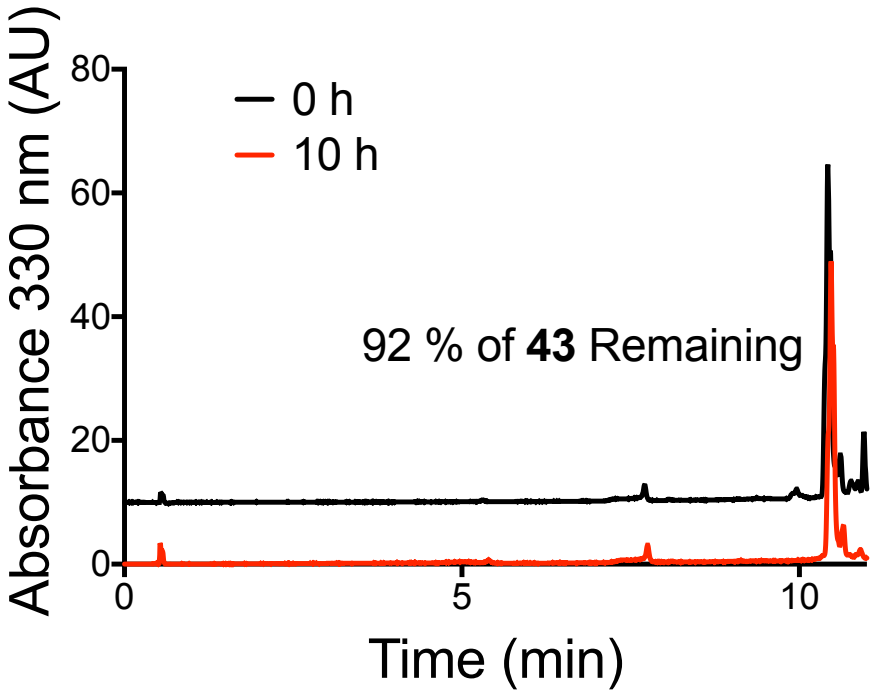

Figure 4.16 Cellular stability of photocaged sphingosine compound, **43**. **43** was added to HeLa cell lysate and a lipid extraction performed immediately or after a 10 h incubation at 37 ºC. The extracted lipid fractions were analyzed by HPLC and stability calculated by integration of the 330 nm absorbance peak of **43**.

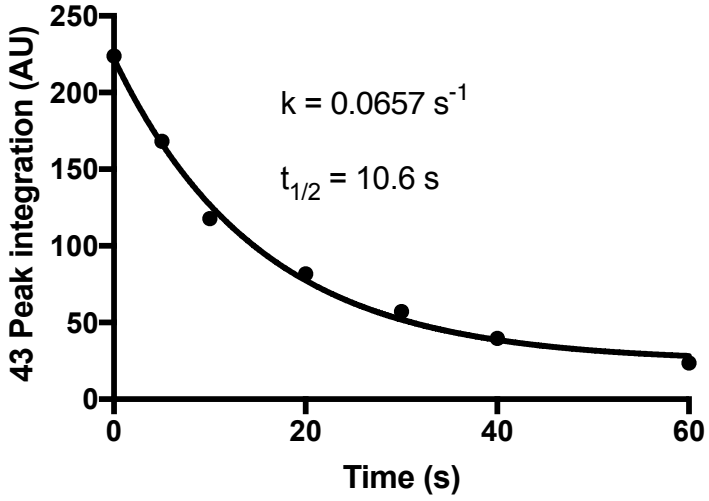

Figure 4.17 Photouncaging of compound **43** by UV light. Conversion of **43** by 360 nm light was monitored by HPLC using absorbance at 330 nm. Integration of the absorbance peak was plotted relative to time using GraphPad Prism software and the corresponding data fit shown ($k = 0.0657\ s^{-1}$, $t_{1/2} = 10.6$ s).

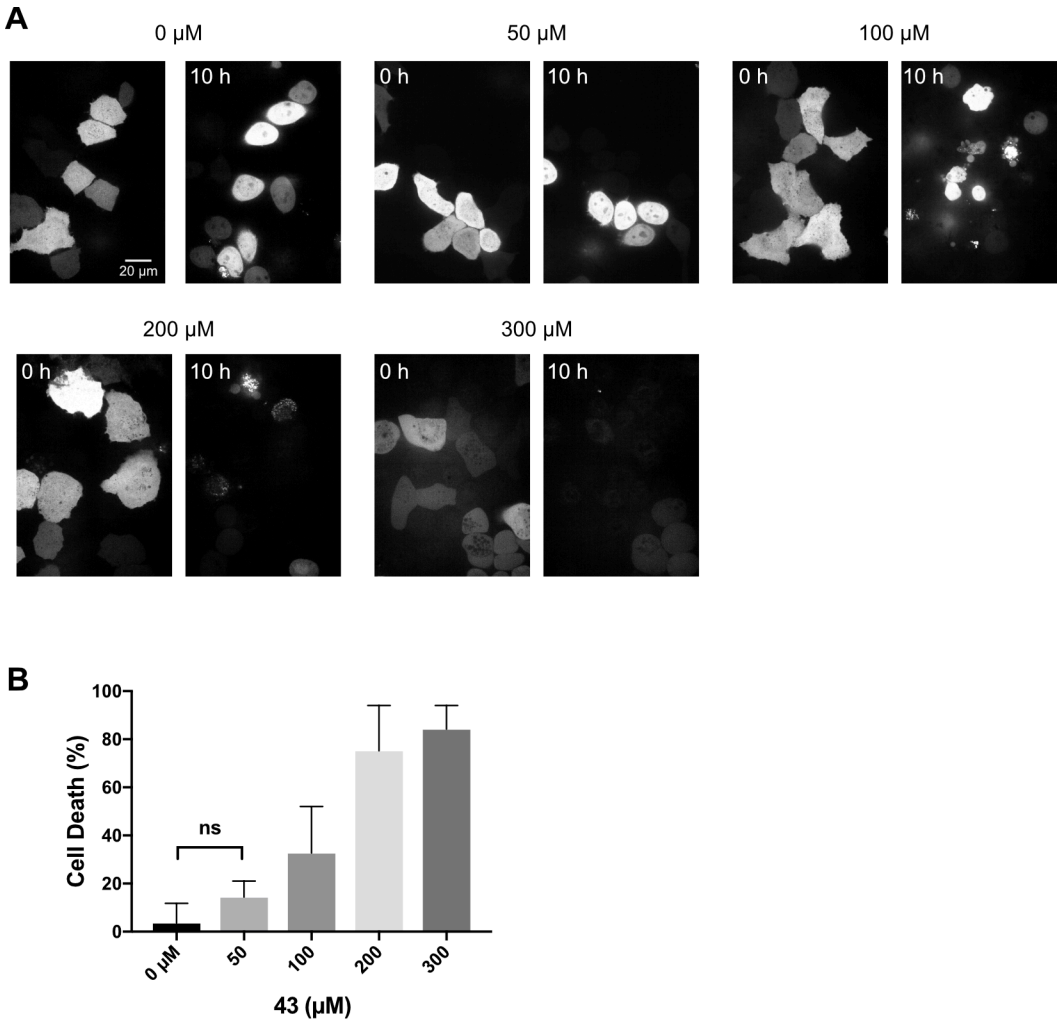

Figure 4.18 Dose response of sphingosine uncaging in cells. A, HeLa cells expressing Bax-GFP were treated with photocaged sphingosine **43** at a range of concentrations and then uncaged using microscopy Method C and imaged for 10 h. Cell death increased with increasing concentration of **43**. B, For each condition, images were taken every 30 min over 10 h at five different locations of the cell culture using microscopy Method A. Percent cell death was monitored using Bax-GFP localization and values shown as means ± SD.

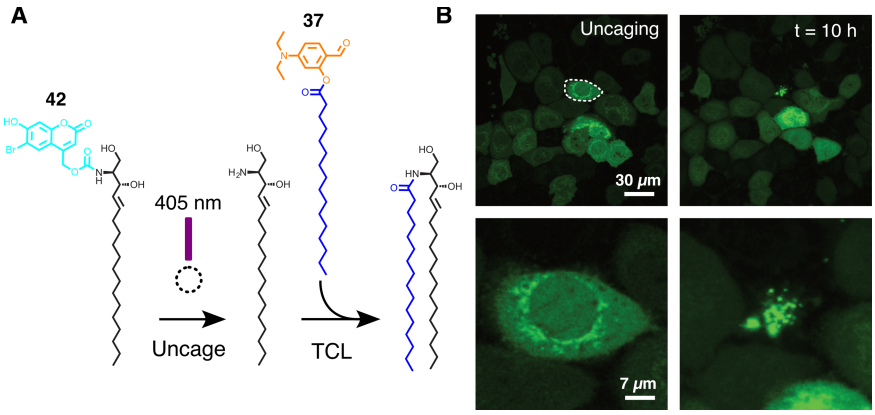

Figure 4.19 Photocontrolled initiation of TCL. A, Photocaged sphingosine **43** can be uncaged by 405 nm laser light to produce sph and trigger TCL. B, HeLa cells expressing Bax-GFP were incubated with 100 μM **37** and 50 μM **43**. A single cell in the frame was exposed to 405 nm laser within the outlined area (left panels) and the sample imaged over a period of 12 hrs. After 10 h, only the cell in which ceramide synthesis was triggered showed cell death and mitochondrial Bax localization characteristic of C16:0 ceramide-induced apoptosis (right panels) (t = 10 h images are maximum intensity Z-projections).

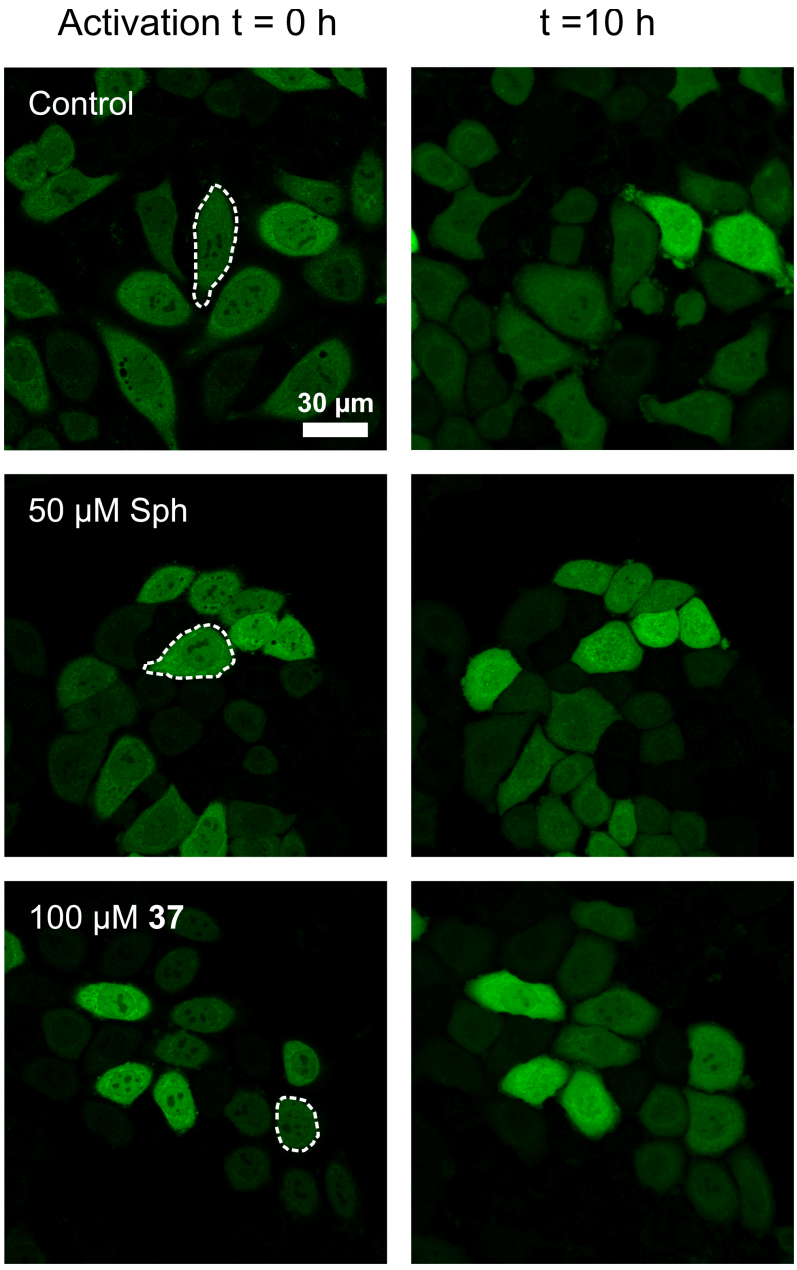

Figure 4.20 Controls for photocontrolled initiation of TCL. HeLa cells expressing Bax-GFP were incubated with 100 µM **37,** 50 µM **43** or no compound. A single cell in the frame was exposed to 405 nm laser within the outlined area (left panels) and the sample imaged over a period of 10 h. After 10 h, the irradiated cells showed no cell death or change in morphology compared to surrounding cells (right panels) (t = 10 h images are maximum intensity Z-projections).

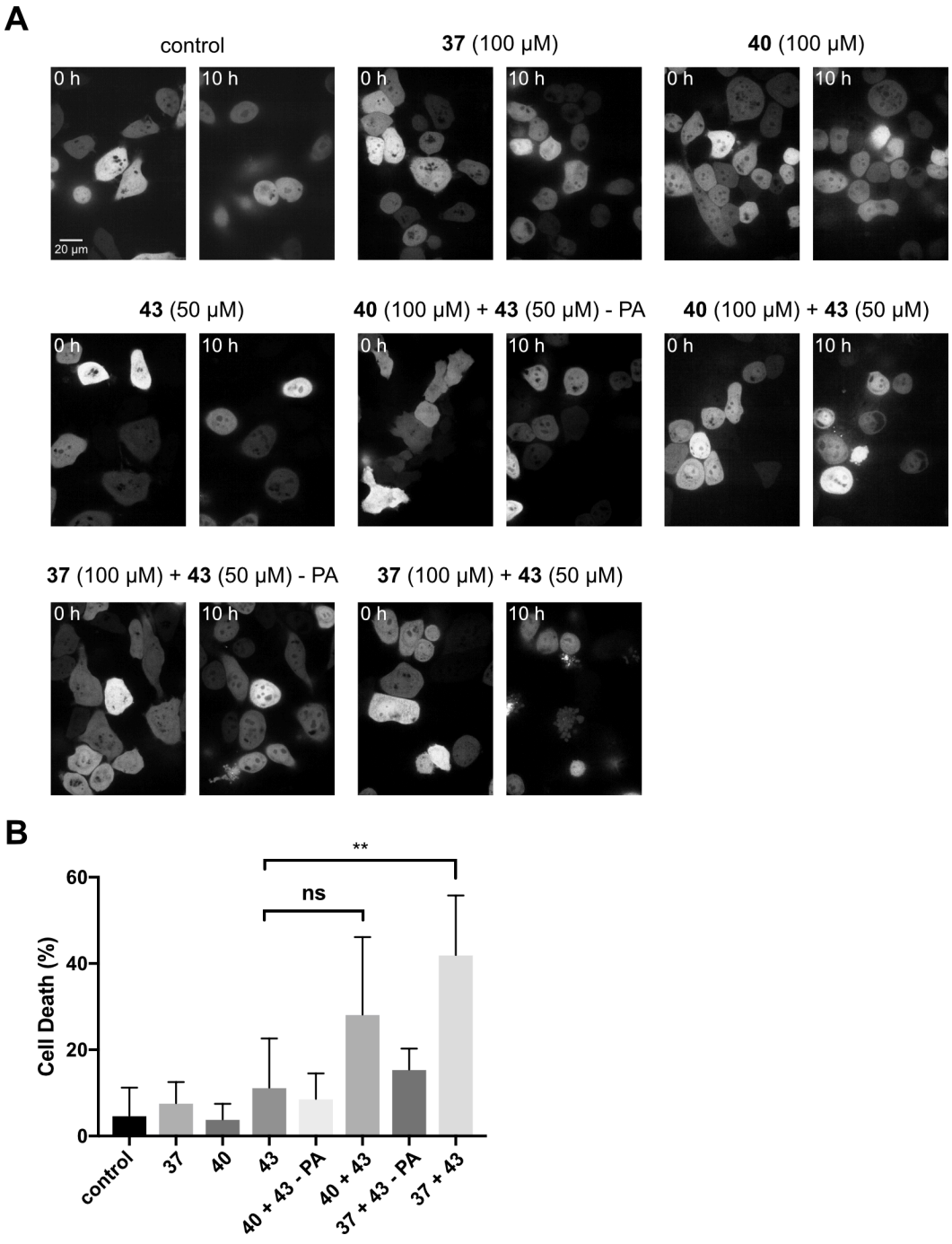

Figure 4.21 Photocontrolled initiation of TCL in multiple cells. A, HeLa cells expressing Bax-GFP were treated with no compound, **37**, **40**, **43**, **40** + **43** (with or without photoactivation (- PA)) or **37** + **43** (with or without photoactivation (- PA)) and then uncaged using microscopy Method C and imaged for 10 h. B, For each condition, images were taken every 30 min over 10 h at five different locations of the cell culture using microscopy Method A. Percent cell death was monitored using Bax-GFP localization and values shown as means ± SD. **$p < 0.01$

4.6 Conclusion

In conclusion, we have implemented an *in situ* synthesis scheme for the direct study of ceramides *in vivo*. Our method enables controlled delivery of specific, full-length ceramides to cells, which is necessary for understanding their specific biological effects. TCL has allowed us to investigate the role of C16:0 ceramide in apoptosis, and demonstrate that ceramide saturation is an important modulator of ceramide-driven apoptosis. Future studies using TCL will prove helpful in understanding the metabolism of *in situ* generated ceramides and their effects on endogenous lipid levels. Furthermore, application of our approach to other lipids may facilitate the study of this often intractable class of biomolecules.

4.7 Experimental Methods

4.7.1 Synthesis of Large Unilamellar Vesicles (LUVs)

5 μmol of dioleoylphosphatidylcholine (DOPC) in a 20 mg/mL $CHCl_3$ solution was added to a glass vial and dried into a film under a stream of nitrogen. 1 mL of buffer (1x PBS or 1x PBS + 5 mM serine) was added to the vial and then the vial tumbled at RT for 1 hr. After tumbling, the formed solution was subjected to 10 freeze/thaw cycles using a dry ice/ethanol bath and a warm water bath with vortexing before every freeze step. The vesicle solution was then extruded 10 times through a 100 nm polycarbonate filter (Whatman, GE Healthcare Bio-Sciences) using an Avanti Mini-Extruder (Avanti Polar Lipids) to produce LUVs.

4.7.2 Traceless Ceramide Ligation in LUVs

To a solution of 5 mM DOPC LUVs was added sphingosine (as a 40 mM solution in MeOH) to a final concentration of 250 μM and **35**, **36**, **37**, **38**, **39** or **40** (as a 20 mM solution in n-butanol) to

a final concentration of 500 μM. The reaction was incubated at 37 ºC in a water bath and 10 μL aliquots taken at specified times for HPLC analysis (Eclipse Plus C8 column (50 or 75 mm), *0-7 min,* 50-95% MeOH in water, *7 min-end*, 95% MeOH in water).

4.7.3 Validation of Cell Fractionation

HeLa cells, maintained in DMEM (10 % FBS, 1 % penicillin/streptomycin) were plated in 10 cm culture dishes and grown to confluency at 37 ºC, 5 % CO_2. Once confluent, cells were detached from their culture dish using a plastic cell scraper and the cell suspension was pelleted by centrifugation at 400 rcf for 5 min. Supernatant was removed and the cell pellets were resuspended in 1 mL fractionation buffer (250 mM sucrose, 20 mM HEPES [pH 7.4], 10 mM KCl, 1.5 mM $MgCl_2$, 1 mM EDTA, 1 mM EGTA). Cells were lysed using a Dounce homogenizer and the lysate transferred to a 1.7 mL Eppendorf tube. The lysate was centrifuged at 700 rcf for 6 min to pellet unbroken cells and nuclei. The supernatant was collected and transferred to a new Eppendorf tube and centrifuged at 10,000 rcf for 10 min to pellet the crude mitochondrial fraction. The supernatant was discarded, and the pellet was resuspended in 100 μL fractionation buffer. Samples were diluted with loading buffer and resolved by electrophoresis using 4–20% SDS–polyacrylamide gels (Bio-Rad) under denaturing and reducing conditions. Proteins were then electrotransferred to a PVDF membrane (Bio-Rad). The membrane was blocked with 3% BSA and then subjected to immunoblot analysis using primary and secondary antibodies from Membrane Fraction WB Cocktail (ab140365) (Abcam) according to the manufacturer's instructions. Chemiluminescent detection was performed by using SuperSignal West Pico PLUS chemiluminescent substrate (ThermoFisher) according to manufacturer's instructions. Membrane images were processed, and band intensities quantified using ImageJ.

4.7.4 MS Detection of Traceless Ceramide Ligation *in vivo*

HeLa cells, maintained in DMEM (10 % FBS, 1 % penicillin/streptomycin) were plated in 6 cm culture dishes and grown to confluency at 37 ºC, 5 % CO_2. Once confluent, media was removed and then the appropriate volume of DMEM (10 % FBS, 1 % penicillin/streptomycin) was added to achieve a final volume of 3 mL media per dish after addition of reaction components. Where indicated, fumonisin B1 was added to a final concentration of 25 μM in 3 mL media. Components of the ligation reaction were prepared as 500 μM solutions in DMEM by diluting stock organic solutions (sphingosine: 40 mM in MeOH, **37i**: 20 mM in n-butanol). **37i** was added to a final concentration of 100 μM in designated plates and the cells incubated at 37 ºC, 5 % CO_2 for 4 h (A 4 h preincubation was used to allow **37i** to internalize in cells. We found this preincubation time resulted in significant levels of ceramide product as detected by MS), after which sphingosine was added to a final concentration of 50 μM in designated plates. Cells were then incubated for 16 h at 37 ºC, 5 % CO_2. After incubation, cells were detached from their culture dish using a plastic cell scraper and the cell suspension (~3 mL) was pelleted by centrifugation at 400 rcf for 5 min. Supernatant was removed and the cell pellets were resuspended in 1 mL fractionation buffer (250 mM sucrose, 20 mM HEPES [pH 7.4], 10 mM KCl, 1.5 mM $MgCl_2$, 1 mM EDTA, 1 mM EGTA). Cells were lysed using a Dounce homogenizer and the lysate transferred to a 1.7 mL Eppendorf tube. The lysate was centrifuged at 700 rcf for 6 min to pellet unbroken cells and nuclei. The supernatant was collected and transferred to a new Eppendorf tube and centrifuged at 10,000 rcf for 10 min to pellet the crude mitochondrial fraction. The supernatant was discarded, and the pellet was resuspended in 100 μL fractionation buffer. Lipids were extracted from the crude mitochondrial fraction using the Bligh and Dyer method.[114] For this, the resuspended crude mitochondrial pellet was transferred to a glass vial and to it was added 350 μL 1:2 $CHCl_3$:MeOH and the vial vortexed for 10 min. Next, 150 μL $CHCl_3$ was added and the vial vortexed for 1 min.

Finally, 150 µL of 1 M NaCl was added and the vial and vortexed for 1 min. The organic layer of the extraction was collected, and solvent removed by rotary evaporation. The residue was dissolved in 200 µL MeOH and analyzed by LC (Eclipse Plus C8 column, *0-7 min,* 50-95% MeOH in water, *7-12 min*, 95% MeOH in water) to an Agilent 6100 Series Single Quadrapole MS (Agilent Technologies) running in Selected Ion Monitoring (SIM) mode for the isotopic ceramide peak ($[M+H]^+$ = 542.5).

4.7.5 MS Quantification of Traceless Ceramide Ligation *in vivo* (Whole-Cell Extract)

The ligation reaction between **37i** and sphingosine was performed in HeLa cells grown in a 6 cm dish as described above. Before cell lysis, cells were counted on a cell counting slide and then lysed as before. A lipid extraction was performed on the entire cell lysate using a modified Bligh and Dyer method. For this, the cell lysate (1 mL) was transferred to a 15 mL falcon tube and to it was added 4 mL 1:2 $CHCl_3$:MeOH and the tube vortexed for 10 min. The extract was then centrifuged at 4000 rcf for 5 min to pellet cellular protein. Next, 1 mL $CHCl_3$ was added and the tube vortexed for 1 min. Finally, 3 mL of 1 M NaCl was added and the tube vortexed for 1 min. The organic layer of the extraction was collected, and solvent removed by rotary evaporation. The residue was dissolved in 200 µL MeOH and analyzed by LC (Eclipse Plus C8 column, *0-7 min,* 50-95% MeOH in water, *7-12 min*, 95% MeOH in water) to an Agilent 6100 Series Single Quadrapole MS (Agilent Technologies) running in SIM mode for the isotopic ceramide peak ($[M+H]^+$ = 542.5). The isotopic ceramide peak was integrated and then moles of ceramide were calculated based on a standard curve for C16:0 ceramide. This procedure was performed in triplicate and samples were normalized to number of cells pre-lysis.

4.7.6 MS Quantification of Traceless Ceramide Ligation *in vivo* (Crude Mitochondrial Fraction)

HeLa cells, maintained in DMEM (10 % FBS, 1 % penicillin/streptomycin) were plated in 6 cm culture dishes and grown to confluency at 37 ºC, 5 % CO_2. Once confluent, media was removed and then the appropriate volume of DMEM (10 % FBS, 1 % penicillin/streptomycin) was added to achieve a final volume of 3 mL media per dish after addition of reaction components. Components of the ligation reaction were prepared as 500 μM solutions in DMEM by diluting stock organic solutions (sphingosine: 40 mM in MeOH, **37i** and **38i**: 20 mM in n-butanol). **37i** and **38i** were added to a final concentration of 100 μM in designated plates and the cells incubated at 37 ºC, 5 % CO_2 for 4 h, after which sphingosine was added to a final concentration of 50 μM in all plates. Cells were then incubated for 16 h at 37 ºC, 5 % CO_2. After incubation, cells were detached from their culture dish using a plastic cell scraper and the cell suspension (~3 mL) was pelleted by centrifugation at 400 rcf for 5 min. Supernatant was removed and cells were resuspended in 1 mL of HBSS and then pelleted by centrifugation at 400 rcf. Supernatant was removed, and the cell pellets were resuspended in 1 mL fractionation buffer (250 mM sucrose, 20 mM HEPES [pH 7.4], 10 mM KCl, 1.5 mM $MgCl_2$, 1 mM EDTA, 1 mM EGTA). Cells were lysed using a Dounce homogenizer and the lysate transferred to a 1.7 mL Eppendorf tube. The lysate was centrifuged at 700 rcf for 6 min to pellet unbroken cells and nuclei. The supernatant was collected and transferred to a new Eppendorf tube and centrifuged at 700 rcf for 6 min again. The supernatant was collected and transferred to a new Eppendorf tube and centrifuged at 10,000 rcf for 10 min to pellet the crude mitochondrial fraction. The supernatant was discarded, and the pellet was resuspended in 100 μL fractionation buffer. Lipids were extracted from the crude mitochondrial fraction using the Bligh and Dyer method.[114] For this, the resuspended crude mitochondrial pellet was transferred to a glass vial and to it was added 350 μL 1:2 $CHCl_3$:MeOH

and the vial vortexed for 10 min. Next, 150 µL $CHCl_3$ was added and the vial vortexed for 1 min. Finally, 150 µL of 1 M NaCl was added and the vial and vortexed for 1 min. The organic layer of the extraction was collected, transferred to a pre-weighed vial, and solvent removed by rotary evaporation. The residue was dissolved in 100 µL MeOH and analyzed by LC (Eclipse Plus C8 column, *0-7 min,* 50-95% MeOH in water, *7-12 min*, 95% MeOH in water) to an Agilent 6100 Series Single Quadrapole MS (Agilent Technologies) running in Selected Ion Monitoring (SIM) mode for the corresponding isotopic ceramide peaks ($[M+H]^+$ = 542.5, isotopic C16:0 ceramide) or ($[M+H]^+$ = 582.6, isotopic C18:1 ceramide). The isotopic ceramide peaks were integrated and then moles of ceramide were calculated based on standard curves for C16:0 and C18:1 ceramide.

4.7.7 WST-1 Viability Assay

HeLa or NIH3T3 cells, maintained in DMEM (10 % FBS, 1 % penicillin/streptomycin) were plated in a 96-well plate at a density of 16,000 cells/well. After 24 h of incubation at 37 ºC, 5 % CO_2, media was removed and then the appropriate volume of DMEM (10 % FBS, 1 % penicillin/streptomycin) was added to achieve a final volume of 100 µL media per well after addition of reaction components (when fumonisin B1 was used, it was added to a final concentration of 25 µM in the media). Components of the ligation reaction were prepared as 500 µM solutions in DMEM by diluting stock organic solutions (sphingosine: 40 mM in MeOH, compounds **37**, **38**, **39**, **40**: 20 mM in n-butanol) (when fumonisin B1 was used, it was added to a final concentration of 25 µM in the media). 20 µL of the 500 µM fatty acid salicylaldehyde ester solution in media was added to designated wells and the cells incubated at 37 ºC, 5 % CO_2 for 4 h, after which varying amounts of the 500 µM sphingosine solution in media was added and the cells incubated again for 16 h at 37 ºC, 5 % CO_2. Additionally, volumes of organic vehicle corresponding to the maximum volumes used in the assay were added to cells and incubated for

the same period. At this point, 10 µL of the WST-1 solution (Sigma-Aldrich) was added to each well and the cells incubated at 37 ºC, 5 % CO_2 for 1 h. Absorbance measurements were taken using a Safire II plate reader (Tecan) at 440 nm using 690 nm as a reference. The background absorbance of the WST-1 reagent in media was subtracted and cell viability was reported as a percentage of the viability of the vehicle control. All conditions were tested in triplicate wells and plotted with error bars representing standard deviation.

4.7.8 Trypan Blue Assay

HeLa cells, maintained in DMEM (10 % FBS, 1 % penicillin/streptomycin, - Phenol Red) (Thermo Fisher) were plated in a 24-well plate (Sigma-Aldrich) at a density of 50,000 cells/well and allowed to attach overnight. Media was removed and then the appropriate volume of DMEM (10 % FBS, 1 % penicillin/streptomycin, -Phenol Red) was added to achieve a final volume of 500 µL media per well after addition of reaction components. Components of the ligation reaction were prepared as 500 µM solutions in DMEM by diluting stock organic solutions (sphingosine: 40 mM in MeOH, **37**: 20 mM in n-butanol). 100 µL of 500 µM **37** in media was added to designated wells and the cells incubated at 37 ºC, 5 % CO_2 for 4 h, after which 40 µL of 500 µM sphingosine in media was added to designated wells and the cells incubated again for 16 h at 37 ºC, 5 % CO_2. Media from each well (500 µL) was then removed and stored in corresponding Eppendorf tubes. Each well was then treated with 100 µL TrypLE dissociation agent (Thermo Fisher) and the dissociated cells were combined with the removed media fraction. 190 µL of each sample was removed from each tube and to it added 10 µL trypan blue solution 0.4% (Thermo Fisher). The trypan blue treated cells were then loaded onto a hemocytometer and cells were counted as either trypan blue excluding (viable) or trypan blue stained (non-viable). Viability is reported as the percentage of

viable cells in the total population. All conditions were tested in triplicate wells and plotted with error bars representing standard deviation.

4.7.9 Caspase Activity in HeLa Cells

HeLa cells, maintained in DMEM (10 % FBS, 1 % penicillin/streptomycin, - Phenol Red) were plated in an 8-well Lab-Tek chamber slide (Sigma-Aldrich) at a density of 32,000 cells/well and allowed to attach overnight. Media was removed and then the appropriate volume of DMEM (10 % FBS, 1 % penicillin/streptomycin, - Phenol Red) was added to achieve a final volume of 500 µL media per well after addition of reaction components (when fumonisin B1 was used, it was added to a final concentration of 25 µM in media). Components of the ligation reaction were prepared as 500 µM solutions in DMEM by diluting stock organic solutions (sphingosine: 40 mM in MeOH, **37**: 20 mM in n-butanol) (when fumonisin B1 was used, it was added to a final concentration of 25 µM in media). 100 µL of 500 µM **37** in media was added to designated wells and the cells incubated at 37 ºC, 5 % CO_2 for 4 h, after which 40 µL of 500 µM sphingosine in media was added to designated wells. Cells were then treated with CellEvent Caspase-3/7 Green (Thermo Fisher) according to the manufacturer's protocol. Cells were maintained at 37 ºC, 5 % CO_2 for 16 h while imaging using microscopy method A.

4.7.10 Bax Localization Experiments

HeLa cells, maintained in DMEM (10 % FBS, 1 % penicillin/streptomycin, -Phenol Red) (Thermo Fisher) were plated in an 8-well Lab-Tek chamber slide (Sigma-Aldrich) at a density of 32,000 cells/well and allowed to attach overnight. Cells were transfected with hBax C3-EGFP (a gift from Richard Youle, Addgene plasmid # 19741) using lipofectamine 2000 (Thermo Fisher) according to the manufacturer's protocol. Components of the ligation reaction were added as described above

and cells incubated for 16 h at 37 ºC, 5 % CO_2. Cells were then treated with MitoTracker Red CMXRos (Thermo Fisher) according to the manufacturer's protocol and imaged using microscopy method A.

4.7.11 Kinetics of Compound 43 Uncaging in LUVs

Large unilamellar vesicles were synthesized using the general procedure. To the vesicle solution was added **43** (20 mM in MeOH) to a final concentration of 100 µM. The solution was then added to a quartz cuvette, sealed with a stopper and exposed to 360 nm light using a photochemical reactor. 20 µL of solution was removed at set time points and aliquots submitted to analysis by HPLC. The depletion of compound **43** was monitored by absorbance at 330 nm and relative concentration determined by integration of the elution peak. Absorbance values were plotted relative to time using GraphPad Prism software and the corresponding data fit shown ($k = 0.0657$ s^{-1}, $t_{1/2} = 10.6$ s).

4.7.12 Cellular Stability of Compound 43

HeLa cell lysate was prepared as above and to it was added **43** (20 mM in MeOH) to a final concentration of 200 µM. The lysate was then aliquoted in 200 µL volumes to 0.7 mL Eppendorf tubes and incubated at 37 ºC. Single 200 µL aliquots were removed at the specified time points and subjected to a whole-cell lipid extraction as above. HPLC analysis was performed and compound stability monitored by absorbance at 330 nm (Eclipse Plus C8 column, *0-10 min,* 5-95% MeOH in water).

4.7.13 Cellular Loading of Compound 43

HeLa cells transiently expressing Bax-EGFP were prepared as before. 500 µL solutions of **36** in

DMEM were prepared by diluting a stock organic solution (**43**: 20 mM in MeOH) to a final concentration of 50 μM in DMEM. Media was removed from three wells of cells in a chamber slide and then media containing the indicated concentration of **43** was added to cells as well as three empty wells containing no cells. The chamber slide was then incubated at 37 ºC, 5 % CO_2 for 1 h. Media was then collected from each well and its fluorescence at 460 nm measured by plate reader. The percent loading was then determined as the difference in mean fluorescence between the cellular and control media. Cellular loading of **43** = 1.3 ± 1.1 %.

4.7.14 Dose Response of Compound 43

HeLa cells transiently expressing Bax-EGFP were prepared as before. 500 μL solutions of the indicated concentration of **43** in DMEM were prepared by diluting a stock organic solution (**43**: 20 mM in MeOH). Media was removed from cells and then media containing the indicated concentration of **43** was added and cells incubated at 37 ºC, 5 % CO_2 for 1 h. Cells were then maintained at 37 ºC, 5 % CO_2, photoactivated using microscopy method C, and imaged using microscopy method A.

4.7.15 Photoactivated Traceless Ceramide Ligation (Single Cells)

HeLa cells transiently expressing Bax-EGFP were prepared as before. Components of the ligation reaction were prepared as 500 μM solutions in DMEM by diluting stock organic solutions (**43**: 20 mM in MeOH, **37**: 20 mM in n-butanol). Media was removed and then the appropriate volume of DMEM (10 % FBS, 1 % penicillin/streptomycin, -Phenol Red) was added to achieve a final volume of 500 μL media per well after addition of reaction components. **37** was added to a final concentration of 100 μM in designated wells and the cells incubated at 37 ºC, 5 % CO_2 for 4 h, after which **43** was added to a final concentration of 50 μM in designated wells and cells incubated

at 37 ºC, 5 % CO_2 for 1 h. Cells were then maintained at 37 ºC, 5 % CO_2 during imaging and photoactivation using microscopy method B.

4.7.16 Photoactivated Traceless Ceramide Ligation (Multiple Cells)

HeLa cells transiently expressing Bax-EGFP were prepared as before. Components of the ligation reaction were prepared as 500 μM solutions in DMEM by diluting stock organic solutions (**43**: 20 mM in MeOH, **37** and **40**: 20 mM in n-butanol). Media was removed and then the appropriate volume of DMEM (10 % FBS, 1 % penicillin/streptomycin, -Phenol Red) was added to achieve a final volume of 500 μL media per well after addition of reaction components. **37** and **40** were added to a final concentration of 100 μM in designated wells and the cells incubated at 37 ºC, 5 % CO_2 for 4 h, after which **43** was added to a final concentration of 50 μM in designated wells and cells incubated at 37 ºC, 5 % CO_2 for 1 h. Cells were then maintained at 37 ºC, 5 % CO_2, photoactivated using microscopy method C, and imaged using microscopy method A.

4.7.17 Statistical Methods

All statistical analysis was performed using Prism 7 software. Where shown, error bars represent standard deviation. In WST-1 assays, significance was determined using an unpaired t-test, assuming consistent SD, and correcting for multiple comparisons using the Holm-Sidak method. When quantifying trypan blue exclusion, caspase 3/7 activity, and punctate Bax localization, significance was determined using an unpaired t-test, assuming consistent SD.

4.7.18 Microscopy

Method A

Imaging was performed on an Axio Observer Z1 inverted microscope (Carl Zeiss Microscopy Gmb, Germany) with Yokogawa CSU-X1 spinning disk confocal unit using a 63x, 1.4 NA oil immersion or 20x, 0.8 NA objective to an ORCA-Flash4.0 V2 Digital CMOS camera (Hamamatsu, Japan). Fluorophores were excited with diode lasers (405 nm; 20mW, 488 nm; 30 mW, 561 nm; 20 mW). Images were acquired using Zen Blue software (Carl Zeiss) and processed using Image J. Where indicated, images are maximum intensity Z-projections generated from a Z-stack in the same X,Y stage position.

Method B

Imaging was performed on an LSM 780 built around an Axio Observer Z1 motorized inverted microscope (Carl Zeiss) with a 63x, 1.40 NA oil immersion objective. EGFP was excited with a 488 nm, 25 mW Argon Laser, green. Compound **43** was uncaged in the indicated regions of a 512 x 512 pixel image by scanning six times in one z-plane with a pixel dwell time of 12.6 µsec/pixel using a 405 nm, 30 mW Diode at 100% power. Images were acquired using Zen Black software (Carl Zeiss) and processed using Image J. Where indicated, images are maximum intensity Z-projections generated from a Z-stack in the same X,Y stage position.

Method C

Photouncaging was performed on an Axio Observer Z1 inverted microscope (Carl Zeiss Microscopy Gmb, Germany) with Yokogawa CSU-X1 spinning disk confocal unit using a 63x, 1.4 NA oil immersion objective to an ORCA-Flash4.0 V2 Digital CMOS camera (Hamamatsu, Japan). Compound **43** was uncaged in one z-plane of each imaging region (the whole frame at 63x magnification) by using a 10 s exposure with the 405 nm (20 mW) laser.

4.7.19 Synthesis of 2-formylphenyl palmitate (35)

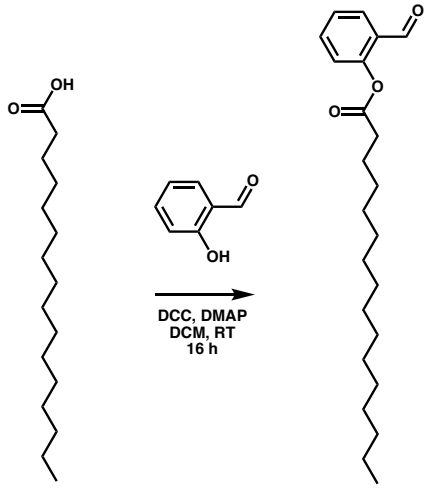

Scheme 4.1 Synthesis of 2-formylphenyl palmitate (**35**)

Palmitic acid (19.5 mg, 76 µmol) was dissolved in 500 µL dry DCM. A 1 M solution of N,N′-Dicyclohexylcarbodiimide in DCM (100 µL, 100 µmol) was added and the reaction stirred at RT for 1 h under inert atmosphere. 4-(dimethylamino)pyridine (15.2 mg, 124 µmol) and salicylaldehyde (9.5 mg, 78 µmol) were dissolved in 200 µL dry DCM and added to the reaction mixture before stirring at RT for 16 h under inert atmosphere. Insoluble material was filtered from the mixture and the solution concentrated under reduced pressure and purified by prep TLC (2.5:97.5 EtOAc:Hex). The band containing the product was washed with DCM and then solvent removed under reduced pressure. The residue was dissolved in $CHCl_3$, filtered through a 0.2 µm filter and solvent removed under reduced pressure, affording a colorless solid (23.1 mg, 84.3% yield). 1H NMR ($CDCl_3$, 500 MHz, δ): 10.10 (s, 1H), 7.87 (dd, J = 7.8, 1.7 Hz, 1H), 7.61 (m, 1H), 7.37 (m, 1H), 7.15 (m, 1H), 2.64 (t, J = 7.7 Hz, 2H), 1.76 (m, 2H), 1.45-1.16 (m, 24H), 0.85 (t, J = 7.0 Hz, 3H). 13C NMR ($CDCl_3$, 125 MHz, δ): 188.9, 172.3, 152.0, 135.5, 131.0, 128.3, 126.5, 123.7, 34.4, 32.1, 29.9, 29.8, 29.7, 29.6, 29.5, 29.4, 24.9, 22.9, 14.4. MS (ESI) calculated $[M+CH_3]^+$: 375.3, found: 375.3.

4.7.20 Synthesis of 2-formyl-5-methoxyphenyl palmitate (36)

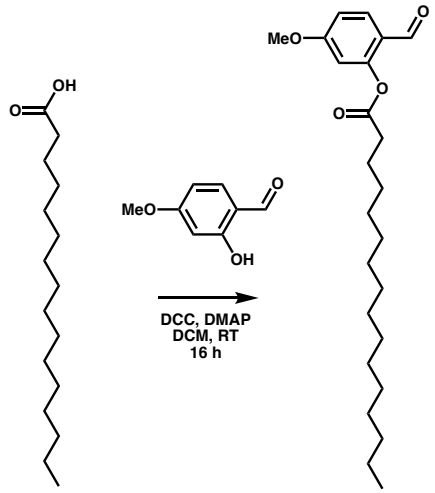

Scheme 4.2 Synthesis of 2-formyl-5-methoxyphenyl palmitate (**36**)

Palmitic acid (19.6 mg, 76 μmol) was dissolved in 500 μL dry DCM. A 1 M solution of N,N′-dicyclohexylcarbodiimide in DCM (100 μL, 100 μmol) was added and the reaction stirred at RT for 1 h under inert atmosphere. 4-(dimethylamino)pyridine (16.2 mg, 132 μmol) and 4-methoxysalicylaldehyde (11.9 mg, 78 μmol) were dissolved in 200 μL dry DCM and added to the reaction mixture before stirring at RT for 16 h under inert atmosphere. Insoluble material was filtered from the mixture and the solution concentrated under reduced pressure and purified by prep TLC (1:9 EtOAc:Hex). The band containing the product was washed with DCM and then solvent removed under reduced pressure. The residue was dissolved in $CHCl_3$, filtered through a 0.2 μm filter and solvent removed under reduced pressure, affording a colorless solid (11.6 mg, 38.9% yield). 1H NMR ($CDCl_3$, 500 MHz, δ): 9.94 (s, 1H), 7.79 (d, J = 8.6 Hz, 1H), 6.86 (dd, J = 8.6 Hz, 1H), 6.64 (d, J = 2.4 Hz, 1H), 3.86 (s, 3H), 2.63 (t, J = 7.8 Hz, 2H), 1.76 (m, 2H), 1.19-1.45 (m, 24 H), 0.86 (t, J = 6.8 Hz, 3H). 13C NMR ($CDCl_3$, 125 MHz, δ): 187.3, 171.9, 165.2,

153.6, 132.7, 121.8, 112.3, 108.7, 55.8, 34.2, 31.9, 29.7, 29.6, 29.5, 29.4, 29.3, 29.2, 24.7, 22.7, 14.1. MS (ESI) calculated $[M+H]^+$: 391.3, found: 391.2.

4.7.21 Synthesis of 5-(diethylamino)-2-formylphenyl palmitate (37)

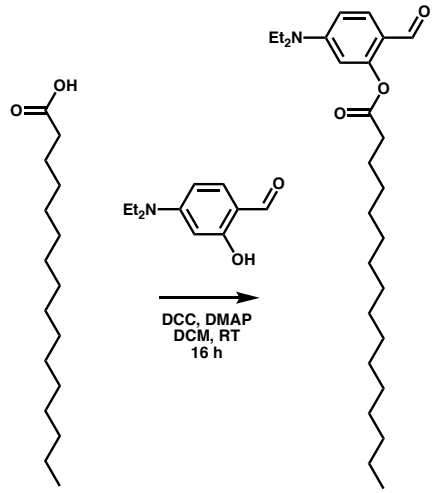

Scheme 4.3 Synthesis of 5-(diethylamino)-2-formylphenyl palmitate (**37**)

Palmitic acid (20.2 mg, 79 μmol) was dissolved in 500 μL dry DCM. A 1 M solution of N,N′-dicyclohexylcarbodiimide in DCM (100 μL, 100 μmol) was added and the reaction stirred at RT for 1 h under inert atmosphere. 4-(dimethylamino)pyridine (16.2 mg, 132 μmol) and 4-(diethylamino)salicylaldehyde (16.1 mg, 83 μmol) were dissolved in 200 μL dry DCM and added to the reaction mixture before stirring at RT for 16 h under inert atmosphere. Insoluble material was filtered from the mixture and the solution concentrated under reduced pressure and purified by prep TLC (1:9 EtOAc:Hex). The band containing the product was washed with DCM and then solvent removed under reduced pressure. The residue was dissolved in $CHCl_3$, filtered through a 0.2 μm filter and solvent removed under reduced pressure, affording a colorless solid (27.3 mg, 80.2% yield). 1H NMR ($CDCl_3$, 500 MHz, δ): 9.74 (s, 1H), 7.66 (d, J = 8.9 Hz, 1H), 6.56 (d, J = 8.9 Hz, 1H), 6.26 (s, 1H), 3.39 (q, J = 7.1 Hz, 4H), 2.62 (t, J = 7.8 Hz, 2H), 1.75 (m, 2H), 1.21-

1.42 (m, 24H), 1.18 (t, J = 7.0 Hz, 6H), 0.85 (t, J = 7.1 Hz, 3H). 13C NMR ($CDCl_3$, 125 MHz, δ): 186.8, 172.4, 154.2, 152.9, 133.6, 116.8, 109.0, 105.0, 45.3, 34.5, 32.1, 29.9, 29.8, 29.7, 29.6, 29.5, 29.4, 24.9, 22.9, 14.4, 12.6. MS (ESI) calculated $[M+H]^+$: 432.3, found: 432.3.

4.7.22 Synthesis of 5-(diethylamino)-2-formylphenyl palmitate-1,2,3,4-$^{13}C_4$ (37i)

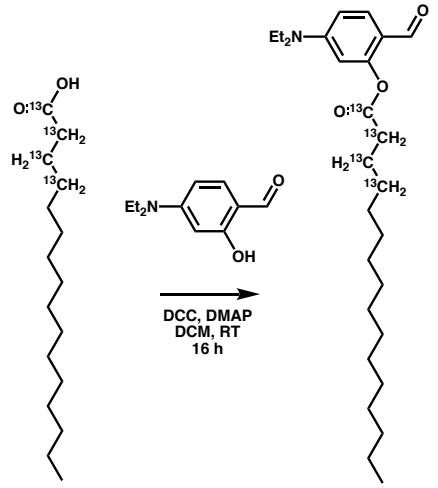

Scheme 4.4 Synthesis of 5-(diethylamino)-2-formylphenyl palmitate-1,2,3,4-$^{13}C_4$ (**37i**)

Palmitic-1,2,3,4-$^{13}C_4$ acid (Cambridge Isotope Laboratories) (20.0 mg, 77 µmol) was dissolved in 500 µL dry DCM. A 1 M solution of N,N′-dicyclohexylcarbodiimide in DCM (100 µL, 100 µmol) was added and the reaction stirred at RT for 1 h under inert atmosphere. 4-(dimethylamino)pyridine (14.0 mg, 115 µmol) and 4-(diethylamino)salicylaldehyde (16.3 mg, 84 µmol) were dissolved in 200 µL dry DCM and added to the reaction mixture before stirring at RT for 16 h under inert atmosphere. Insoluble material was filtered from the mixture and the solution concentrated under reduced pressure and purified by prep TLC (1:9 EtOAc:Hex). The band containing the product was washed with DCM and then solvent removed under reduced pressure. The residue was dissolved in $CHCl_3$, filtered through a 0.2 µm filter and solvent removed under reduced pressure, affording a colorless solid (24.3 mg, 72.6 % yield). 1H NMR ($CDCl_3$, 500 MHz, δ): 9.76 (s, 1H), 7.67 (d, J = 8.9 Hz, 1H), 6.54 (dd, J = 8.9, 2.5 Hz, 1H), 6.25 (d, J = 2.5 Hz, 1H), 3.41 (q, J = 7.1 Hz, 4H), 2.76 (m, 1H), 2.51 (m, 1H), 1.92 (m, 2H), 1.85-1.23 (m, 24H), 1.21 (t, J = 7.1 Hz, 6H), 0.88 (t, J = 7.1 Hz, 3H). 13C NMR ($CDCl_3$, 125 MHz, δ): 186.9, 172.8, 172.3, 153.4, 133.7, 116.8, 108.9, 104.8, 45.2, 35.0, 34.8, 34.6, 34.3, 32.3, 30.0, 29.8, 29.7, 29.5, 29.4,

26.1, 25.8, 25.5, 25.4, 25.1, 24.8, 23.1, 14.5, 12.9. MS (ESI) calculated $[M+H]^+$: 436.4, found: 436.4.

4.7.23 Synthesis of 5-(diethylamino)-2-formylphenyl oleate (38)

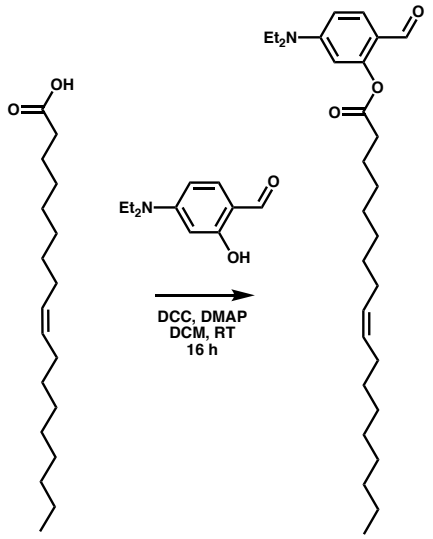

Scheme 4.5 Synthesis of 5-(diethylamino)-2-formylphenyl oleate (**38**)

Oleic acid (10.3 mg, 35.4 μmol) was dissolved in 200 μL dry DCM. A 1 M solution of N,N′-dicyclohexylcarbodiimide in DCM (40 μL, 40 μmol) was added and the reaction stirred at RT for 1 h under inert atmosphere. 4-(dimethylamino)pyridine (9.0 mg, 46.5 μmol) and 4-(diethylamino)salicylaldehyde (9.0 mg, 73.7 μmol) were dissolved in 100 μL dry DCM and added to the reaction mixture before stirring at RT for 16 h under inert atmosphere. Insoluble material was filtered from the mixture and the solution concentrated under reduced pressure and purified by prep TLC (1:9 EtOAc:Hex). The band containing the product was washed with DCM and then solvent removed under reduced pressure affording a colorless oil which was dissolved in 1:1 MeOH:CH_3CN and further purified by HPLC to afford a colorless oil (5.2 mg, 31.2% yield). (Eclipse Plus C8 column, *0-7 min,* 50-95% MeOH in water, *7-12 min*, 95% MeOH in water). 1H

NMR ($CDCl_3$, 500 MHz, δ): 9.74 (s, 1H), 7.64 (d, J = 8.9 Hz, 1H), 6.52 (dd, J = 2.4, 8.9 Hz, 1H), 6.24 (d, J = 2.4 Hz, 1H), 5.32 (m, 2H), 3.38 (q, J = 6.9 Hz, 4H), 2.62 (t, J = 7.8 Hz, 2H), 2.00 (m, 4H), 1.77 (m, 2H), 1.45-1.21 (m, 22H), 1.19 (t, J = 6.9 Hz, 6H), 0.86 (t, J = 6.9 Hz, 3H). 13C NMR ($CDCl_3$, 125 MHz, δ): 186.4, 172.1, 154.0, 153.0, 133.3, 130.0, 129.7, 116.4, 108.5, 104.4, 44.8, 34.3, 31.9, 29.7, 29.5, 29.3, 29.2, 29.1, 27.2, 24.7, 22.7, 14.1, 12.4. MS (ESI) calculated $[M+H]^+$: 458.4, found: 458.4.

4.7.24 Synthesis of 5-(diethylamino)-2-formylphenyl oleate-U-$^{13}C_{18}$ (38i)

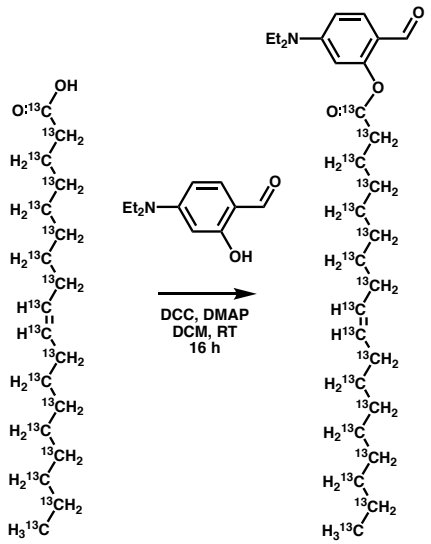

Scheme 4.6 Synthesis of 5-(diethylamino)-2-formylphenyl oleate-U-$^{13}C_{18}$ (**38i**)

Oleic-U-$^{13}C_{18}$ acid (Cambridge Isotope Laboratories) (5.0 mg, 17 µmol) was dissolved in 200 µL dry DCM. A 1 M solution of N,N′-dicyclohexylcarbodiimide in DCM (20 µL, 20 µmol) was added and the reaction stirred at RT for 1 h under inert atmosphere. 4-(dimethylamino)pyridine (4.1 mg, 33.3 µmol) and 4-(diethylamino)salicylaldehyde (4.8 mg, 25 µmol) were dissolved in 100 µL dry DCM and added to the reaction mixture before stirring at RT for 16 h under inert atmosphere. Insoluble material was filtered from the mixture and the solution concentrated under reduced

pressure and purified by prep TLC (1:9 EtOAc:Hex). The band containing the product was washed with DCM and then solvent removed under reduced pressure. The residue was dissolved in $CHCl_3$, filtered through a 0.2 µm filter and solvent removed under reduced pressure, affording a colorless oil. 1H NMR ($CDCl_3$, 500 MHz, δ): 9.76 (s, 1H), 7.68 (d, J = 8.9 Hz, 1H), 6.55 (d, J = 8.9 Hz, 1H), 6.25 (s, 1H), 5.53 – 5.16 (m, 2H), 3.42 (q, J = 7.1 Hz, 4H), 2.83-2.48 (m, 2H), 2.21-1.85 (m, 4H), 1.85 – 1.05 (m, 28H), 1.05 – 0.71 (m, 3H). 13C NMR ($CDCl_3$, 125 MHz, δ): 186.6, 172.5, 172.0, 154.0, 153.1, 133.5, 130.0, 129.9, 129.7, 116.3, 108.5, 104.4, 44.8, 36.4, 36.1, 36.0, 35.7, 34.6, 34.4, 34.2, 33.9, 32.2, 32.0, 31.9, 31.7, 31.6, 30.0, 29.8, 29.7, 29.6, 29.5, 29.4, 29.3, 29.2, 29.1, 27.5, 27.4, 27.3, 27.2, 27.1, 27.0, 26.9, 25.0, 24.9, 24.8, 24.7, 24.6, 24.5, 24.4, 23.0, 22.7, 22.4, 14.3, 14.2, 14.0, 12.5. MS (ESI) calculated $[M+H]^+$: 476.4, found: 476.4.

4.7.25 Synthesis of 5-(diethylamino)-2-formylphenyl stearate (39)

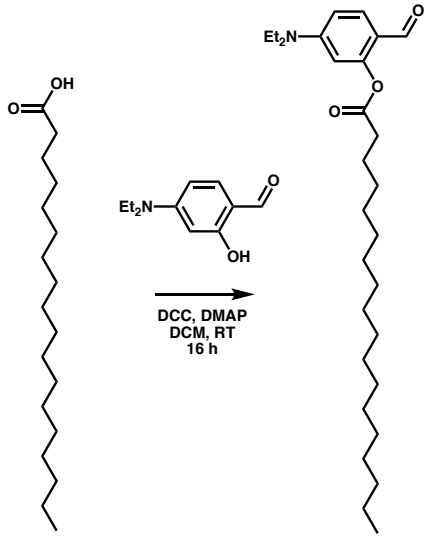

Scheme 4.7 Synthesis of 5-(diethylamino)-2-formylphenyl stearate (**39**)

Stearic acid (20 mg, 70 µmol) was dissolved in 500 µL dry DCM and to this solution was added dicyclohexylcarbodiimide in DCM (70 µL, 70 µmol) and the mixture stirred at RT for 1 hr. 4-

(dimethylamino)pyridine (13 mg, 105 μmol) and 4-(diethylamino)salicylaldehyde (15 mg, 77 μmol) were added and the reaction stirred overnight at RT under inert atmosphere. Insoluble material was filtered from the mixture and the solution concentrated under reduced pressure and purified by preparatory TLC (1:9 EtOAc:Hex). The band containing the product was washed with DCM and then solvent removed under reduced pressure. The residue was dissolved in $CHCl_3$, filtered through a 0.2 μm filter and solvent removed under reduced pressure, affording a colorless solid (13.4 mg, 41.5 % yield). 1H NMR ($CDCl_3$, 500 MHz, δ): 9.73 (s, 1H), 7.63 (d, J = 8.9 Hz, 1H), 6.51 (dd, J = 8.9, 2.5 Hz, 1H), 6.22 (d, J = 2.5 Hz, 1H), 3.38 (q, J = 7.2 Hz, 4H), 2.62 (t, J = 7.6 Hz, 2H), 1.76 (m, 2H), 1.43-1.21 (m, 28H), 1.18 (t, J = 7.2 Hz, 6H), 0.85 (t, J = 7.0 Hz, 3H). 13C NMR ($CDCl_3$, 125 MHz, δ): 186.7, 172.4, 154.2, 153.2, 133.6, 116.4, 108.6, 104.5, 45.0, 34.5, 32.1, 29.9, 29.8, 29.7, 29.6, 29.5, 29.4, 24.9, 22.9, 14.4, 12.7. MS (ESI) calculated $[M+H]^+$: 460.4, found: 460.4.

4.7.26 Synthesis of 5-(diethylamino)-2-formylphenyl nervonate (40)

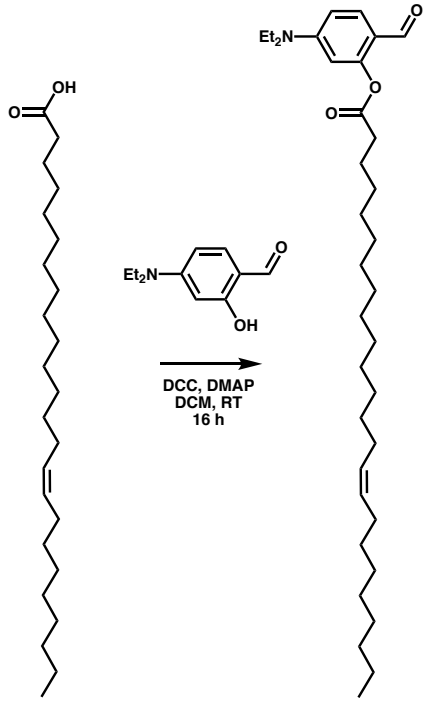

Scheme 4.8 Synthesis of 5-(diethylamino)-2-formylphenyl nervonate (**40**)

Nervonic acid (10.5 mg, 28.7 μmol) was dissolved in 200 μL dry DCM. A 1 M solution of N,N′-dicyclohexylcarbodiimide in DCM (40 μL, 40 μmol) was added and the reaction stirred at RT for 1 h under inert atmosphere. 4-(dimethylamino)pyridine (7.4 mg, 60.6 μmol) and 4-(diethylamino)salicylaldehyde (6.5 mg, 33.6 μmol) were dissolved in 100 μL dry DCM and added to the reaction mixture before stirring at RT for 16 h under inert atmosphere. Insoluble material was filtered from the mixture and the solution concentrated under reduced pressure and purified by preparatory TLC (1:9 EtOAc:Hex). The band containing the product was washed with DCM and then solvent removed under reduced pressure affording a colorless solid which was dissolved in 1:1 MeOH:CH_3CN and further purified by HPLC to afford a colorless solid (4.6 mg, 31.1% yield). (Eclipse Plus C8 column, *0-7 min,* 50-95% MeOH in water, *7-12 min*, 95% MeOH in water). 1H NMR ($CDCl_3$, 500 MHz, δ): 9.74 (s, 1H), 7.66 (d, J = 8.9 Hz, 1H), 6.52 (dd, J = 2.6,

8.9 Hz, 1H), 6.23 (d, J = 2.6 Hz, 1H), 5.33 (m, 2H), 3.40 (q, J = 7.1 Hz, 4H), 2.62 (t, J = 7.5 Hz, 2H), 2.00 (m, 4H), 1.76 (m, 2H), 1.44-1.21 (m, 32H), 1.19 (t, J = 6.9 Hz, 6H), 0.86 (t, J = 6.9 Hz, 3H). 13C NMR ($CDCl_3$, 125 MHz, δ): 187.0, 172.6, 154.5, 153.5, 133.8, 130.4, 116.9, 109.0, 104.9, 45.3, 34.8, 32.4, 30.3, 30.2, 30.1, 30.0, 29.8, 29.7, 27.7, 25.2, 23.2, 14.6, 12.9. MS (ESI) calculated $[M+H]^+$: 542.5, found: 542.5.

4.7.27 Synthesis of 7-((benzyloxy)methoxy)-6-bromo-4-(hydroxymethyl)-2H-chromen-2-one (41)

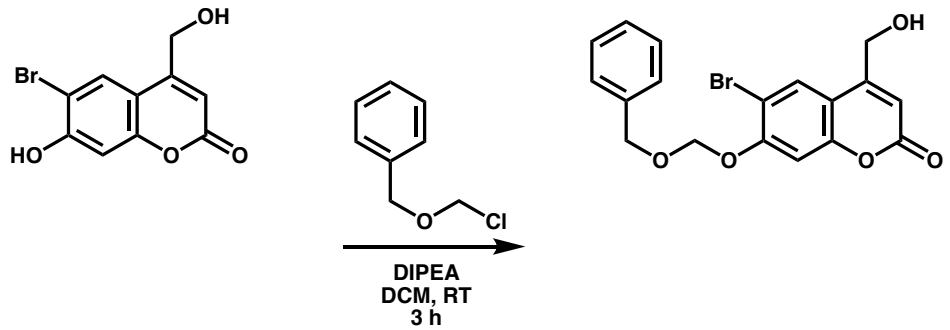

Scheme 4.9 Synthesis of 7-((benzyloxy)methoxy)-6-bromo-4-(hydroxymethyl)-2H-chromen-2-one (**41**)

6-bromo-7-hydroxy-4-(hydroxymethyl)-2H-chromen-2-one[128] (50 mg, 184 μmol) was dissolved in 300 μL dry DCM and DIPEA (97 μL, 553 μmol) was added. ((chloromethoxy)methyl)benzene (51 μL, 369 μmol) was added and the reaction stirred under Ar at RT for 3 hrs. The reaction mixture was diluted with DCM and then washed with water and brine. The organic fraction was dried *in vacuo,* the residue dissolved in a minimal volume of DCM and then purified by preparative TLC (6:94 MeOH:DCM). The band containing the product was washed with 1:9 MeOH:DCM and then solvent removed under reduced pressure. The residue was dissolved in $CHCl_3$, filtered through a 0.2 μm filter and solvent removed under reduced pressure to afford a pale pink solid (44 mg, 61% yield). 1H NMR ($(CD_3)_2SO$), 500 MHz, δ): 7.94 (s, 1H), 7.33 (m, 5H), 6.36 (t, J = 1.5

Hz, 1H), 5.65 (t, J = 5.5 Hz, 1H), 5.55 (s, 2H), 4.73 (m, 4H). 13C NMR ($CHCl_3$, 125 MHz, δ): 161.3, 156.3, 154.1, 153.6, 136.5, 128.7, 128.3, 128.2, 127.7, 113.0, 110.4, 108.6, 104.1, 93.0, 70.9, 60.8. MS (ESI) calculated $[M+H]^+$: 391.0 and 393.0, found: 391.0 and 393.0

4.7.28 Synthesis of (7-((benzyloxy)methoxy)-6-bromo-2-oxo-2H-chromen-4-yl)methyl (E)-(1,3-dihydroxyoctadec-4-en-2-yl)carbamate (42)

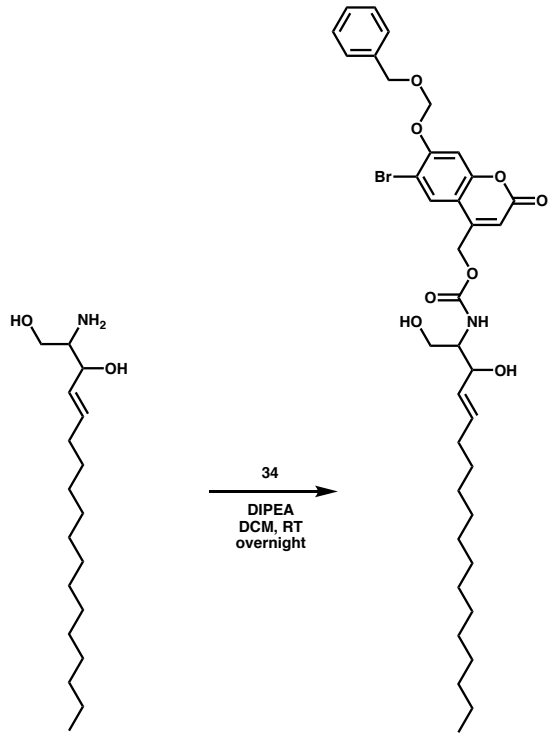

Scheme 4.10 Synthesis of (7-((benzyloxy)methoxy)-6-bromo-2-oxo-2H-chromen-4-yl)methyl (E)-(1,3-dihydroxyoctadec-4-en-2-yl)carbamate (**42**)

41 (15.2 mg, 38 µmol) and 4-nitrobenzyl chloroformate (7.4 mg, 33 µmol) were dissolved in 400 µL dry DCM. DIPEA (15 µL, 86 µmol) was added and the solution stirred under Ar at RT for 1 h after which D-*erythro*-sphingosine (5.0 mg, 17 µmol) was added and the reaction stirred under Ar at RT overnight. The reaction mixture was dried under reduced pressure and the residue dissolved in a minimal volume of MeOH before filtering through cotton and purification by HPLC to yield

a colorless solid (2.2 mg, 18% yield). (Zorbax SB-C18 column, *0-10 min,* 60-100% MeOH in water, *10-18 min*, 100% MeOH in water). 1H NMR ($CDCl_3$, 500 MHz, δ): 7.86 (s, 1H), 7.32 (m, 5H), 6.37 (s, 1H), 5.79 (m, 2H), 5.55 (dd, J = 6.2, 15.3 Hz, 1H), 5.41 (s, 2H), 5.23 (s, 2H), 4.73 (s, 2H), 4.38 (s, 1H), 4.01 (d, J = 10.6 Hz, 1H), 3.75 (m, 1H), 3.67 (m, 1H), 3.47 (s, 2H), 2.37 (s, 1H), 2.05 (m, 2H), 1.43-1.15 (m, 22H), 0.86 (t, J = 7.2 Hz, 3H). 13C NMR ($CDCl_3$, 125 MHz, δ): 160.5, 156.6, 155.4, 154.4, 149.1, 136.5, 134.9, 128.8, 128.4, 128.3, 127.8, 112.8, 111.4, 108.8, 104.3, 93.1, 75.1, 71.0, 62.3, 61.7, 55.8, 51.1, 32.5, 32.2, 29.9, 29.8, 29.7, 29.6, 29.4, 29.3, 22.9, 14.1. MS (ESI) calculated $[M\text{-}H_2O+H]^+$: 698.3 and 700.3, found: 698.3 and 700.3.

4.7.29 Synthesis of (6-bromo-7-hydroxy-2-oxo-2*H*-chromen-4-yl)methyl (*E*)-(1,3-dihydroxyoctadec-4-en-2-yl)carbamate (43)

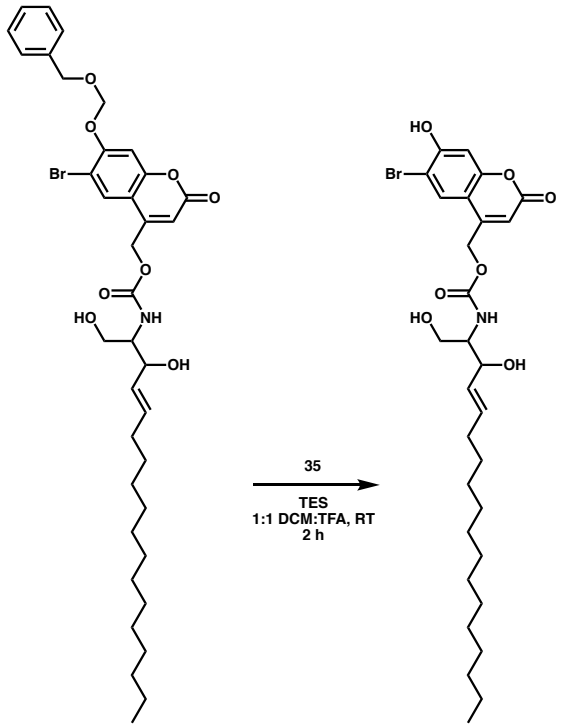

Scheme 4.11 Synthesis of (6-bromo-7-hydroxy-2-oxo-2*H*-chromen-4-yl)methyl (*E*)-(1,3-dihydroxyoctadec-4-en-2-yl)carbamate (**43**)

42 (1.1 mg, 1.5 µmol) was dissolved in 150 µL of 1:1 DCM:TFA with triethylsilane (0.5 µL, 3.1 µmol) and stirred for 2 h at RT protected from light. The reaction mixture was dried under reduced pressure and the residue dissolved in a minimal volume of MeOH before purification by HPLC to yield a colorless solid (0.9 mg, 98% yield). (Zorbax SB-C18 column, *0-10 min,* 60-100% MeOH in water, *10-18 min*, 100% MeOH in water). 1H NMR ($CDCl_3$, 500 MHz, δ): 7.62 (s, 1H), 7.00 (s, 1H), 6.35 (s, 1H), 5.97 (bs, 1H), 5.86 (m, 1H), 5.72 (m, 1H), 5.36 (m, 2H), 5.20 (m, 2H), 4.35 (s, 1H), 3.74 (m, 2H), 1.72 (m, 2H), 1.23 (m, 22H), 0.86 (t, J = 7.1 Hz, 3H). 13C NMR ($CDCl_3$, 125 MHz, δ): 160.3, 155.4, 154.8, 152.1, 129.3, 129.1, 126.8, 111.4, 106.9, 104.7, 79.4, 79.2, 61.9,

54.2, 29.9, 29.8, 29.7, 29.6, 29.3, 22.9, 14.4. MS (ESI) calculated $[M\text{-}H_2O+H]^+$: 578.2 and 580.2, found: 578.2 and 580.2.

Synthesis of C16:0 Ceramide (44)

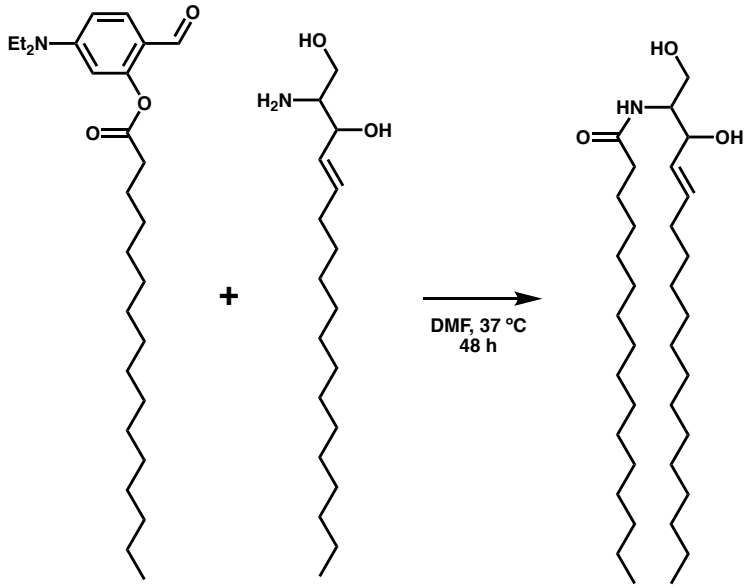

Scheme 4.12 Synthesis of C16:0 Ceramide (**44**)

Sphingosine (7.1 mg, 24 µmol) and **30** (7.2 mg, 17 µmol) were dissolved in 500 µL dry DMF. The reaction was stirred at 37 ºC for 48 hrs. Solvent was removed under reduced pressure then the residue dissolved in a minimal volume of HPLC grade MeOH and purified by HPLC to afford a colorless solid (1.8 mg, 20.1% yield). (Eclipse Plus C8 column, *0-7 min,* 50-95% MeOH in water, *7-12 min*, 95% MeOH in water). 1H NMR (CD_3OD, 500 MHz, δ): 5.70 (m, 1H), 5.49 (m, 1H), 4.06 (m, 1H), 3.88 (m, 1H), 3.74 (d, J = 5.0 Hz, 2H), 2.22 (t, J = 7.6 Hz, 2H), 2.07 (m, 2H), 1.61 (m, 2H), 1.45-1.25 (m, 46H), 0.92 (t, J = 7.1 Hz, 6H). 13C NMR (CD_3OD, 125 MHz, δ): 176.4, 134.9, 131.5, 73.8, 62.5, 56.9, 37.5, 33.6, 33.2, 31.0, 30.9, 30.8, 30.7, 30.6, 27.3, 23.9, 14.6. MS (ESI) calculated $[M+H]^+$: 538.5, found: 538.5.

Notes about the chapter:

Chapter four, in full, is a reprint (with co-author permission) of the material as it appears in the publication; **A. K. Rudd,** N. K. Devaraj "Traceless Synthesis of Ceramides in Living Cells Reveals Saturation Dependent Apoptotic Effects," *Proc. Natl. Acad. Sci. U.S.A.,* 2018, 115(29) 7485-7490. I would like to thank Neal Devaraj for his invaluable advice and assistance in preparing the manuscript. The author of the dissertation is the primary author of this manuscript.

CHAPTER 5

5 Amphiphile-Mediated Depalmitoylation of Proteins in Living Cells

5.1 Introduction

Cellular proteins undergo numerous post-translational modifications (PTMs), including phosphorylation, nitrosylation, glycosylation, ubiquitination, methylation, and lipidation.[132] These modifications play essential roles in the structure, localization, and activity of proteins in cells, and their dysregulation can result in disease.[133] Protein S-palmitoylation is an essential PTM in which a palmitate group is linked to proteins through a reversible thioester bond with cysteine residues.[134,135] Defects in palmitoylation can have devastating biological consequences and are implicated in several disorders, including Alzheimer's disease,[136] diabetes,[137] and cancer.[134] Despite tremendous interest in S-palmitoylation, methods for in vivo remodeling of protein lipidation are limited in scope.[134,138] While inhibitors, such as 2-bromopalmitate, block the enzymes responsible for S-palmitoylation, they cannot cleave S-palmitoyl groups from currently lipidated proteins and are known to irreversibly inhibit several enzymes involved in lipid biosynthesis.[134] Therefore, we sought to engineer a small molecule for direct and chemoselective depalmitoylation of S-palmitoyl groups in vivo.

We conceived a method for depalmitoylation of membrane-associated proteins based on the chemoselective reaction of N-terminal cysteines with thioesters through native chemical ligation (NCL)[78] (Figure 5.1A). Previous work in our group has demonstrated that amphiphilic NCL precursors can react spontaneously and rapidly under physiological conditions to yield stable lipid products.[80,139,140] We hypothesized that a small, cysteine-containing amphiphile could be utilized for the selective depalmitoylation of native membrane-anchored proteins in vivo. We

anticipated that using an amphiphilic reactant would ensure localization in the membrane, enhancing the reaction rate and selectivity of reaction with membrane-bound proteins bearing thioesters. This amphiphile-mediated depalmitoylation (AMD) approach would offer the advantage of direct cleavage of S-palmitoyl groups from endogenous proteins in a way that is nondestructive towards the rest of the protein.

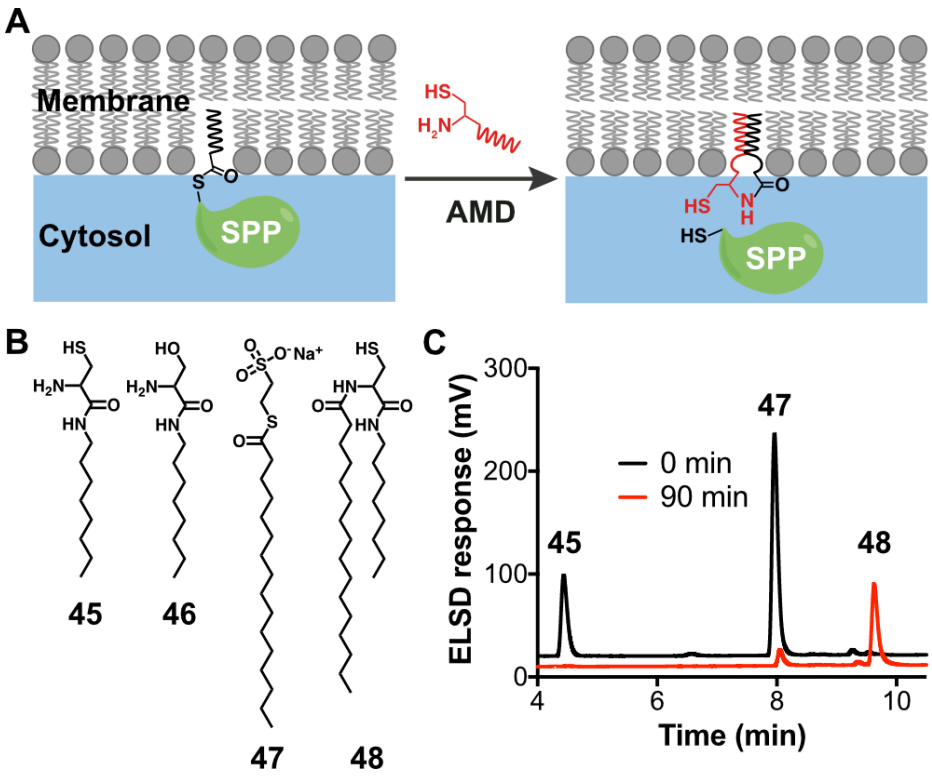

Figure 5.1 Amphiphile-mediated depalmitoylation (AMD). (A) Schematic representation of the depalmitoylation of an S-palmitoylated protein (SPP) by AMD. (B) Chemical structures of compounds used in this study. (C) HPLC/ELSD traces of the reaction between alkyl cysteine **45** (5 mM) and MESNA thiopalmitate **47** (5 mM) to form the N-acylated product **48**.

5.2 Design of a Reactive Amphiphile

In designing a reactive amphiphile, we sought to balance lipophilicity and aqueous solubility to promote both cell permeability and membrane affinity. Therefore, we employed a lipophilic alkyl chain of moderate length, octylamine, coupled to cysteine for the synthesis of the depalmitoylating agent **1** (Figure 5.1B, Figure 5.2). To determine if **45** could cleave the thioester linkage of S-palmitoyl groups under physiological conditions, we performed preliminary tests in the presence of S-palmitoyl sodium 2-mercaptoethanesulfonate (MESNA) **47** (Figure 5.1B, Figure 5.3), an S-palmitoylated protein (SPP) surrogate. We found that the reaction between **45** and **47** proceeded rapidly and irreversibly at ambient temperature and cleaved the model S-palmitoyl group to yield **48** (Figure 5.1B), a stable, N-acylated product (Figure 5.1C, Figure 5.4). To confirm that the observed reaction is due to NCL and not direct aminolysis, we synthesized the alkyl derivative **46**, an analog of **45** in which the thiol group is replaced with an alcohol (Figure 5.2). Compound **46** should have similar physical properties to **45** but be unable to engage in NCL[141] (Figure 5.1B). As expected, the reaction between **46** and **47** under the same conditions yielded no ligation product, demonstrating that the observed reaction proceeds through NCL (Figure 5.4). Having confirmed the efficient reaction of **45** with thioesters in aqueous buffer, we wanted to determine if AMD could be used to cleave palmitoyl groups from S-palmitoylated proteins in vivo. HRas is a member of the Ras family of GTPases, which function as key regulatory proteins in cell differentiation, proliferation, and survival.[142] Mutations in HRas are associated with several cancers,[143] as well as Costello syndrome, a severe congenital disorder for which there is no cure.[144,145] Therefore, there is significant interest in developing therapeutics which target HRas signaling.[146,147] However, Ras proteins are challenging to target and have even been deemed "undruggable".[146] In mammalian cells, HRas is palmitoylated at the Golgi complex before being trafficked to the plasma membrane. Once at the plasma membrane, HRas can be enzymatically

depalmitoylated, triggering its movement back to the Golgi, where it can repeat this cycle.[148] Because of its biological and clinical importance, we chose to target HRas for depalmitoylation by the alkyl cysteine **45**.

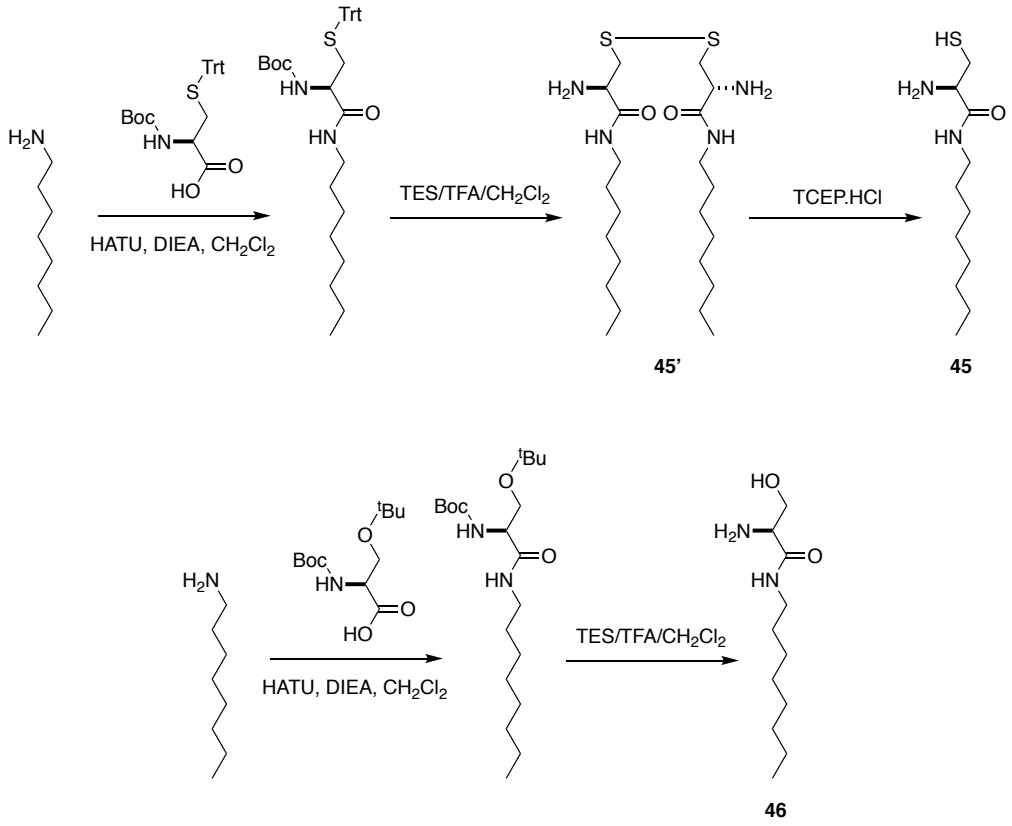

Figure 5.2 Synthesis of H_2N-*L*-Cys-Oct (**45**) and H_2N-*L*-Ser-Oct (**46**).

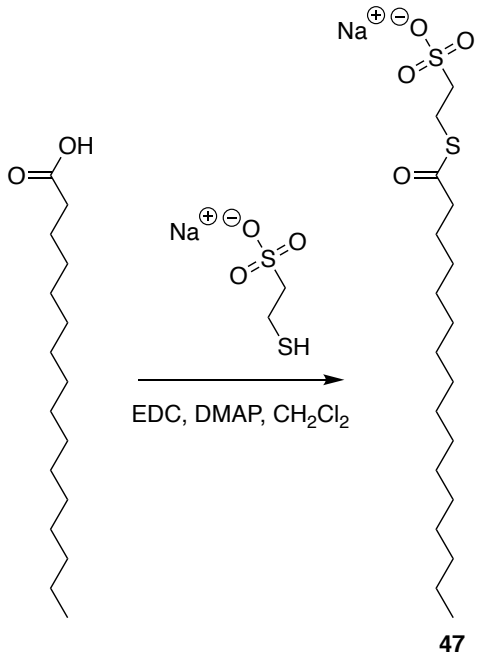

Figure 5.3 Synthesis of MESNA thiopalmitate (**47**).

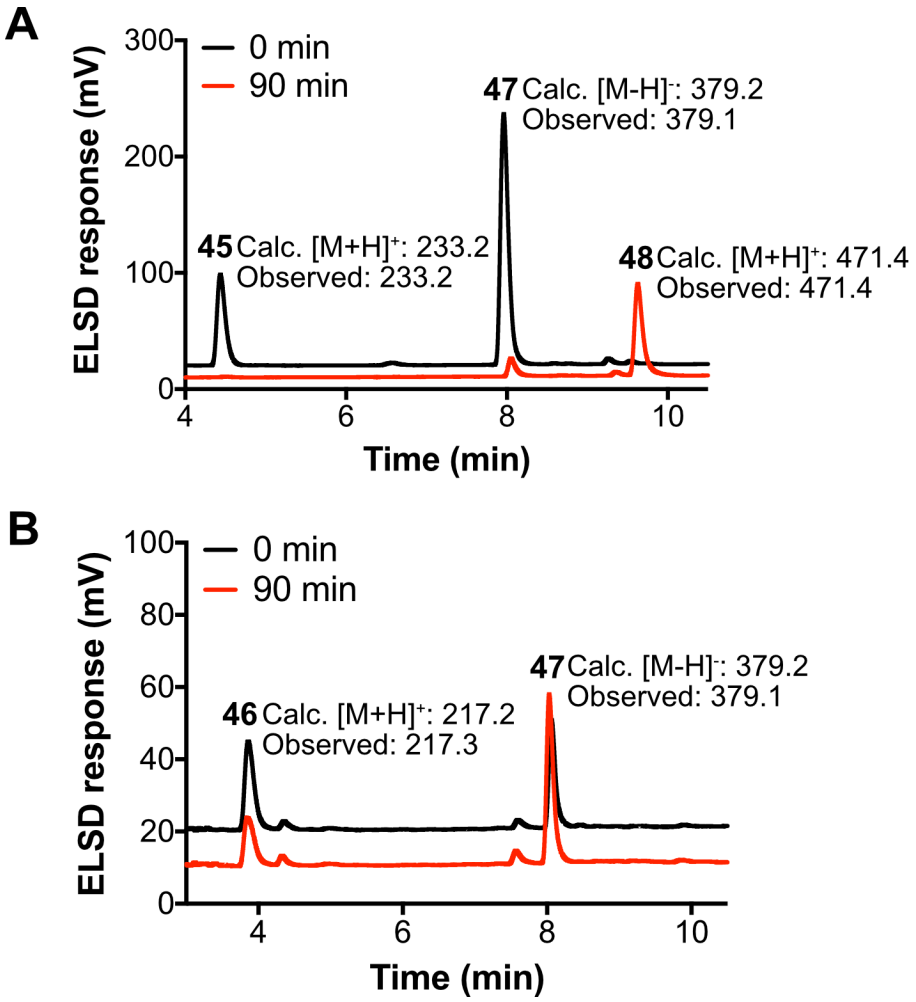

Figure 5.4 In vitro analysis of AMD reaction. (A) HPLC traces of the reaction between **45** and **47** in vitro to form **48**. (B) HPLC traces show no reaction between **46** and **47**. MS (ESI) spectra were integrated for each peak to confirm compound identity. Calculated and observed major MS peaks are listed next to corresponding ELSD peaks.

5.3 Depalmitoylation of Proteins in Live Cells

For use in cells, a stock solution of 50 mM **45** or **46** was prepared in DMSO with the addition of 2 equivalents [100 mM] tris(2-carboxyethyl)phosphine hydrochloride (TCEP.HCl), a preservative to prevent oxidation in storage (Figure 5.5). Before use, stocks were diluted to the desired concentration in cell media. To determine if **45** can trigger depalmitoylation in live cells, HeLa cells were treated with a range of concentrations of **45** (0.31-1.25 µmol/10^7 cells) for 20 min. The palmitoylation state of endogenous HRas after treatment with **45** was detected using an acyl resin-assisted capture method (Figure 5.6A,B).[149] We found that HRas palmitoylation decreased

in a dose-dependent manner and near complete depalmitoylation of HRas was observed upon treatment of HeLa cells with 1.25 μmol/10^7 cells **45**. To exclude the possibility that the observed reduction in HRas palmitoylation was due to the preservative TCEP or a non-specific effect of the amphiphile, we performed the same experiments in the presence of TCEP alone or compound **46** (Figure 5.6C-D). Under these conditions, no significant depalmitoylation was observed, indicating that the depalmitoylation of HRas is dependent on the cysteine moiety present in **45.** HRas undergoes natural cycles of palmitoylation and depalmitoylation by the palmitoyl acyltransferase DHHC9/GCP16, and acyl protein thioesterases 1 and 2 (APT-1/2), respectively.[150] To determine if the observed reduction in HRas palmitoylation was due to cleavage of palmitoyl groups by **45**, or the result of endogenous thioesterase activity, we treated cells with **45** in the presence of an inhibitor of APT-1/2, palmostatin B (PB).[151,152] We found that **45** (1.25 μmol/10^7 cells) efficiently depalmitoylated HRas, even in the presence of PB (Figure 5.6E-F), suggesting that it acts by directly cleaving S-palmitoyl groups and not through alternative biological mechanisms. Additionally, no significant depalmitoylation was observed when cells were treated with PB, or PB and TCEP alone (Figure 5.6E-F). To confirm that the reaction between **45** and biological thioesters resulted in the expected N-acylated product **48**, we treated HeLa cells with **45** and then performed a lipid extraction and mass spectrometric analysis. We detected the expected AMD product, **48**, when cells were treated with **1** but not when cells were treated with TCEP preservative alone (Figure 5.7). To determine the scope of protein depalmitoylation by AMD in HeLa cells, we detected the palmitoylation levels of eight known palmitoylated proteins after treatment with **45**. We found that AMD reduced the palmitoylation level of five of the tested proteins (Gα(i), lyric/metadherin, CD44, SNAP25 and HRas) by >80%. Palmitoylation levels in three other proteins (flotillin-1, flotillin-2 and calnexin), however, were only reduced by 19-40% (Figure 5.8). The reduced activity of AMD towards flotillins may be due to their association with membrane

rafts, which could restrict access of **1** to their S-palmitoylation site.[153] Calnexin, on the other hand, is localized in ER membranes,[154] and thus may be less susceptible to depalmitoylation as compared to plasma membrane proteins.

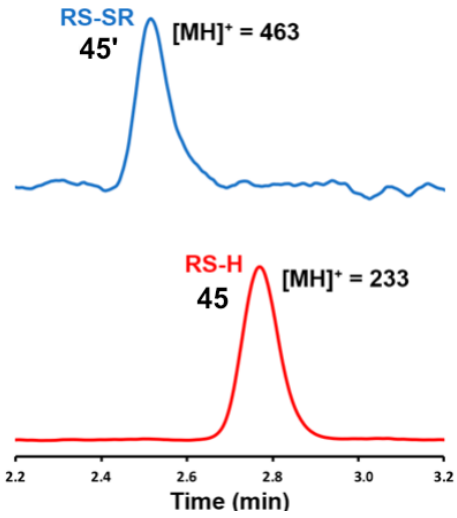

Figure 5.5 HPLC/ELSD traces of a 5 mM solution of **45'** in the absence (*top*) and presence (*bottom*) of TCEP (5 mM), showing the reduction of disulfide (**45'**, RS-SR) to thiol (**45**, RSH).

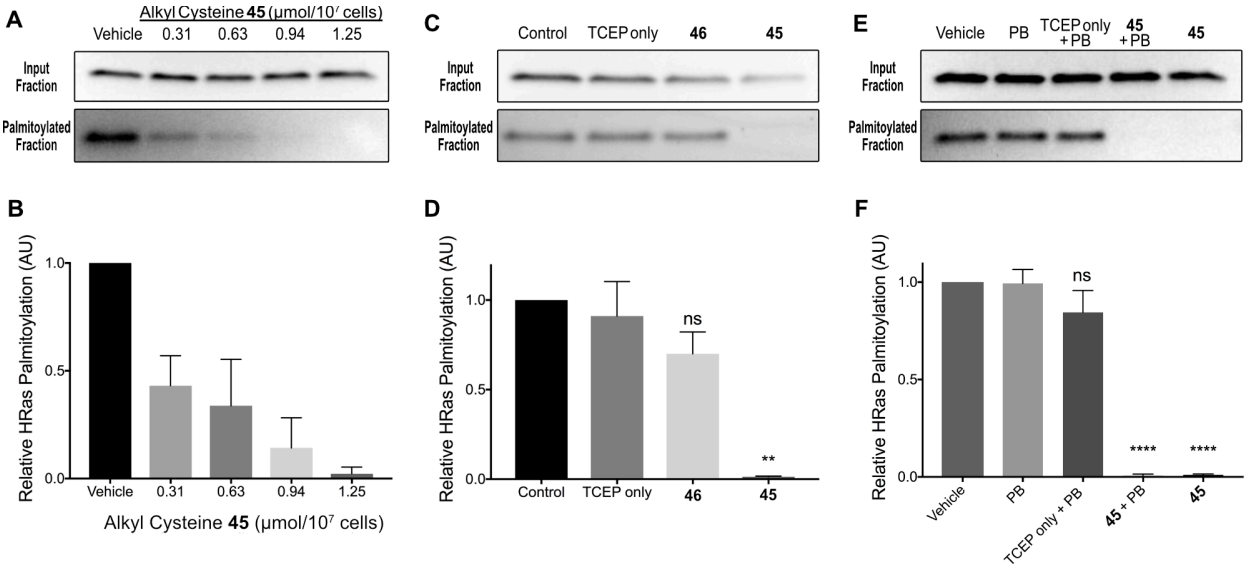

Figure 5.6 Depalmitoylation of HRas in HeLa cells. (A-F) Western blot detection of endogenous HRas in acyl resin-assisted capture fractions. The input fraction contains all cellular proteins. The palmitoylated fraction contains only S-palmitoylated proteins. Assays were performed in three biological replicates with the vehicle or control normalized to 1. Values are shown as means ± SD. Statistically significant differences in palmitoylation between TCEP only (D) or PB (F) and the other means are indicated: **P<0.01, ****P<0.0001. ns, not significant.

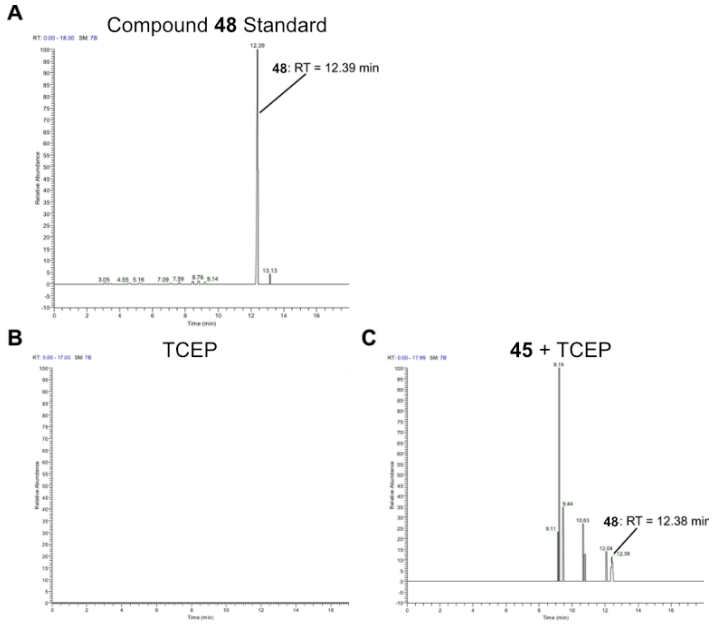

Figure 5.7 LC MS/MS traces of selected reaction monitoring for the AMD product **48** in HeLa cell lipid extracts. (A) Standard injection of **48**. (B) Lipid extract from HeLa cells treated with TCEP control. (C) Lipid extract from HeLa cells treated with **45** and TCEP. Peaks corresponding to **48** are labeled with corresponding retention time (RT).

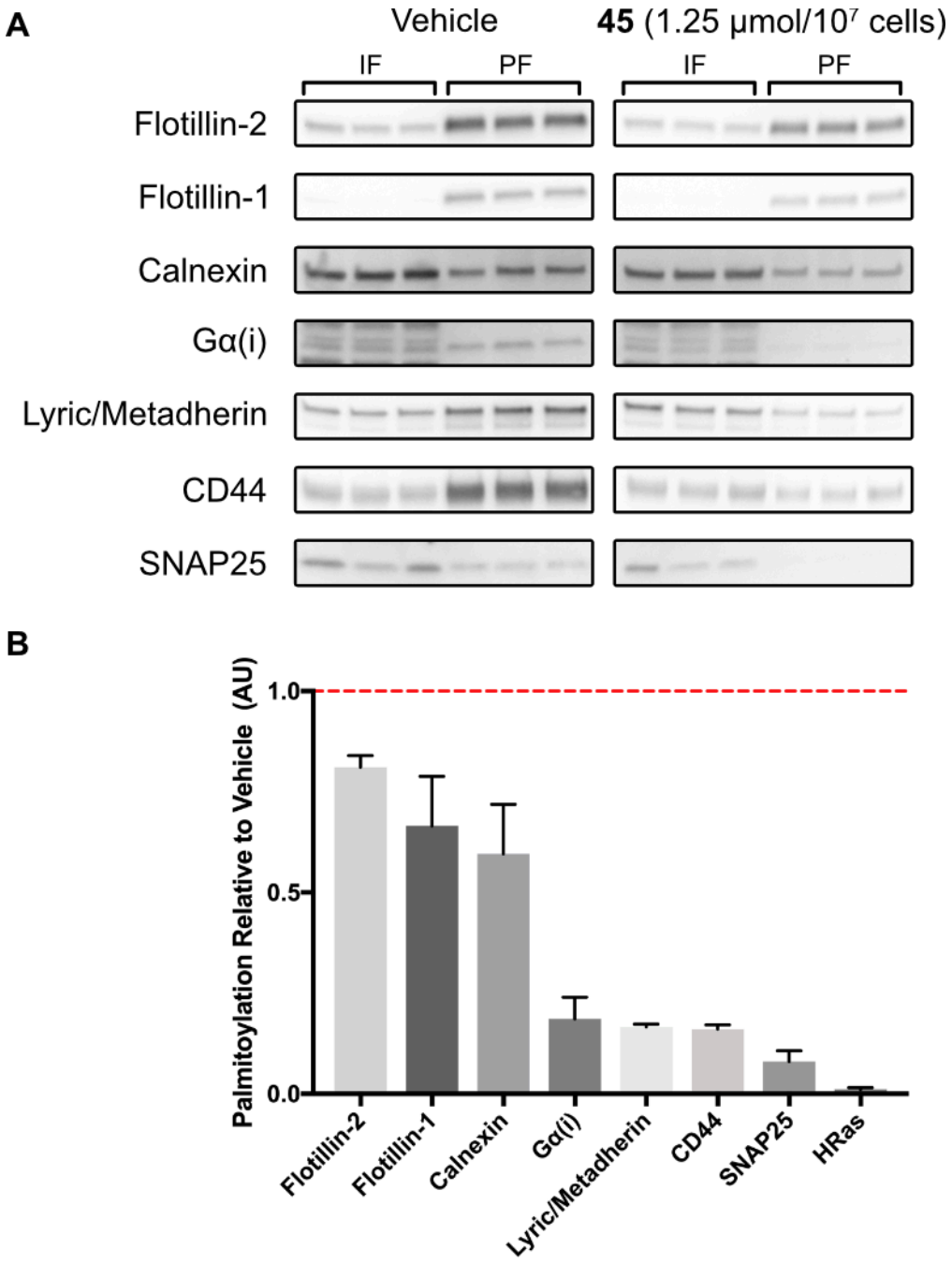

Figure 5.8 Depalmitoylation of proteins in HeLa cells. (A) Western blot detection of endogenous S-palmitoylated proteins in acyl resin-assisted capture fractions after treatment with vehicle or **45** (1.25 µmol/10^7 cells). The input fraction (IF) contains all cellular proteins. The palmitoylated fraction (PF) contains only S-palmitoylated proteins. Assays were performed in three biological replicates. (B) Quantification of protein palmitoylation in cells treated with **45** (1.25 µmol/10^7 cells) relative to cells treated with vehicle. Values are shown as means ± SD.

5.4 Functional Results of HRas Depalmitoylation

Previous studies have shown that the cysteine palmitoylation sites of HRas are necessary for its localization to the plasma membrane. Mutation of these sites results in a distinct shift in HRas localization from the plasma membrane to ER/Golgi membranes and cytosol.[148,150] To investigate the ability of AMD to trigger changes in HRas localization, we transiently transfected HeLa cells with a plasmid encoding for EGFP-HRas. Initially, EGFP-HRas was observed primarily at the plasma membrane, indicative of its S-palmitoylated state (Figure 5.9A).[150] After treatment with **45** (1.25 μmol/10^7 cells) for 20 min, EGFP-HRas localization at the plasma membrane decreased and was accompanied by an increase in fluorescence at inner cellular membranes, adopting a distribution consistent with depalmitoylated HRas (Figure 5.9A, Figure 5.10).[150] Controls with compound **46** (Figure 5.9B, Figure 5.10) or TCEP alone (Figure 5.9C, Figure 5.10) showed no change in fluorescence localization. Furthermore, cells transfected with plasmid encoding EGFP-KRas4b, a Ras isoform tethered to the plasma membrane by an electrostatic interaction instead of S-palmitoylation, and treated with **45** (1.25 μmol/10^7 cells), showed no change in protein localization (Figure 5.9D, Figure 5.10). Statistical analysis of several hundred cells under each condition demonstrated a significant change in plasma membrane protein localization only in EGFP-HRas transfected cells treated with **45** (Figure 5.9E, Figure 5.11). To determine if treatment with **45** has any effect on Ras signaling pathways, we analyzed the phosphorylation of AKT1 (pS473) and ERK1/2 (pY204/pY187), two downstream effectors regulated by Ras.[155] We found that treatment of HeLa cells with **45** (1.25 μmol/10^7 cells) resulted in a significant decrease in AKT1 phosphorylation, but not ERK1/2 phosphorylation, after EGF stimulation (Figure 5.12). Interestingly, treatment of T24 cells, a bladder cancer cell line with an oncogenic HRas mutation,[156] with **45** resulted in near complete abrogation of AKT1 and ERK1/2

phosphorylation (Figure 5.13). These results suggest that cells with hyperactive HRas may be uniquely susceptible to signaling inhibition by AMD.[157]

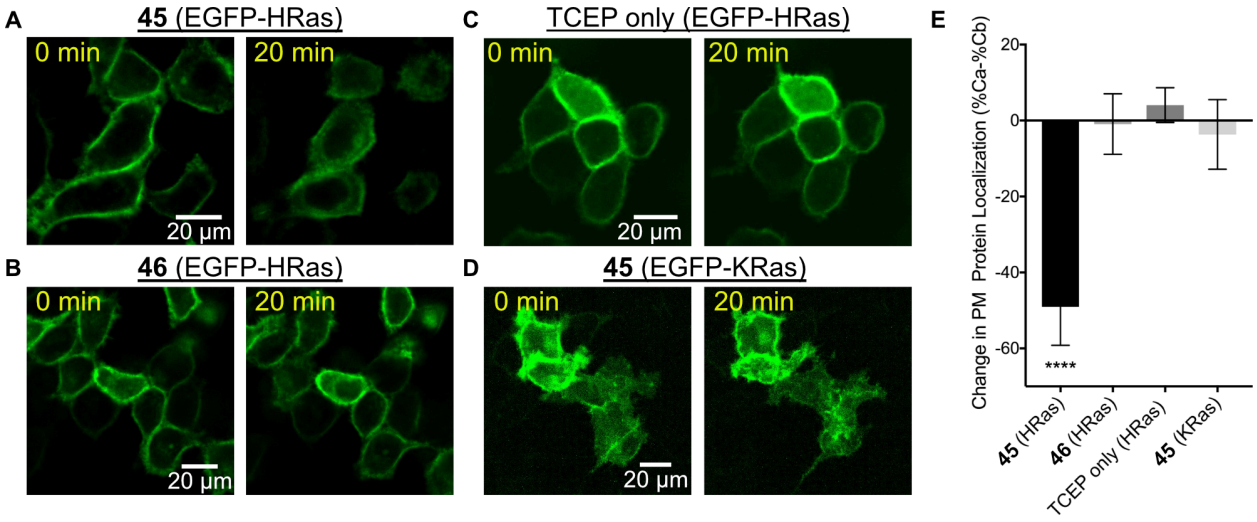

Figure 5.9 AMD induces translocation of EGFP-HRas from the plasma membrane (PM). Fluorescence microscopy images of HeLa cells expressing EGFP-HRas (A-C) or EGFP-KRas4b (D) before and after treatment with **45** (A and D), **46** (B) or TCEP only (C). (E) Change in PM localization of EGFP-HRas or EGFP-KRas4b within large populations of cells after treatment with **45**, **46**, or TCEP only. The difference between the percentage of cells showing EGFP localization at the plasma membrane after (%Ca) and before (%Cb) treatment is shown. Values are reported as means ± SD. Statistically significant changes in protein localization after treatment are indicated: ****P<0.0001.

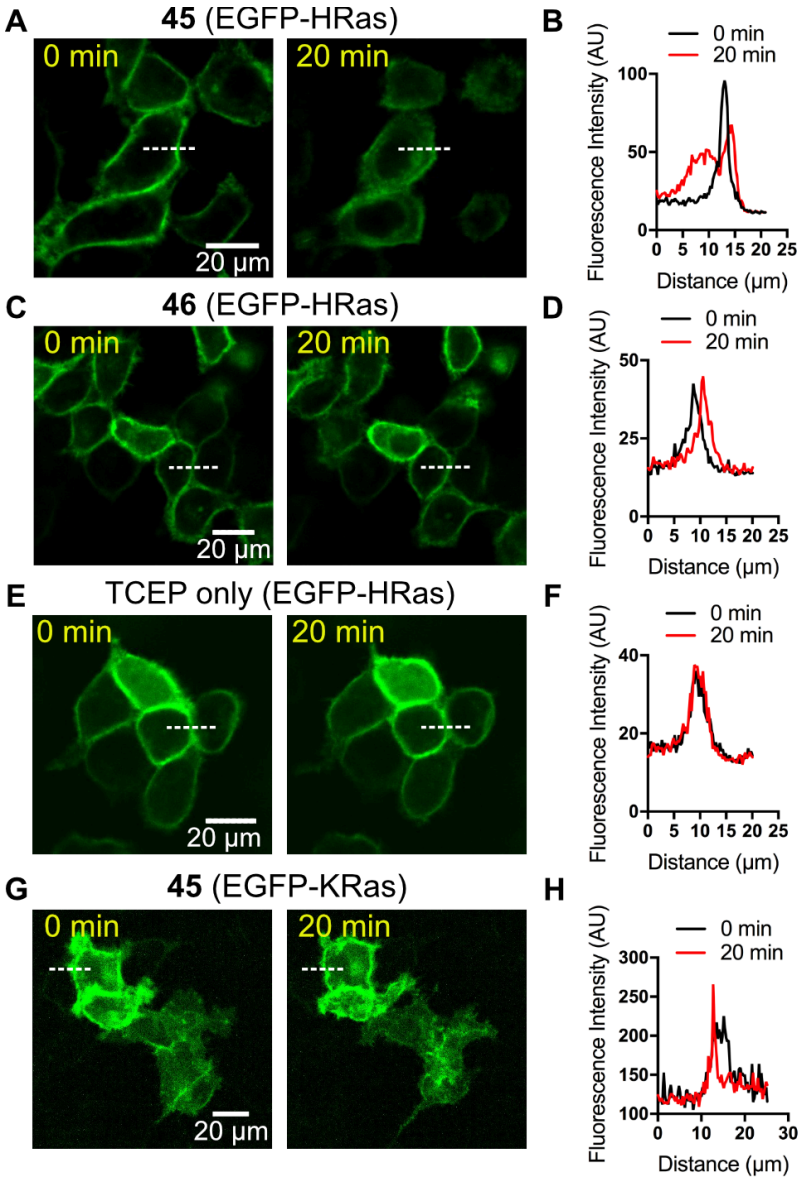

Figure 5.10 Depalmitoylation of HRas in HeLa cells. Fluorescence microscopy images and intensity profiles [along white dashed lines] of HeLa cells expressing EGFP-HRas (A-F) or EGFP-KRas (G-H) before and after treatment with **45** (A,B,G and H) (1.25 μmol/10^7 cells), **46** (C and D) (1.25 μmol/10^7 cells) or TCEP only (E and F).

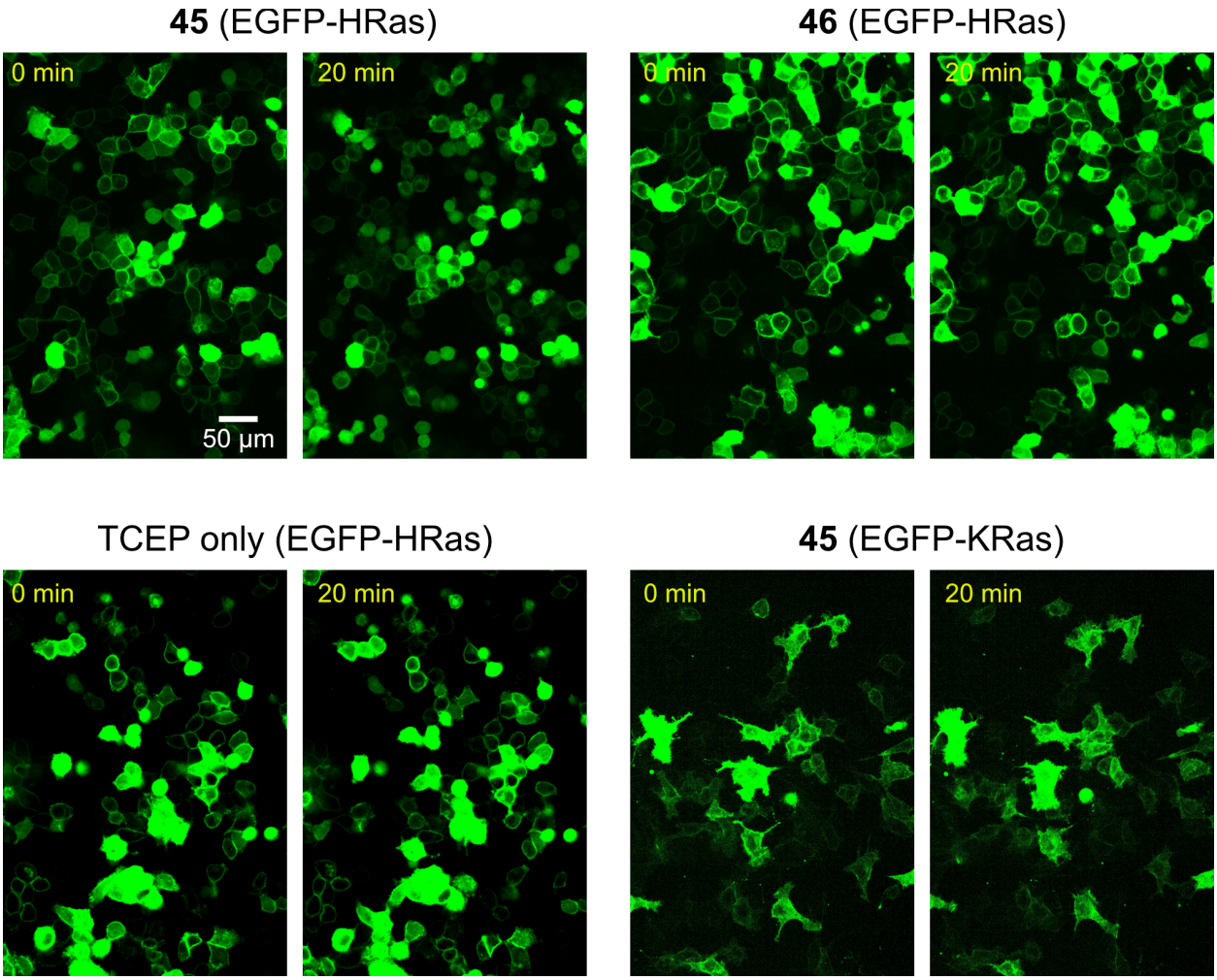

Figure 5.11 Depalmitoylation of HRas in HeLa cells. Representative fluorescence microscopy images of HeLa cells expressing EGFP-HRas or EGFP-KRas before and after treatment with **45** (1.25 µmol/10^7 cells), **46** (1.25 µmol/10^7 cells) or TCEP only.

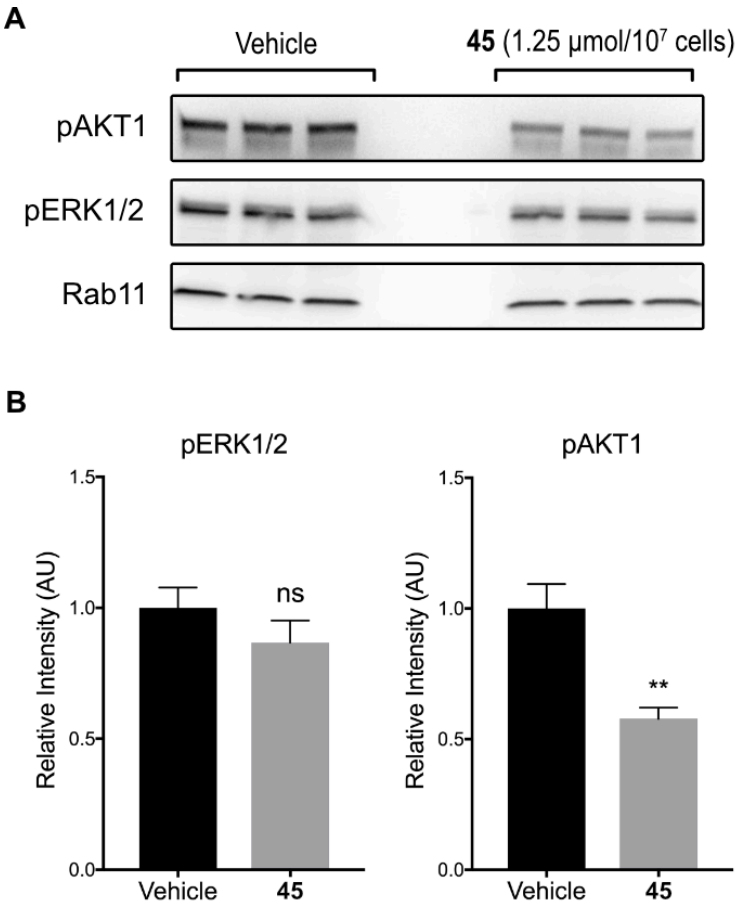

Figure 5.12 AKT1 and ERK1/2 phosphorylation after AMD in HeLa cells. (A) Western blot detection of phosphorylated AKT1 (pS473) and ERK1/2 (pY204/187) after treatment with Vehicle or **45** (1.25 µmol/10^7 cells) and stimulation with EGF (100 ng/µL). Rab11 was used as a loading control. (B) Assays were performed in three biological replicates. The intensity of the protein band in each condition was normalized to the intensity of the corresponding loading control (Rab11). The values within individual replicates were normalized to the vehicle condition and reported as means ± SD. ns, not significant, **P<0.01.

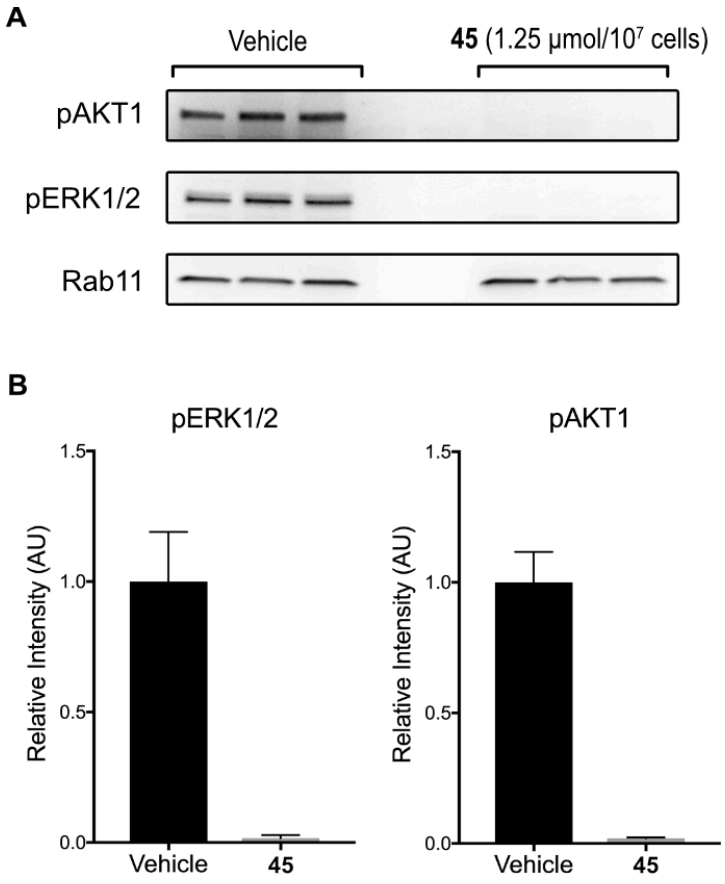

Figure 5.13 AKT1 and ERK1/2 phosphorylation after AMD in T24 cells. (A) Western blot detection of phosphorylated AKT1 (pS473) and ERK1/2 (pY204/187) after treatment with Vehicle or **45** (1.25 µmol/10^7 cells). Rab11 was used as a loading control. (B) Assays were performed in three biological replicates. The intensity of the protein band in each condition was normalized to the intensity of the corresponding loading control (Rab11). The values within individual replicates were normalized to the vehicle condition and reported as means ± SD.

5.5 Therapeutic Depalmitoylation in INCL Disease

Palmitoylation plays a crucial role in directing protein localization and function, and disruption of these processes can lead to disease.[158] Infantile neuronal ceroid lipofuscinosis (INCL) is a degenerative and fatal disease caused by mutations in the palmitoyl-protein thioesterase-1 (PPT1) gene.[159] PPT1 is a thioesterase responsible for the depalmitoylation of many S-palmitoylated proteins. Mutations which disrupt its activity result in intracellular accumulation of palmitoylated proteins, leading to cell apoptosis and neurodegeneration.[160] Although rare, INCL is a devastating disease, and currently there exist few treatment options and no cure.[161,162] We postulated that AMD could mimic the thioesterase activity of PPT1 and may help reverse the accumulation of palmitoylated proteins caused by INCL. To evaluate the potential of **45** for the treatment of INCL, we obtained patient-derived INCL lymphoblasts and determined their tolerance of **45** over a 24 h period. We found that doses up to 0.08 μmol/10^7 cells did not decrease cell viability compared to the nontreated control (Figure 5.14A). To determine if AMD could decrease the accumulation of S-palmitoylated proteins in INCL cells,[159,160] we treated INCL lymphoblasts with **45** (0.05 μmol/10^7 cells) for 24 h. We then detected the palmitoylation level of GAP43, a protein which accumulates at the ER in INCL cells[160] and is known to have increased levels of palmitoylation in PPT1 knockout models.[159] We found that **45** significantly reduced the level of GAP43 palmitoylation in INCL cells (Figure 5.14B,C). Treatment of INCL lymphoblasts with TCEP only or **46** did not result in a significant change in GAP43 palmitoylation. This suggests that AMD may help to counteract the increased protein palmitoylation and ER accumulation associated with INCL and could offer a therapeutic benefit.

In conclusion, we have developed a small-molecule depalmitoylation strategy for the cleavage of S-palmitoyl groups in vivo. The efficacy of AMD in vivo and its ability to hit disease-relevant targets suggest it has potential therapeutic value.

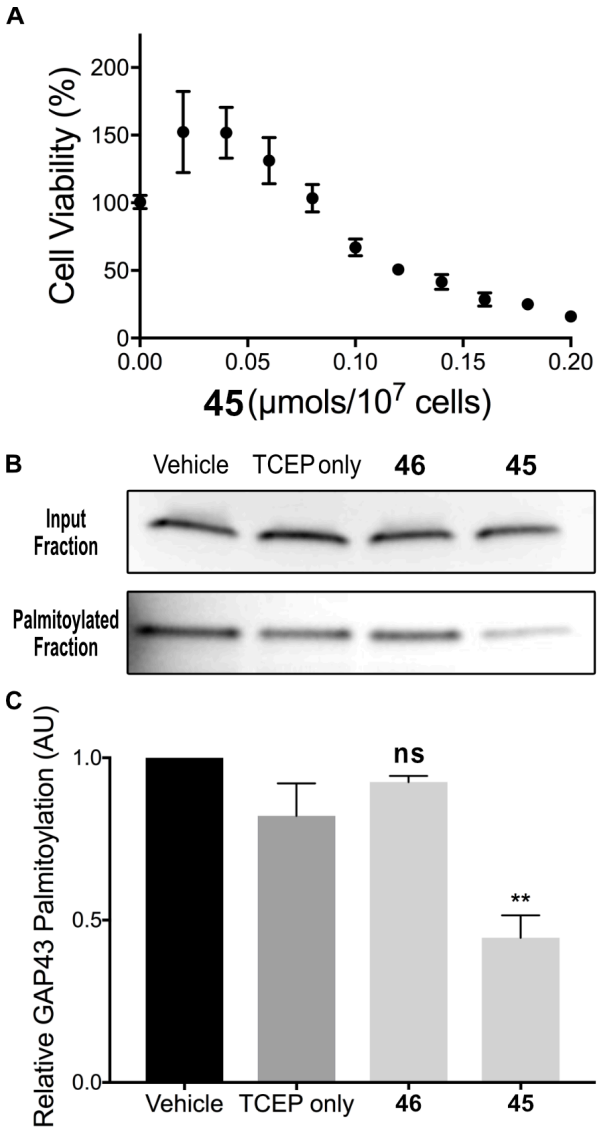

Figure 5.14 Depalmitoylation of GAP43 in INCL fibroblasts. (A) Viability of INCL lymphoblasts after treatment with **45** for 24 h as determined by a WST-1 assay. (B, C) Western blot detection of endogenous GAP43 in acyl resin-assisted capture fractions. The input fraction contains all cellular proteins. The palmitoylated fraction contains only S-palmitoylated proteins. Assays were performed in three biological replicates with the vehicle normalized to 1. Values are shown as means ± SD. Statistically significant differences in palmitoylation between TCEP only and the other means is indicated: **P<0.01. ns, not significant.

5.6 Experimental Methods

5.6.1 HPLC Analysis

HPLC analysis was performed on an Agilent 1260 Infinity system equipped with a Varian 380-LC evaporative light scattering detector (ELSD) and an Agilent 6120 Single Quad MS.

5.6.2 AMD Model Reaction

H_2N-*L*-Cys-Oct ∪ H_2N-*L*-Cys-Oct **(45')** or H_2N-*L*-Ser-Oct (**46**) was combined with MESNA thiopalmitate (**47**) in NaH_2PO_4 buffer (200 mM, pH 7.1) containing 10 mM tris(2-carboxyethyl)phosphine hydrochloride (TCEP) at a final concentration of 5 mM for each reactant. The reaction was stirred at 25 ºC and aliquots taken at the specified time points and subjected to HPLC/ELSD/MS analysis (Eclipse Plus C8 analytical column, 50-95% *MeOH* in H_2O with 0.1% TFA, 0-7 min; 95% *MeOH* in H_2O with 0.1% TFA, 7 min-end).

5.6.3 Microscopy

Imaging was performed on an Axio Observer Z1 inverted microscope (Carl Zeiss Microscopy Gmb, Germany) with Yokogawa CSU-X1 spinning disk confocal unit using a 63x, 1.4 NA oil immersion or 20x, 0.8 NA objective to an ORCA-Flash4.0 V2 Digital CMOS camera (Hamamatsu, Japan). For live cell imaging, an incubation chamber with temperature and CO_2 controllers (World Precision Instruments) was utilized. Fluorophores were excited with s diode laser (488 nm; 30 mW). Images were acquired using Zen Blue software (Carl Zeiss) and processed using Image J.[163]

5.6.4 Cell Culture

Infantile Neuronal Ceroid Lipofuscinosis (INCL) human lymphoblasts (GM16083) were obtained from Coriell Institute (Camden, NJ). T24 cells (ATCC HTB-4) were obtained from ATCC. Cells were maintained in DMEM (HeLa cells) or RPMI 1640 (INCL lymphoblasts and T24 cells)

supplemented with penicillin (50 units/mL), streptomycin (50 μg/mL) and 10% FBS (HeLa cells and T24 cells) or 15 % FBS (INCL Lymphoblasts) at 37 ºC, 5% CO_2.

5.6.5 Plasmid Construction

mEGFP-HRas was a gift from Karel Svoboda[164] (Addgene plasmid # 18662), mEGFP-N1 was a gift from Michael Davidson (Addgene plasmid # 54767) and Hs.KRAS4b was a gift from Dominic Esposito (Addgene plasmid # 83129). EGFP-KRas4b was constructed using Gibson Assembly (New England Biolabs). The vector mEGFP-N1 was linearized using HindIII and inserts were prepared by PCR amplification of Hs.KRAS4b with the following primers: KRAS4bfwd, 5'-GGA-CTC-AGA-TCT-CGA-GCT-CAA-ATG-ACT-GAA-TAT-AAA-CTT-GTG-G-3'; KRAS4brev, 5'-CCG-TCG-ACT-GCA-GAA-TTC-GAT-TAC-ATA-ATT-ACA-CAC-TTT-GTC-TTT-G-3'. The resulting construct was sequenced to verify its identity. Plasmids used for transfection were prepared using a plasmid maxiprep kit (EZgene).

5.6.6 Live-Cell Imaging of HeLa Cells

HeLa cells were plated at 40,000 cells/well in an 8-well Lab-Tek chamber slide (ThermoFisher) and allowed to adhere overnight. Cells were transfected with mEGFP-HRas or mEGFP-KRas4b using Lipofectamine 2000 (ThermoFisher) according to the manufacturer's protocol. 50 mM stocks of compounds **45** and **46** were prepared by dissolving the solid compound in DMSO containing 100 mM tris(2-carboxyethyl)phosphine hydrochloride (TCEP) as a preservative. From these stocks, a solution of 200 μM [**45** or **46**] (with 400 μM TCEP), or 400 μM TCEP was prepared in OptiMEM media. Before imaging, cells were exchanged into OptiMEM media. The diluted solutions were added to the indicated final concentration within individual wells of the chamber slide and cells imaged while maintaining 37 ºC, 5% CO_2 in the incubation chamber. Images were acquired in 6 different locations across a minimum of 2 independent experiments. The percentage

of cells exhibiting GFP fluorescence at the plasma membrane before and after treatment in each location was counted. An unpaired t test was performed to determine the significance of the means before and after treatment.

5.6.7 Acyl Resin-Assisted Capture Detection of Protein Palmitoylation in HeLa Cells

HeLa cells were grown to confluency in 10 cm plates. Stock solutions of compounds were prepared in DMSO as before and diluted to the final indicated concentration in 5.5 mL of OptiMEM media before adding to cells. Cells were incubated at 37 ºC for 20 min and then media removed and 3 mL of HBSS added to each plate. Cells were detached using a cell scraper, pelleted by centrifugation at 1,000 rcf for 5 min and the pellet processed using a CAPTUREome S-Palmitoylated Protein Kit (Badrilla, UK) according to the manufacturer's protocol. Samples were resolved by electrophoresis using 4–20% SDS–polyacrylamide gels (Bio-Rad) under denaturing and reducing conditions. Proteins were then electrotransferred to a PVDF membrane (Bio-Rad). The membrane was blocked with 3% BSA and then subjected to immunoblot analysis using Anti-GTPase HRAS antibody (ab97488) (Abcam), Calnexin Antibody (2433S) (Cell Signaling Technology), Gα(i) Antibody (5290S) (Cell Signaling Technology), SNAP25 Antibody (5308S) (Cell Signaling Technology), Flotillin-2 Antibody (3436S) (Cell Signaling Technology), CD44 Antibody (3570S) (Cell Signaling Technology), Lyric/Metadherin Antibody (14065S) (Cell Signaling Technology), Flotillin-1 Antibody (3253S) (Cell Signaling Technology) and secondary goat anti-rabbit IgG-HRP (sc-2030) (Santa Cruz Biotechnology) or goat anti-mouse IgG HRP (ThermoFisher). Chemiluminescent detection was performed by using SuperSignal West Pico PLUS chemiluminescent substrate (ThermoFisher) according to the manufacturer's instructions.

5.6.8 Acyl Resin-Assisted Capture Detection of GAP43 Palmitoylation in INCL Lymphoblasts

INCL Lymphoblasts were adjusted to 1,000,000 cells/mL in 20 mL of OptiMem Media. Stock solutions of compounds were prepared in DMSO as before and diluted to the indicated final concentration in the cell suspension. Cells were transferred to T25 flasks and incubated at 37 ºC for 20 min. Cells were pelleted by centrifugation at 1,000 rcf for 5 min and the pellet processed using a CAPTUREome S-Palmitoylated Protein Kit (Badrilla, UK) according to the manufacturer's protocol. Samples were resolved by electrophoresis using 4–20% SDS–polyacrylamide gels (Bio-Rad) under denaturing and reducing conditions. Proteins were then electrotransferred to a PVDF membrane (Bio-Rad). The membrane was blocked with 3% BSA and then subjected to immunoblot analysis using GAP-43 (B-5) Antibody (sc-17790) (Santa Cruz Biotechnology) and secondary antibody goat anti-mouse IgG HRP (ThermoFisher). Chemiluminescent detection was performed by using SuperSignal West Pico PLUS chemiluminescent substrate (ThermoFisher) according to the manufacturer's instructions.

5.6.9 Statistical Analysis of Acyl Resin-Assisted Capture Detection Assays

Assays were performed in 3 biological replicates. Each replicate involved the analysis of 4 to 5 conditions side-by-side. Western blots were analyzed using ImageJ[163]. The intensity of the protein band in each cleaved bound fraction (palmitoylated protein fraction) was normalized to the intensity of the corresponding input fraction (total protein fraction). The values within individual replicates were normalized to the control or vehicle condition and reported as means ± SD. An unpaired t test was performed to determine the significance between means.

5.6.10 Detection of AKT1 and ERK1/2 Phosphorylation in HeLa Cells

HeLa cells were grown to confluency in 6 cm plates and then serum starved overnight in OptiMEM. Stock solutions of compounds were prepared in DMSO as before and diluted to the

final indicated concentration in 2 mL of OptiMEM media before adding to cells. Cells were incubated at 37 ºC for 20 min and then stimulated with 100 ng/µL EGF (ThermoFisher) for 5 min. Media was then removed and cells washed once with HBSS. 1.5 mL of HBSS was then added to each plate. Cells were detached using a cell scraper, pelleted by centrifugation at 1,000 rcf for 5 min and the pellet processed using M-PER™ Mammalian Protein Extraction Reagent (ThermoFisher) with the addition of Halt Protease Inhibitor Cocktail (ThermoFisher) and 1 mM sodium orthovanadate. Samples were resolved by electrophoresis using 4–20% SDS–polyacrylamide gels (Bio-Rad) under denaturing and reducing conditions. Proteins were then electrotransferred to a PVDF membrane (Bio-Rad). The membrane was blocked with 3% BSA and then subjected to immunoblot analysis using AKT/MAPK Signaling Pathway Antibody Cocktail (ab151279) (Abcam) and secondary goat anti-rabbit IgG-HRP (sc-2030) (Santa Cruz Biotechnology). Chemiluminescent detection was performed by using SuperSignal West Pico PLUS chemiluminescent substrate (ThermoFisher) according to the manufacturer's instructions.

5.6.11 Statistical Analysis of AKT1 and ERK1/2 Phosphorylation in HeLa Cells

Assays were performed in 3 biological replicates. Western blots were analyzed using ImageJ[163]. The intensity of the protein band in each condition was normalized to the intensity of the corresponding loading control (Rab11). The values within individual replicates were normalized to the vehicle condition and reported as means ± SD. An unpaired t test was performed to determine the significance between means.

5.6.12 Detection of AKT1 and ERK1/2 Phosphorylation in T24 Cells

T24 cells were grown to confluency in 6 cm plates. Stock solutions of compounds were prepared in DMSO as before and diluted to the final indicated concentration in 2 mL of OptiMEM media before adding to cells. Cells were incubated at 37 ºC for 1 h and then media removed and 1.5 mL

of HBSS added to each plate. Cells were detached using a cell scraper, pelleted by centrifugation at 1,000 rcf for 5 min and the pellet processed using M-PER™ Mammalian Protein Extraction Reagent (ThermoFisher) with the addition of Halt Protease Inhibitor Cocktail (ThermoFisher) and 1 mM sodium orthovanadate. Samples were resolved by electrophoresis using 4–20% SDS–polyacrylamide gels (Bio-Rad) under denaturing and reducing conditions. Proteins were then electrotransferred to a PVDF membrane (Bio-Rad). The membrane was blocked with 3% BSA and then subjected to immunoblot analysis using AKT/MAPK Signaling Pathway Antibody Cocktail (ab151279) (Abcam) and secondary goat anti-rabbit IgG-HRP (sc-2030) (Santa Cruz Biotechnology). Chemiluminescent detection was performed by using SuperSignal West Pico PLUS chemiluminescent substrate (ThermoFisher) according to the manufacturer's instructions.

5.6.13 Statistical Analysis of AKT1 and ERK1/2 Phosphorylation in T24 Cells

Assays were performed in 3 biological replicates. Western blots were analyzed using ImageJ[163]. The intensity of the protein band in each condition was normalized to the intensity of the corresponding loading control (Rab11). The values within individual replicates were normalized to the vehicle condition and reported as means ± SD.

5.6.14 WST-1 Viability Assay INCL Lymphoblasts

INCL lymphoblasts were plated at 100,000 cells/well in 80 µL of OptiMEM in a 96 well plate. Stock organic solutions were prepared as before and then diluted to 5x stock solutions in OptiMEM. 20 µL of the OptiMEM stocks was then added to the appropriate wells to achieve the indicated final concentration of the compound in 100 µL of cell suspension. After a 24 h incubation, 10 µL of WST-1 reagent (Sigma-Aldrich) was added to each well and cells incubated for 1 h at 37 ºC, 5% CO_2. Absorbance measurements were taken using a Safire II plate reader (Tecan) at 440 nm using 690 nm as a reference. The background absorbance of the WST-1 reagent

in media was subtracted and cell viability was reported as a percentage of the viability of the non-treated control cells. All conditions were tested in 4 replicate wells and values reported as means ± SD.

5.6.15 MS Detection of AMD Product

HeLa cells were grown to confluency in two 6 cm plates. Once confluent, media was removed and cells washed 1x with HBSS. Stock solutions were prepared as before. From these stocks, solutions of 200 μM **1** (with 400 μM TCEP) or 400 μM TCEP were prepared in OptiMEM media. To each plate was added 3 mL OptiMEM + 400 μM TCEP or OptiMEM + 200 μM **45** (with 400 μM TCEP). Cells were incubated at 37 ºC for 20 min and then media removed and 3 mL of HBSS added to each plate. Cells were detached using a cell scraper, pelleted by centrifugation at 1,000 rcf for 5 min and the pellet subjected to a lipid extraction using the Bligh and Dyer method.[114] Lipid extracts were analyzed for the presence of the AMD product palmityl-N-*L*-Cys-Oct (**48**) using reverse phase chromatography on an HP 1100 LC station to a Thermo LCQdeca-MS running in ESI Positive Ion Mode. MS/MS analysis was performed on the $[M+H]^+$ peak of **48** (m/z 471) then selected reaction monitoring on the fragmentation peak (m/z 130) (Figure S5).

5.6.16 Synthesis - General Considerations

Commercially available N-Boc-*L*-Cys(Trt)-OH, O-(7-azabenzotriazol-1-yl)-1,1,3,3-tetramethyl-uronium hexafluorophosphate (HATU), *N*,*N*-diisopropylethylamine (DIEA), octylamine, trifluoroacetic acid (TFA), triethylsilane (TES), dimethyl sulfoxide (DMSO), tris(2-carboxyethyl)phosphine hydrochloride (TCEP.HCl) and N-*tert*-butylhydroxylamine hydrochloride (NtBuHA) were obtained from Sigma-Aldrich. Deuterated chloroform ($CDCl_3$) and methanol (CD_3OD) were obtained from Cambridge Isotope Laboratories. All reagents obtained from commercial suppliers were used without further purification unless otherwise noted.

Analytical thin-layer chromatography was performed on E. Merck silica gel 60 F_{254} plates. Compounds, which were not UV active, were visualized by dipping the plates in a ninhydrin or potassium permanganate solution and heating. Silica gel flash chromatography was performed using E. Merck silica gel (type 60SDS, 230-400 mesh). Solvent mixtures for chromatography are reported as v/v ratios. HPLC analysis was carried out on an Eclipse Plus C8 analytical column with *Phase A*/*Phase B* gradients [*Phase A*: H_2O with 0.1% formic acid; *Phase B*: MeOH with 0.1% formic acid]. HPLC purification was carried out on Zorbax SB-C18 semipreparative column with *Phase A*/*Phase B* gradients [*Phase A*: H_2O with 0.1% formic acid; *Phase B*: MeOH with 0.1% formic acid]. Proton nuclear magnetic resonance (^{1}H NMR) spectra were recorded on a Varian VX-500 MHz or Jeol Delta ECA-500 MHz spectrometers, and were referenced relative to residual proton resonances in $CDCl_3$ (at δ 7.24 ppm) or CD_3OD (at δ 4.87 or 3.31 ppm). ^{1}H NMR splitting patterns are assigned as singlet (s), doublet (d), triplet (t), quartet (q) or pentuplet (p). All first-order splitting patterns were designated on the basis of the appearance of the multiplet. Splitting patterns that could not be readily interpreted are designated as multiplet (m) or broad (br). Carbon nuclear magnetic resonance (^{13}C NMR) spectra were recorded on a Varian VX-500 MHz or Jeol Delta ECA-500 MHz spectrometers, and were referenced relative to residual proton resonances in $CDCl_3$ (at δ 77.23 ppm) or CD_3OD (at δ 49.15 ppm). Electrospray Ionization-Time of Flight (ESI-TOF) spectra were obtained on an Agilent 6230 Accurate-Mass TOFMS mass spectrometer.

5.6.17 Synthesis of N-Boc-*L*-Cys(Trt)-Oct

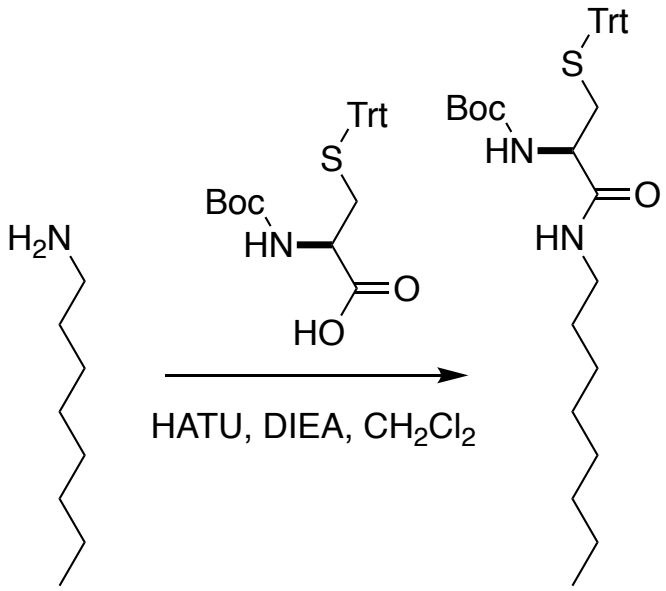

Scheme 5.1 Synthesis of N-Boc-*L*-Cys(Trt)-Oct

A solution of N-Boc-*L*-Cys(Trt)-OH (250.0 mg, 539.3 μmol) in CH_2Cl_2 (5 mL) was stirred at 0 ºC for 10 min, and then HATU (225.5 mg, 593.2 μmol) and DIEA (375.7 μL, 2.16 mmol) were successively added. After 10 min stirring at 0 ºC, octylamine (89.1 μL, 539.3 μmol) was added. After 1 h stirring at rt, the reaction mixture was washed with HCl(5%) (3 × 2.5 mL) and $NaHCO_3$(sat) (3 × 2.5 mL). The organic layer was dried (Na_2SO_4), filtered and concentrated, providing a yellow oil, which was purified by flash chromatography (0-2% MeOH in CH_2Cl_2), affording 295.9 mg of N-Boc-*L*-Cys(Trt)-Oct as a pale yellow oil [95%, R_f = 0.40 (1% MeOH in CH_2Cl_2)]. ^{1}H NMR ($CDCl_3$, 500.13 MHz, δ): 7.41 (d, *J* = 8.0 Hz, 5H, 5 × CH_{Ar}), 7.35-7.15 (m, 10H, 10 × CH_{Ar}), 6.04-5.89 (m, 1H, 1 × NH), 4.92-4.69 (m, 1H, 1 × NH), 3.90-3.72 (m, 1H, 1 × CH), 3.26-3.04 (m, 2H, 1 × CH_2), 2.79-2.68 (m, 1H, 0.5 × CH_2), 2.59-2.37 (m, 1H, 0.5 × CH_2), 1.35-1.15 (m, 12H, 6 × CH_2), 1.41 (s, 9H, 3 × CH_3), 0.86 (t, *J* = 6.9 Hz, 3H, 1 × CH_3). ^{13}C NMR ($CDCl_3$, 125.77 MHz, δ): 170.3, 155.5, 144.5, 129.7, 128.2, 127.0, 80.4, 67.3, 53.6, 39.6, 38.8,

31.9, 29.5, 29.4, 29.3, 28.4, 26.9, 22.8, 14.2. MS (ESI-TOF) [m/z (%)]: 597 ([M +Na]$^+$, 100), 575 ([MH]$^+$, 68]. HRMS (ESI-TOF) calculated for [$C_{35}H_{46}N_2O_3SNa$] ([M +Na]$^+$) 597.3121, found 597.3124.

5.6.18 Synthesis of H_2N-*L*-Cys-Oct ∪ H_2N-*L*-Cys-Oct (45')*

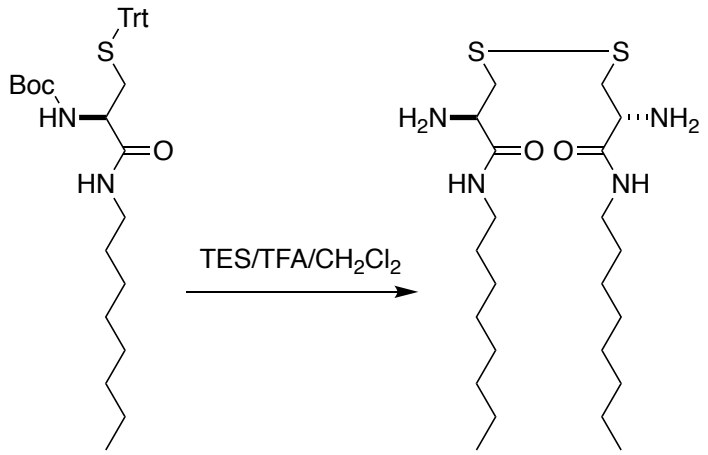

Scheme 5.2 Synthesis of H_2N-*L*-Cys-Oct ∪ H_2N-*L*-Cys-Oct (**45'**)

A solution of N-Boc-*L*-Cys(Trt)-Oct (10.0 mg, 17.4 μmol) in 500 μL of TFA/CH_2Cl_2/TES (225:225:50) was stirred at rt for 30 min. After removal of the solvent, the residue was dried under high vacuum for 3 h. Then, the corresponding residue was diluted in MeOH (250 μL), filtered using a 0.2 μm syringe-driven filter, and the crude solution was purified by HPLC, affording 3.27 mg of the H_2N-*L*-Cys-Oct ∪ H_2N-*L*-Cys-Oct (**45'**) as a colorless film [81%, t_R = 6.6 min (Zorbax SB-C18 semipreparative column, 50% *Phase A* in *Phase B*, 5 min, and then 5% *Phase A* in *Phase B*, 10 min)]. As a disulfide (RS-SR): t_R = 2.52 min (Eclipse Plus C8 analytical column, 5% *Phase A* in *Phase B*, 5.5 min)] (Figure S4). ^{1}H NMR (CD_3OD, 500.13 MHz, δ): 4.11-3.91 (m, 2H, 2 × CH), 3.36-3.32 (m, 2H, 2 × CH), 3.29-3.21 (m, 4H, 2 × CH_2), 3.09-2.92 (m, 2H, 2 × CH), 1.65-1.47 (m, 4H, 2 × CH_2), 1.45-1.21 (m, 20H, 10 × CH_2), 0.91 (t, *J* = 6.8 Hz, 6H, 2 × CH_3). ^{13}C NMR

(CD_3OD, 125.77 MHz, δ): 170.2, 53.6, 40.9, 40.8, 33.1, 30.5, 30.4, 30.3, 28.1, 23.8, 14.5. MS (ESI-TOF) [m/z (%)]: 485 ([M +Na]$^+$, 100), 463 ([MH]$^+$, 33]. HRMS (ESI-TOF) calculated for [$C_{22}H_{46}N_4O_2S_2Na$] ([M +Na]$^+$) 485.2954, found 485.2947. HRMS (ESI-TOF) calculated for [$C_{22}H_{47}N_4O_2S_2$] ([MH]$^+$) 463.3135, found 463.3128.

* Air oxidation of the thiol (RSH) causes the disulfide bond (RS-SR) formation.

5.6.19 Synthesis of H_2N-*L*-Cys-Oct (45)

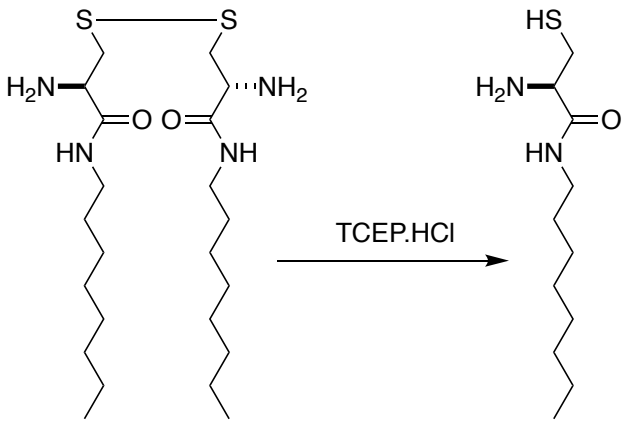

Scheme 5.3 Synthesis of H_2N-*L*-Cys-Oct (**45**)

A solution of H_2N-*L*-Cys-Oct ∪ H_2N-*L*-Cys-Oct (**45'**, 1.0 mg, 4.3 μmol) in 861.5 μL of a 5 mM solution of TCEP.HCl in H_2O (or DMSO) was stirred at rt for 5 min. Then, it was analyzed by HPLC and/or used directly for the depalmitoylation experiments. As a free thiol (R-SH): t_R = 2.77 min (Eclipse Plus C8 analytical column, 5% *Phase A* in *Phase B*, 5.5 min)] (Figure S4). MS (ESI-TOF) [m/z (%)]: 233 ([MH]$^+$, 100).

5.6.20 Synthesis of N-Boc-*L*-Ser(ᵗBu)-Oct

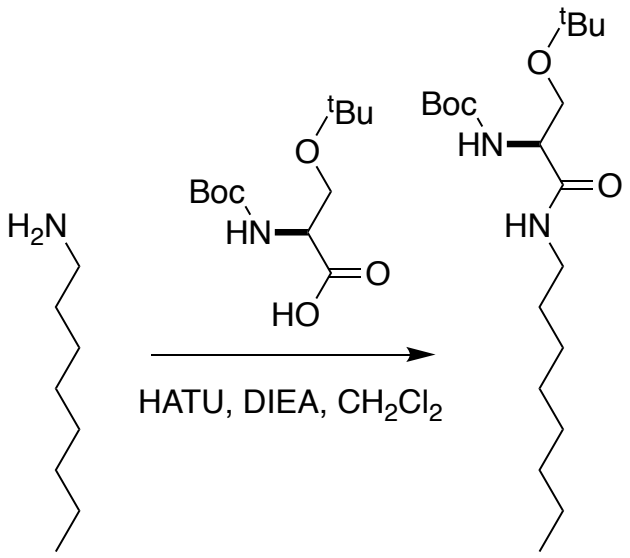

Scheme 5.4 Synthesis of N-Boc-*L*-Ser(ᵗBu)-Oct

A solution of N-Boc-*L*-Ser(ᵗBu)-OH (100.0 mg, 382.8 μmol) in CH_2Cl_2 (4 mL) was stirred at 0 ºC for 10 min, and then HATU (160.1 mg, 421.1 μmol) and DIEA (266.7 μL, 1.53 mmol) were successively added. After 10 min stirring at 0 ºC, octylamine (63.3 μL, 382.8 μmol) was added. After 1 h stirring at rt, the reaction mixture was washed with HCl(5%) (3 × 2 mL) and $NaHCO_3$(sat) (3 × 2 mL). The organic layer was dried (Na_2SO_4), filtered and concentrated, providing a yellow oil, which was purified by flash chromatography (0-5% MeOH in CH_2Cl_2), affording 128.9 mg of N-Boc-*L*-Ser(ᵗBu)-Oct as white crystals [91%, R_f = 0.42 (5% MeOH in CH_2Cl_2)]. ^{1}H NMR ($CDCl_3$, 500.13 MHz, δ): 6.69-6.41 (m, 1H, 1 × NH), 5.54-5.31 (m, 1H, 1 × NH), 4.21-4.00 (m, 1H, 1 × CH), 3.86-3.66 (m, 1H, 0.5 × CH_2), 3.43-3.29 (m, 1H, 0.5 × CH_2), 3.29-3.19 (m, 2H, 1 × CH_2), 1.51-1.46 (m, 2H, 1 × CH_2), 1.44 (s, 9H, 3 × CH_3), 1.34-1.20 (m, 10H, 5 × CH_2), 1.18 (s, 9H, 3 × CH_3), 0.86 (t, *J* = 6.9 Hz, 3H, 1 × CH_3). ^{13}C NMR ($CDCl_3$, 125.77 MHz, δ): 170.6, 155.7, 80.0, 74.0, 62.0, 54.3, 39.6, 38.8, 31.9, 29.6, 29.4, 28.5, 27.6, 27.0, 22.8, 14.2. MS (ESI-TOF) [m/z

(%)]: 373 ([MH]$^+$, 100]. HRMS (ESI-TOF) calculated for [$C_{20}H_{41}N_2O_4$] ([MH]$^+$) 373.3061, found 373.3058.

5.6.21 Synthesis of H_2N-*L*-Ser-Oct (46)

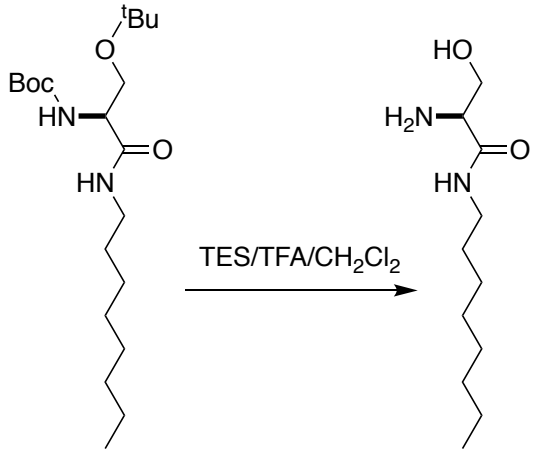

Scheme 5.5 Synthesis of H_2N-*L*-Ser-Oct (**46**)

A solution of N-Boc-*L*-Ser(^{t}Bu)-Oct (20.0 mg, 53.7 μmol) in 500 μL of TFA/CH_2Cl_2/TES (225:225:50) was stirred at rt for 30 min. After removal of the solvent, the residue was dried under high vacuum for 3 h. Then, the corresponding residue was diluted in MeOH (250 μL), filtered using a 0.2 μm syringe-driven filter, and the crude solution was purified by HPLC, affording 10.1 mg of the H_2N-*L*-Ser-Oct (**46**) as a colorless film [87%, t_R = 6.3 min (Zorbax SB-C18 semipreparative column, 50% *Phase A* in *Phase B*, 5 min, and then 5% *Phase A* in *Phase B*, 10 min)]. ^{1}H NMR (CD_3OD, 500.13 MHz, δ): 3.92-3.87 (m, 1H, 1 × CH), 3.86-3.81 (m, 1H, 0.5 × CH_2), 3.80-3.74 (m, 1H, 0.5 × CH_2), 3.26-3.22 (t, *J* = 7.0 Hz, 2H, 1 × CH_2), 1.59-1.47 (m, 2H, 1 × CH_2), 1.36-1.23 (m, 10H, 5 × CH_2), 0.90 (t, *J* = 7.0 Hz, 3H, 1 × CH_3). ^{13}C NMR (CD_3OD, 125.77 MHz, δ): 168.4, 62.0, 56.5, 40.7, 33.0, 30.4, 30.4, 30.3, 28.0, 23.7, 14.4. MS (ESI-TOF) [m/z (%)]:

217 ([MH]$^+$, 100]. HRMS (ESI-TOF) calculated for [$C_{11}H_{25}N_2O_2$] ([MH]$^+$) 217.1911, found 217.1912.

5.6.22 Synthesis of MESNA thiopalmitate (47)[139]

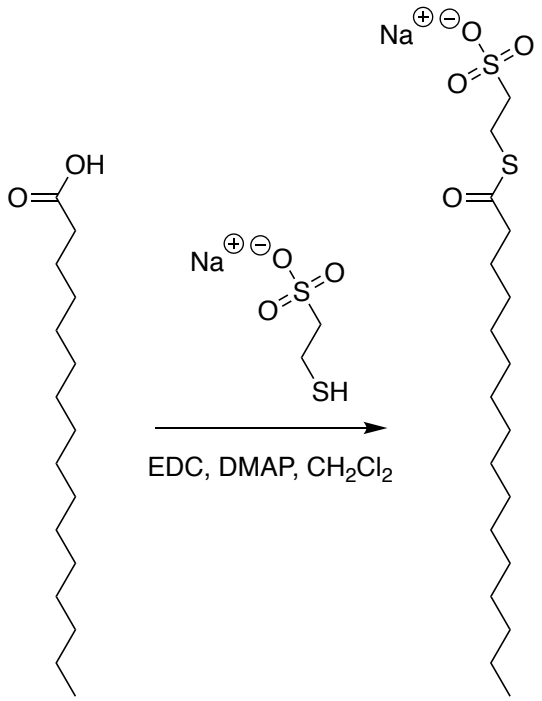

Scheme 5.6 Synthesis of Synthesis of MESNA thiopalmitate (**47**)

A solution of palmitic acid (171.8 mg, 670.0 μmol) in CH_2Cl_2 (5 mL) was stirred at 0 ºC for 10 min, and then DMAP (7.4 mg, 60.9 μmol) and EDC.HCl (128.4 mg, 670.0 μmol) were successively added. After 10 min stirring at 0 ºC, sodium 2-mercaptoethanesulfonate[165] (MESNA, 100.0 mg, 609.1 μmol) was added. After 5 h stirring at rt, the mixture was extracted with H_2O (2 × 3 mL) and the combined aqueous phases were washed with EtOAc (3 mL). After evaporation of H_2O under reduced pressure, the residue was washed with CH_3CN (5 mL), and then filtered to yield 189.3 mg of **3** as a white solid [77%]. ^{1}H NMR (d_6-DMSO, 500.13 MHz, δ): 3.08-2.96 (m, 2H, 1 × CH_2), 2.62-2.50 (m, 4H, 2 × CH_2), 1.62-1.45 (m, 2H, 1 × CH_2), 1.34-1.14 (m, 24H, 12 ×

CH_2), 0.85 (t, J = 7.0 Hz, 3H, 1 × CH_3). ^{13}C NMR (d_6-DMSO, 125.77 MHz, δ): 198.7, 50.9, 43.3, 31.3, 29.1, 29.1, 29.1, 29.0, 29.0, 29.0, 28.9, 28.8, 28.7, 28.2, 25.1, 24.3, 22.1, 14.0. MS (ESI-TOF) [m/z (%)]: 379 ([M -Na]$^-$, 100). HRMS (ESI-TOF) calculated for $C_{18}H_{35}O_4S_2$ ([M -Na]$^-$) 379.1971, found 379.1973.

5.6.23 Synthesis of Palmityl-N-*L*-Cys-Oct (48)

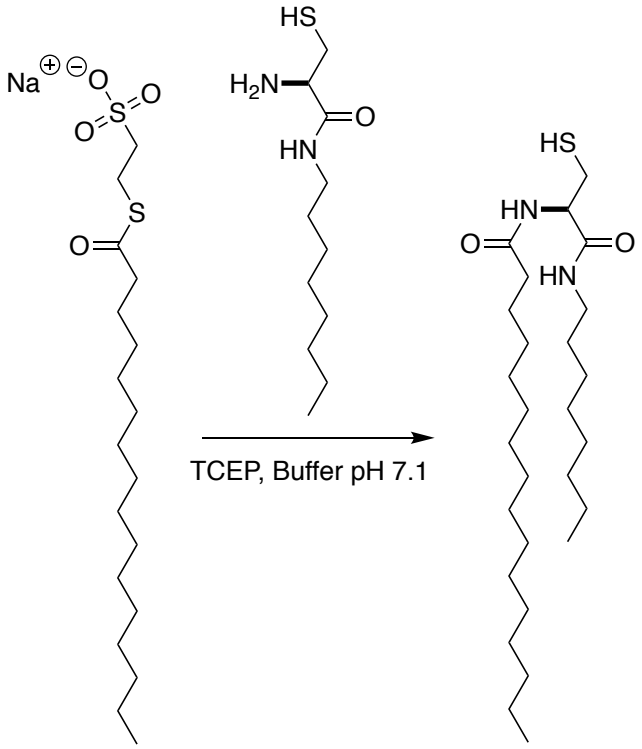

Scheme 5.7 Synthesis of Palmityl-N-*L*-Cys-Oct (**48**)

H_2N-*L*-Cys-Oct (**45**, 3.00 mg, 12.93 μmol) and MESNA thiopalmitate (**47**, 5.20 mg, 12.93 μmol) were dissolved in 1.29 mL of 20 mM TCEP.HCl in 200 mM NaH_2PO_4 pH 7.1 buffer and stirred under N_2 at rt. After 30 min, the corresponding mixture was filtered using a 0.2 μm syringe-driven filter, and the crude solution was purified by HPLC, affording 4.92 mg of the amidophospholipid **48** as a colorless oil [81%, t_R = 8.1 min (Zorbax SB-C18 semipreparative column, 100 % Phase B,

20.5 min), t_R = 5.01 min (Eclipse Plus C8 analytical column, 5% *Phase A* in *Phase B*, 5.5 min)]. MS (ESI-TOF) [m/z (%)]: 493 ([M +Na]$^+$, 18), 471 ([MH]$^+$, 100]. HRMS (ESI-TOF) calculated for [$C_{27}H_{55}N_2O_2S$] ([MH]$^+$) 471.3984, found 471.3982.

Notes about the chapter:

Chapter five, in full, is a reprint (with co-author permission) of the material as it appears in the publication; **A. K. Rudd**, R. J. Brea, N. K. Devaraj "Amphiphile-Mediated Depalmitoyolation of Proteins in Living Cells," *J. Am. Chem. Soc.*, 2018, 140 (50) 17374-17378. I would like to sincerely thank Roberto Brea for his assistance with this work. Roberto Brea synthesized all compounds presented in this chapter and provided valuable scientific advice. I thank Neal Devaraj for his guidance and insight in designing experiments and preparing the manuscript. The author of the dissertation is the primary author of this manuscript.

References

(1) The Chevreul Life http://www.cyberlipid.org/chevreul/life0002.htm.

(2) List, G. R. Giants of the Past Michel Eugéne Chevreul http://lipidlibrary.aocs.org/History/content.cfm?ItemNumber=39262.

(3) Membrane Permeability 100 Years since Ernest Overton. **1999**, 1–18.

(4) Gorter, E. On Bimolecular Layers of Lipids on the Chromocytes of the Blood. *J. Exp. Med.* **1925**, *41*, 439–443.

(5) Steinberg, D. In Celebration of the 100th Anniversary of the Lipid Hypothesis of Atherosclerosis. *J. Lipid Res.* **2013**, *54*, 2946–2949.

(6) Spector, A. A.; Kim, H.-Y. Discovery of Essential Fatty Acids. *J. Lipid Res.* **2015**, *56*, 11–21.

(7) List, G. R.; Bibus, D. Giants of the Past Ralph Theodore Holman http://lipidlibrary.aocs.org/History/content.cfm?ItemNumber=39266.

(8) Dennis, E. A. Lipidomics Joins the Omics Evolution. *Proc. Natl. Acad. Sci. U. S. A.* **2009**, *106*, 2089–2090.

(9) LIPID MAPS Structure Database.

(10) Sletten, E. M.; Bertozzi, C. R. Bioorthogonal Chemistry: Fishing for Selectivity in a Sea of Functionality. *Angew. Chem. Int. Ed. Engl.* **2009**, *48*, 6974–6998.

(11) Höglinger, D.; Haberkant, P.; Aguilera-Romero, A.; Riezman, H.; Porter, F. D.; Platt, F. M.; Galione, A.; Schultz, C. Intracellular Sphingosine Releases Calcium from Lysosomes. *Elife* **2015**, *4*, e10616.

(12) Frank, J. A.; Yuschenko, D. A.; Hodson, D. J.; Lipstein, N.; Nagpal, J.; Rutter, G. A.; Rhee, J.-S.; Gottschalk, A.; Brose, N.; Schultz, C.; et al. Photoswitchable Diacylglycerols Enable Optical Control of Protein Kinase C. *Nat. Chem. Biol.* **2016**, *12*, 755–762.

(13) Budin, I.; Rond, T. De; Chen, Y.; Chan, L. J. G.; Petzold, C. J.; Keasling, J. D. Viscous Control of Cellular Respiration by Membrane Lipid Composition. *Science* **2018**, *1189*, 1186–1189.

(14) Zhu, T.; Szostak, J. Coupled Growth and Division of Model Protocell Membranes. *J. Am. Chem. Soc.* **2009**, *131*, 5705–5713.

(15) Hardy, M. D.; Yang, J.; Selimkhanov, J.; Cole, C. M.; Tsimring, L. S.; Devaraj, N. K. Self-Reproducing Catalyst Drives Repeated Phospholipid Synthesis and Membrane Growth. **2015**, *112*, 8187–8192.

(16) Budin, I.; Devaraj, N. K. Membrane Assembly Driven by a Biomimetic Coupling Reaction. *J. Am. Chem. Soc.* **2012**, *134*, 751–753.

(17) Hartman, N. C.; Groves, J. T. Signaling Clusters in the Cell Membrane. *Curr. Opin. Cell Biol.* **2011**, *23*, 370–376.

(18) Baumgart, T.; Capraro, B. R.; Zhu, C.; Das, S. L. Thermodynamics and Mechanics of Membrane Curvature Generation and Sensing by Proteins and Lipids. *Annu. Rev. Phys. Chem.* **2011**, *62*, 483–506.

(19) Hancock, W. O. Bidirectional Cargo Transport: Moving beyond Tug of War. *Nat. Rev. Mol. Cell Biol.* **2014**, *15*, 615–628.

(20) Nadolski, M. J.; Linder, M. E. Protein Lipidation. *FEBS J.* **2007**, *274*, 5202–5210.

(21) Hicke, L.; Dunn, R. Regulation of Membrane Protein Transport by Ubiquitin and Ubiquitin-Binding Proteins. *Annu. Rev. Cell Dev. Biol.* **2003**, *19*, 141–172.

(22) Mikelj, M.; Praper, T.; Demič, R.; Hodnik, V.; Turk, T.; Anderluh, G. Electroformation of Giant Unilamellar Vesicles from Erythrocyte Membranes under Low-Salt Conditions. *Anal. Biochem.* **2013**, *435*, 174–180.

(23) Girard, P.; Pécréaux, J.; Lenoir, G.; Falson, P.; Rigaud, J.-L.; Bassereau, P. A New Method for the Reconstitution of Membrane Proteins into Giant Unilamellar Vesicles. *Biophys. J.* **2004**, *87*, 419–429.

(24) Varnier, A.; Kermarrec, F.; Blesneac, I.; Moreau, C.; Liguori, L.; Lenormand, J. L.; Picollet-D'hahan, N. A Simple Method for the Reconstitution of Membrane Proteins into Giant Unilamellar Vesicles. *J. Membr. Biol.* **2010**, *233*, 85–92.

(25) Bier, F. F.; von Nickisch-Rosenegk, M.; Teschke, T. Construction of an Artificial Cell Membrane Anchor Using DARC as a Fitting for Artificial Extracellular Functionalities of Eukaryotic Cells. *J. Nanobiotechnology* **2012**, *10*, 1.

(26) Noireaux, V.; Libchaber, A. A Vesicle Bioreactor as a Step toward an Artificial Cell Assembly. *Proc. Natl. Acad. Sci. U. S. A.* **2004**, *101*, 17669–17674.

(27) Erhart, D.; Zimmermann, M.; Jacques, O.; Wittwer, M. B.; Ernst, B.; Constable, E.; Zvelebil, M.; Beaufils, F.; Wymann, M. P. Chemical Development of Intracellular Protein Heterodimerizers. *Chem. Biol.* **2013**, *20*, 549–557.

(28) Ishida, M.; Watanabe, H. Synthetic Self-Localizing Ligands That Control the Spatial Location of Proteins in Living Cells. *J. Am. Chem. Soc.* **2013**, *135*, 12684–12689.

(29) Kennedy, M.; Hughes, R.; Peteya, L. Rapid Blue-Light-Mediated Induction of Protein Interactions in Living Cells. *Nat. Methods* **2010**, *7*, 12–16.

(30) Uhlenheuer, D. a; Wasserberg, D.; Haase, C.; Nguyen, H. D.; Schenkel, J. H.; Huskens, J.;

Ravoo, B. J.; Jonkheijm, P.; Brunsveld, L. Directed Supramolecular Surface Assembly of SNAP-Tag Fusion Proteins. *Chemistry* **2012**, *18*, 6788–6794.

(31) Keppler, A.; Gendreizig, S.; Gronemeyer, T.; Pick, H.; Vogel, H.; Johnsson, K. A General Method for the Covalent Labeling of Fusion Proteins with Small Molecules in Vivo. *Nat. Biotechnol.* **2003**, *21*, 86–89.

(32) Hinner, M. J.; Johnsson, K. How to Obtain Labeled Proteins and What to Do with Them. *Curr. Opin. Biotechnol.* **2010**, *21*, 766–776.

(33) Johnsson, K. Visualizing Biochemical Activities in Living Cells. *Nat. Chem. Biol.* **2009**, *5*, 63–65.

(34) Lukinavičius, G.; Umezawa, K.; Olivier, N.; Honigmann, A.; Yang, G.; Plass, T.; Mueller, V.; Reymond, L.; Corrêa, I. R.; Luo, Z.-G.; et al. A Near-Infrared Fluorophore for Live-Cell Super-Resolution Microscopy of Cellular Proteins. *Nat. Chem.* **2013**, *5*, 132–139.

(35) Sun, X.; Zhang, A.; Baker, B.; Sun, L.; Howard, A.; Buswell, J.; Maurel, D.; Masharina, A.; Johnsson, K.; Noren, C. J.; et al. Development of SNAP-Tag Fluorogenic Probes for Wash-Free Fluorescence Imaging. *Chembiochem* **2011**, *12*, 2217–2226.

(36) Chidley, C.; Haruki, H.; Pedersen, M. G.; Muller, E.; Johnsson, K. A Yeast-Based Screen Reveals That Sulfasalazine Inhibits Tetrahydrobiopterin Biosynthesis. *Nat. Chem. Biol.* **2011**, *7*, 375–383.

(37) Chidley, C.; Mosiewicz, K.; Johnsson, K. A Designed Protein for the Specific and Covalent Heteroconjugation of Biomolecules. *Bioconjug. Chem.* **2008**, *19*, 1753–1756.

(38) Lemercier, G.; Gendreizig, S.; Kindermann, M.; Johnsson, K. Inducing and Sensing Protein--Protein Interactions in Living Cells by Selective Cross-Linking. *Angew. Chem. Int. Ed. Engl.* **2007**, *46*, 4281–4284.

(39) Gu, G. J.; Friedman, M.; Jost, C.; Johnsson, K.; Kamali-Moghaddam, M.; Plückthun, A.; Landegren, U.; Söderberg, O. Protein Tag-Mediated Conjugation of Oligonucleotides to Recombinant Affinity Binders for Proximity Ligation. *N. Biotechnol.* **2013**, *30*, 144–152.

(40) Engin, S.; Fichtner, D.; Wedlich, D.; Fruk, L. SNAP-Tag as a Tool for Surface Immobilization. *Curr. Pharm. Des.* **2013**, *19*, 5443–5448.

(41) Mollwitz, B.; Brunk, E.; Schmitt, S.; Pojer, F.; Bannwarth, M.; Schiltz, M.; Rothlisberger, U.; Johnsson, K. Directed Evolution of the Suicide Protein O^6-Alkylguanine-DNA Alkyltransferase for Increased Reactivity Results in an Alkylated Protein with Exceptional Stability. *Biochemistry* **2012**, *51*, 986–994.

(42) Erhart, D. Control of Cellular Signals in Time and Space, University of Basel, 2012.

(43) Lee, H.; Venable, R. M.; Mackerell, A. D.; Pastor, R. W. Molecular Dynamics Studies of Polyethylene Oxide and Polyethylene Glycol: Hydrodynamic Radius and Shape

Anisotropy. *Biophys. J.* **2008**, *95*, 1590–1599.

(44) Kurfürst, M. Detection and Molecular Weight Determination of Polyethylene Glycol-Modified Hirudin by Staining after Sodium Dodecyl Sulfate-Polyacrylamide Gel Electrophoresis. *Anal. Biochem.* **1992**, *248*, 244–248.

(45) Pautot, S.; Frisken, B.; Weitz, D. Production of Unilamellar Vesicles Using an Inverted Emulsion. *Langmuir* **2003**, *19*, 2870–2879.

(46) Veatch, S. L.; Keller, S. L. Separation of Liquid Phases in Giant Vesicles of Ternary Mixtures of Phospholipids and Cholesterol. *Biophys. J.* **2003**, *85*, 3074–3083.

(47) Feigenson, G. W.; Buboltz, J. T. Ternary Phase Diagram of Dipalmitoyl-PC/Dilauroyl-PC/Cholesterol: Nanoscopic Domain Formation Driven by Cholesterol. *Biophys. J.* **2001**, *80*, 2775–2788.

(48) Banala, S.; Arnold, A.; Johnsson, K. Caged Substrates for Protein Labeling and Immobilization. *Chembiochem* **2008**, *9*, 38–41.

(49) Moscho, A.; Orwar, O. W. E.; Chiu, D. T.; Modi, B. P.; Zare, R. N. Rapid Preparation of Giant Unilamellar Vesicles. *Proc. Natl. Acad. Sci.* **1996**, *93*, 11443–11447.

(50) Kahya, N.; Scherfeld, D.; Bacia, K.; Schwille, P. Lipid Domain Formation and Dynamics in Giant Unilamellar Vesicles Explored by Fluorescence Correlation Spectroscopy. *J. Struct. Biol.* **2004**, *147*, 77–89.

(51) Mufamadi, M. S.; Pillay, V.; Choonara, Y. E.; Du Toit, L. C.; Modi, G.; Naidoo, D.; Ndesendo, V. M. K. A Review on Composite Liposomal Technologies for Specialized Drug Delivery. *J. Drug Deliv.* **2011**, *2011*, 939851.

(52) Torchilin, V. P. Recent Advances with Liposomes as Pharmaceutical Carriers. *Nat. Rev. Drug Discov.* **2005**, *4*, 145–160.

(53) Noireaux, V.; Maeda, Y. T.; Libchaber, A. Development of an Artificial Cell, from Self-Organization to Computation and Self-Reproduction. *Proc. Natl. Acad. Sci. U. S. A.* **2011**, *108*, 3473–3480.

(54) Shin, J.; Noireaux, V. An E. Coli Cell-Free Expression Toolbox: Application to Synthetic Gene Circuits and Artificial Cells. *ACS Synth. Biol.* **2012**, *1*, 29–41.

(55) Nourian, Z.; Roelofsen, W.; Danelon, C. Triggered Gene Expression in Fed-Vesicle Microreactors with a Multifunctional Membrane. *Angew. Chemie* **2012**, *124*, 3168–3172.

(56) Dezi, M.; Cicco, A. Di. Detergent-Mediated Incorporation of Transmembrane Proteins in Giant Unilamellar Vesicles with Controlled Physiological Contents. *Proc. Natl. Acad. Sci.* **2013**, *110*, 7276–7281.

(57) Stachowiak, J. C.; Schmid, E. M.; Ryan, C. J.; Ann, H. S.; Sasaki, D. Y.; Sherman, M. B.;

Geissler, P. L.; Fletcher, D. A.; Hayden, C. C. Membrane Bending by Protein-Protein Crowding. *Nat. Cell Biol.* **2012**, *14*, 944–949.

(58) Song, W.; Yu, Z.; Madden, M. M.; Lin, Q. A Bioorthogonal Chemistry Strategy for Probing Protein Lipidation in Live Cells. *Mol. Biosyst.* **2010**, *6*, 1576–1578.

(59) Edelstein, A.; Amodaj, N.; Hoover, K.; Vale, R.; Stuurman, N. Computer Control of Microscopes Using MManager. *Curr. Protoc. Mol. Biol.* **2010**, *Chapter 14*, Unit14.20.

(60) Klán, P.; Šolomek, T.; Bochet, C. Photoremovable Protecting Groups in Chemistry and Biology: Reaction Mechanisms and Efficacy. *Chem. Rev.* **2012**, *113*, 119–191.

(61) Trigo, F. F.; Papageorgiou, G.; Corrie, J. E. T.; Ogden, D. Laser Photolysis of DPNI-GABA, a Tool for Investigating the Properties and Distribution of GABA Receptors and for Silencing Neurons in Situ. *J. Neurosci. Methods* **2009**, *181*, 159–169.

(62) Trigo, F. F.; Corrie, J. E. T.; Ogden, D. Laser Photolysis of Caged Compounds at 405 Nm: Photochemical Advantages, Localisation, Phototoxicity and Methods for Calibration. *J. Neurosci. Methods* **2009**, *180*, 9–21.

(63) Banala, S.; Arnold, A.; Johnsson, K. Caged Substrates for Protein Labeling and Immobilization. *Chembiochem* **2008**, *9*, 38–41.

(64) Holthuis, J. C. M.; Menon, A. K. Lipid Landscapes and Pipelines in Membrane Homeostasis. *Nature* **2014**, *510*, 48–57.

(65) Shindou, H.; Hishikawa, D.; Harayama, T.; Yuki, K.; Shimizu, T. Recent Progress on Acyl CoA: Lysophospholipid Acyltransferase Research. *J. Lipid Res.* **2009**, *50 Suppl*, S46–S51.

(66) Lipowsky, R. Remodeling of Membrane Compartments: Some Consequences of Membrane Fluidity. *Biol. Chem.* **2014**, *395*, 253–274.

(67) Cepińska, M. N.; Veenhuis, M.; van der Klei, I. J.; Nagotu, S. Peroxisome Fission Is Associated with Reorganization of Specific Membrane Proteins. *Traffic* **2011**, *12*, 925–937.

(68) Rocha, S.; De Keersmaecker, H.; Hutchison, J. A.; Vanhoorelbeke, K.; Martens, J. A.; Hofkens, J.; Uji-I, H. Membrane Remodeling Processes Induced by Phospholipase Action. *Langmuir* **2014**, *30*, 4743–4751.

(69) Brown, W. J.; Chambers, K.; Doody, A. Phospholipase A2 (PLA2) Enzymes in Membrane Trafficking: Mediators of Membrane Shape and Function. *Traffic* **2003**, *4*, 214–221.

(70) Vogel, V.; Sheetz, M. Local Force and Geometry Sensing Regulate Cell Functions. *Nat. Rev. Mol. Cell Biol.* **2006**, *7*, 265–275.

(71) Jiang, Z.; de Messieres, M.; Lee, J. C. Membrane Remodeling by Alpha-Synuclein and Effects on Amyloid Formation. *J Am Chem Soc* **2013**, *135*, 15970–15973.

(72) Schlame, M.; Acehan, D.; Berno, B.; Xu, Y.; Valvo, S.; Ren, M.; Stokes, D. L.; Epand, R. M. The Physical State of Lipid Substrates Provides Transacylation Specificity for Tafazzin. *Nat. Chem. Biol.* **2012**, *8*, 862–869.

(73) Lozano, M. M.; Liu, Z.; Sunnick, E.; Janshoff, A.; Kumar, K.; Boxer, S. G. Colocalization of the Ganglioside G M1 and Cholesterol Detected by Secondary Ion Mass Spectrometry. *J. Am. Chem. Soc.* **2013**, *135*, 5620–5630.

(74) Hanson, J. M.; Gettel, D. L.; Tabaei, S. R.; Jackman, J.; Kim, M. C.; Sasaki, D. Y.; Groves, J. T.; Liedberg, B.; Cho, N. J.; Parikh, A. N. Cholesterol-Enriched Domain Formation Induced by Viral-Encoded, Membrane-Active Amphipathic Peptide. *Biophys. J.* **2016**, *110*, 176–187.

(75) McLean, L. R.; Phillips, M. C. Mechanism of Cholesterol and Phosphatidylcholine Exchange or Transfer between Unilamellar Vesicles. *Biochemistry* **1981**, *20*, 2893–2900.

(76) Vázquez, O.; Seitz, O. Templated Native Chemical Ligation: Peptide Chemistry beyond Protein Synthesis. *J. Pept. Sci.* **2014**, *20*, 78–86.

(77) Raibaut, L.; Ollivier, N.; Melnyk, O. Sequential Native Peptide Ligation Strategies for Total Chemical Protein Synthesis. *Chem. Soc. Rev.* **2012**, *41*, 7001.

(78) Dawson, P.; Muir, T.; Clark-Lewis, I.; Kent, S. Synthesis of Proteins by Native Chemical Ligation. *Science* **1994**, *266*, 776–779.

(79) Mitteilung, P.; Wieland, V. T.; Bokelmann, E.; Bauer, L.; Ulrich, H.; Hans, L. Uber Peptidsynthesen. 8. Mitteilung. **1953**, *104*.

(80) Brea, R. J.; Cole, C. M.; Devaraj, N. K. In Situ Vesicle Formation by Native Chemical Ligation. *Angew. Chem. Int. Ed.* **2014**, *53*, 14102–14105.

(81) Cole, C. M.; Brea, R. J.; Kim, Y. H.; Hardy, M. D.; Yang, J.; Devaraj, N. K. Spontaneous Reconstitution of Functional Transmembrane Proteins during Bioorthogonal Phospholipid Membrane Synthesis. *Angew. Chemie - Int. Ed.* **2015**, *54*, 12738–12742.

(82) Ruff, Y.; Garavini, V.; Giuseppone, N. Reversible Native Chemical Ligation: A Facile Access to Dynamic Covalent Peptides. *J. Am. Chem. Soc.* **2014**, *136*, 6333–6339.

(83) McLean, L. R.; Phillips, M. C. Kinetics of Phosphatidylcholine and Lysophosphatidylcholine Exchange between Unilamellar Vesicles. *Biochemistry* **1984**, *23*, 4624–4630.

(84) Walde, P.; Cosentino, K.; Engel, H.; Stano, P. Giant Vesicles: Preparations and Applications. *Chembiochem* **2010**, *11*, 848–865.

(85) Fan, J.; Sammalkorpi, M.; Haataja, M. Formation and Regulation of Lipid Microdomains in Cell Membranes: Theory, Modeling, and Speculation. *FEBS Lett.* **2010**, *584*, 1678–1684.

(86) Simons, K.; Gerl, M. J. Revitalizing Membrane Rafts: New Tools and Insights. *Nat. Rev. Mol. Cell Biol.* **2010**, *11*, 688–699.

(87) Hanzal-Bayer, M. F.; Hancock, J. F. Lipid Rafts and Membrane Traffic. *FEBS Lett.* **2007**, *581*, 2098–2104.

(88) Gassart, A. De; Ge, C.; Fe, B. Lipid Raft – Associated Protein Sorting in Exosomes. *Proteins* **2003**, *102*, 4336–4344.

(89) Michel, V.; Bakovic, M. Lipid Rafts in Health and Disease. *Biol. Cell* **2007**, *99*, 129–140.

(90) Chazal, N.; Gerlier, D. Virus Entry, Assembly, Budding, and Membrane Rafts. *Microbiol. Mol. Biol. Rev.* **2003**, *67*, 226–237.

(91) Leser, G. P.; Lamb, R. A. Influenza Virus Assembly and Budding in Raft-Derived Microdomains: A Quantitative Analysis of the Surface Distribution of HA, NA and M2 Proteins. *Virology* **2005**, *342*, 215–227.

(92) Baumgart, T.; Hess, S. T.; Webb, W. W. Imaging Coexisting Fluid Domains in Bilmembrane Models Coupling Curbature and Line Tension. *Nature* **2003**, *425*, 821–824.

(93) Yeung, T.; Grinstein, S. Lipid Signaling and the Modulation of Surface Charge during Phagocytosis. *Immunol. Rev.* **2007**, *219*, 17–36.

(94) Shi, X.; Bi, Y.; Yang, W.; Guo, X.; Jiang, Y.; Wan, C.; Li, L.; Bai, Y.; Guo, J.; Wang, Y.; et al. Ca2+ Regulates T-Cell Receptor Activation by Modulating the Charge Property of Lipids. *Nature* **2013**, *493*, 111–115.

(95) Tatsuta, T.; Scharwey, M.; Langer, T. Mitochondrial Lipid Trafficking. *Trends Cell Biol.* **2014**, *24*, 44–52.

(96) Varkey, J.; Isas, J. M.; Mizuno, N.; Jensen, M. B.; Bhatia, V. K.; Jao, C. C.; Petrlova, J.; Voss, J. C.; Stamou, D. G.; Steven, A. C.; et al. Membrane Curvature Induction and Tubulation Are Common Features of Synucleins and Apolipoproteins. *J. Biol. Chem.* **2010**, *285*, 32486–32493.

(97) Peter, B. J.; Kent, H. M.; Mills, I. G.; Vallis, Y.; Butler, P. J. G.; Evans, P. R.; McMahon, H. T. BAR Domains as Sensors of Membrane Curvature: The Amphiphysin BAR Structure. *Science* **2004**, *303*, 495–499.

(98) Pujals, S.; Miyamae, H.; Afonin, S.; Murayama, T.; Hirose, H.; Nakase, I.; Taniuchi, K.; Umeda, M.; Sakamoto, K.; Ulrich, A. S.; et al. Curvature Engineering: Positive Membrane Curvature Induced by Epsin N-Terminal Peptide Boosts Internalization of Octaarginine. *ACS Chem. Biol.* **2013**, *8*, 1894–1899.

(99) Stagg, S. M.; LaPointe, P.; Balch, W. E. Structural Design of Cage and Coat Scaffolds That Direct Membrane Traffic. *Curr. Opin. Struct. Biol.* **2007**, *17*, 221–228.

(100) Grösch, S.; Schiffmann, S.; Geisslinger, G. Chain Length-Specific Properties of Ceramides. *Prog. Lipid Res.* **2012**, *51*, 50–62.

(101) Chavez, J. A.; Summers, S. A. A Ceramide-Centric View of Insulin Resistance. *Cell Metab.* **2012**, *15*, 585–594.

(102) Trajkovic, K.; Hsu, C.; Chiantia, S.; Rajendran, L.; Wenzel, D.; Wieland, F.; Schwille, P.; Brügger, B.; Simons, M. Ceramide Triggers Budding of Exosome Vesicles into Multivesicular Endosomes. *Science* **2008**, *319*, 1244–1247.

(103) Montefusco, D. J.; Chen, L.; Matmati, N.; Lu, S.; Newcomb, B.; Cooper, G. F.; Hannun, Y. A.; Lu, X. Distinct Signaling Roles of Ceramide Species in Yeast Revealed Through Systematic Perturbation and Systems Biology Analyses. *Sci. Signal.* **2013**, *6*, 14.

(104) Pettus, B. J.; Chalfant, C. E.; Hannun, Y. A. Ceramide in Apoptosis: An Overview and Current Perspectives. *Biochim. Biophys. Acta* **2002**, *1585*, 114–125.

(105) Morad, S. A. F.; Cabot, M. C. Ceramide-Orchestrated Signalling in Cancer Cells. *Nat. Rev. Cancer* **2013**, *13*, 51–65.

(106) Sot, J.; Goñi, F. M.; Alonso, A. Molecular Associations and Surface-Active Properties of Short- and Long-N-Acyl Chain Ceramides. *Biochim. Biophys. Acta - Biomembr.* **2005**, *1711*, 12–19.

(107) Ogretmen, B.; Pettus, B. J.; Rossi, M. J.; Wood, R.; Usta, J.; Szulc, Z.; Bielawska, A.; Obeid, L. M.; Hannun, Y. A. Biochemical Mechanisms of the Generation of Endogenous Long Chain Ceramide in Response to Exogenous Short Chain Ceramide in the A549 Human Lung Adenocarcinoma Cell Line. *J. Biol. Chem.* **2002**, *277*, 12960–12969.

(108) Mullen, T. D.; Hannun, Y. A.; Obeid, L. M. Ceramide Synthases at the Centre of Sphingolipid Metabolism and Biology. *Biochem. J.* **2012**, *441*, 789–802.

(109) Kim, Y. A.; Ramirez, D. M. C.; Costain, W. J.; Johnston, L. J.; Bittman, R. A New Tool to Assess Ceramide Bioactivity: 6-Bromo-7-Hydroxycoumarinyl-Caged Ceramide. *Chem. Commun.* **2011**, *47*, 9236–9238.

(110) Li, X.; Lam, H. Y.; Zhang, Y.; Chan, C. K. Salicylaldehyde Ester-Induced Chemoselective Peptide Ligations: Enabling Generation of Natural Peptidic Linkages at the Serine/Threonine Sites. *Org. Lett.* **2010**, *12*, 1724–1727.

(111) Brea, R. J.; Bhattacharya, A.; Devaraj, N. K. Spontaneous Phospholipid Membrane Formation by Histidine Ligation. *Synlett* **2017**, *28*, 108–112.

(112) Wieckowski, M. R.; Giorgi, C.; Lebiedzinska, M.; Duszynski, J.; Pinton, P. Isolation of

Mitochondria-Associated Membranes and Mitochondria from Animal Tissues and Cells. *Nat. Protoc.* **2009**, *4*, 1582–1590.

(113) Merrill, A. H.; Van Echten, G.; Wang, E.; Sandhoff, K. Fumonisin B1 Inhibits Sphingosine (Sphinganine) N-Acyltransferase and de Novo Sphingolipid Biosynthesis in Cultured Neurons in Situ. *J. Biol. Chem.* **1993**, *268*, 27299–27306.

(114) Bligh, E. G.; Dyer, W. J. A Rapid Method of Total Lipid Extraction and Purification. *Can. J. Biochem. Physiol.* **1959**, *37*, 911–917.

(115) Thomas, R. L.; Matsko, C. M.; Lotze, M. T.; Amoscato, A. A. Mass Spectrometric Identification of Increased C16 Ceramide Levels During Apoptosis. *J. Biol. Chem.* **1999**, *274*, 30580–30588.

(116) Osawa, Y.; Uchinami, H.; Bielawski, J.; Schwabe, R. F.; Hannun, Y. A.; Brenner, D. A. Roles for C16-Ceramide and Sphingosine 1-Phosphate in Regulating Hepatocyte Apoptosis in Response to Tumor Necrosis Factor-α. *J. Biol. Chem.* **2005**, *280*, 27879–27887.

(117) Mesicek, J.; Lee, H.; Feldman, T.; Jiang, X.; Skobeleva, A.; Berdyshev, E. V; Haimovitz-Friedman, A.; Fuks, Z.; Kolesnick, R. Ceramide Synthases 2, 5, and 6 Confer Distinct Roles in Radiation-Induced Apoptosis in HeLa Cells. *Cell. Signal.* **2010**, *22*, 1300–1307.

(118) Kolesnick, R. N.; Goñi, F. M.; Alonso, A. Compartmentalization of Ceramide Signaling: Physical Foundations and Biological Effects. *J. Cell. Physiol.* **2000**, *184*, 285–300.

(119) van Blitterswijk, W. J.; van der Luit, A. H.; Veldman, R. J.; Verheij, M.; Borst, J. Ceramide: Second Messenger or Modulator of Membrane Structure and Dynamics? *Biochem. J.* **2003**, *369*, 199–211.

(120) Pastorino, J. G.; Tafani, M.; Rothman, R. J.; Marcinkeviciute, A.; Hoek, J. B.; Farber, J. L.; Marcineviciute, A. Functional Consequences of the Sustained or Transient Activation by Bax of the Mitochondrial Permeability Transition Pore. *J. Biol. Chem.* **1999**, *274*, 31734–31739.

(121) Lee, H.; Rotolo, J. a.; Mesicek, J.; Penate-Medina, T.; Rimner, A.; Liao, W.-C.; Yin, X.; Ragupathi, G.; Ehleiter, D.; Gulbins, E.; et al. Mitochondrial Ceramide-Rich Macrodomains Functionalize Bax upon Irradiation. *PLoS One* **2011**, *6*, e19783.

(122) Taha, T. A.; Mullen, T. D.; Obeid, L. M. A House Divided: Ceramide, Sphingosine, and Sphingosine-1-Phosphate in Programmed Cell Death. *Biochim. Biophys. Acta - Biomembr.* **2006**, *1758*, 2027–2036.

(123) von Haefen, C.; Wieder, T.; Gillissen, B.; Stärck, L.; Graupner, V.; Dörken, B.; Daniel, P. T. Ceramide Induces Mitochondrial Activation and Apoptosis via a Bax-Dependent Pathway in Human Carcinoma Cells. *Oncogene* **2002**, *21*, 4009–4019.

(124) Wolter, K. G.; Hsu, Y. Te; Smith, C. L.; Nechushtan, A.; Xi, X. G.; Youle, R. J.

Movement of Bax from the Cytosol to Mitochondria during Apoptosis. *J. Cell Biol.* **1997**, *139*, 1281–1292.

(125) Hou, Q.; Jin, J.; Zhou, H.; Novgorodov, S. a; Bielawska, A.; Szulc, Z. M.; Hannun, Y. a; Obeid, L. M.; Hsu, Y.-T. Mitochondrially Targeted Ceramides Preferentially Promote Autophagy, Retard Cell Growth, and Induce Apoptosis. *J. Lipid Res.* **2011**, *52*, 278–288.

(126) Mullen, T. D.; Spassieva, S.; Jenkins, R. W.; Kitatani, K.; Bielawski, J.; Hannun, Y. a; Obeid, L. M. Selective Knockdown of Ceramide Synthases Reveals Complex Interregulation of Sphingolipid Metabolism. *J. Lipid Res.* **2011**, *52*, 68–77.

(127) Pinto, S. N.; Silva, L. C.; Futerman, A. H.; Prieto, M. Effect of Ceramide Structure on Membrane Biophysical Properties: The Role of Acyl Chain Length and Unsaturation. *Biochim. Biophys. Acta - Biomembr.* **2011**, *1808*, 2753–2760.

(128) Luo, J.; Uprety, R.; Naro, Y.; Chou, C.; Nguyen, D. P.; Chin, J. W.; Deiters, A. Genetically Encoded Optochemical Probes for Simultaneous Fluorescence Reporting and Light Activation of Protein Function with Two-Photon Excitation. *J. Am. Chem. Soc.* **2014**, *136*, 15551–15558.

(129) Ramirez, D. M. C.; Pitre, S. P.; Kim, Y. A.; Bittman, R.; Johnston, L. J. Photouncaging of Ceramides Promotes Reorganization of Liquid-Ordered Domains in Supported Lipid Bilayers. *Langmuir* **2013**, *29*, 3380–3387.

(130) Bieberich, E. Ceramide in Stem Cell Differentiation and Embryo Development: Novel Functions of a Topological Cell-Signaling Lipid and the Concept of Ceramide Compartments. *J. Lipids* **2011**, *2011*, 1–11.

(131) Cutler, R. G.; Kelly, J.; Storie, K.; Pedersen, W. A.; Tammara, A.; Hatanpaa, K.; Troncoso, J. C.; Mattson, M. P. Involvement of Oxidative Stress-Induced Abnormalities in Ceramide and Cholesterol Metabolism in Brain Aging and Alzheimer's Disease. *Proc. Natl. Acad. Sci. USA* **2004**, *101*, 2070–2075.

(132) Prabakaran, S.; Lippens, G.; Steen, H.; Gunawardena, J. Post-Translational Modification: Nature's Escape from Genetic Imprisonment and the Basis for Dynamic Information Encoding. *Wiley Interdiscip. Rev. Syst. Biol. Med.* **2012**, *4*, 565–583.

(133) Vidal, C. J. *Post-Translational Modifications in Health and Disease*; Springer New York: New York, NY, 2011.

(134) Yeste-Velasco, M.; Linder, M. E.; Lu, Y.-J. Protein S-Palmitoylation and Cancer. *Biochim. Biophys. Acta* **2015**, *1856*, 107–120.

(135) Rocks, O.; Gerauer, M.; Vartak, N.; Koch, S.; Huang, Z.-P.; Pechlivanis, M.; Kuhlmann, J.; Brunsveld, L.; Chandra, A.; Ellinger, B.; et al. The Palmitoylation Machinery Is a Spatially Organizing System for Peripheral Membrane Proteins. *Cell* **2010**, *141*, 458–471.

(136) Meckler, X.; Roseman, J.; Das, P.; Cheng, H.; Pei, S.; Keat, M.; Kassarjian, B.; Golde, T.

E.; Parent, A. T.; Thinakaran, G. Reduced Alzheimer's Disease ß-Amyloid Deposition in Transgenic Mice Expressing S-Palmitoylation-Deficient APH1aL and Nicastrin. *J. Neurosci.* **2010**, *30*, 16160–16169.

(137) Berchtold, L. A.; Storling, Z. M.; Ortis, F.; Lage, K.; Bang-Berthelsen, C.; Bergholdt, R.; Hald, J.; Brorsson, C. A.; Eizirik, D. L.; Pociot, F.; et al. Huntingtin-Interacting Protein 14 Is a Type 1 Diabetes Candidate Protein Regulating Insulin Secretion and ß-Cell Apoptosis. *Proc. Natl. Acad. Sci.* **2011**, *108*, E681–E688.

(138) Blaskovic, S.; Blanc, M.; van der Goot, F. G. What Does S-Palmitoylation Do to Membrane Proteins? *FEBS J.* **2013**, *280*, 2766–2774.

(139) Brea, R. J.; Rudd, A. K.; Devaraj, N. K. Nonenzymatic Biomimetic Remodeling of Phospholipids in Synthetic Liposomes. *Proc. Natl. Acad. Sci.* **2016**, *113*, 8589–8594.

(140) Brea, R. J.; Cole, C. M.; Lyda, B. R.; Ye, L.; Prosser, R. S.; Sunahara, R. K.; Devaraj, N. K. In Situ Reconstitution of the Adenosine A2A Receptor in Spontaneously Formed Synthetic Liposomes. *J. Am. Chem. Soc.* **2017**, *139*, 3607–3610.

(141) Yan, L. Z.; Dawson, P. E. Synthesis of Peptides and Proteins without Cysteine Residues by Native Chemical Ligation Combined with Desulfurization. *J. Am. Chem. Soc.* **2001**, *123*, 526–533.

(142) Malumbres, M.; Barbacid, M. RAS Oncogenes: The First 30 Years. *Nat. Rev. Cancer* **2003**, *3*, 459–465.

(143) Fernandez-Medarde, A.; Santos, E. Ras in Cancer and Developmental Diseases. *Genes Cancer* **2011**, *2*, 344–358.

(144) Aoki, Y.; Niihori, T.; Kawame, H.; Kurosawa, K.; Ohashi, H.; Tanaka, Y.; Filocamo, M.; Kato, K.; Suzuki, Y.; Kure, S.; et al. Germline Mutations in HRAS Proto-Oncogene Cause Costello Syndrome. *Nat. Genet.* **2005**, *37*, 1038–1040.

(145) Gripp, K. W.; Lin, A. E. Costello Syndrome: A Ras/Mitogen Activated Protein Kinase Pathway Syndrome (Rasopathy) Resulting from HRAS Germline Mutations. *Genet. Med.* **2012**, *14*, 285–292.

(146) Papke, B.; Der, C. J. Drugging RAS: Know the Enemy. *Science* **2017**, *355*, 1158–1163.

(147) Calvo, F.; Agudo-Ibáñez, L.; Crespo, P. The Ras-ERK Pathway: Understanding Site-Specific Signaling Provides Hope of New Anti-Tumor Therapies. *BioEssays* **2010**, *32*, 412–421.

(148) Goodwin, J. S.; Drake, K. R.; Rogers, C.; Wright, L.; Lippincott-Schwartz, J.; Philips, M. R.; Kenworthy, A. K. Depalmitoylated Ras Traffics to and from the Golgi Complex via a Nonvesicular Pathway. *J. Cell Biol.* **2005**, *170*, 261–272.

(149) Forrester, M. T.; Hess, D. T.; Thompson, J. W.; Hultman, R.; Moseley, M. A.; Stamler, J.

S.; Casey, P. J. Site-Specific Analysis of Protein S-Acylation by Resin-Assisted Capture. *J. Lipid Res.* **2011**, *52*, 393–398.

(150) Agudo-Ibáñez, L.; Herrero, A.; Barbacid, M.; Crespo, P. H-Ras Distribution and Signaling in Plasma Membrane Microdomains Are Regulated by Acylation and Deacylation Events. *Mol. Cell. Biol.* **2015**, *35*, 1898–1914.

(151) Rusch, M.; Zimmermann, T. J.; Bürger, M.; Dekker, F. J.; Görmer, K.; Triola, G.; Brockmeyer, A.; Janning, P.; Böttcher, T.; Sieber, S. A.; et al. Identification of Acyl Protein Thioesterases 1 and 2 as the Cellular Targets of the Ras-Signaling Modulators Palmostatin B and M. *Angew. Chemie Int. Ed.* **2011**, *50*, 9838–9842.

(152) Dekker, F. J.; Rocks, O.; Vartak, N.; Menninger, S.; Hedberg, C.; Balamurugan, R.; Wetzel, S.; Renner, S.; Gerauer, M.; Schölermann, B.; et al. Small-Molecule Inhibition of APT1 Affects Ras Localization and Signaling. *Nat. Chem. Biol.* **2010**, *6*, 449–456.

(153) Babuke, T.; Tikkanen, R. Dissecting the Molecular Function of Reggie/Flotillin Proteins. *Eur. J. Cell Biol.* **2007**, *86*, 525–532.

(154) Rajagopalan, S.; Xu, Y.; Brenner, M. B. Retention of Unassembled Components of Integral Membrane Proteins by Calnexin. *Science* **1994**, *263*, 387–390.

(155) De Luca, A.; Maiello, M. R.; D'Alessio, A.; Pergameno, M.; Normanno, N. The RAS/RAF/MEK/ERK and the PI3K/AKT Signalling Pathways: Role in Cancer Pathogenesis and Implications for Therapeutic Approaches. *Expert Opin. Ther. Targets* **2012**, *16*, S17–S27.

(156) Reddy, E. P.; Reynolds, R. K.; Santos, E.; Barbacid, M. A Point Mutation Is Responsible for the Acquisition of Transforming Properties by the T24 Human Bladder Carcinoma Oncogene. *Nature* **1982**, *300*, 149–152.

(157) Kiessling, M. K.; Curioni-Fontecedro, A.; Samaras, P.; Atrott, K.; Cosin-Roger, J.; Lang, S.; Scharl, M.; Rogler, G. Mutant HRAS as Novel Target for MEK and MTOR Inhibitors. *Oncotarget* **2015**, *6*, 42183–42196.

(158) Sanders, S. S.; Martin, D. D. O.; Butland, S. L.; Lavallée-Adam, M.; Calzolari, D.; Kay, C.; Yates, J. R.; Hayden, M. R. Curation of the Mammalian Palmitoylome Indicates a Pivotal Role for Palmitoylation in Diseases and Disorders of the Nervous System and Cancers. *PLOS Comput. Biol.* **2015**, *11*, e1004405.

(159) Zhang, Z.; Lee, Y.-C.; Kim, S.-J.; Choi, M. S.; Tsai, P.-C.; Xu, Y.; Xiao, Y.-J.; Zhang, P.; Heffer, A.; Mukherjee, A. B. Palmitoyl-Protein Thioesterase-1 Deficiency Mediates the Activation of the Unfolded Protein Response and Neuronal Apoptosis in INCL. *Hum. Mol. Genet.* **2006**, *15*, 337–346.

(160) Kim, S.-J.; Zhang, Z.; Hitomi, E.; Lee, Y.-C.; Mukherjee, A. B. Endoplasmic Reticulum Stress-Induced Caspase-4 Activation Mediates Apoptosis and Neurodegeneration in INCL. *Hum. Mol. Genet.* **2006**, *15*, 1826–1834.

(161) Sarkar, C.; Chandra, G.; Peng, S.; Zhang, Z.; Liu, A.; Mukherjee, A. B. Neuroprotection and Lifespan Extension in Ppt1 −/− Mice by NtBuHA: Therapeutic Implications for INCL. *Nat. Neurosci.* **2013**, *16*, 1608–1617.

(162) Levin, S. W.; Baker, E. H.; Zein, W. M.; Zhang, Z.; Quezado, Z. M. N.; Miao, N.; Gropman, A.; Griffin, K. J.; Bianconi, S.; Chandra, G.; et al. Oral Cysteamine Bitartrate and N-Acetylcysteine for Patients with Infantile Neuronal Ceroid Lipofuscinosis: A Pilot Study. *Lancet Neurol.* **2014**, *13*, 777–787.

(163) Schneider, C. A.; Rasband, W. S.; Eliceiri, K. W. NIH Image to ImageJ: 25 Years of Image Analysis. *Nat. Methods* **2012**, *9*, 671–675.

(164) Yasuda, R.; Harvey, C. D.; Zhong, H.; Sobczyk, A.; van Aelst, L.; Svoboda, K. Supersensitive Ras Activation in Dendrites and Spines Revealed by Two-Photon Fluorescence Lifetime Imaging. *Nat. Neurosci.* **2006**, *9*, 283–291.

(165) Rise, F.; Undheim, K. Sodium 2-Mercaptoethanesulfonate in Reversible Adduct Formation and Water Solubilization. *Acta Chem. Scand.* **1989**, *43*, 489–492.